In presenting the dissertation as a partial fulfillment of the requirements for an advanced degree from the Georgia Institute of Technology, I agree that the Library of the Institute shall make it available for inspection and circulation in accordance with its regulations governing materials of this type. I agree that permission to copy from, or to publish from, this dissertation may be granted by the professor under whose direction it was written, or, in his absence, by the Dean of the Graduate Division when such copying or publication is solely for scholarly purposes and does not involve potential financial gain. It is understood that any copying from, or publication of, this dissertation which involves potential financial gain will not be allowed without written permission.

7/25/68

INTERACTION OF A TWO-DIMENSIONAL, COMPRESSIBLE, TURBULENT FREE JET WITH A CROSSFLOWING FREE STREAM

A THESIS

Presented to

The Faculty of the Division of Graduate

Studies and Research

by

Frank Buck Tatom

In Partial Fulfillment

of the Requirements for the Degree

Doctor of Philosophy

in the School of Mechanical Engineering

Georgia Institute of Technology

April, 1971

INTERACTION OF A TWO-DIMENSIONAL, COMPRESSIBLE,

TURBULENT FREE JET WITH A CROSSFLOWING FREE STREAM

Approved:

Chairman

Date approved by Chairman: May 17, 1971

ACKNOWLEDGMENTS

Assistance and support to the author in carrying out the investigation, culminating in this thesis, was derived from a number of sources. In this regard I would like to recognize certain individuals who made special contributions.

First to my wife, Roberta, without whose understanding and willingness to sacrifice, this study could never have even commenced, I offer my sincerest expression of gratitude and love.

For his guidance and support, I wish to thank my major advisor, Dr. S. P. Kezios, whose continual confidence in me proved essential to the successful completion of this work. To the members of my thesis committee, Dr. P. Desai, Dr. H. M. McMahon, Dr. J. C. Wu and Dr. P. Durbetaki, I express my appreciation for their conscientious efforts in the form of advice, review of my work, and constructive comments.

A special word of thanks is due to Assistant Professor D. W. Kraus for his invaluable aid regarding the translation of Russian literature. The encouragement offered by Dr. S. V. Shelton and his willingness to listen to my ideas, is gratefully acknowledged. I would also like to thank Mr. J. W. Segers for his patience and advice regarding problems associated with the digital computer.

To my brother, Dr. John W. Tatom, Vanderbilt University, I express my deepest gratitude for his interest and advice. To my

mother for the moral support she offered me, I in return offer her my sincere thanks and affection.

Dr. E. A. Coxe, Clemson University provided me with valuable advice regarding his own experience concerned with a related problem, and for this advice and his encouragement I am most grateful. In this regard I am indebted to Assistant Professor J. F. Thompson, Mississippi State University, for his advice pertaining to a related problem, and also pertaining to computer graphics.

In addition to those already noted, who through personal contact provided direct assistance to me, I would also like to recognize a number of individuals with whom correspondence proved most helpful. These include Dr. F. Maurer, Institute for Applied Gasdynamics, Linderhöhe, West Germany; Mr. H. Endo, National Aerospace Laboratory, Tokyo, Japan; Dr. A. J. Chorin, New York University; Dr. R. D. Richtmyer, University of Colorado; Mr. R. G. Graham, Northrop Corporation; Dr. S. M. Scala, General Electric Corporation; and Mr. A. M. O. Smith, McDonnell Douglas Corporation. Each of these demonstrated a spirit of cooperation in response to my inquiries which I sincerely appreciate.

To the U. S. Department of Health, Education and Welfare and to the Schlumberger Foundation, both of which provided me with financial support, I express my sincere appreciation.

Notwithstanding the gratitude and appreciation which I wish to convey to those already noted, there remains One to whom I owe an infinitely greater debt. To the Omnipotent and Omniscient God who gave me the desire to study the wonders of His universe and blessed me with the capability to understand a small part, I give special thanks.

TABLE OF CONTENTS

Page

ACKNOWLEDGMENTS ii

LIST OF TABLES viii

LIST OF ILLUSTRATIONS ix

SUMMARY xii

NOMENCLATURE xv

Chapter

I. INTRODUCTION 1

Background
Statement of the Problem
Jet Characteristics
Free Stream Characteristics
Physical Boundaries of the Problem
Significance of Time in the Problem
Nature and Extent of the Desired Solution
General Flow Pattern
Plane Turbulent Jet
Two-Dimensional Deflected Turbulent Jet

II. PREVIOUS RELATED STUDIES 12

Deflected Jets
Turbulent Flow Characteristics
Straight Turbulent Flow
Turbulent Free Jets
Turbulent Boundary Layers
Turbulent Flow in Ducts
Curved Turbulent Flow
Computational Fluid Dynamics

III. ANALYTICAL DEVELOPMENT 58

Coordinate Systems
Parabolic Coordinates
Rectangular Coordinates
Relation Between Rectangular and Parabolic Coordinates
Location of Jet Centerline

Chapter Page

III. ANALYTICAL DEVELOPMENT (Continued)

Non-Dimensionalization Procedure
Governing Equations
  Classical Form
  Time-Averaged Equations
  Conservation-Law Form
Molecular Transport Models
Turbulent Transport Models
Variation of Molecular Transport Properties
Variation of Turbulent Transport Properties
  Calculation of Jet Eddy Viscosity
  Calculation of Boundary Layer Eddy Viscosity
  Calculation of Slot Eddy Viscosity
  General Logic for Calculation of Eddy Viscosity
  Calculation of Eddy Diffusivities
Boundary Conditions
  Free Flow Region
  Slot Flow Region
Initial Conditions

IV. NUMERICAL TECHNIQUE 122

Grid System
Finite-Difference Approximations for Spatial Derivatives
Interpolation and Numerical Integration Procedures
Time-Marching Procedures for Interior Points
Time-Marching Procedures for Boundary Points
  Free Flow Region
  Slot Flow Region
Stability and Convergence Considerations
Digital Computer Program
Computer Graphics

V. DISCUSSION OF RESULTS 149

Test Case No. 1 (Low Subsonic Jet/
  Low Subsonic Free Stream)
  Analysis of Test Conditions
  Predicted Flow Pattern
  Comparison with Experimental Data
Test Case No. 2 (Transonic Jet/
  High Subsonic Free Stream)
  Analysis of Test Conditions
  Predicted Flow Pattern
  Comparison with Experimental Data
Important Features of Deflected Jets

Chapter

V. DISCUSSION OF RESULTS (Continued)

Observations Concerning Numerical Computation of Turbulent Compressible Flow
Initial Conditions
Boundary Conditions
Time-Marching Technique and Mass Diffusion

VI. CONCLUSIONS 214

Deflected Jets
Turbulent Flow Characteristics
Computational Fluid Dynamics

VII. RECOMMENDATIONS 220

Deflected Jets
Turbulent Flow Characteristics
Computational Fluid Dynamics

APPENDIX

A. CALCULATION OF THE ISENTROPIC JET EXIT CONDITIONS 224

B. DEVELOPMENT OF THE TIME-AVERAGED EQUATIONS GOVERNING TURBULENT FLOW. 226

Expansion of Terms Containing Products and Sums
Rules for Neglecting Terms
Time-Averaged Equation of State
Time-Averaged Continuity Equation
Time-Averaged Momentum Equations
Time-Averaged Energy Equation

C. TRANSVERSE VARIATION OF EDDY VISCOSITY. 243

D. CALCULATION OF DISTANCE ALONG A PARABOLA. 246

E. ENERGY BOUNDARY CONDITION AT AN INSULATED WALL WITH THERMAL CAPACITANCE 249

F. CALCULATION OF INITIAL CONDITIONS 252

Free Flow Region
Slot Flow Region

G. FINITE-DIFFERENCE EQUATIONS 260

APPENDIX Page

H. DESCRIPTION OF DIGITAL COMPUTER PROGRAM 263

General Characteristics
Subroutines and Function Subprograms
Program Terminology
Input Items
Output Items
Computer Logic

I. SIMPLIFIED ANALYSIS OF TRAVERSE OF THE JET BY THE FREE STREAM 289

BIBLIOGRAPHY 294

VITA 303

LIST OF TABLES

Table		Page
1.	Input Parameters for Test Case No. 1.	151
2.	Input Parameters for Test Case No. 2.	171
3.	Subroutines of DEFJET	266
4.	Function Subprograms of DEFJET.	269
5.	Important FORTRAN Variables	270
6.	Input Data for DEFJET	275

LIST OF ILLUSTRATIONS

Figure		Page
1.	General Characteristics of a Plane Turbulent Jet.	7
2.	General Flow Pattern of Two-Dimensional Deflected Turbulent Jet	9
3.	Sketch of the General Flow Regions.	59
4a.	Parabolic Coordinate System	61
4b.	Rectangular Coordinate System	61
5.	Rectangular Grid System	124
6.	Parabolic Grid System	125
7.	Parabolic Grid System for the Free Flow, Overall View, Low Subsonic Jet/Low Subsonic Free Stream (Test Case No. 1)	155
8.	Fluid Velocity in the Free Flow, Overall View, Low Subsonic Jet/Low Subsonic Free Stream (Test Case No. 1)	156
9.	Streamlines in the Free Flow, Overall View, Low Subsonic Jet/Low Subsonic Free Stream (Test Case No. 1)	158
10.	Isotachs in the Free Flow, Overall View, Low Subsonic Jet/Low Subsonic Free Stream (Test Case No. 1)	159
11.	Lines of Constant Eddy Viscosity in the Free Flow, Overall View, Low Subsonic Jet/Low Subsonic Free Stream (Test Case No. 1)	160
12.	Parabolic Grid System for the Free Flow, Enlarged View, Low Subsonic Jet/Low Subsonic Free Stream (Test Case No. 1)	162
13.	Fluid Velocity in the Free Flow, Enlarged View, Low Subsonic Jet/Low Subsonic Free Stream (Test Case No. 1)	163

Figure — Page

14. Streamlines in the Free Flow, Enlarged View, Low Subsonic Jet/Low Subsonic Free Stream (Test Case No. 1) 164

15. Isotachs in the Free Flow, Enlarged View, Low Subsonic Jet/Low Subsonic Free Stream (Test Case No. 1) 165

16. Lines of Constant Eddy Viscosity in the Free Flow, Enlarged View, Low Subsonic Jet/Low Subsonic Free Stream (Test Case No. 1) 167

17. Measured and Predicted Jet Paths, Low Subsonic Jet/ Low Subsonic Free Stream (Test Case No. 1). 169

18. Parabolic Grid System for the Free Flow, Overall View, Transonic Jet/High Subsonic Free Stream (Test Case No. 2) 174

19. Fluid Velocity in the Free Flow, Overall View, Transonic Jet/High Subsonic Free Stream (Test Case No. 2) 176

20. Streamlines in the Free Flow, Overall View, Transonic Jet/High Subsonic Free Stream (Test Case No. 2) 178

21. Isotachs in the Free Flow, Overall View, Transonic Jet/High Subsonic Free Stream (Test Case No. 2) 179

22. Lines of Constant Eddy Viscosity in the Free Flow, Overall View, Transonic Jet/High Subsonic Free Stream (Test Case No. 2) 181

23. Isobars in the Free Flow, Overall View, Transonic Jet/High Subsonic Free Stream (Test Case No. 2) 182

24. Parabolic Grid System for the Free Flow, Enlarged View, Transonic Jet/High Subsonic Free Stream (Test Case No. 2) 183

25. Fluid Velocity in the Free Flow, Enlarged View, Transonic Jet/High Subsonic Free Stream (Test Case No. 2) 185

Figure Page

26. Streamlines in the Free Flow, Enlarged View, Transonic Jet/High Subsonic Free Stream (Test Case No. 2) 186

27. Isotachs in the Free Flow, Enlarged View, Transonic Jet/High Subsonic Free Stream (Test Case No. 2) 187

28. Lines of Constant Eddy Viscosity in the Free Flow, Enlarged View, Transonic Jet/High Subsonic Free Stream (Test Case No. 2) 189

29. Isobars in the Free Flow, Enlarged View, Transonic Jet/High Subsonic Free Stream (Test Case No. 2) 190

30. Pressure Distribution Along the Plate, Transonic Jet/High Subsonic Free Stream (Test Case No. 2) 192

31. Predicted Jet Paths, Transonic Jet/High Subsonic Free Stream (Test Case No. 2) 195

32. Streamlines in the Free Flow, Test Case No. 1 at Time Zero. 198

33. Streamlines in the Free Flow, Test Case No. 1 after 500 Time Steps. 199

34. Streamlines in the Free Flow, Test Case No. 1 after 1000 Time Steps 200

35. Streamlines in the Free Flow, Test Case No. 1 after 2078 Time Steps 201

36. Streamlines in the Free Flow, Test Case No. 1 after 4154 Time Steps 202

37. Control Volume at the Surface of the Wall 250

38. Flow Chart of the Main Routine, DEFJET. 276

39. Flow Chart of the Subroutine LW1. 283

40. Flow Chart of the Subroutine LW2. 286

41. Relative Position of Streamlines $\psi_{\ell es}$ and ψ_{tes} with Respect to Jet Centerline. 290

SUMMARY

An analytical study is conducted which is concerned with the interaction of a two-dimensional compressible, turbulent free jet with a crossflowing free stream. The jet issues from a slot in a flat plate with the slot axis perpendicular to the plate and the latter parallel to the free stream. Only jets with sonic or subsonic exit velocities are considered along with a subsonic free stream. Due to the sweeping action of the latter, the emerging jet is deflected in the downstream direction. Analytical prediction is sought of the steady-state flow pattern at specified points throughout the flow field (including the interior of the slot). Such predictions must satisfy the fundamental governing equations subject to the appropriate boundary conditions.

The time-averaged governing equations are set up in rectangular coordinates for the flow in the slot. Because previous experimental data indicate that the jet path resembles a parabola, the equations for the flow region above the plate are formulated in parabolic coordinates. The phenomenological approach to turbulence is utilized. Considerable effort is directed toward the development of methods of calculating eddy viscosity, eddy mass diffusivity and eddy thermal diffusivity for the types of turbulent flow present in the problem.

Because of the complexity of the governing equations only a numerical solution is feasible. A transient numerical technique similar to the Lax-Wendroff two-step method is used to solve the governing

equations in finite-difference form. The numerical scheme is programmed for the UNIVAC-1108 digital computer.

Two test cases, corresponding to actual test conditions for which experimental data are available, are considered. In the first case, low subsonic flow conditions are present both in the jet and free stream, while in the second the jet is transonic and the free stream is high subsonic. Because of limitations regarding computer availability, steady-state solutions are not achieved for either case. Quantitative pictures of the deflected jet flow patterns, however, are achieved. The predicted patterns contain several features which have not been previously reported. In general the predicted flow fields are in agreement with the available experimental data, although there exist several significant differences.

In developing the time-averaged version of the governing equations for turbulent compressible flow certain double-correlation terms, consisting of the time-averaged products of the density fluctuation and the fluctuations of the velocity components, are produced. These terms are shown to represent turbulent mass self-diffusion which appears to be significant in turbulent compressible flow. Another important observation, concerning turbulent flow in general is that an exact analogy between turbulent stress-strain relations and laminar stress-strain relations (without boundary layer simplifications) is both useful and valid.

With regard to computational fluid dynamics the results of the study indicate that the use of artificial viscosity by some investigators

quite likely represents an empirical approximation to the more physically acceptable concepts of eddy viscosity and related parameters. This conclusion in turn implies that some of the instabilities associated with computational fluid dynamics may represent, or be related to, the physical instabilities characteristic of turbulent flow.

NOMENCLATURE*

English Letters

Symbol	Definition
a	speed of sound.
A_i	term in conservation-law form of governing equations for rectangular coordinates [see Equation (III-98)].
b	characteristic jet width.
b_o	half-width of jet exit slot.
b_w	width of jet exit slot.
B_i	term in conservation-law form of governing equations for rectangular coordinates [see Equation (III-99)].
c_p	heat capacity with constant pressure.
c_v	heat capacity with constant volume.
c_w	heat capacity of wall.
C	empirical curvature constant used by Sawyer [52] and Endo [20].
C_i	term in conservation-law form of governing equations in rectangular coordinates [see Equation (III-100)].
C_∞	force coefficient of jet.
D	diameter of jet exit for round jet.
e	specific internal energy.
e_o	specific stagnation internal energy.
E_i	term in conservation law form of governing equations for parabolic coordinates [see Equation (III-102)].

*In general all terms are expressed in dimensionless form and thus have no units. Dimensional quantities where occurring are denoted by the superscript ^ and have units in accordance with the English engineering system.

Symbol	Definition
f	Fanning friction factor.
$f(\ )$	function of ( ).
F_i	term in conservation-law form of governing equations for parabolic coordinates [see Equation (III-103)].
G_i	term in conservation-law form of governing equations for parabolic coordinates [see Equation (III-104)].
h	specific enthalpy.
h_w	slot breadth, the major dimension of the slot (perpendicular to the plane in which the problem is defined).
H	metric factor.
J	number of u-grid lines.
k	thermal conductivity.
K	number of v-grid lines.
ℓ	mixing length.
L	characteristic length.
M	number of x-grid lines.
N	number of y-grid lines.
p	absolute pressure.
q	molecular heat flux.
r	turbulent heat flux.
R	specific gas constant.
R	cylindrical coordinate.
$R_{jc\ell}$	radius of curvature of jet centerline.
s	distance along jet centerline.
t	time.

Symbol	Definition
T	absolute temperature.
u	parabolic coordinate.
v	parabolic coordinate.
w	local magnitude of velocity.
w_u	u-component of velocity.
w_v	v-component of velocity.
w_x	x-component of velocity.
w_y	y-component of velocity.
w_{je}	characteristic jet exit velocity.
w_∞	free stream velocity at infinity.
x	rectangular coordinate.
y	rectangular coordinate.
z	coordinate normal to u-v plane in parabolic coordinates, x-y plane in rectangular coordinates, and R-ϕ in cylindrical coordinates.

Greek Letters

α	inclination angle of jet axis to free stream direction.
α_o	initial inclination angle of jet axis to free stream direction.
γ	ratio of heat capacities.
γ_t	intermittency factor for turbulent flow.
Γ_i	term in conservation-law form of governing equations for parabolic coordinates [see Equation (III-104)].
$\delta_{1/2}$	jet half-thickness [transverse distance from jet centerline to point where $w = 1/2(w_{jc\ell}+w_\infty)$].
$\delta_{b\ell}$	boundary-layer thickness.

Symbol	Definition
$\delta^*_{b\ell}$	boundary layer displacement thickness.
ϵ_h	eddy thermal diffusivity.
ϵ_m	eddy viscosity.
ϵ_ρ	eddy mass self-diffusivity.
ζ	curvilinear coordinate measured along jet axis.
η	curvilinear coordinate measured normal to jet axis.
θ_j	displacement thickness of jet as defined by Equation (II-23).
λ	second coefficient of viscosity.
μ	first coefficient of viscosity.
ν	kinematic viscosity.
ρ	density.
ρ_w	density of wall.
σ	spreading coefficient.
σ_{ij}	viscous stress tensor.
σ_w	shear stress at the wall.
τ_{ij}	turbulent stress tensor.
ϕ	cylindrical coordinate.
ψ	stream function.

Dimensionless Groups

N_{Ma}	Mach number, w/a.
N_{Pr}	Prandtl number, $\mu c_p/k$.
$(N_{Pr})_t$	turbulent Prandtl number, ϵ_m/ϵ_h.
N_{Re}	Reynolds number, $\rho wL/\mu$.

Symbol	Definition
$(N_{Re})_t$	eddy Reynolds number, $(w_{jc\ell}-w_\infty)\delta_{1/2}/(\epsilon_m)_j$.
$(N_{Sc})_t$	turbulent Schmidt number, ϵ_m/ϵ_ρ.

Subscripts

bℓ	boundary layer.
bℓi	boundary layer, inner region.
bℓo	boundary layer, outer region.
cℓ	centerline.
e	isentropic exit condition.
j	u-incrementation.
j	jet flow.
k	v-incrementation.
ℓep	leading edge of plate.
ℓes	leading edge of slot.
m	x-incrementation.
n	y-incrementation.
o	stagnation condition.
ref	reference value.
rp	reattachment point.
s	slot flow.
t	turbulent.
tep	trailing edge of plate.
tes	trailing edge of slot.
u	pertaining to u-coordinate.
v	pertaining to v-coordinate.

Symbol	Definition
w	wall.
∞	free stream.

Superscripts

ℓ	time-incrementation.
-	time-averaged component.
'	fluctuating component.
^	dimensional quantity (the absence of this superscript implies a dimensionless quantity).

CHAPTER I

INTRODUCTION

Background

The interaction of a fluid jet with a free stream in a crossflow configuration produces a flow pattern which is of considerable practical significance. A wide variety of applications for this type of jet interaction exists. Examples include attitude control systems for guided missiles, thrust-vector control systems for rocket motors, fuel injection in supersonic burners, in-flight venting of interstage compartments of ascending space vehicles, overfire jets in boilers and incinerators, jet flaps for conventional aircraft, and air curtains. The transition flight phase for VTOL (Vertical Take-Off and Landing) aircraft also involves such an interaction. This wide variety of applications represents a broad range of flow conditions, from two-dimensional, laminar, incompressible flow of a single nonreacting species, to three-dimensional, turbulent, supersonic flow of a multi-species reacting gas mixture. Furthermore, the characteristics of the flow which are of interest vary from one application to another. In one case the jet penetration height or trajectory may be of primary importance, while in another the pressure distribution on the surface through which the jet issues is the principal flow characteristic of interest. In still another case the item of major concern is the discharge coefficient of the jet exit.

The considerable number of applications, coupled with the wide range of flow conditions, and the varied interests regarding the flow characteristics have in turn produced a number of different approaches to the problem. Because of the basic complexity of the flow field, much of the analytical work has been based on either potential flow theory or integral mass-momentum conservation concepts. Only a limited effort has been made to solve the problem analytically by satisfying the basic governing equations. Pertinent experimental studies are relatively numerous and cover a wide variety of test conditions. Unfortunately due to the number of test variables involved, there does not appear to be a general method for correlating the test results. This situation tends to produce a new correlation procedure for each new experimental study.

An ultimate goal in the study of free jets in crossflow is the development of a general technique capable of predicting the behavior of any such jet from the simplest case to the most complex. The most reasonable approach to such a goal consists of an orderly number of steps, each of which provides a basis for the development of the next. At the present time the most complex analytical case which has been rigorously treated appears to be a two-dimensional laminar incompressible jet issuing through a flat plate into a free stream with a laminar boundary layer on the plate surface [1]*.

A reasonable step forward analytically would involve the case of a two-dimensional *turbulent, compressible* jet issuing through a flat

---

*Numbers in brackets [ ] denote references cited in the Bibliography.

plate into a free stream with a *turbulent* boundary layer on the surface of the plate. This case poses the basic problem treated in this dissertation.

Statement of the Problem

In rigorously describing the problem under consideration there are five items to be defined as follows:

1. Characteristics of the jet.
2. Characteristics of the free stream.
3. Physical boundaries of the problem.
4. Significance of time in the problem.
5. Precise nature and extent of the desired solution.

Although these items are interdependent, for purposes of discussion they are treated individually in the five subdivisions which follow.

Jet Characteristics

The jet is produced by the turbulent efflux of a compressible fluid from a rectangular duct, which is of such dimensions as to produce two-dimensional flow. The exit plane of the duct coincides with a slot cut in the surface of a flat plate. The plate is perpendicular to the direction of flow in the duct. The flow in the latter is sonic or subsonic and the fluid involved is a calorically perfect ideal gas, which is identical to the fluid in the free-stream flow over the plate. Due to the sweeping action of the free stream, the emerging jet is deflected toward the downstream direction of the free stream.

Free Stream Characteristics

The general pattern of the free stream, upstream of the region of interaction, is that pattern characteristic of subsonic, compressible, two-dimensional flow over an adiabatic flat plate with a turbulent boundary layer. As already noted, the free-stream fluid is identical to that in the jet. Due to the presence of free-stream turbulence (or a tripping device at the leading edge of the plate) no laminar boundary layer occurs.

Physical Boundaries of the Problem

Two regions must be considered in the problem: (1) the flow in the duct or slot, and (2) the flow above the flat plate. These regions are considered to lie within certain physical boundaries. The latter are not necessarily solid surfaces but instead are the outer limits of the spatial domain of the problem. The physical boundaries of the slot or duct flow (referred to hereafter as the "slot-flow region") consist of an entrance plane which is assumed to exist a large distance upstream, the two duct walls which channel the flow, and finally the exit plane of the duct.

For the flow above the plate (referred to hereafter as the "free-flow region"), the plane in which the plate lies forms one of the four boundaries. The plate extends a finite distance both upstream and downstream. A second physical boundary, perpendicular to the direction of the free stream flow, is located upstream of the leading edge of the flat plate. The distance upstream is sufficiently great to prevent any disturbance generated by the presence of the jet from reaching this

second boundary. Downstream of the trailing edge of the plate a third boundary is located. As with the upstream case, this boundary lies in a plane normal to the free stream flow and must be sufficiently removed from the jet so that no flow disturbance produced by the latter can reach the boundary. The fourth boundary coincides with a streamline which is located at a distance above the plate which is so great that the disturbance produced by the jet causes no effect on the streamline, which is thus parallel to the plate.

Significance of Time in the Problem

The flow field which is of primary interest is that which exists under steady-state conditions. Periodic or fluctuating flow patterns, if they exist with steady-state boundary conditions, are of considerable interest. Transient effects, which may initially occur in generating steady-state conditions are of secondary interest only.

Nature and Extent of the Desired Solution

Within the physical boundaries described, analytical prediction of the steady-state flow variables (velocity, pressure, temperature, and density) is desired at a specified number of points throughout the two flow regions. This analytical prediction must satisfy the fundamental governing equations and appropriate boundary conditions. Because of the complexity of the governing equations, a numerical approach involving the use of digital computers is envisioned.

General Flow Pattern

Although a quantitative solution to the problem as posed does not exist, a qualitative description of the general flow pattern can be

developed. In describing such a flow pattern a basic understanding of the characteristics of turbulent plane jets is useful. Thus, before any attempt is made to describe a deflected jet, a brief description of the flow pattern associated with plane free jets is in order.

Plane Turbulent Jet

The behavior of turbulent plane jets under a variety of test conditions has been observed and analyzed. Based on such observation and analysis, certain fundamental features of such jets can be defined. For the case of a plane turbulent jet issuing into a parallel uniform free stream the general flow pattern is indicated in Figure 1.

As noted in the figure there exists an *initial region* of the jet flow field, within which the jet velocity profiles are not fully developed. If the exit velocity is assumed to be uniform, it can be seen that within a portion of the initial region the jet velocity is equal to the jet velocity at the exit. This wedge-shaped region is referred to as the *potential core*. The outer boundaries of the initial region are represented by the locus of points at which the jet velocity approaches the free stream velocity. That portion of the initial region between the potential core and the outer boundaries is the *mixing layer*.

Downstream of the initial region the mixing layers merge to form the *transitional region*. Within this relatively small region the rate of spread of the jet increases nonlinearly. The velocity profiles resemble those of a fully developed turbulent jet, but these profiles are not truly similar. In many analyses, because of its relatively small size, and due to a lack of understanding as to its true nature, the transitional region is neglected.

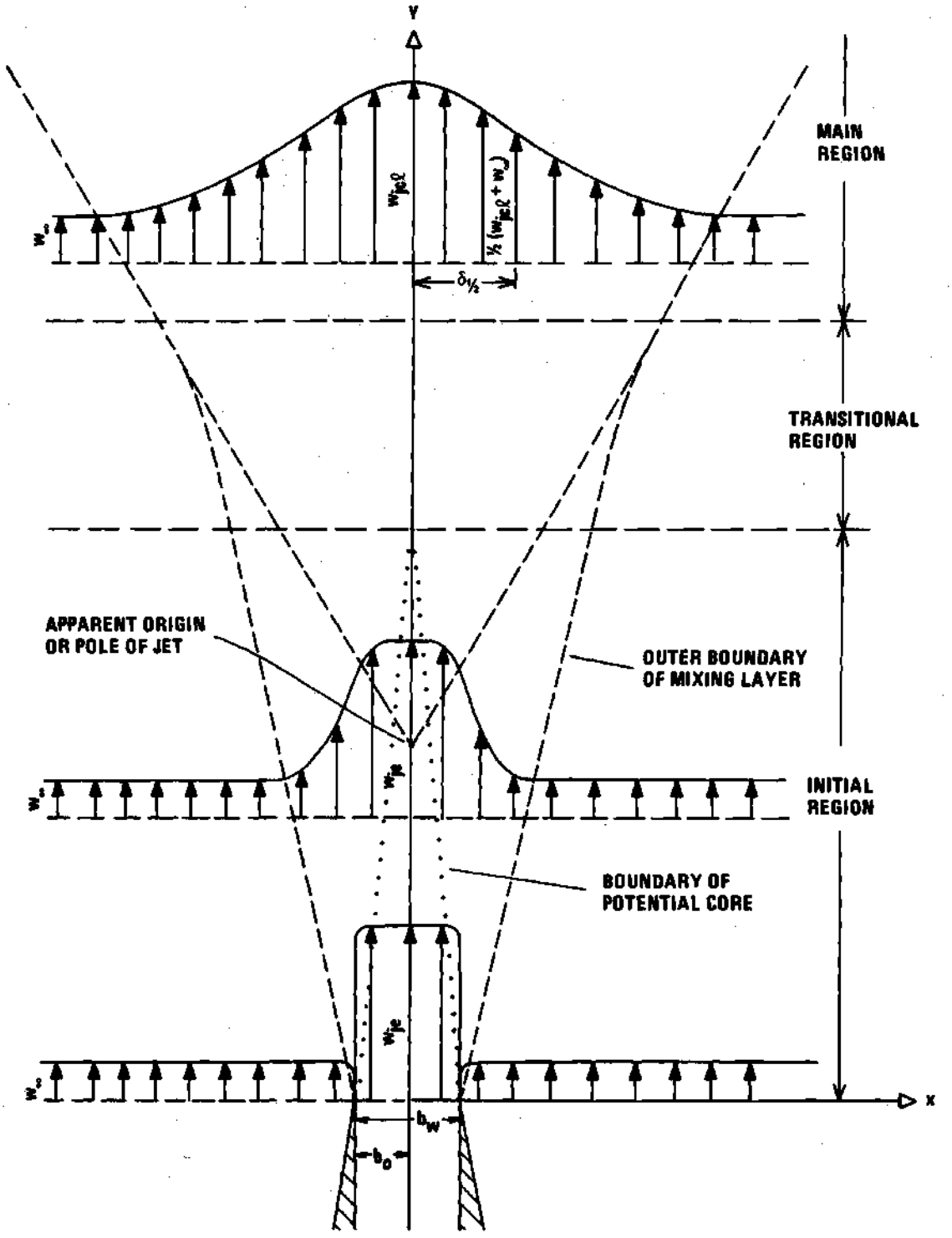

Figure 1. General Characteristics of a Plane Turbulent Jet

The *main* or *primary region* of the jet occurs downstream of the transitional region. The velocity profiles within this portion of the flow field are characteristic of fully developed turbulent flow and are similar. Notice should be taken that the rate of spread of the jet in the main region is linear and also greater than the corresponding rate in the initial region. If the outer boundaries of the main region are extrapolated upstream, their intersection with the plane of symmetry of the jet is designated as the *apparent origin* or *pole* of the jet. The main region extends downstream until the jet centerline velocity is essentially equal to the free stream velocity.

Within the main region of the jet the two parameters which are of primary interest are the jet centerline velocity $\hat{w}_{jc\ell}$ which generally decreases with distance downstream, and the jet half-width $\hat{\delta}_{1/2}$. The latter parameter is defined as the transverse distance from the jet centerline to that point where the velocity component parallel to the jet axis equals the arithmetic mean of the jet centerline velocity and the free-stream velocity.

Two-Dimensional Deflected Turbulent Jet

For the case of the two-dimensional deflected turbulent jet the general flow pattern is presented in Figure 2. The jet emerges from the slot in the flat plate and encounters the turbulent boundary layer generated by the uniform free stream flowing over the flat plate. The initial angle between the jet and the free stream is the inclination angle α_o. As the jet penetrates the boundary layer the former is deflected downstream. If the jet is sufficiently strong it may pass completely

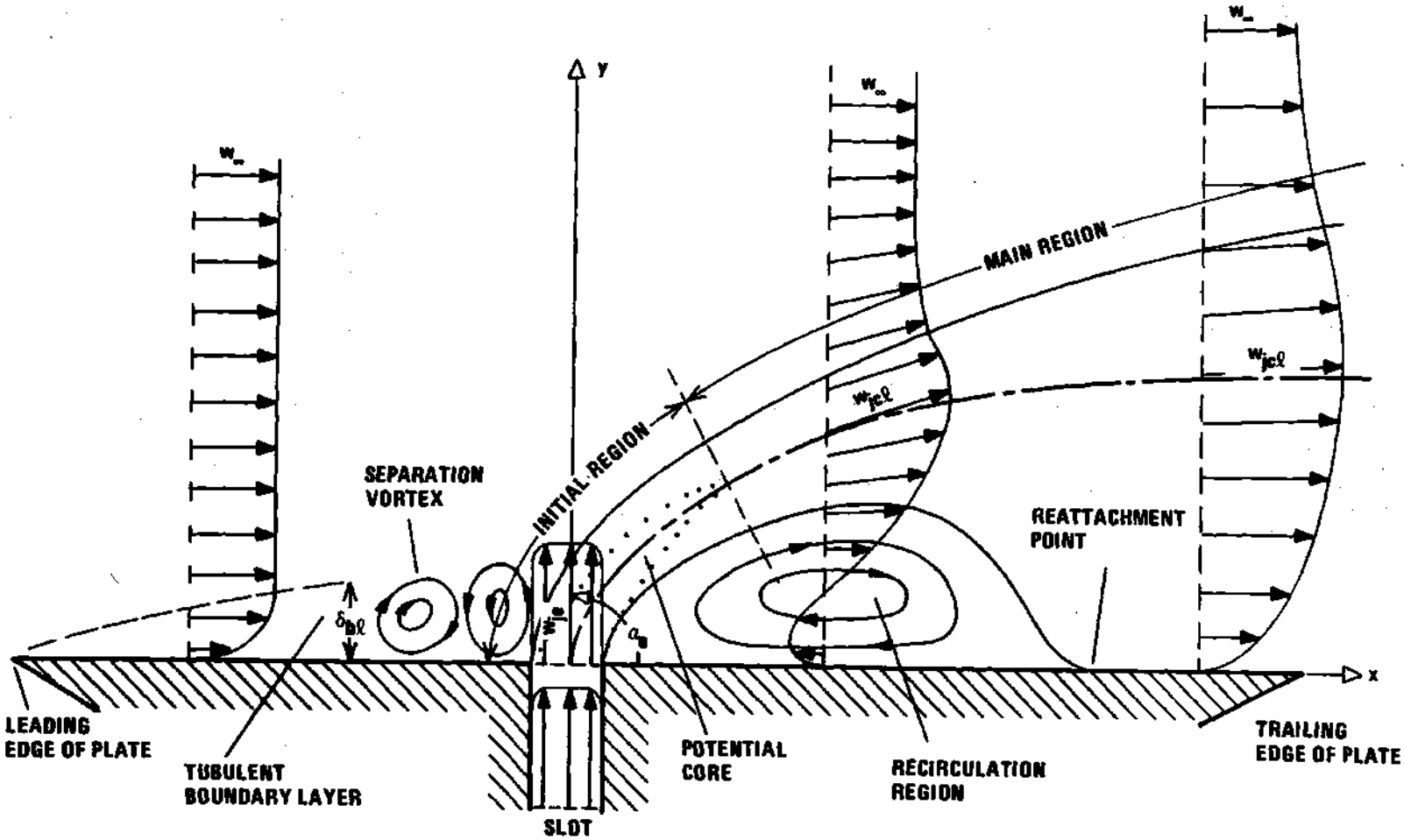

Figure 2. General Flow Pattern of Two-Dimensional Deflected Turbulent Jet

through the boundary layer and arch out into the free stream. The deflected jet resembles in many ways the plane jet already discussed. The potential core is again present and an initial region can be identified. The jet exit velocity profile, however, may not be uniform or symmetrical due to the transverse pressure gradient across the slot exit. In addition, the outer boundaries of the jet are difficult to define, and the question of similarity of the fully developed turbulent velocity profiles is not readily answered. Due to uncertainty regarding both spreading rate and the similarity of the velocity profiles, no distinction between the transitional and main regions can be easily established. It is important to note that the jet centerline or axis coincides with the locus of points of maximum velocity.

In some cases the adverse pressure gradient produced by the jet interacting with the free stream causes the boundary layer to separate from the plate before the jet is encountered. In this situation, two vortices rotating in opposite directions may possibly form immediately upstream of the jet.

Downstream, as a result of the induced flow produced by the jet, a recirculation region forms. Within this region the pressure is somewhat lower than the free stream value. The outer boundary to this recirculation region is represented by the streamline originating at the downstream lip of the slot. This streamline initially proceeds outward, away from the plate, but subsequently curves back and reattaches to the plate at some distance downstream. The behavior of this stagnation streamline represents the well-known Coanda effect.

The jet centerline velocity is constantly deflected in the direction of the free stream. At some distance downstream the centerline velocity direction coincides with that of the free stream. At this point the flow pattern resembles that of a wall jet in a moving stream. Further downstream (if the trailing edge of the plate is not encountered) the jet centerline velocity is reduced to the point where it is indistinguishable from the free stream velocity. At this point the flow essentially becomes a simple turbulent boundary layer.

The preceding description provides an overall picture of the nature of the problem. Such a picture proves useful both in surveying the literature for related studies as well as in developing an analytical model to provide a quantitative solution.

CHAPTER II

PREVIOUS RELATED STUDIES

The pertinent literature for the problem under consideration can be divided into three major parts as follows:

1. Deflected jets.
2. Turbulent flow characteristics.
3. Computational fluid dynamics.

The three subsequent major subdivisions deal with these subjects. All symbols, unless otherwise noted, are consistent with the Nomenclature.

Deflected Jets

There exists a sizeable amount of literature concerned with the problem of deflected jets. An excellent summary of much of this literature is found in a report by Spring, Street, and Amick [2]. Examination of this summary report reveals that much of the experimental work which has been carried out has involved circular or three-dimensional deflected jets. This is to be expected for two reasons: First, the task of experimentally producing a true two-dimensional deflected jet is considerably more difficult than that of producing the circular or three-dimensional case; second, in many practical applications, the latter type is actually involved. Although circular or three-dimensional deflected jets are of considerable importance, in order to limit the scope of the current survey, only studies involving the

two-dimensional case are discussed. Furthermore, those two-dimensional cases which involve a supersonic free stream and/or a supersonic jet exit velocity are beyond the scope of the current problem and therefore no attempt is made to cover them.

With the restricted noted, the number of references is reduced to approximately 15. In studying this literature there are two specific objectives to keep in mind. First, with regard to analytical studies, care must be taken to benefit from past experience while not duplicating past work. The second objective is concerned with obtaining and evaluating experimental data from earlier studies. These data must be of such a nature and in such a form as to provide a basis for comparison with predictions of the analytical model to be developed.

One of the first serious analytical studies of deflected jets, both plane and round, was conducted by Davis [3], with regard to the use of such jets to improve furnace combustion (overfire jets). Davis performed a simplified dynamic analysis of the jet trajectory based on the assumption that the deflected jet velocity was the resultant of the velocity of the corresponding straight jet and the velocity of the deflecting free stream. The resulting equation for the centerline of a plane deflected jet was

$$\hat{x}_{jc\ell} = \frac{\hat{w}_\infty \hat{y}_{jc\ell}(\hat{y}_{jc\ell}+4\hat{b}_w \sin\alpha_o)}{7.72\hat{b}_w \hat{w}_{je} \sin^2\alpha_o}\left(\frac{\hat{T}_{je}}{\hat{T}_\infty}\right)^{1/3} + \hat{y}_{jc\ell}\cot\alpha_o \qquad \text{(II-1)}$$

where $\hat{x}$ = distance downstream along plate *from the jet exit.*

For the case of an initial inclination angle α_o of 90°, Equation (II-1) reduces to

$$\hat{x}_{jc\ell} = \frac{\hat{w}_\infty \hat{y}_{jc\ell}(\hat{y}_{jc\ell}+4\hat{b}w)}{7.72\hat{b}_w \hat{w}_{je}} \left(\frac{\hat{T}_{je}}{\hat{T}_\infty}\right)^{1/3} \qquad (\alpha_o=90°) \qquad \text{(II-2)}$$

Both of the preceding equations can be seen to represent parabolas. Davis compared his calculated jet trajectories with observed flame contours produced by overfire jets, as reported by Robey and Harlow [4]. The comparison indicated general agreement between the calculations and observations.

Ivanov [5] presented experimental data from five tests involving low subsonic deflected jets. The slot breadth-to-width ratio $\hat{h}_w/\hat{b}_w$ ranged from 5 to 22.25. The ratio of jet exit velocity $\hat{w}_{je}$ to free-stream velocity $\hat{w}_\infty$ ranged from 5 to 20. At the jet exit plane the jet axis was normal to the direction of flow of the free stream. The data consisted of velocity measurements along the jet centerline along with the Cartesian coordinates of the centerline. Based on dimensional analysis Ivanov developed the following relation for the jet centerline:

$$\frac{a\hat{x}_{jc\ell}}{\hat{b}_o} = 1.9 \frac{\hat{\rho}_\infty \hat{w}_\infty^2}{\hat{\rho}_{je}\hat{w}_{je}^2} \left(\frac{a\hat{y}_{jc\ell}}{\hat{b}_o}\right)^{2.5} \qquad \text{(II-3)}$$

where

a = structure coefficient of the jet (ranging from .08 to .12).

$\hat{x}$ = distance downstream along the plate *from the jet exit.*

This equation is identical with that for a parabola if the exponent is reduced from 2.5 to 2.

Lowry and Turner [6] conducted a wind tunnel investigation involving a deflected jet on a 35° swept wing. The jet exit Mach number (=0.3) was equal to that of the free stream. The ratio of slot breadth-to-width ranged from 70 to 300. The inclination angle α_o was 120°. Jet stagnation pressure $\hat{p}_{jo}$ was equal to free-stream stagnation pressure $\hat{p}_{\infty o}$. The only experimental data reported were the rolling-moment coefficients as a function of angle-of-attack of the wing. The general conclusion was reached that a jet with stagnation pressure equal to free stream stagnation pressure could be used in an emergency as a control device in place of a higher pressure jet alone, or a jet and spoiler combination.

Taylor [7] presented an analytical model in which the free stream was represented by potential flow over an obstacle. The jet, which was initially at right angles to the free stream, was assumed to possess a constant momentum flow rate at any cross section normal to the curved jet axis, with a transverse pressure gradient produced by centrifugal force. The pressure immediately downstream of the jet was assumed to be constant and equal to the ambient pressure. The shape of the jet centerline was determined by matching the pressure in the jet, produced by centrifugal force, to the pressure distribution produced by the free stream flowing over the surface of a blunt body. The closest force balance was obtained when the body shape was described in cylindrical coordinates by the relation

$$\left(\frac{\hat{R}_{jc\ell}}{\hat{R}_{jc\ell o}}\right)^{1-n} = \frac{\sin(n\phi_{jc\ell})}{n(\sin\phi_{jc\ell})} \qquad \text{(II-4)}$$

where

n = 0.43.

$\hat{R}_{jc\ell}$ = radial position of jet centerline.

$\phi_{jc\ell}$ = angular position of jet centerline measured from the upwind direction.

$\hat{R}_{jc\ell o}$ = radial position of jet centerline for ϕ=0.

The value of $\hat{R}_{jc\ell o}$ was related to the flow velocities according to the relation*

$$\hat{R}_{jc\ell o} = \frac{2\hat{w}_{je}^2 \hat{b}_w}{\hat{w}_\infty^2}\left(\frac{2-n}{3}\right) \qquad \text{(II-5)}$$

Taylor noted that the body shape represented by Equation (II-4) closely resembled a parabola which, in the same coordinate system, is described by the relation

$$\left(\frac{\hat{R}_{jc\ell}}{\hat{R}_{jc\ell o}}\right)^{0.5} = \frac{\sin(0.5\phi_{jc\ell})}{0.5\sin\phi_{jc\ell}} \qquad \text{(II-6)}$$

In a later work [8], Ivanov presented (along with the five test cases already discussed) experimental data for 13 additional test cases.

---

*In Reference 7, the factor of 2 appears to have been omitted from the expression for $\hat{R}_{jc\ell o}$.

The ranges of the test variables were essentially the same as before, with the exception that two new variables were introduced. These two variables were the initial inclination angle of the jet to the free stream α_o and the ratio of jet exit temperature to free stream temperature ($\hat{T}_{je}/\hat{T}_\infty$). Tests were run for α_o values of 90° and 120°, and temperature ratios of 1.0 and 2.0. The data consisted of the same type of measurements as before. For the jet centerline Ivanov recommended the empirical equation,

$$\frac{\hat{ax}_{jc\ell}}{\hat{b}_o} = 1.9\,\frac{\hat{\rho}_\infty \hat{w}_\infty^2}{\hat{\rho}_{je}\hat{w}_{je}^2}\left(\frac{\hat{ay}_{jc\ell}}{\hat{b}_o}\right)^{2.5} - \left(\frac{\hat{ay}_{jc\ell}}{\hat{b}_o}\right)\tan(\alpha_o - 90°) \qquad \text{(II-7)}$$

Equation (II-7) reduces to Equation (II-3) for α_o=90°. For the problem under consideration, Ivanov's data appear to be the best available with regard to jet centerline location and jet centerline velocity variation.

Jet flap aerodynamics was the subject of a study by Williams, Butler, and Wood [9]. The study included the analysis of experimental data previously collected [10,11,12]. The behavior of jet flaps was described in terms of lift, stalling behavior, pitching moments, downwash, sideslip derivatives and ground effects. Most of the experimental results were presented in terms of coefficients of lift, drag, pitching moment, thrust, and flow rate, as well as derivatives of these coefficients. The jet exit velocity was subsonic and the free stream Reynolds number ranged from 5×10^4 to 8×10^5. A complete description of all test variables was not given. Notice was taken that the lift generated by

the jet was several times greater than the corresponding vertical component of the jet momentum flow rate.

Heyser and Maurer [13] carried out an experimental study involving a comparison between solid and jet spoilers. The jets were oriented at right angles to the free stream. Sonic velocity was obtained at the jet exit while the free stream Mach number ranged from .86 to 2.84. The slot breadth-to-width ratios were 48 and 144. Pressure measurements were taken along the flat plate through which the jet issued. Several Schlierien photographs were taken to obtain an overall view of the flow pattern. The pressure distribution produced by the deflected jet resembled that produced by a solid spoiler with a high pressure region just upstream of the jet and a low pressure region immediately downstream of the jet. This pressure data appears to be the best available for a two-dimensional deflected jet.

Abramovich [14] developed an analytical model in which the jet was treated as a solid aerodynamic shape with a normal force coefficient c_n. The jet centerline was determined by a force balance between the aerodynamic drag and the centrifugal force produced by the curvature of the jet. For the case of the jet oriented at an initial inclination angle α_o the resulting expression was*

$$\hat{y}_{jc\ell} = \frac{2\hat{b}_w\hat{\rho}_{je}\hat{w}_{je}^2\sin\alpha_o}{c_n\hat{\rho}_\infty\hat{w}_\infty^2}\left(\sqrt{\frac{c_n\hat{\rho}_\infty\hat{w}_\infty^2\hat{x}_{jc\ell}}{\hat{b}_w\hat{\rho}_{je}\hat{w}_{je}^2\sin\alpha_o} + \cot^2\alpha_o} - \cot\alpha_o\right) \qquad \text{(II-8)}$$

*As originally presented in Reference 14, Equation (II-8) contained a typographical error in that $\sin\alpha_o$ was squared.

where $\hat{x}$ = distance downstream along the plate *from the jet exit.*

Abramovich indicated that values of C_n ranged from 1 to 3. For the case of the jet normal to the free stream, the equation for the centerline reduces to

$$\hat{x}_{jc\ell} = \frac{C_n \hat{\rho}_\infty \hat{w}_\infty^2}{4\hat{b}_w \hat{\rho}_{je} \hat{w}_{je}^2} \hat{y}_{jc\ell}^2 \quad (\alpha_o = 90°) \tag{II-9}$$

This relation is the equation for a parabola.

A potential flow analysis of the two-dimensional deflected jet was performed by Ting, Libby, and Ruger [15]. The technique was applicable to cases where only a small difference between the free stream and jet stagnation pressures occurred. A solution was obtained by perturbation theory whereby the potential flow solution corresponding to the case of equal stagnation pressures was corrected to account for the pressure difference. No results were presented and no comparison with experimental data was made.

Vizel and Mostinskii [16] carried out a simplified aerodynamic analysis of plane and circular deflected jets, relying heavily on the experimental data of Ivanov. Their approach was similar to that of Abramovich. The analytical model was based on the overall conservation of the x- and y-components of momentum, combined with the jet treated as an aerodynamic shape, characterized by a force coefficient C_∞ (equal to 5.0). For the jet axis the resulting expression was

$$\frac{\hat{x}_{jc\ell}}{\hat{b}_w} = \frac{1}{4}\frac{C_\infty \hat{\rho}_\infty \hat{w}_\infty^2}{\hat{\rho}_{je}\hat{w}_{je}^2 \sin\alpha_o}\left(\frac{\hat{y}_{jc\ell}}{\hat{b}_w}\right)^2 + \left(\frac{\hat{y}_{jc\ell}}{\hat{b}_w}\right)\cot\alpha_o \qquad \text{(II-10)}$$

where $\hat{x}$ = distance downstream along the plate from the jet exit.

For the case of α_o=90° the jet centerline relation becomes

$$\frac{\hat{x}_{jc\ell}}{\hat{b}_w} = \frac{1}{4}\frac{C_\infty \hat{\rho}_\infty \hat{w}_\infty^2}{\hat{\rho}_{je}\hat{w}_{je}^2}\left(\frac{\hat{y}_{jc\ell}}{\hat{b}_w}\right)^2 \quad (\alpha_o=90°) \qquad \text{(II-11)}$$

which is again the equation for a parabola. A comparison of Equations (II-9) and (II-11) reveals that they are identical except for the value of C_∞, defined by Vizel and Mostinskii, differing from that of C_n as defined by Abramovich. By means of Equation (II-11), Vizel and Mostinskii apparently achieved better agreement with Ivanov's data than could be achieved by means of the relation developed by Abramovich.

In an analytical study by Ackerberg and Pal [17] two approaches involving potential flow were described. The first approach was applicable to jets with the jet exit width much smaller than the radius of curvature of the jet axis. The jet width was assumed to remain essentially constant and the jet velocity was assumed to vary transversely in the form of a potential vortex. Downstream of the jet the pressure was assumed to be constant and equal to the ambient pressure. Upstream, by means of conformal mapping combined with force balancing, the upstream free streamline was obtained. By the first approach two

relations were derived for the case of the jet exhausting at right angles to the free stream. First, in the immediate vicinity of the jet exit

$$X_{jc\ell} \sim Y_{jc\ell}^2 + O(Y_{jc\ell}^4) \qquad \text{(II-12)}$$

where

$$X_{jc\ell} = \hat{x}_{jc\ell}/\hat{b}_w.$$

$$Y_{jc\ell} = \sqrt{\frac{\hat{\rho}_\infty \hat{w}_\infty^2}{\hat{\rho}_{je} \hat{w}_{je}^2}} \left(\frac{\hat{y}_{jc\ell}}{\hat{b}_w}\right)$$

$\hat{x}$ = distance downstream along the plate *from the jet exit.*

The second relation applied to regions at great distances from the jet exit and was of the form

$$X_{jc\ell} \sim \left(\frac{Y_{jc\ell}+\pi/2A_o^2}{2A_o}\right)^2 - \frac{1}{2} A_o \ell n \left(\frac{Y_{jc\ell}+\pi/2A_o^2}{2A_o}\right)^2 + A_1 \qquad \text{(II-13)}$$

where

$A_o = -0.797.$

$A_1 = 1.175$ (experimentally derived).

A variational approach developed by Pal represented the second method for solving the problem. This approach was mathematically quite involved and made use of the generalized Dirichlet integral, conformal mapping, and the Ritz-Galerkin method to obtain a variational integral.

The final outcome was a numerical solution which was presented in the form of a table.

Ackerberg and Pal compared their theoretical predictions with the earlier work of Taylor and with the experimental data of Ivanov as reported by Vizel and Mostinskii. In general the theoretical curves of the two authors displayed greater penetration than those of Taylor, which in turn represented greater penetration than measured by Ivanov.

Girshovich has presented two studies of the deflected jet. In the first of these [18], the primary region of the jet was considered. Curvilinear coordinates were employed with the governing equations for the jet reducing to the familiar boundary layer equations. The upstream and downstream boundary conditions were similar to those set forth by Taylor. Girshovich noted that the approach was applicable only to a certain range of values of α_0 but stated that this range must be established by experiment. Furthermore, the analytical model was observed to be inapplicable for cases involving extreme curvature. In the course of his analytical development Girshovich introduced several terms which are not clearly defined. In addition, his final relation for the velocity profile of the deflected jet contains terms which must be evaluated by the solution of addition equations, involving the centerline velocity and the jet half-thickness. A numerical solution involving some iteration appears necessary. To find the jet centerline the use of potential flow was proposed. A line source parallel to the direction of the free stream was to be superimposed on a uniform flow potential to produce the desired flow pattern. No comparison with experimental data

was presented by Girshovich nor were any numerical results or closed-form expressions provided for the calculation of the properties of the deflected jet.

In his second study [19], Girshovich concentrated on the flow in the initial region of the deflected jet. As before, curvilinear coordinates were employed, with the governing equations being reduced to the boundary layer equations. Unfortunately, as with the earlier paper, some difficulty is encountered in following Girshovich's work because of the introduction of undefined terms in his analytical development, coupled with the presence of several apparent typographical errors. Experimental data for velocity ratios ($\hat{w}_{je}/\hat{w}_{\infty}$) ranging from 3.52 to 9.81 were compared with analytical predictions with apparently satisfactory agreement. Due to the lack of a complete definition of the test conditions for his experiment, combined with his use of undefined terms in the plotted data, no meaningful comparison in the current study can be made with either the analytical or experimental results of Girshovich. One significant conclusion drawn by Girshovich was that his jet trajectories were not in complete agreement with experimental data because of his assumption that pressure downstream of the jet was equal to the free-stream pressure. He indicated that the actual pressure was somewhat lower than the ambient value due to the "rarefaction in the dead zone behind the jet," and suggested that the magnitude of the rarefaction should be determined by experiment.

Coxe [1] carried out an analytical and experimental investigation of a two-dimensional laminar incompressible deflected jet exhausting at

right angles to a laminar free stream flowing over a flat plate. Two cases were considered, one involving a second flat plate parallel to the first plate, producing a confined jet, and the other case without the second plate, thus producing an unconfined jet. His analytical model was based on the fundamental governing equations for conservation of mass and momentum. These equations were satisfied by the use of vorticity and stream functions. A transient finite-difference approach was used in obtaining a solution. No-slip boundary conditions at the surface of the flat plate were applied. For the jet exit condition three different velocity profiles were considered: (1) unrestricted, (2) slug flow, and (3) parabolic. For the unrestricted case no velocity profile was assumed. Instead, the profile was allowed to adjust itself for a given mass flow rate. Computational difficulties were encountered in this case and also in the case of a slug flow profile. The use of the parabolic profile produced the best results. For the upstream and downstream boundary conditions Coxe essentially assumed that all streamlines were parallel to the flat plate. Some computational difficulty was encountered along the downstream boundary.

The experimental data collected by Coxe consisted of photographs of smoke streamlines. Velocity ratios $\hat{w}_{je}/\hat{w}_{\infty}$ ranged from 0.471 to 1.49. The free-stream Reynolds numbers were quite low (to maintain laminar flow) with values from 715 to 1060. Likewise the jet exit Reynolds numbers were also low with values from 90 to 180. The experimental data was in reasonable agreement with the analytical predictions. Coxe concluded that the use of a parabola to represent the jet centerline

appeared to be a satisfactory first approximation. He recommended that a curvilinear coordinate system involving orthogonal families of either parabolas or hyperbolas be considered for use in further studies. He appeared to favor hyperbolas over parabolas. The recommendation was also made that a coordinate transformation be utilized to maximize the number of computational grid points in the immediate vicinity of the jet. As already noted the work by Coxe appears to be the first attempt at a rigorous solution to the two-dimensional deflected jet problem.

The analytical and experimental study by Endo [20] involved a jet located at the trailing edge of a flat plate, exhausting at inclination angles of 0°, 10°, and 30° into a free stream flowing over both sides of the plate. The free-stream velocity ranged from 40 ft/sec to 66 ft/sec, while the jet exit Reynolds number was held constant at 1.5×10^4. Such a Reynolds number represents a jet exit velocity of approximately 230 ft/sec. Endo measured the transverse velocity profiles for various distances downstream. He also measured the static pressure distribution and turbulent intensity at various points in the jet. The velocity profiles which he obtained appeared to possess similarity.

The analytical model developed by Endo was based on the conservation of mass and momentum, for an incompressible fluid, in curvilinear coordinates, ζ and η. The ζ-axis was positioned along the jet axis (the locus of the maximum jet velocity for a given distance downstream from the jet exit); the η-coordinate was oriented normal to the ζ-axis with positive values of η corresponding to the convex side of the jet and negative values to the concave side. The resulting differential

equations were similar to the boundary layer equations used by Girshovich except that certain terms involving radius of curvature of the jet were retained. Of special interest was the manner in which Endo treated the turbulent shear stress in the jet. A discussion of this point is included in the subsequent portion of this chapter, devoted to turbulent flow characteristics.

Based on the assumption of similarity Endo succeeded in integrating the differential equations to obtain the variation of the velocity component with respect to η. He presented the solution in the form of a nondimensional table similar to that used in laminar boundary layer analysis. A comparison by him between analytical prediction and experimental data indicated very satisfactory agreement. Notice should be taken however that this comparison was based in part upon an empirical relation derived by Bradbury [21] for a plane turbulent jet. Endo's general conclusion was that similarity does occur in the curved two-dimensional jet.

In summary, with regard to two-dimensional deflected jets there appear to be essentially three significant points. First, the various equations for the jet centerline, based both on theory and experiment, generally indicate that the shape of the centerline resembles a parabola. Second, the only available experimental data for jet centerline location and velocity measurements is that reported by Ivanov [5,8]. Finally, the experimental results of Heyser and Maurer [13] represent the only available data, concerned with the pressure distribution, characteristic of the class of deflected jets under consideration.

Turbulent Flow Characteristics

In describing turbulent transport processes there are two basic concepts, namely, *statistical* and *phenomenological*. The statistical concept is generally accepted to be the more fundamental, but due to a lack of understanding of the statistical functions describing turbulent motion, only limited success has been achieved with this method [22]. The phenomenological concept, on the other hand, has been used successfully in a number of different types of turbulent flow. Phenomenological theories can be divided into two categories: (1) deductive approaches, such as those proposed by Boussinesq [23], Prandtl [24], Taylor [25], and von Karman [26], involving the concepts of eddy viscosity and mixing length; and (2) inductive approaches as proposed by Reichardt [27], involving the use of the Gaussian error integral and related functions to represent the distribution of momentum flux and other properties in turbulent flow. The inductive approach, while useful in certain cases, does not appear compatible with the objective of the current study because a basic part of this objective is the solution of the fundamental governing equations. The deductive approach, with the concept of eddy viscosity, on the other hand, appears quite adaptable to the solution of such equations.

Based on the preceding discussion, certain restrictions in the scope of this portion of the literature survey appear in order. In general only studies which are concerned with deductive phenomenological theories are covered. Notice should be taken that the authors of some of the literature discussed are not in agreement with the concept of

eddy viscosity or mixing length. In many cases, however, experimental results as well as analytical models can be interpreted in terms of such parameters. In order to provide some organization to the discussion it is useful to assign classifications to various types of turbulent flow as follows:

1. Straight turbulent flow
    a. turbulent free jets
    b. turbulent boundary layers
    c. turbulent flow in ducts
2. Curved turbulent flow

Subsequent subdivisions of this portion of the literature survey are organized according to these classifications.

Straight Turbulent Flow

As the name implies, straight turbulent flow involves flow without appreciable curvature. Thus centrifugal forces are generally not present and this in turn reduces the likelihood of transverse pressure gradients. Examples of straight turbulent flow include turbulent free jets, turbulent boundary layers on flat plates, turbulent flow in ducts, turbulent wall jets on flat plates, and turbulent wakes. The first three of these types of flow are especially pertinent to the problem under consideration.

Turbulent Free Jets. Albertson, Dai, Jensen, and Rouse [28] carried out a study, primarily experimental in nature, concerned with turbulent submerged (free) jets. Based on the experimental data for a two-dimensional jet, the centerline velocity $\hat{w}_{jcl}$ in the fully

established flow, was observed to vary with downstream position $\hat{y}$ according to the relation

$$\frac{\hat{w}_{jc\ell}}{\hat{w}_{je}}\sqrt{\frac{\hat{y}}{\hat{b}_w}} = 2.28 \qquad \text{(II-14)}$$

The transverse distribution of velocity was described by the equation

$$\log_{10}\left(\frac{\hat{w}_y}{\hat{w}_{je}}\sqrt{\frac{\hat{y}}{\hat{b}_w}}\right) = 0.36 - 1.84\left(\frac{\hat{x}}{\hat{y}}\right)^2 \qquad \text{(II-15)}$$

where

$\hat{x}$ = transverse distance measured from jet centerline (always positive).

Although no relation was given for the variation of eddy viscosity $(\hat{\epsilon}_m)_j$ with position, an analysis of the plotted curves indicates that such variation was of the form

$$(\hat{\epsilon}_m)_j = \hat{w}_{jc\ell}(0.006\hat{y}-0.01\hat{x}) \qquad \text{(II-16)}$$

Equation (II-16) indicates a linear decrease in eddy viscosity with transverse position. A combination of Equations (II-14) and (II-16) yields the relation that eddy viscosity increases according to the square root of the distance downstream.

Reichardt [27] presented some of the earliest experimental data on two-dimensional turbulent jets. He measured both temperature and

velocity profiles and also the spreading rate of the jet. According to his experimental data the jet velocity profiles were exponential in form. This experimental observation regarding the variation of the jet velocity with transverse position proved to be quite significant in the development and application of his inductive theory of turbulence. Reichardt also observed that the turbulent Prandtl number (the ratio of eddy viscosity, $\hat{\epsilon}_m$, to the eddy thermal diffusivity, $\hat{\epsilon}_h$) was equal to 0.57 for plane turbulent jets.

Hinze [22] presented a discussion of nonisotropic free turbulence, characteristic of free jets and wakes. His discussion of jets was limited to round free jets and thus is not especially pertinent to the current study. It is of interest to note, however, that as reported by Hinze the eddy viscosity varies only slightly with radial position in the round jet.

Schlichting [29], based on the earlier analysis by Goertler [30], and the experimental work by Reichardt, for a plane free jet exhausting into a stationary medium, presented the following expression for the eddy viscosity:

$$(\hat{\epsilon}_m)_j = 0.037\hat{\delta}_{1/2}\hat{w}_{jc\ell} \qquad \text{(II-17)}$$

The author indicated that the assumption of eddy viscosity remaining constant over the width of the jet was in good agreement with experiment. He also demonstrated by an order-of-magnitude approximation that

$$\hat{w}_{jc\ell} \propto \hat{y}^{-1/2} \tag{II-18}$$

$$\hat{\delta}_{1/2} \propto \hat{y} \tag{II-19}$$

Abramovich [14] presented an extensive discussion of the general problem of plane turbulent gas jets. His primary approach was semi-empirical in nature and relied heavily on experimental data. Only limited attention was given to turbulent transport phenomena, but a number of useful relations and charts were developed for the calculation of various jet characteristics, including the length of the potential core of the jet, the variation of the jet centerline velocity with distance downstream, and the jet thickness as a function of distance downstream.

Bradbury [21] carried out a combined analytical and experimental study of turbulent plane jets exhausting into a slow-moving parallel airstream. The transverse variation of turbulent shear stress, eddy viscosity, intensity, and intermittency were plotted based on experimental data along with plots of velocity profiles, jet width variation with distance downstream, and jet centerline velocity decay. For the latter, based on experimental data the following relation was proposed:

$$\left(\frac{\hat{w}_{jc\ell}}{\hat{w}_{je}}\right)^2 = 0.00575(\hat{y}-\hat{y}_o)/\hat{b}_w \tag{II-20}$$

where $\hat{y}_o$ = location of "apparent origin" of fully-developed turbulent flow.

For the growth of the jet thickness Bradbury gave the relation

$$\frac{\hat{\delta}_{1/2}}{\hat{b}_w} = \frac{0.123(\hat{y}/\hat{b}_w - \hat{y}_o/\hat{b}_w)}{1 + 0.0755(\hat{y}/\hat{b}_w - \hat{y}_o/\hat{b}_w)^{1/2}} \qquad \text{(II-21)}$$

The observation that the measured eddy viscosity, corrected by the intermittency factor, was roughly constant in the transverse plane, was also made by Bradbury.

Zakkay and Krause [31] carried out an experimental study involving high-speed, compressible coaxial jets with the objective of determining the radial variation of eddy viscosity. For both subsonic and supersonic flow conditions hydrogen, argon, and xenon were exhausted by the inner jet with air exhausted by the outer jet. One of the conclusions which was reached was that for cases involving gases with nearly the same molecular weight, only small radial variations of eddy viscosity occurred.

Korst and Chow [32] developed a procedure for calculating the eddy viscosity in compressible flow involving the mixing of two streams. The fundamental equation was

$$(\hat{\epsilon}_m)_j = \frac{\hat{y}}{2\sigma_{II}^2}(\hat{w}_a + \hat{w}_b) \qquad \text{(II-22)}$$

where

$\hat{w}_a$ = velocity of stream "a."

$\hat{w}_b$ = velocity of stream "b."

σ_{II} = spreading coefficient for two streams.

Calculation of σ_{II} was semi-empirical in nature and involved the influence of the ambient temperatures, the stagnation temperature, the Crocco numbers ($\hat{w}/\sqrt{2\hat{c}_p\hat{T}_o}$) and the velocity ratio ($\hat{w}_a/\hat{w}_b$) for the two streams.

In an extension of Bradbury's earlier work, Bradbury and Riley [33] carried out an experimental study of a plane turbulent jet exhausting into a parallel free stream with the latter possessing appreciable velocity. Experimental data of the same type as that in Reference 21 was presented. The data of Bradbury and Riley indicate that the eddy Reynolds number $(N_{Re})_t = (\hat{w}_{jc\ell}-\hat{w}_\infty)\hat{\delta}_{1/2}/(\hat{\epsilon}_m)_j$ in such a flow varies from an upstream value of the same magnitude (~33.4) encountered with a plane jet exhausting into a stationary medium, to a downstream value (~19.4) characteristic of self-preserving wake flow. The experimental results were generalized in the form of a table which provided the variation of the eddy Reynolds number with distance downstream $(\hat{y}-\hat{y}_o)$. For nondimensionalization of this distance the concept of the momentum thickness of the jet, $\hat{\theta}_j$ was introduced as follows:

$$\hat{\theta}_j = \frac{\hat{\rho}\int_{-\infty}^{\infty}\hat{w}_j(\hat{w}_j-\hat{w}_\infty)d\hat{x}}{\hat{\rho}\hat{w}_\infty^2} \qquad \text{(II-23)}$$

As before in Bradbury's work the distance $\hat{y}_o$ represents the shift in the effective origin of the jet. The authors indicated that this shift was too large to ignore. Unfortunately they did not provide a means for predicting this quantity.

Tomich and Weger [34] conducted a combined analytical and experimental study involving turbulent compressible axisymmetric jets. They proposed the following relation for eddy viscosity:

$$(\hat{\epsilon}_m)_j = \frac{\hat{\rho}_{c\ell}}{\hat{\rho}} (0.00972-0.00751N_{Ma}+0.00298N_{Ma}^2)\left(\frac{\hat{\rho}_\infty}{\hat{\rho}_{je}}\right)^{1/2} \hat{w}_{je}\hat{D}f \qquad \text{(II-24)}$$

where

$$f = \begin{cases} 0.2 & (\hat{y}/\hat{D} \le 4.73\sqrt{\hat{\rho}_{je}/\hat{\rho}_\infty}) \\ 1.0 & (\hat{y}/\hat{D} > 4.73\sqrt{\hat{\rho}_{je}/\hat{\rho}_\infty}) \end{cases}$$

The governing equations developed by Tomich and Weger were the boundary layer equations for conservation of mass, momentum and energy. Their numerical solution appeared to be in reasonable agreement with their experimental data.

Bauer [35] in an analytical study of a supersonic axisymmetric multispecies turbulent jet, assumed no radial variation of eddy viscosity. For the axial variation he used the relation

$$(\hat{\epsilon}_m)_j = \frac{\hat{y}}{4\sigma^2} (\hat{w}_{max}+\hat{w}_{min}) \qquad \text{(II-25)}$$

where

σ = spreading coefficient (=15.3).

$\hat{w}_{max}$ = maximum velocity at a given axial position.

$\hat{w}_{min}$ = minimum velocity at a given axial position.

Bauer assumed a turbulent Prandtl number equal to 0.92. In relating turbulent stresses to velocity gradients in cylindrical coordinates, he used the following expressions:

$$-\overline{(\hat{\rho}\hat{w}_y)'\hat{w}_r'} = \begin{cases} \bar{\rho}(\hat{\epsilon}_m)_j \dfrac{\partial \bar{\hat{w}}_y}{\partial \hat{r}} & \text{(II-26a)} \\ \bar{\rho}(\hat{\epsilon}_m)_j \dfrac{\partial \bar{\hat{w}}_r}{\partial \hat{y}} & \text{(II-26b)} \end{cases}$$

$$-\overline{(\hat{\rho}\hat{w}_r)'\hat{w}_y'} = \begin{cases} \bar{\rho}(\hat{\epsilon}_m)_j \dfrac{\partial \bar{\hat{w}}_r}{\partial \hat{y}} & \text{(II-27a)} \\ \bar{\rho}(\hat{\epsilon}_m)_j \dfrac{\partial \bar{\hat{w}}_r}{\partial \hat{r}} & \text{(II-27b)} \end{cases}$$

$$-\overline{(\hat{\rho}\hat{w}_y)'\hat{w}_y'} = \bar{\rho}(\hat{\epsilon}_m)_j \frac{\partial \bar{\hat{w}}_y}{\partial \hat{y}} \qquad \text{(II-28)}$$

$$-\overline{(\hat{\rho}\hat{w}_r)'\hat{w}_r'} = \bar{\rho}(\hat{\epsilon}_m)_j \frac{\partial \bar{\hat{w}}_r}{\partial \hat{r}} \qquad \text{(II-29)}$$

Special notice should be taken that two different expressions for turbulent shear stresses were utilized by Bauer as indicated by the form of Equations (II-26) and (II-27). Furthermore, none of these relations is analogous in form to its laminar stress-strain counterpart. The best agreement between his numerical predictions and previous experimental data was achieved using Equations (II-26a) and (II-27a), but Bauer concluded that his shear stress relation contained simplifications which limited the accuracy of his results.

Turbulent Boundary Layers. There exists a great mass of literature devoted to turbulent boundary layers. Fundamental references

include the works of Schlichting [28], and Pai [36]. One of the first analytical studies of turbulent boundary layers involving compressible fluids was carried out by Van Driest [37]. In developing the time-averaged equations for compressible turbulent flow, the instantaneous values of certain products such as $\hat{\rho}\hat{w}_x$ were expressed in the form

$$\hat{\rho}\hat{w}_x = \overline{(\hat{\rho}\hat{w}_x)} + (\hat{\rho}\hat{w}_x)' \tag{II-30}$$

In introducing the turbulent shear stresses, Van Driest assumed the following type of relations:

$$\overline{(\hat{\rho}\hat{w}_x)'w_y'} = \bar{\rho}(\hat{\epsilon}_m)_{b\ell} \frac{\partial \bar{\hat{w}}_x}{\partial \hat{y}} \tag{II-31}$$

Triple correlations of the form $\overline{\rho' w_x' w_y'}$ were neglected. For mixing length the assumption of a linear variation with distance from the wall was made. The turbulent Prandtl number was taken as unity. Based on this approach Van Driest developed a set of turbulent, compressible, boundary layer equations. From these equations he derived analytical expressions for the velocity and temperature profiles and the turbulent shear stress at the wall.

An analytical study conducted by Kleinstein [38] was concerned with turbulent incompressible boundary layers. Primary attention was directed toward that portion of the boundary layer near the wall. By imposing the condition that the eddy viscosity must vary continuously and smoothly in this region, and by taking the velocity as the

independent variable, Kleinstein developed an eddy viscosity model which yielded an integrable closed-form expression for the velocity distribution.

Maise and McDonald [39] carried out an analytical study involving the mixing length and eddy viscosity in turbulent compressible boundary layers. Based on the analysis of earlier experimental data they concluded that the effects of compressibility on mixing length were small. Compressibility appeared to have a greater influence on the eddy viscosity, especially in the outer region of the boundary layer. In general, the authors observed that the eddy viscosity decreased with increasing Mach number.

A general discussion of turbulent boundary layers was presented by Bradshaw [39]. He discussed the generation of shear stresses in turbulent flow, the inner region of the turbulent boundary layer, the outer region, and calculation methods. In general Bradshaw did not favor the concepts of mixing length and eddy viscosity in calculating turbulent stresses. Instead he proposed use of the turbulent energy equation for this purpose. He indicated that compressibility should not greatly affect turbulence for cases involving velocities less than hypersonic.

An extensive analytical study of turbulent boundary layers was reported by Cebeci, Smith, and Wang [40]. Two models for calculation of eddy viscosity were used. In the inner region the expression for eddy viscosity was

$$(\hat{\epsilon}_m)_{b\ell i} = .16\hat{y}^2\left\{1 - \exp\left[-\frac{y}{26}\left(\frac{\bar{\hat{\sigma}}_w}{\bar{\rho}} + \frac{d\bar{\beta}}{d\hat{x}}\frac{\hat{y}}{\bar{\beta}}\right)^{1/2}\right]\right\}^2 \left|\frac{d\bar{\hat{w}}_x}{d\hat{y}}\right| \qquad \text{(II-32)}$$

In the outer region,

$$(\hat{\epsilon}_m)_{b\ell o} = .0168\hat{w}_\infty\hat{\delta}^*_{b\ell}[1.0+5.5(\hat{y}/\hat{\delta}_b)^6]^{-1} \qquad \text{(II-33)}$$

The authors indicated that the boundary between the two regions was determined by the point at which $(\hat{\epsilon}_m)_{b\ell i} = (\hat{\epsilon}_m)_{b\ell o}$. The turbulent Prandtl number was taken to be .9.

Turbulent Flow in Ducts. Turbulent flow through various shaped conduits has been the subject of considerable investigation. Hinze [22], Schlichting [29], Pai [36], and Knudsen and Katz [42] provide excellent summaries of studies of such flow. In general all of these authorities agree that parallel turbulent flow between two plates is quite similar to turbulent flow through a circular pipe, and thus relationships derived or observed for one case should prove applicable to the other. Thus this segment of the literature survey is primarily concerned with turbulent flow in circular pipes and between flat plates.

Based on the experimental data of Nikuradse [43], for the mixing length in smooth circular pipes with Reynolds numbers above 10^5, Schlichting proposed the relation

$$\frac{\hat{\ell}}{\hat{R}_p} = 0.14 - 0.08\left(1 - \frac{\hat{x}}{\hat{R}_p}\right)^2 - 0.06\left(1 - \frac{\hat{x}}{\hat{R}_p}\right)^4 \qquad \text{(II-34)}$$

where

$\hat{R}_p$ = radius of the pipe.

$\hat{x}$ = distance from the wall.

Notice should be taken that Equation (II-34), when taken in conjunction with the conventional definition of eddy viscosity, produces zero values for the latter along the pipe centerline. This result conflicts with the experimental data of Laufer [44] for turbulent pipe flow. In the inner turbulent core Laufer's data indicated that the eddy viscosity was non-zero and essentially constant with respect to radial position. Page, Schlinger, Breux and Sage [45] obtained similar results for flow between parallel plates. This conflict does not appear too serious because along the centerline of a pipe, as expected, Laufer's data indicated that the turbulent shear stress is zero.

Hinze, based on the assumption of a linear distribution of turbulent shear stress outside the wall region for the eddy viscosity developed the relation

$$(\hat{\epsilon}_m)_s = \frac{\bar{\hat{\sigma}}_w \hat{D}}{2\bar{\hat{\rho}}} (1-\xi) / \left(\frac{d\bar{\hat{w}}_y}{d\xi}\right) \qquad \text{(II-35)}$$

where

$\bar{\hat{\sigma}}_w$ = shear stress at the wall.

ξ $2\hat{x}/\hat{D}$

$\hat{x}$ = distance from the wall.

With regard to the turbulent Prandtl number, Hinze reported values ranging from 0.65 to 0.72.

The turbulent velocity profiles for flow between parallel plates was the subject of a second study by Laufer [46]. Based on an analysis of the resulting experimental data, Pai [47] derived the following expression for the velocity distribution:

$$\frac{\bar{\hat{w}}_y}{(\hat{w}_y)_{max}} = 1.0 - .3293(1-2\hat{x}/\hat{D})^2 - .6707(1-2\hat{x}/\hat{D})^{32} \qquad \text{(II-36)}$$

where $\hat{x}$ = distance from the wall.

It should be noted, however, that the coefficients and exponents of the second and third terms on the right side of Equation (II-36) are actually functions of the Reynolds number, and the values given correspond to a Reynolds number of 13,500.

In an effort to relate wall shear stress to friction factors, Knudsen and Katz pointed out that the Fanning friction factor f is related to the wall shear stress as follows:

$$f = \frac{2\bar{\sigma}_w}{\bar{\rho}(\hat{w}_y)^2_{mean}} \qquad \text{(II-37)}$$

where

$$(\hat{w}_y)_{mean} = \int_0^{\hat{b}_w} \bar{w}_y d\hat{x}/\hat{b}_w$$

Furthermore the authors provided numerical results which indicated that the friction factor for flow between plates can be calculated by the following semi-empirical relation derived by Drew, Koo, and McAdams [48]:

$$f = 0.00140 + 0.125(N_{Re})_b^{-0.32} \qquad \text{(II-38)}$$

where

$$(N_{Re})_b = \frac{2\hat{b}_w(\hat{w}_y)_{mean}\bar{\hat{\rho}}}{\hat{\mu}}$$

Also of interest were the values of turbulent Prandtl numbers, reported by Knudsen and Katz, ranging from 0.6 to 1.0.

Curved Turbulent Flow

The effect of curvature on turbulent flow has been the subject of a limited number of studies. Eskinazi and Yeh [49] in a study of turbulent flow in a curved channel, noted that turbulent intensity and turbulent shear stresses were greater in the vicinity of the outer (concave) wall of the channel than in the vicinity of the inner (convex) wall. Their analysis indicated that the turbulent shear stress was positive near the inner wall and this suppressed the production of turbulent energy. Near the outer wall the same stress was negative, which increased the production of turbulent energy. The authors noted that this was analogous to the stability criterion for revolving fluids as set forth by Rayleigh [50]. In effect this stability criterion indicated that, for any revolving fluid (compressible or incompressible) in the absence of viscosity, a stable flow can exist only when the circulation or angular momentum increases with radial position.

The behavior of turbulent wall jets on curved surfaces was the one of the subjects of an experimental study by Bradshaw and Gee [51]. The observation was made that in the outer mixing layer of the wall jet

the growth rate of the jet thickness was approximately linear but roughly 50 per cent greater than the corresponding growth rate of a similar wall jet on a flat plate. One possible explanation for the increased mixing in the outer layer was the existence of a negative radial gradient of angular momentum, which was considered an unstable condition in accordance with Rayleigh's criterion.

Sawyer [52] presented an analysis of a two-dimensional reattaching turbulent jet with attention given to the effects of curvature on entrainment. The observation was made that, based on earlier experimental data by the author [53], a two-dimensional curved jet exhibited no obvious asymmetry. Furthermore the rate of spread of such a jet was essentially the same as that for a plane jet. Sawyer indicated that because of centrifugal forces the entrainment rate of the convex side of the jet should be larger than that on the concave side. Such a difference could occur without producing asymmetry in the velocity profiles *only because there was transverse flow across the jet axis* from the convex to the concave side. Of special significance was the first-order theory presented by Sawyer to predict the effects of curvature on the turbulent mixing process. In terms of eddy viscosity Sawyer's turbulent shear relation was

$$\bar{\tilde{\tau}}_{\eta\zeta} = \bar{\tilde{\rho}}(\hat{\epsilon}_m)_{jc\ell}\left(\frac{\partial\tilde{\bar{w}}_\zeta}{\partial\hat{\eta}} - C\,\frac{\bar{w}_\zeta}{\hat{R}_{jc\ell}}\right) \qquad \text{(II-39)}$$

where C = empirical constant.

Based on the analysis of the experimental data the value of C was found to be 5.29.

An investigation of a curved turbulent mixing layer was performed by Margolis and Lumley [54]. Their experimental data indicated that turbulence was suppressed near a convex wall (where the radial gradient of angular momentum is positive). Near a concave wall (where the same gradient is negative) turbulence was promoted.

An investigation by Guitton [55], which involved both experimental and analytical studies of turbulent wall jets over curved surfaces, produced results consistent with those already discussed. Based on experimental data the observation was made that a concave wall jet grew less rapidly than a plane wall jet. In the analytical model the turbulent shear stress was expressed as

$$\bar{\tau}_{\eta\zeta} = \bar{\rho}\hat{\epsilon}_m\left(\frac{\partial\bar{\hat{w}}_\zeta}{\partial\hat{\eta}} - \frac{\bar{\hat{w}}_\zeta}{\hat{R}_{jc\ell}+\hat{\eta}}\right) \qquad \text{(II-40)}$$

The eddy viscosity was assumed to be constant with respect to the transverse coordinate $\hat{\eta}$. A comparison of Equation (II-40) with (II-39), as proposed by Sawyer, reveals that Guitton's expression does not contain any empirical constant in the second term on the right side.

Wyngard, Tennekes, Lumley, and Margolis [56] carried out an extension to the earlier work by Margolis and Lumley. They observed that in a turbulent curved mixing layer for unstable cases (involving negative radial gradients of angular momentum) the rate of turbulent energy production was greater than similar production rates for stable

cases (involving positive radial gradients of angular momentum).

As previously noted in the discussion of deflected jets, Endo [20] carried out an investigation involving a curved two-dimensional jet. In developing his analytical model he assumed a turbulent shear stress relation of the same form as Equation (II-39), which was used by Sawyer. According to Endo's analysis the value of the empirical constant C varied from approximately ten in the initial region to a final value of three in the main region. Also of significance is the fact that Endo, like Sawyer, concluded that *mass flow occurs across the jet centerline* (from the convex to the concave side).

Based on the literature survey of turbulent flow, a number of items are worthy of note. First, with regard to turbulent plane jets, the most general study from both experimental and analytical standpoints is that by Bradbury and Riley [33]. This study appears to offer a reasonable method of calculating eddy viscosity for a plane turbulent jet. The second item of interest is concerned with the calculation of eddy viscosity in turbulent boundary layers for compressible flow. The work by Maise and McDonald [39] combined with that by Cebeci, Smith and Wang [40] provide promising methods of determining values for the eddy viscosity in both the inner and outer regions of the boundary layer. For turbulent flow in ducts, the approach suggested by Hinze [22] for calculating eddy viscosity seems most acceptable. Such an approach however, necessitates knowledge of the shear stress at the wall. The latter can be expressed in terms of the Fanning friction factor, which can be calculated by means of the relation developed by Drew, Koo and McAdams [48].

Two points concerned with curved turbulent flow are of special interest. First, turbulence is affected by the curvature of the flow field. Second, for the case of a curved jet, there appears to be mass flow across the jet centerline from the convex to the concave side of the jet.

Computational Fluid Dynamics

The governing equations for fluid motion consist of a set of nonlinear partial differential equations. Because of their complexity for most situations, analytical solutions are possible only when the equations are greatly simplified. If the fundamental equations are to be solved, for most cases a numerical approach is required. The latter in turn normally necessitates the use of a digital computer. A considerable amount of literature has recently been generated concerning this general subject [57]. As with the preceding portions of this literature survey, certain restrictions on the material to be covered are necessary. In general, only numerical procedures which have some application to turbulent compressible flow are of interest. In this regard notice should be taken that the governing equations for this type of flow may be classified as *mixed hyperbolic-parabolic* [58,59]. Thus, solutions to both hyperbolic and parabolic (but not elliptic) equations are of major concern.

Von Newmann and Richtmyer [60] carried out an analytical study which was involved with the numerical calculation of shock wave propagation in a compressible fluid. The transient one-dimensional inviscid equations of motion, written in Lagrangian coordinates, were modified

to include certain nonlinear terms to represent the dissipative mechanism present in the vicinity of the shock. These terms, commonly referred to as "artificial viscosity" were defined in such a manner as to satisfy the Rankine-Hugoniot equations for a normal shock. The authors developed the finite-difference equations corresponding to the differential equations. By means of Fourier series expansions they studied the stability criteria for the difference equations and arrived at the following *sufficient* condition for stability

$$\Delta\hat{t} \leq \frac{\hat{\rho}_o \Delta\hat{x}}{\sqrt{\gamma \hat{p} \hat{\rho}}} \qquad \text{(II-41)}$$

where $\hat{\rho}_o$ = initial density.

Courant, Isaacson, and Rees [61] presented a discussion on nonlinear hyperbolic equations. Two finite-difference schemes were described, one using a curvilinear grid and the other using a rectangular grid. The techniques were applicable to hyperbolic systems of quasi-linear first-order partial differential equations. Necessary and sufficient conditions for convergence were developed.

In a numerical study by Lax and Wendroff [62] the governing equations for transient, one-dimensional, inviscid, compressible fluid dynamics were arranged in such a manner so that the quantities to be conserved were mass, momentum, and total energy (internal plus kinetic). This arrangement of the equations is referred to as the *conservation law form*. A finite difference technique, which is generally referred to as the "Lax-Wendroff one-step method" was developed for solving the equations. The technique possessed second-order accuracy in time. The

necessary and sufficient stability criterion was shown to be that *the rate of propagation of signals in the difference scheme must be at least as large as the true maximum signal speed.* This criteria can be written as

$$\Delta\hat{t} \leq \frac{\Delta\hat{x}}{\hat{w} + \hat{a}} \tag{II-42}$$

The authors utilized the concept of artificial viscosity to allow for shocks.

Rusanov [63] presented a numerical technique also utilizing the concept of artificial viscosity for multi-dimensional fluid dynamic problems involving shocks. Eulerian coordinates and the conservation law form of the governing equations were utilized. Only first-order accuracy in time was achieved, but stability requirements were similar to those of the Lax-Wendroff one-step method. It should be noted that artificial viscosity was used by Rusanov, not only to allow for shocks, but also to stabilize the first-order numerical scheme.

A survey of finite difference methods for transient fluid dynamics was reported by Richtmyer [64]. Various schemes for the solution of hyperbolic systems were described and compared. In addition, another numerical technique, which was ascribed to Lax and Wendroff was discussed. This technique, which was called the "Lax-Wendroff two-step method," possessed second-order accuracy in time but was somewhat simpler than the one-step method. For two-dimensional flow with a square grid, Richtmyer showed that in the case of inviscid compressible

flow the necessary and sufficient condition for stability was

$$\Delta\hat{t} < \frac{\Delta\hat{x}}{(\hat{w}+\hat{a})\sqrt{2}} \qquad \text{(II-43)}$$

Thommen [65,66] presented the results of a numerical study involving two-dimensional supersonic/subsonic viscous flow over a flat plate. Only laminar flow was treated, but the entire Navier-Stokes equations were considered. An attempt was made to obtain the steady-state solution to the problem by numerically solving the unsteady or transient equations. The Lax-Wendroff one-step method was employed. Although no comparison was made with experimental data, the calculated flow field resembled that for a laminar boundary layer on a flat plate. Thommen encountered instabilities with his scheme for Reynolds numbers in excess of several hundred. Also at the leading edge of the flat plate, when a rectangular grid was used instead of a square grid, oscillation in the calculated values of pressure and density occurred. Thommen presented an approximate stability analysis for one-dimensional compressible viscous flow. The most general criterion he arrived at was the following implicit relation:

$$(N''_{Re})_\infty \Delta\hat{x} \geq \frac{\hat{\mu}''\Delta\hat{t}/\Delta\hat{x}}{\hat{\rho}} \left\{[1-(\Delta\hat{t}/\Delta\hat{x})^2(\hat{w}+\hat{a})^2]^{-1} + [1-(\Delta\hat{t}/\Delta\hat{x})^2(\hat{w}-\hat{a})^2]^{-1}\right\} \qquad \text{(II-44)}$$

where

$$(N''_{Re})_\infty = \frac{\hat{\rho}_\infty \hat{w}_\infty \hat{x}}{\hat{\mu}''} .$$

$$\hat{\mu}'' = 2\hat{\mu} + \hat{\lambda}.$$

It should be noted that Equation (II-44) does not take into account heat transfer. In general this implicit relation indicates that as the product of the Reynolds number and the space increment increases the ratio of the time increment to space increment can also be increased without loss of stability.

The concept of solving the steady compressible Navier-Stokes equations by means of an asymptotic solution of the time-dependent flow has also been proposed by Crocco [67]. The author attempted to avoid the instability associated with first-order techniques by utilizing a special set of difference equations. These difference equations, which possessed satisfactory stability characteristics, only became consistent with the differential equations as the time-dependence vanished. Several numerical experiments were conducted with this technique for the case of quasi-one dimensional supersonic flow in a divergent duct with various back pressures applied. Acceptable results were obtained for Reynolds numbers below 160. Above this value a wavy pattern in the density distribution in the duct was produced which was physically unrealistic.

Burnstein [68] carried out an analytical study of inviscid supersonic flow (Mach number = 4.3) around a rectangular body using the Lax-Wendroff one-step method. Instabilities in the numerical computational occurred in two regions: along the detached shock and in

the vicinity of the corner of the body. In these two regions artificial viscosity was utilized to stabilize the solution. With the introduction of such a term, the calculated flow field was in good agreement with experimental data. Notice should be taken that artificial viscosity as employed by Burnstein was somewhat complex and was a nonisotropic parameter, which was introduced into the continuity and energy equations as well as into the momentum equations.

Morretti and Abbett [69] utilized a transient approach in solving the mixed supersonic/subsonic inviscid flow around a blunt body. By means of a nonlinear coordinate transformation, the surface of the blunt body and the moving bow shock were assigned fixed positions in the grid system, without the need for irregular grid points or interpolation. The finite-difference technique, employed for the interior points, was of second-order accuracy and appears to be essentially the same as the Lax-Wendroff one-step method. Points along the shock and the blunt body were coupled to the interior points by a quasi one-dimensional transient method of characteristics. With a relatively coarse grid, reasonably good flow predictions were obtained, based on comparison with experiment.

Prediction of turbulent compressible two-dimensional flow fields was described by Trulio, Carr, Niles, and Rentfrow [70]. A transient approach was used along with a non-linear coordinate transformation for an example problem involving flow around a right circular cylinder. Generation and shedding of vortices were predicted. Very few details of the actual numerical procedure were described.

Richtmyer and Morton [71] have provided an excellent reference on numerical techniques for initial value problems. Considerable attention is devoted to stability criteria in general. One-dimensional fluid dynamics and multi-dimensional fluid dynamic techniques are discussed. The authors in general appear to favor the Lax-Wendroff two-step method over all other techniques for compressible fluid flow. It is of special significance to note that in the introduction to their text, concerning the lack of rigorous mathematical proofs of convergence and consistency for many new numerical techniques, Richtmyer and Morton stated, ". . . if we were to wait for convergence proofs and error estimates for the new methods, most of the computers now in use in technology and industry would come grinding to a halt."

In a study pertaining to the calculation of detached shocks ahead of blunt bodies, Lapidus [72] encountered instabilities in the same regions as had been encountered by Burnstein. To overcome these instabilities, Lapidus introduced an artificial viscosity based on the absolute value of the difference in the velocity components at adjacent grid points. This model for artificial viscosity was simpler than that used by Burnstein, but was also nonisotropic and was applied to all conservation equations. The basic numerical technique employed by Lapidus was the Lax-Wendroff two-step method.

Scala and Gordon [73,74] in a study involving laminar compressible flow over a cylinder, developed a numerical technique especially designed for mixed hyperbolic-parabolic equations. The authors, based on their own earlier analysis of the reflection of a shock wave at a

surface [75], classified all terms in the equations for conservation of mass, momentum, and energy as either parabolic or hyperbolic. The parabolic terms generally involved viscosity. Two separate numerical techniques were employed, one for the parabolic terms and the other for the hyperbolic. For the former, an alternating explicit-implicit scheme previously developed by Gordon [76] was used. For the hyperbolic terms, the equations were reduced to a normal form and differencing was accomplished according to the sign of the characteristics, as suggested by Courant, Isaacson and Rees. A nonlinear coordinate transformation was used to concentrate or "squeeze" points into a particular region of interest. The resulting predictions for flow over a cylinder appeared quite reasonable, although no comparison with experimental data was presented. The stability criterion for the nonviscous hyperbolic system was*

$$\hat{\Delta t} \leq \frac{1}{(|\hat{w}_r|+\hat{a})/\Delta\hat{R} + (|\hat{w}_\phi|+\hat{a})/(\hat{R}\Delta\phi)} \qquad \text{(II-45)}$$

Scala and Gordon noted that no answer was available to the question of existence and uniqueness of a solution to the Navier-Stokes equations. Furthermore the consistency of their finite difference equations and the convergence of the numerical solution could not be precisely established.

Prediction of the flow in turbulent boundary layers, both

---

*It should be noted that, due to a typographical error, in Reference 73 and 74, in the second term in the denominator of Equation (II-45) the radius $\hat{R}$ was omitted.

compressible and incompressible were described by Smith and Cebeci [77], and in a later study by Cebeci, Smith, and Wang [41]. The eddy viscosity models used in these studies have been discussed already. The governing equations were assumed to be the time-averaged steady-state boundary layer equations with turbulence taken into account by means of the Reynolds stresses. The equations were transformed twice: first by the Probstein-Elliot transformation [78], and then by the Levy-Lees transformation [79]. The resulting equations were numerically solved by an iterative finite-difference technique with the calculations proceeding from upstream to downstream.

Coxe [1], in his study of a laminar, incompressible, two-dimensional deflected jet, as noted previously, utilized a time-dependent finite-difference technique. Because his problem dealt with an incompressible fluid, his equations were mixed parabolic-elliptic. Thus at each time step there was the requirement for simultaneous solution of a set of nonlinear algebraic equations for all grid points.

In another study involving incompressible viscous flow, Chorin [80] introduced the concept of artificial compressibility, in order to eliminate the need for simultaneous solution of nonlinear algebraic equations. In effect the continuity equation for incompressible flow was modified to resemble the corresponding equation for transient compressible flow. An artificial density and an artificial equation of state were developed. As steady-state conditions were approached, the terms containing the artificial density approached zero and in the limit, as time approached infinity, the modified equations reduced to

the actual equations for incompressible viscous flow. This technique can be seen to resemble that proposed by Crocco. Chorin used the leap-frog scheme [64] to obtain central space and time derivatives. Viscous dissipative terms were differenced according to the Dufort-Frankel pattern [81]. The stability criterion for the numerical technique was found to be

$$\Delta\hat{t} \leq \frac{2(\Delta\hat{x})_{min}}{N^{1/2}(1+\sqrt{5})}\sqrt{\hat{\delta}} \qquad \text{(II-46)}$$

where

N = number of dimensions.

$\hat{\delta}$ = artificial compressibility $(\hat{p}/\hat{\rho})$.

Chorin conducted several numerical experiments involving channel flow and thermal convection with apparently satisfactory results, although no comparison with experimental data was provided.

Skoglund, Cole and Staiano [82] conducted an investigation of the relative merits of various numerical techniques as applied to supersonic compressible boundary layers with shock waves. After an extensive literature survey the authors selected the Rusanov method and the Lax-Wendroff one-step method for further study. For a one-dimensional test case involving the propagation of a shock wave, both methods produced satisfactory results. For a two-dimensional test problem involving the interaction of a shock wave with a laminar boundary layer, the Rusanov technique produced results which were considerably less accurate than those produced by the Lax-Wendroff method. In utilizing the latter, however, the need arose for an excessive number of grid points. To

avoid this problem a nonlinear coordinate transformation, utilizing the hyperbolic tangent, was employed. This transformation was of the form

$$X = a_1 \tanh(a_2 \hat{x}) \qquad \text{(II-48)}$$

where

X = transformed coordinate.

a_1 = arbitrary constant.

a_2 = arbitrary constant.

$\hat{x}$ = original coordinate.

Such a transformation causes the coordinate X to approach a constant, a_1, when $\hat{x}$ approaches infinity. In general, based on the results obtained, the authors indicated that the Lax-Wendroff one-step method produced the most promising results, although the Rusanov method was simpler.

A useful discussion of finite-difference techniques as applied to problems involving mixed supersonic/subsonic flow has been presented by Jenkins [83]. The author cited seven examples of such mixed flow, including the deflected jet problem currently under consideration. He concluded that transient finite-difference techniques appeared to offer the best promise for the solution of such problems. The use of coordinate stretching also appeared to Jenkins to be a means of extending the range of Reynolds numbers for which numerical solutions were feasible.

Bauer [35] in his study of a turbulent axisymmetric jet, which as already discussed, utilized the Rusanov method for the numerical

solution of the time-averaged governing equations. No attempt was made by Bauer to determine the effect of turbulence on the stability criteria as set forth by Rusanov. The author noted, however, that when turbulence was represented by the use of eddy viscosity, the overall stability of the numerical technique should be improved.

The importance of boundary conditions in the numerical solution of fluid dynamic problems was the subject of a discussion by Morretti [84]. He noted that, in general, accurate representation of the boundary conditions was essential to an accurate numerical solution. The fallacy of using the principle of "mirror image" points to satisfy conditions along a solid surface was clearly demonstrated. In general Morretti favored the use of the method of characteristics to couple the boundary points to the interior points of the flow field. He also indicated the need for extending the free flow region to infinity to allow accurate free stream boundary conditions to be defined. Although Morretti was primarily concerned with compressible inviscid flow he indicated that a similar need for accurate boundary condition description existed in viscous flow problems.

An interesting variation of the two-step Lax-Wendroff method was utilized by MacCormack [85]. The author was concerned with viscous compressible flow associated with hypervelocity impact. In MacCormack's variation on the spatial derivatives of the governing equation in conservation law form were approximated by alternating backward and forward finite differences.

Lomax [86] recently carried out a numerical experiment comparing the performance of various numerical procedures as applied to the solution of the one-dimensional inviscid wave propagation problem. He achieved the best results using MacCormack's variation of the Lax-Wendroff two-step method.

The literature survey of computational fluid dynamics reveals several important points. First, the concept of obtaining steady-state solutions by means of the transient version of the governing equations appears to be the most promising approach to the solution of the equations governing fluid flow. For the case of compressible flow, the most tested and successful transient techniques are the Lax-Wendroff two-step method and the Rusanov method. The former appears more accurate but the latter is simpler. Stability criteria for these transient techniques appear to be related physically to the rate of propagation of a pressure wave through the moving fluid, but such criteria are based on linear approximations to the nonlinear system of governing equations. For problems involving the Navier-Stokes equations, currently no precise proof is available for such fundamental points as the proper posing of the problem, consistency of the finite-difference approximation of the partial differential equations, and convergence of the numerical solution to the solution of the latter equations.

CHAPTER III

ANALYTICAL DEVELOPMENT

In order to obtain a solution to the deflected jet problem an analytical model must be formulated which realistically describes the physical phenomena involved. Important features of this model are: (1) coordinate sytems used, (2) non-dimensionalization procedure, (3) governing equations, (4) molecular transport models, (5) turbulent transport models, (6) variation of molecular transport properties, (7) variation of turbulent transport properties, (8) boundary conditions, and (9) initial conditions. Subsequent portions of this chapter deal with each of the preceding points.

Coordinate Systems

Fundamental to the development of an analytical model is the selection of the most suitable coordinate system or systems. Such selection should be based primarily on the geometry of the problem, including both the flow pattern and the location of the physical boundaries. For the deflected jet problem there are two general flow regions, namely, the slot flow and the free flow regions and they are shown in Figure 3. For two-dimensional flow in a slot the use of rectangular coordinates appears natural and logical. For the free flow, however, rectangular coordinates are not in general compatible with the general flow pattern (except possibly in the boundary layer flow near

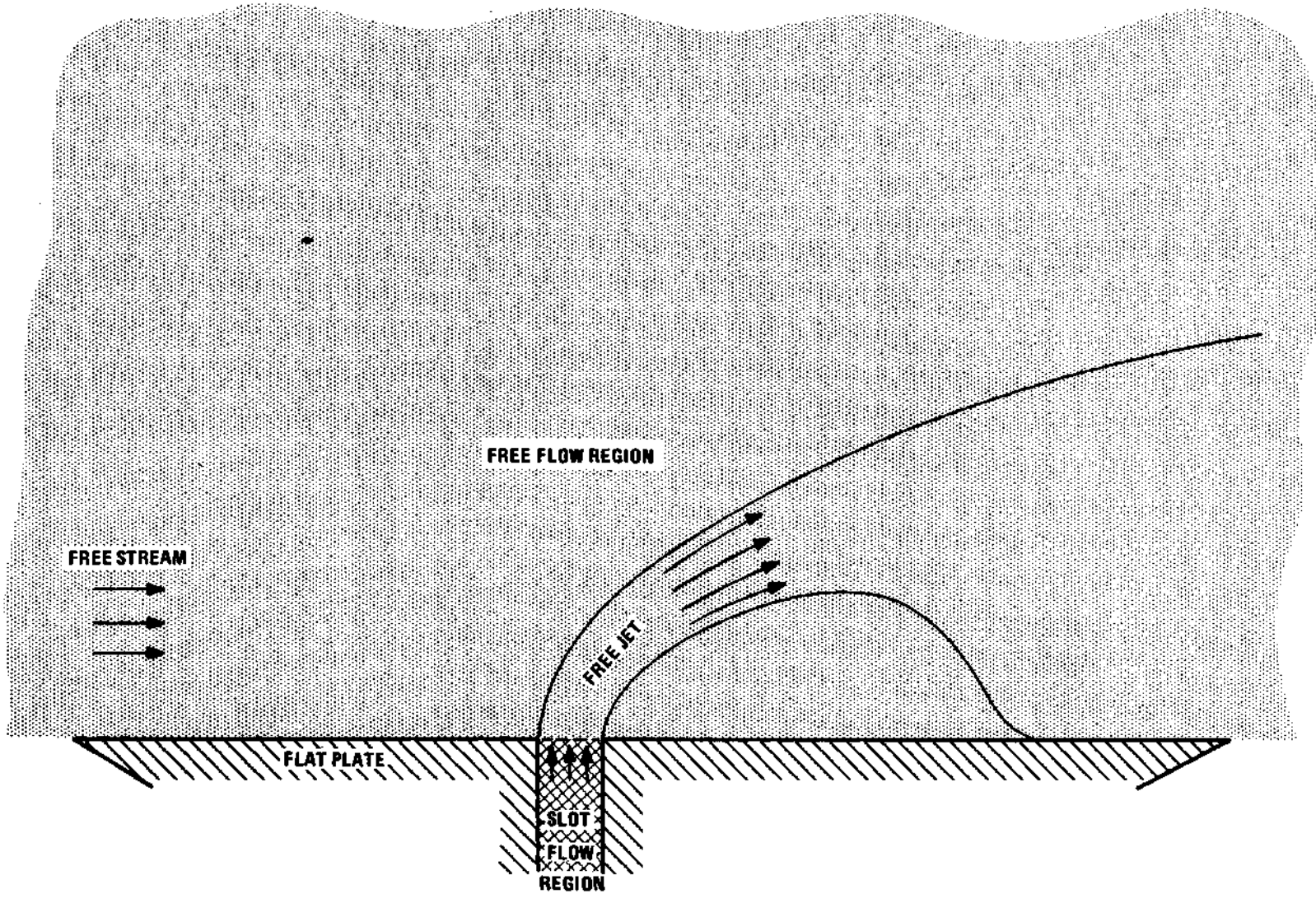

Figure 3. Sketch of the General Flow Regions

the surface of the plate). As noted in Chapter II, experimental studies as well as simplified analytical models have generally indicated that the jet centerline resembles a parabola. In this regard the recommendation by Coxe [1] concerning the use of hyperbolic or parabolic coordinates appears especially significant. Although Coxe favored the hyperbolic coordinate system, a thorough comparison of the features of the two systems indicates that parabolic coordinates are the more suitable system in which to describe the free flow.

Parabolic Coordinates

The parabolic coordinate system is shown in Figure 4a. The parabolas have a common focus, which is the origin of the system, and a common axis. The family of parabolas along which $\hat{u}$ is held constant (referred to as the u-parabolas) is orthogonal to the family along which $\hat{v}$ is held constant (the v-parabolas) [87]. The latus rectum of each u-parabola is $2\hat{u}^2$, and for each v-parabola the latus rectum is $2\hat{v}^2$.

For the case of a free stream flowing from left to right the jet axis should closely correspond to a v-parabola. As indicated in Figure 4 this parabola is designed $\hat{v}_{c\ell}$. Eight other significant parabolas are indicated in the figure. The $\hat{u}_1$ and $\hat{v}_1$ parabolas coincide with the surface of the flat plate. The $\hat{v}_{tes}$ and $\hat{v}_{\ell es}$ parabolas originate at the trailing edge and leading edge of the slot, respectively. The parabolas originating at the trailing edge and leading edge of the plate are respectively designated $\hat{u}_{tep}$ and $\hat{v}_{\ell ep}$. The upstream and downstream physical boundaries of the free flow region are represented by the parabolas $\hat{v}_\infty$ and $\hat{u}_\infty$. Because of the nature of parabolic coordinates

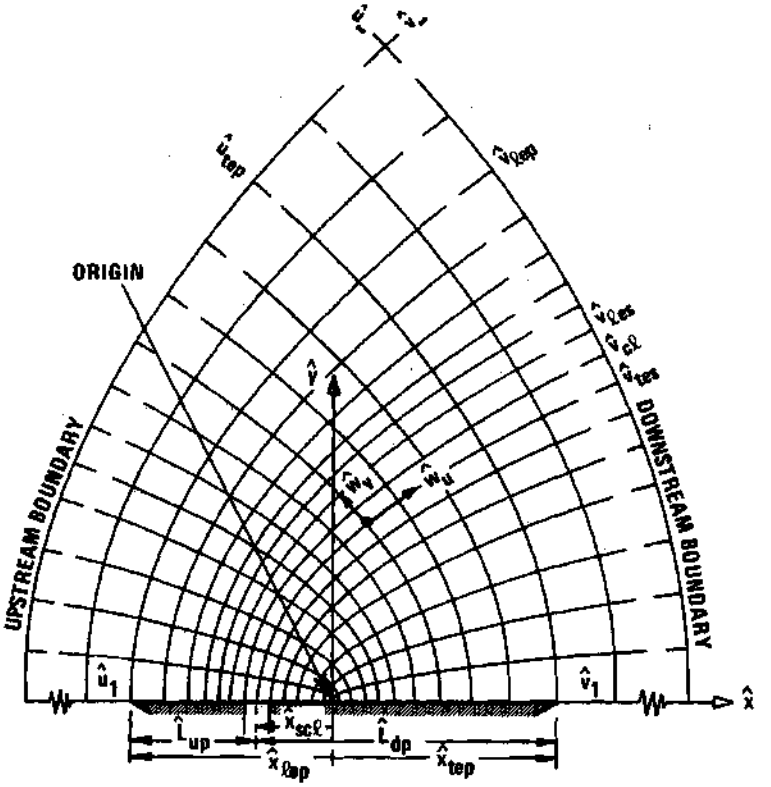

Figure 4a. Parabolic Coordinate System

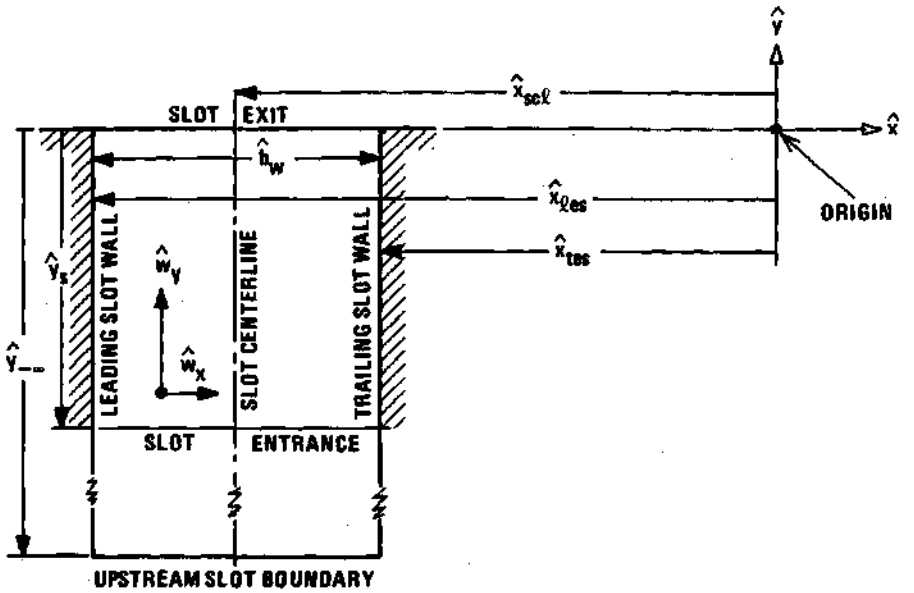

Figure 4b. Rectangular Coordinate System

it can be seen that the free flow region is completely enclosed by the four parabolas $\hat{u}_1$, $\hat{v}_1$, $\hat{u}_\infty$, and $\hat{v}_\infty$. The parabolas generally conform to the physical boundaries for the free flow set forth in the statement of the problem in Chapter I, except for the requirement in the latter for a physical boundary along a streamline located a great distance above and parallel to the plate. This difference in the shape of the boundaries is inherent, due to the nature of parabolic coordinates, but it should be of little significance if $\hat{u}_\infty$ and $\hat{v}_\infty$ are sufficiently large.

The parabolic velocity components are $\hat{w}_u$ and $\hat{w}_v$. These components are defined everywhere except at the origin which is a singular point. The metric factors $\hat{H}_u$ and $\hat{H}_v$ are related to the coordinates by the relations [88]

$$\hat{H}_u = \sqrt{\hat{u}^2 + \hat{v}^2} \qquad \text{(III-1)}$$

$$\hat{H}_v = \sqrt{\hat{u}^2 + \hat{v}^2} \qquad \text{(III-2)}$$

Because these factors are always equal, they are jointly represented by the symbol $\hat{H}$. Thus

$$\hat{H} = \hat{H}_u = \hat{H}_v \qquad \text{(III-3)}$$

Rectangular Coordinates

For the slot flow the rectangular coordinate system used is shown in Figure 4b. For convenience the origin of the rectangular

coordinate system coincides with the origin of the parabolic system, with the x-axis forming the common axis for all parabolas. For the case of a free stream velocity in the positive x-direction, the slot, with a length of $\hat{L}_s$ and a width of $\hat{b}_w$, is located in the third quadrant with the slot longitudinal axis, at $\hat{x}_{sc\ell}$, parallel to the y-axis. The two walls of the slot are located at $\hat{x}_{\ell es}$ and $\hat{x}_{tes}$. The slot entrance is at $\hat{y}_s = -\hat{L}_s$. The slot exit corresponds to $\hat{y} = 0$. The upstream physical boundary of the slot flow region is at $\hat{y}_{-\infty}$. Notice should be taken that this boundary at $\hat{y}_{-\infty}$ is considerably further upstream than the slot entrance at $\hat{y}_s$.

The location of the slot relative to the leading and trailing edges of the plate is given in terms of two distances. The distance from the slot centerline to the leading edge of the plate is denoted by $\hat{L}_{up}$ while the distance from the slot centerline to the trailing edge of the plate is represented by $\hat{L}_{dp}$. Notice should be taken that $\hat{L}_{up}$ and $\hat{L}_{dp}$ represent absolute values and therefore are always positive.

The velocity components in the x- and y-directions are respectively $\hat{w}_x$ and $\hat{w}_y$. For the slot flow to produce a jet, w_y must be positive in general. The x-component $\hat{w}_x$ should be small and may be either positive or negative.

Relationship Between Rectangular and Parabolic Coordinates

For the two coordinate systems with common origins, the relations for $\hat{x}$ and $\hat{y}$ in terms of $\hat{u}$ and $\hat{v}$ are

$$\hat{x} = (\hat{u}^2 - \hat{v}^2)/2 \qquad \text{(III-4)}$$

$$\hat{y} = \hat{u}\hat{v} \tag{III-5}$$

The inverse relations are

$$\hat{u} = \sqrt{\hat{x} + \sqrt{\hat{x}^2+\hat{y}^2}} \tag{III-6}$$

$$\hat{v} = \sqrt{-\hat{x} + \sqrt{\hat{x}^2+\hat{y}^2}} \tag{III-7}$$

For convenience certain dimensions in the free flow region can be expressed in rectangular coordinates. These include the x-coordinate of the leading edge of the plate,

$$\hat{x}_{\ell ep} = -\hat{v}^2_{\ell ep}/2 \tag{III-8}$$

and the x-coordinate of the trailing edge of the plate,

$$\hat{x}_{tep} = \hat{u}^2_{tep}/2 \tag{III-9}$$

In similar fashion the x-coordinates of the leading and trailing edges of the slot can be expressed by the relations

$$\hat{x}_{\ell es} = -\hat{v}^2_{\ell es}/2 \tag{III-10}$$

$$\hat{x}_{tes} = -\hat{v}^2_{tes}/2 \tag{III-11}$$

The relations for $\hat{w}_x$ and $\hat{w}_y$ in terms of $\hat{w}_u$ and $\hat{w}_v$ are

$$\hat{w}_x = (\hat{w}_u\hat{u}-\hat{w}_v\hat{v})/\hat{H} \tag{III-12}$$

$$\hat{w}_y = (\hat{w}_u\hat{v}+\hat{w}_u\hat{u})/\hat{H} \tag{III-13}$$

The inverse relations for $\hat{w}_u$ and $\hat{w}_v$ are

$$\hat{w}_u = (\hat{w}_x\hat{u}+\hat{w}_y\hat{v})/H \tag{III-14}$$

$$\hat{w}_v = (\hat{w}_y\hat{u}-\hat{w}_x\hat{v})/\hat{H} \tag{III-15}$$

Notice should be taken that

$$\left.\begin{aligned}\hat{w}_x &= \hat{w}_v\\ \hat{w}_y &= \hat{w}_u\end{aligned}\right\} \quad (u=0) \tag{III-16}$$

and

$$\left.\begin{aligned}\hat{w}_x &= \hat{w}_u\\ \hat{x}_y &= \hat{w}_v\end{aligned}\right\} \quad (v=0) \tag{III-17}$$

These equalities represent a desirable feature of the parabolic system because, in the jet exit plane, they permit precise matching of vector components in parabolic coordinates with components in rectangular coordinates.

Location of Jet Centerline

As already noted, the $\hat{v}_{c\ell}$-parabola is designed to correspond generally to the jet centerline. To accomplish this the value of $\hat{v}_{c\ell}$ must be consistent with the various expressions for the jet axis as discussed in Chapter II. The simple expression developed by Vizel and Mostinskii [16], for the case of $\alpha_o=90°$, as given by Equation (II-11) appears to best represent experimental data. This expression can be written as

$$\frac{\hat{x}_{jc\ell}}{\hat{b}_w} = \frac{1}{4}\frac{C_\infty \hat{\rho}_\infty \hat{w}_\infty^2}{\hat{\rho}_{je}\hat{w}_{je}^2}\left(\frac{\hat{y}_{jc\ell}}{\hat{b}_w}\right)^2 + \frac{\hat{x}_{sc\ell}}{\hat{b}_w} \qquad \text{(III-18)}$$

Notice should be taken that the constant distance $\hat{x}_{sc\ell}$ has been added to the right-hand side of the original expression in order to take into account the location of the common origin of the parabolic and rectangular coordinates. Now, based on the relation between parabolic coordinates and rectangular coordinates as given by Equations (III-4) and (III-5),

$$\hat{x}_{jc\ell} = (\hat{u}^2-\hat{v}_{c\ell}^2)/2 \qquad \text{(III-19)}$$

and

$$\hat{y}_{jc\ell} = \hat{u}\hat{v}_{jc\ell} \qquad \text{(III-20)}$$

Then

$$\hat{x}_{jc\ell} = \frac{1}{2}\left[\left(\frac{\hat{y}_{jc\ell}}{\hat{v}_{c\ell}}\right)^2 - \hat{v}_{c\ell}^2\right] \qquad \text{(III-21)}$$

Comparison of Equations (III-18) and (III-21) reveals that for consistency the value of $\hat{v}_{c\ell}$ must satisfy the relation

$$\hat{v}_{c\ell} = \sqrt{\frac{2\hat{b}_w\hat{\rho}_{je}\hat{w}_{je}^2}{C_\infty\hat{\rho}_\infty\hat{w}_\infty^2}} \qquad \text{(III-22)}$$

In addition the value of $\hat{x}_{sc\ell}$ is determined by the relation

$$\hat{x}_{sc\ell} = \frac{-\hat{b}_w\hat{\rho}_{je}\hat{w}_{je}^2}{\hat{C}_\infty\hat{\rho}_\infty\hat{w}_\infty^2} \qquad \text{(III-23)}$$

Thus the approximate location of the jet centerline can be expressed in parabolic coordinates as a simple ratio of certain fundamental parameters associated with the free stream and the jet.

Non-Dimensionalization Procedure

In order to broaden the application of any solution to the deflected jet problem, non-dimensionalization of all coordinates and flow properties must be introduced. This process should be carried out in such a manner as to leave the governing equations essentially unaffected with regard to their form. As already implied, the parabolic shape of the jet axis appears to be the most significant feature of the flow problem. One of the bases for the development of dimensionless quantities is therefore the requirement that $v_{c\ell}$ (the dimensionless

version of $\hat{v}_{c\ell}$) has a magnitude of unity. By assigning such a value to $v_{c\ell}$, comparison of the predictions of the analytical model with experimental data is simplified, as discussed in Chapter V.

Based on Equation (III-22), to set $v_{c\ell}$ to unity the basic relation is

$$v_{c\ell} \equiv \hat{v}_{c\ell} \sqrt{\frac{2\hat{b}_w \hat{\rho}_{je} \hat{w}_{je}^2}{C_\infty \hat{\rho}_\infty \hat{w}_\infty^2}} \qquad \text{(III-24)}$$

The square of the denominator in the preceding relation has the dimensions of length and represents twice the distance from the origin to the slot centerline. This quantity is defined as the significant length $\hat{L}$ in problem as follows:

$$\hat{L} \equiv \frac{2\hat{b}_w \hat{\rho}_{je} \hat{w}_{je}^2}{C_\infty \hat{\rho}_\infty \hat{w}_\infty^2} \qquad \text{(III-25)}$$

The dimensionless coordinates can be seen to be

$$u \equiv \hat{u}/\sqrt{\hat{L}} \qquad \text{(III-26)}$$

$$v \equiv \hat{v}/\sqrt{\hat{L}} \qquad \text{(III-27)}$$

$$x \equiv \hat{x}/\hat{L} \qquad \text{(III-28)}$$

$$y \equiv \hat{y}/\hat{L} \qquad \text{(III-29)}$$

and the dimensionless metric factor for parabolic coordinates,

$$H \equiv \hat{H}/\sqrt{\hat{L}} \tag{III-30}$$

In addition to the requirements that $v_{c\ell}$ be unity, the requirement that the isentropic jet exit velocity w_{je} be unity is also stipulated. This is equivalent to taking $\hat{w}_{je}$ as the characteristic velocity of the flow. Calculation of this parameter is described in Appendix A. Dimensionless velocity components are defined as follows:

$$w_u \equiv \hat{w}_u/\hat{w}_{je} \tag{III-31}$$

$$w_v \equiv \hat{w}_v/\hat{w}_{je} \tag{III-32}$$

$$w_x \equiv \hat{w}_x/\hat{w}_{je} \tag{III-33}$$

$$w_y \equiv \hat{w}_y/\hat{w}_{je} \tag{III-34}$$

As a third requirement in the nondimensionalizing process, the isentropic jet exit density ρ_{je} is set equal to unity. This introduces $\hat{\rho}_{je}$ as the characteristic density of the problem. Thus

$$\rho \equiv \hat{\rho}/\hat{\rho}_{je} \tag{III-35}$$

Calculation of $\hat{\rho}_{je}$ is also described in Appendix A.

The final requirement is that c_p be equal to unity. This implies that $\hat{c}_\rho$, which is assumed constant, is taken as the fourth characteristic parameter. Thus

$$c_\rho \equiv \hat{c}_\rho / \hat{c}_\rho \tag{III-36}$$

The dimensionless version of all remaining parameters can be derived based on the general requirement that the governing equations in dimensionless form (as presented in the next subsection) to be of the same form as the dimensional version. By fundamental dimensional analysis this yields the following dimensionless definitions:

$$t \equiv \hat{t}\hat{w}_{je}/\hat{L} \tag{III-37}$$

$$p \equiv \hat{p}/(\hat{\rho}_{je}\hat{w}_{je}^2) \tag{III-38}$$

$$h \equiv \hat{h}/\hat{w}_{je}^2 \tag{III-39}$$

$$T \equiv \hat{T}\hat{c}_p/\hat{w}_{je}^2 \tag{III-40}$$

$$e \equiv \hat{e}/\hat{w}_{je}^2 \tag{III-41}$$

$$c_v \equiv \hat{c}_v/\hat{c}_p \tag{III-42}$$

$$R \equiv \hat{R}/\hat{c}_p \tag{III-43}$$

$$k \equiv \hat{k}/(\hat{L}\hat{c}_p\hat{w}_{je}\hat{\rho}_{je}) \tag{III-44}$$

$$\mu \equiv \hat{\mu}/(\hat{L}\hat{w}_{je}\hat{\rho}_{je}) \tag{III-45}$$

$$\epsilon_\rho \equiv \hat{\epsilon}_\rho/(\hat{L}\hat{w}_{je}) \tag{III-46}$$

$$\epsilon_m \equiv \hat{\epsilon}_m/(\hat{L}\hat{w}_{je}) \tag{III-47}$$

$$\epsilon_h \equiv \hat{\epsilon}_h/(\hat{L}\hat{w}_{je}) \tag{III-48}$$

Notice should be taken that based on Equation (III-37) one unit of dimensionless time represents the time required for a particle, traveling at the isentropic jet exit speed, to travel twice the distance along the x-axis from the origin to the slot centerline.

In all subsequent discussion, unless otherwise noted, all parameters are dimensionless. For brevity, however, the word "dimensionless" will not be used.

Governing Equations

For two-dimensional flow of a nonreacting gas there are five primary flow properties: density, pressure, temperature, and the two components of velocity. The five equations which must be satisfied are the equation of state, the continuity equation for conservation of mass, the two Navier-Stokes equations for conservation of the two components of momentum, and the energy equation for conservation of energy. All

of these equations are well known and their derivations are presented in numerous texts [29,42,89,90].

Classical Form

The instantaneous values of the five primary properties can be calculated by means of the five equations already noted. First, the equation of state for an ideal gas is

$$p = RT\rho \tag{III-49}$$

For the problem under consideration two coordinate systems are utilized and thus, for the remaining four equations, the need arises for two versions of each equation. For the rectangular version there is no particular problem. For the parabolic version, however, the equations are in an unfamiliar form and considerable care must be exercised in their development. By the use of general orthogonal curvilinear coordinates and metric factors [88], however, these equations can be written out without any significant difficulty.

Accordingly, for the continuity equation in rectangular coordinates,

$$\frac{\partial \rho}{\partial t} + \frac{\partial(\rho w_x)}{\partial x} + \frac{\partial(\rho w_y)}{\partial y} = 0 \tag{III-50}$$

and in parabolic coordinates,

$$\frac{\partial \rho}{\partial t} + \frac{1}{H}\left[\frac{\partial(\rho w_u)}{\partial u} + \frac{\partial(\rho w_v)}{\partial v}\right] + \frac{1}{H^3}(\rho w_u u + \rho w_v v) = 0 \tag{III-51}$$

For conservation of momentum in rectangular coordinates the x-component and y-component equations in terms of stress, in the absence of body forces, are, respectively

$$\rho\left(\frac{\partial w_x}{\partial t} + w_x \frac{\partial w_x}{\partial x} + w_y \frac{\partial w_x}{\partial y}\right) = \frac{\partial \sigma_{xx}}{\partial x} + \frac{\partial \sigma_{xy}}{\partial y} \qquad \text{(III-52)}$$

and

$$\rho\left(\frac{\partial w_y}{\partial t} + w_x \frac{\partial w_y}{\partial x} + w_y \frac{\partial w_y}{\partial y}\right) = \frac{\partial \sigma_{xy}}{\partial x} + \frac{\partial \sigma_{yy}}{\partial y} \qquad \text{(III-53)}$$

In parabolic coordinates, the u-momentum and v-momentum equations are

$$\rho\left[\frac{\partial w_u}{\partial t} + \frac{1}{H}\left(w_u \frac{\partial w_u}{\partial u} + w_v \frac{\partial w_u}{\partial v}\right) - \frac{w_v}{H^3}(w_v u - w_u v)\right] = \frac{1}{H}\left(\frac{\partial}{\partial u}\sigma_{uu} + \frac{\partial}{\partial v}\sigma_{vu}\right) + \frac{1}{H^3}(u\sigma_{uu} + 2v\sigma_{uv} - u\sigma_{vv}) \qquad \text{(III-54)}$$

and

$$\rho\left[\frac{\partial w_v}{\partial t} + \frac{1}{H}\left(w_u \frac{\partial w_v}{\partial u} + w_v \frac{\partial w_v}{\partial v}\right) - \frac{w_u}{H^3}(w_u v - w_v u)\right] = \frac{1}{H}\left(\frac{\partial}{\partial u}\sigma_{uv} + \frac{\partial}{\partial v}\sigma_{rv}\right) + \frac{1}{H^3}(-v\sigma_{uu} + 2u\sigma_{uv} + v\sigma_{vv}) \qquad \text{(III-55)}$$

For the current case it is convenient to write the momentum equation in a slightly different form. If the continuity equation in rectangular coordinates, Equation (III-50), is multiplied by w_x and the result added to the x-momentum equation, the result is

$$\frac{\partial(\rho w_x)}{\partial t} + \frac{\partial}{\partial x}\left[(\rho w_x)w_x\right] + \frac{\partial}{\partial y}\left[(\rho w_x)w_y\right] = \frac{\partial \sigma_{xx}}{\partial x} + \frac{\partial \sigma_{xy}}{\partial y} \qquad \text{(III-56)}$$

Likewise if the continuity equation is multiplied by w_y and added to the y-momentum equation, the resulting relation is

$$\frac{\partial(\rho w_y)}{\partial t} + \frac{\partial}{\partial x}\left[(\rho w_y)w_x\right] + \frac{\partial}{\partial y}\left[(\rho w_y)w_y\right] = \frac{\partial \sigma_{xy}}{\partial x} + \frac{\partial \sigma_{yy}}{\partial y} \qquad \text{(III-57)}$$

In parabolic coordinates if the continuity equation is multiplied by w_u and then added to the u-momentum equation, there results

$$\frac{\partial(\rho w_u)}{\partial t} + \frac{1}{H}\left\{\frac{\partial}{\partial u}\left[(\rho w_u)w_u\right] + \frac{\partial}{\partial v}\left[(\rho w_u)w_v\right]\right\} + \frac{1}{H^3}\left[u(\rho w_u)w_u + 2v(\rho w_u)w_v - u(\rho w_v)w_v\right] = \frac{1}{H}\left(\frac{\partial \sigma_{uu}}{\partial u} + \frac{\partial \sigma_{uv}}{\partial v}\right) + \frac{1}{H^3}\left(u\sigma_{uu} + 2v\sigma_{uv} - u\sigma_{vv}\right) \qquad \text{(III-58)}$$

In similar fashion multiplication of the continuity equation by w_v and addition to the v-momentum equation yields

$$\frac{\partial(\rho w_v)}{\partial t} + \frac{1}{H}\left\{\frac{\partial}{\partial u}\left[(\rho w_v)w_u\right] + \frac{\partial}{\partial v}\left[(\rho w_v)w_v\right]\right\} + \frac{1}{H^3}\left[-v(\rho w_u)w_u + 2u(\rho w_v)w_u + v(\rho w_v)w_v\right] + \frac{1}{H}\left(\frac{\partial \sigma_{uv}}{\partial u} + \frac{\partial \sigma_{vv}}{\partial v}\right) + \frac{1}{H^3}\left(-v\sigma_{uu} + 2u\sigma_{uv} + v\sigma_{vv}\right) \qquad \text{(III-59)}$$

For the energy equation there exist several different versions [88,89]. The form given in Reference 89, involving the sum of internal plus kinetic energy, appears most suitable for the current analytical model. In rectangular coordinates the equation is

$$\frac{\partial(\rho e_o)}{\partial t} + \frac{\partial}{\partial x}(\rho e_o w_x) + \frac{\partial}{\partial y}(\rho e_o w_y) = -\left(\frac{\partial}{\partial x} q_x + \frac{\partial}{\partial y} q_y\right)$$

$$+ \frac{\partial}{\partial x}(\sigma_{xx} w_x + \sigma_{xy} w_y) + \frac{\partial}{\partial y}(\sigma_{xy} w_x + \sigma_{yy} w_y) \qquad \text{(III-60)}$$

Likewise in parabolic coordinates the same version of the energy equation becomes

$$\frac{\partial}{\partial t}(\rho e_o) + \frac{1}{H}\left[\frac{\partial}{\partial u}(\rho e_o w_u) + \frac{\partial}{\partial v}(\rho e_o w_v)\right] + \frac{1}{H^3}(u\rho e_o w_u + v\rho e_o w_v) =$$

$$- \frac{1}{H}\left(\frac{\partial q_u}{\partial u} + \frac{\partial q_v}{\partial v}\right) - \frac{1}{H^3}(u q_u + v q_v)$$

$$+ \frac{1}{H}\left[\frac{\partial}{\partial u}(\sigma_{uu} w_u + \sigma_{uv} w_v) + \frac{\partial}{\partial v}(\sigma_{uv} w_u + \sigma_{vv} w_v)\right]$$

$$+ \frac{1}{H^3}(u\sigma_{uu} w_u + u\sigma_{uv} w_v + v\sigma_{uv} w_u + v\sigma_{vv} w_v) \qquad \text{(III-61)}$$

Time-Averaged Equations

In the manner developed by Reynolds [91], for the case of turbulent flow, the instantaneous values of the flow variables are divided into a time-averaged component and a fluctuating component. Thus

$$\rho = \bar{\rho} + \rho'$$

$$p = \bar{p} + p'$$

$$T = \bar{T} + T'$$

$$w_x = \bar{w}_x + w'_x$$

$$w_y = \bar{w}_y + w'_y$$

$$w_u = \bar{w}_u + w'_u$$

$$w_v = \bar{w}_v + w'_v$$

$$e = \bar{e} + e'$$

$$e_o = \bar{e}_o + e'_o$$

$$h = \bar{h} + h'$$

$$\sigma_{xx} = \bar{\sigma}_{xx} + \sigma'_{xx}$$

$$\sigma_{xy} = \bar{\sigma}_{xy} + \sigma'_{xy}$$

$$\sigma_{yy} = \bar{\sigma}_{yy} + \sigma'_{yy}$$

$$\sigma_{uu} = \bar{\sigma}_{uu} + \sigma'_{uu}$$

$$\sigma_{uv} = \bar{\sigma}_{uv} + \sigma'_{uv}$$

$$\sigma_{vv} = \bar{\sigma}_{vv} + \sigma'_{vv}$$

$$q_x = \bar{q}_x + q'_x$$

$$q_y = \bar{q}_y + q_y'$$

$$q_u = \bar{q}_u + q_u'$$

$$q_v = \bar{q}_v + q_v'$$

In addition, after Van Driest [37], it is useful in certain cases to treat the quantities of momentum per unit volume and energy per unit volume in a manner similar to that for the other variables. Thus

$$(\rho w_x) = (\overline{\rho w_x}) + (\rho w_x)'$$

$$(\rho w_y) = (\overline{\rho w_y}) + (\rho w_y)'$$

$$(\rho w_u) = (\overline{\rho w_u}) + (\rho w_u)'$$

$$(\rho w_v) = (\overline{\rho w_v}) + (\rho w_v)'$$

$$(\rho e) = (\overline{\rho e}) + (\rho e)'$$

$$(\rho e_o) = (\overline{\rho e_o}) + (\rho e_o)'$$

An expansion of each of these last six relations is provided in Appendix B.

To obtain the time-averaged equations, the expression for the instantaneous value of each flow variable must be substituted into

Equations (III-49), (III-50), (III-51), (III-56), (III-57), (III-58), (III-59), (III-60), and (III-61) as shown in Appendix B. The resulting expressions are time-averaged over a time period which is large compared with the mean time period of the fluctuations. After application of fundamental rules for time-averaging, as well as certain simplifying assumptions which are covered in Appendix B, the desired equations for turbulent flow are obtained.

Based on the introduction of the preceding concepts, the time-averaged equation of state is, as shown in Appendix B,

$$\bar{p} = R(\bar{T}\bar{\rho}+\overline{T'\rho'}) \qquad \text{(III-62)}$$

The first term in parentheses in Equation (III-62) is interpreted as representing the equilibrium pressure $\bar{p}_s$ while the second is interpreted as the turbulent pressure $\bar{p}_t$. Thus the following definitions are assumed:

$$\bar{p}_s \equiv R\bar{T}\bar{\rho} \qquad \text{(III-63)}$$

and

$$\bar{p}_t \equiv R\overline{T'\rho'} \qquad \text{(III-64)}$$

For conservation of mass the time-averaged equation in rectangular coordinates is

$$\frac{\partial \bar{\rho}}{\partial t} + \frac{\partial(\bar{\rho}\bar{w}_x)}{\partial x} + \frac{\partial(\overline{\rho' w'_x})}{\partial x} + \frac{\partial(\bar{\rho}\bar{w}_y)}{\partial y} + \frac{\partial(\overline{\rho' w'_y})}{\partial y} = 0 \qquad \text{(III-65)}$$

and in parabolic coordinates,

$$\frac{\partial \bar{\rho}}{\partial t} + \frac{1}{H}\left[\frac{\partial}{\partial u}(\bar{\rho}\bar{w}_u) + \frac{\partial}{\partial u}(\overline{\rho' w'_u}) + \frac{\partial}{\partial v}(\bar{\rho}\bar{w}_v) + \frac{\partial}{\partial v}(\overline{\rho' w'_v})\right]$$

$$+ \frac{1}{H^3}\left[u(\bar{\rho}\bar{w}_u + \overline{\rho' w'_u}) + v(\bar{\rho}\bar{w}_v + \overline{\rho' w'_v})\right] = 0 \qquad \text{(III-66)}$$

In the two preceding equations certain double correlation terms ($\overline{\rho' w'_x}$, $\overline{\rho' w'_y}$, $\overline{\rho' w'_u}$, and $\overline{\rho' w'_v}$) can be identified. These terms, as noted by Shapiro [92] represent apparent mass flow which is hereafter referred to as turbulent mass diffusion.* For brevity the following definitions are used:

$$\bar{m}_x \equiv \overline{\rho' w'_x} \qquad \text{(III-67)}$$

$$\bar{m}_y \equiv \overline{\rho' w'_y} \qquad \text{(III-68)}$$

$$\bar{m}_u \equiv \overline{\rho' w'_u} \qquad \text{(III-69)}$$

$$\bar{m}_v \equiv \overline{\rho' w'_v} \qquad \text{(III-70)}$$

---

*Actually these terms are the turbulent counterpart of molecular diffusion terms which are "hidden" in the single species continuity equation.

Substitution of these four definitions into the continuity equations yields

$$\frac{\partial\bar{\rho}}{\partial t} + \frac{\partial(\bar{\rho}\bar{w}_x)}{\partial x} + \frac{\partial\bar{m}_x}{\partial x} + \frac{\partial(\bar{\rho}\bar{w}_y)}{\partial y} + \frac{\partial\bar{m}_y}{\partial y} = 0 \qquad \text{(III-71)}$$

and

$$\frac{\partial\bar{\rho}}{\partial t} + \frac{1}{H}\left[\frac{\partial(\bar{\rho}\bar{w}_u)}{\partial u} + \frac{\partial\bar{m}_u}{\partial u} + \frac{\partial(\bar{\rho}\bar{w}_v)}{\partial v} + \frac{\partial\bar{m}_v}{\partial v}\right]$$

$$+ \frac{1}{H^3}\left[u(\bar{\rho}\bar{w}_u+\bar{m}_u) + v(\bar{\rho}\bar{w}_v+\bar{m}_v)\right] = 0 \qquad \text{(III-72)}$$

For conservation of x-momentum in rectangular coordinates the time-averaged equation is

$$\frac{\partial(\overline{\rho w_x})}{\partial t} + \frac{\partial(\bar{\rho}\bar{w}_x\bar{w}_x)}{\partial x} + \frac{\partial(\bar{\rho}\bar{w}_x\bar{w}_y)}{\partial y} = \frac{\partial\bar{\sigma}_{xx}}{\partial x} + \frac{\partial\bar{\sigma}_{xy}}{\partial y} - \frac{\partial}{\partial x}\left(\bar{\rho}\overline{w'_x w'_x}\right.$$

$$\left. + 2\bar{w}_x\overline{\rho' w'_x}\right) - \frac{\partial}{\partial y}\left(\bar{\rho}\overline{w'_x w'_y}+\bar{w}_x\overline{\rho' w'_y}+\bar{w}_y\overline{\rho' w'_x}\right) \qquad \text{(III-73)}$$

Likewise for y-momentum,

$$\frac{\partial(\overline{\rho w_y})}{\partial t} + \frac{\partial(\bar{\rho}\bar{w}_y\bar{w}_x)}{\partial x} + \frac{\partial(\bar{\rho}\bar{w}_y\bar{w}_y)}{\partial y} = \frac{\partial\bar{\sigma}_{xy}}{\partial x} + \frac{\partial\bar{\sigma}_{yy}}{\partial y} - \frac{\partial}{\partial x}\left(\bar{\rho}\overline{w'_x w'_y}\right.$$

$$\left. +\bar{w}_y\overline{\rho' w'_x}+\bar{w}_x\overline{\rho' w'_y}\right) - \frac{\partial}{\partial y}\left(\bar{\rho}\overline{w'_y w'_y}+2\bar{w}_y\overline{\rho' w'_y}\right) \qquad \text{(III-74)}$$

In parabolic coordinates the time-averaged u-momentum equation is

$$\frac{\partial(\overline{\rho w_u})}{\partial t} + \frac{1}{H}\left[\frac{\partial}{\partial u}(\bar{\rho}\bar{w}_u\bar{w}_u) + \frac{\partial}{\partial v}(\bar{\rho}\bar{w}_u\bar{w}_v)\right] + \frac{1}{H^3}(u\bar{\rho}\bar{w}_u\bar{w}_u + 2v\bar{\rho}\bar{w}_u\bar{w}_v - u\bar{\rho}\bar{w}_v\bar{w}_v) =$$

$$\frac{1}{H}\left(\frac{\partial\bar{\sigma}_{uu}}{\partial u} + \frac{\partial\bar{\sigma}_{uv}}{\partial v}\right) + \frac{1}{H^3}(u\bar{\sigma}_{uu} + 2v\bar{\sigma}_{uv} - u\bar{\sigma}_{vv}) - \frac{1}{H}\left[\frac{\partial}{\partial u}(\bar{\rho}\overline{w'_u w'_u}\right.$$

$$\left. + 2\bar{w}_u\overline{\rho' w'_u}) + \frac{\partial}{\partial v}(\bar{\rho}\overline{w'_u w'_v} + \bar{w}_u\overline{\rho' w'_v} + \bar{w}_v\overline{\rho' w'_u})\right] - \frac{1}{H^3}[u(\bar{\rho}\overline{w'_u w'_u} + 2w_u\overline{\rho' w'_u})$$

$$+ 2v(\bar{\rho}\overline{w'_u w'_v} + \bar{w}_u\overline{\rho' w'_v} + \bar{w}_v\overline{\rho' w'_u}) - u(\bar{\rho}\overline{w'_v w'_v} + 2\bar{w}_v\overline{\rho' w'_v})] \qquad \text{(III-75)}$$

For v-momentum,

$$\frac{\partial(\overline{\rho w_v})}{\partial t} + \frac{1}{H}\left[\frac{\partial}{\partial u}(\bar{\rho}\bar{w}_v\bar{w}_u) + \frac{\partial}{\partial v}(\bar{\rho}\bar{w}_v\bar{w}_v)\right] + \frac{1}{H^3}(-v\bar{\rho}\bar{w}_u\bar{w}_u + 2u\bar{\rho}\bar{w}_v\bar{w}_u + v\bar{\rho}\bar{w}_v\bar{w}_v) =$$

$$\frac{1}{H}\left(\frac{\partial\bar{\sigma}_{uv}}{\partial u} + \frac{\partial\bar{\sigma}_{vv}}{\partial v}\right) + \frac{1}{H^3}(-v\bar{\sigma}_{uu} + 2u\bar{\sigma}_{uv} + v\bar{\sigma}_{vv}) - \frac{1}{H}\left[\frac{\partial}{\partial u}(\bar{\rho}\overline{w'_u w'_v}\right.$$

$$\left. + \bar{w}_u\overline{\rho' w'_v} + \bar{w}_v\overline{\rho' w'_u}) + \frac{\partial}{\partial v}(\bar{\rho}\overline{w'_v w'_v} + 2\bar{w}_v\overline{\rho' w'_v})\right] - \frac{1}{H^3}[-v(\bar{\rho}\overline{w'_u w'_u}$$

$$+ 2\bar{w}_u\overline{\rho' w'_u}) + 2u(\bar{\rho}\overline{w'_u w'_v} + \bar{w}_u\overline{\rho' w'_v} + \bar{w}_v\overline{\rho' w'_u}) + v(\bar{\rho}\overline{w'_v w'_v} + 2\bar{w}_v\overline{\rho' w'_v})] \qquad \text{(III-76)}$$

Notice should be taken that the time derivative term in each of the four preceding equations actually consists of two terms based on the expansion procedure outlined in Appendix B. For *compactness*, however, in the momentum equations (and also in the energy equation) these terms are written in the Van Driest form.

In Equations (III-73), (III-74), (III-75), and (III-76), the well-known Reynolds or turbulent stresses can be identified in the form of double correlation terms involving velocity components. Of special significance is the fact that in both coordinate systems each turbulent stress is the exact counterpart of an ordinary viscous stress. For convenience the following notation is introduced:

$$\bar{\tau}_{xx} \equiv -\overline{\rho w'_x w'_x} \qquad \text{(III-77)}$$

$$\bar{\tau}_{xy} \equiv -\overline{\rho w'_x w'_y} \qquad \text{(III-78)}$$

$$\bar{\tau}_{yy} \equiv -\overline{\rho w'_y w'_y} \qquad \text{(III-79)}$$

$$\bar{\tau}_{uu} \equiv -\overline{\rho w'_u w'_u} \qquad \text{(III-80)}$$

$$\bar{\tau}_{uv} \equiv -\overline{\rho w'_u w'_v} \qquad \text{(III-81)}$$

$$\bar{\tau}_{vv} \equiv -\overline{\rho w'_v w'_v} \qquad \text{(III-82)}$$

It is important to note that the turbulent stresses as defined here do not correspond to those defined by Van Driest [37], which are in common use. The reason for using these different definitions is to provide for a more exact analogy between the turbulent and molecular transport terms.

In addition to the turbulent stresses, certain other terms occur involving the product of the turbulent mass diffusion terms and the mean velocity components. These terms also produce momentum fluxes which may be interpreted as stresses. If the definitions for turbulent mass diffusion and turbulent stresses are introduced into the time-averaged momentum equations is rectangular coordinates the results are

$$\frac{\partial(\overline{\rho w}_x)}{\partial t} + \frac{\partial(\bar{\rho}\bar{w}_x\bar{w}_x)}{\partial x} + \frac{\partial(\bar{\rho}\bar{w}_x\bar{w}_y)}{\partial y} = \frac{\partial}{\partial x}(\bar{\sigma}_{xx}+\bar{\tau}_{xx}-2\bar{w}_x\bar{m}_x)$$

$$+ \frac{\partial}{\partial y}(\bar{\sigma}_{xy}+\bar{\tau}_{xy}-\bar{w}_x\bar{m}_y-\bar{w}_y\bar{m}_x) \qquad \text{(III-83)}$$

and

$$\frac{\partial(\overline{\rho w}_y)}{\partial t} + \frac{\partial}{\partial x}(\bar{\rho}\bar{w}_y\bar{w}_x) + \frac{\partial}{\partial y}(\bar{\rho}\bar{w}_y\bar{w}_y) = \frac{\partial}{\partial x}(\bar{\sigma}_{xy}+\bar{\tau}_{xy}-\bar{w}_y\bar{m}_x-\bar{w}_x\bar{m}_y)$$

$$+ \frac{\partial}{\partial y}(\bar{\sigma}_{yy}+\bar{\tau}_{yy}-2\bar{w}_y\bar{m}_y) \qquad \text{(III-84)}$$

In parabolic coordinates, substitution of these definitions for turbulent mass diffusion and turbulent stresses into the time-averaged momentum equations produces

$$\frac{\partial(\overline{\rho w}_u)}{\partial t} + \frac{1}{H}\left[\frac{\partial}{\partial u}(\bar{\rho}\bar{w}_u\bar{w}_u) + \frac{\partial}{\partial v}(\bar{\rho}\bar{w}_u\bar{w}_v)\right] + \frac{1}{H^3}(u\bar{\rho}\bar{w}_u\bar{w}_u+2v\bar{\rho}\bar{w}_u\bar{w}_v$$

$$-u\bar{\rho}\bar{w}_v\bar{w}_v) = \frac{1}{H}\left[\frac{\partial}{\partial u}(\bar{\sigma}_{uu}+\bar{\tau}_{uu}-2\bar{w}_u\bar{m}_u) + \frac{\partial}{\partial v}(\bar{\sigma}_{uv}+\bar{\tau}_{uv}-\bar{w}_u\bar{m}_v\right.$$

$$-\bar{w}_v\bar{m}_u)\Big] + \frac{1}{H^3}\left[u(\bar{\sigma}_{uu}+\bar{\tau}_{uu}-2\bar{w}_u\bar{m}_u) + 2v(\bar{\sigma}_{uv}+\bar{\tau}_{uv}-\bar{w}_u\bar{m}_v-\bar{w}_v\bar{m}_u)\right.$$

$$\left. - u(\bar{\sigma}_{vv}+\bar{\tau}_{vv}-2\bar{w}_v\bar{m}_v)\right] \qquad \text{(III-85)}$$

and

$$\frac{\partial(\overline{\rho w}_v)}{\partial t} + \frac{1}{H}\left[\frac{\partial}{\partial u}(\bar{\rho}\bar{w}_v\bar{w}_u) + \frac{\partial}{\partial v}(\bar{\rho}\bar{w}_v\bar{w}_v)\right] + \frac{1}{H^3}(-v\bar{\rho}\bar{w}_u\bar{w}_u+2u\bar{\rho}\bar{w}_u\bar{w}_v$$

$$+v\bar{\rho}\bar{w}_v\bar{w}_v) = \frac{1}{H}\left[\frac{\partial}{\partial u}(\bar{\sigma}_{uv}+\bar{\tau}_{uv}-\bar{w}_u\bar{m}_v-\bar{w}_v\bar{m}_u) + \frac{\partial}{\partial v}(\bar{\sigma}_{vv}+\bar{\tau}_{vv}\right.$$

$$\left.-2\bar{w}_v\bar{m}_v)\right] + \frac{1}{H^3}\left[-v(\sigma_{uu}+\tau_{uu}-2\bar{w}_u\bar{m}_u) + 2u(\bar{\sigma}_{uv}+\bar{\tau}_{uv}-\bar{w}_u\bar{m}_v-\bar{w}_v\bar{m}_u)\right.$$

$$\left. + v(\bar{\sigma}_{vv}+\bar{\tau}_{vv}-2\bar{w}_v\bar{m}_v)\right] \qquad \text{(III-86)}$$

Development of the time-averaged energy equation, as described in Appendix B, proceeds along lines similar to those used in the momentum equations. For rectangular coordinates the result is

$$\frac{\partial}{\partial t}(\bar{\rho}\bar{e}_o) + \frac{\partial}{\partial x}(\bar{\rho}\bar{e}_o\bar{w}_x) + \frac{\partial}{\partial y}(\bar{\rho}\bar{e}_o\bar{w}_y) = -\left(\frac{\partial\bar{q}_x}{\partial x} + \frac{\partial\bar{q}_y}{\partial y}\right) + \frac{\partial}{\partial x}(\bar{\sigma}_{xx}\bar{w}_x+\bar{\sigma}_{xy}\bar{w}_y)$$

$$+ \frac{\partial}{\partial y}(\bar{\sigma}_{xy}\bar{w}_x+\bar{\sigma}_{yy}\bar{w}_y) - \frac{\partial}{\partial x}(\bar{\rho}\overline{h'w'_x}+\bar{\rho}\overline{w'_xw'_x}\bar{w}_x+\bar{\rho}\overline{w'_xw'_y}\bar{w}_y+\bar{e}_o\overline{\rho'w'_x}$$

$$+\bar{w}_x\bar{w}_x\overline{\rho'w'_x}+\bar{w}_x\bar{w}_y\overline{\rho'w'_y}+\bar{w}_xc_v\overline{\rho't'}) - \frac{\partial}{\partial y}(\bar{\rho}\overline{h'w'_y}+\bar{\rho}\overline{w'_xw'_y}\bar{w}_x+\bar{\rho}\overline{w'_yw'_y}\bar{w}_y$$

$$+\bar{e}_o\overline{\rho'w'_y}+\bar{w}_x\bar{w}_y\overline{\rho'w'_x}+\bar{w}_y\bar{w}_y\overline{\rho'w'_y}+\bar{w}_yc_v\overline{\rho'T'}) \qquad \text{(III-87)}$$

The time-averaged energy equation in parabolic coordinates is

$$\frac{\partial}{\partial t}(\overline{\rho e_o}) + \frac{1}{H}\left[\frac{\partial}{\partial u}(\bar{\rho}\bar{e}_o\bar{w}_u) + \frac{\partial}{\partial v}(\bar{\rho}\bar{e}_o\bar{w}_v)\right] + \frac{1}{H^3}(u\bar{\rho}\bar{e}_o\bar{w}_u + v\bar{\rho}\bar{e}_o\bar{w}_v)$$

$$= -\frac{1}{H}\left(\frac{\partial \bar{q}_u}{\partial u} + \frac{\partial \bar{q}_v}{\partial v}\right) - \frac{1}{H^3}(u\bar{q}_u + v\bar{q}_v) + \frac{1}{H}\left[\frac{\partial}{\partial u}(\bar{\sigma}_{uu}\bar{w}_u\right.$$

$$\left. + \bar{\sigma}_{uv}\bar{w}_v) + \frac{\partial}{\partial v}(\bar{\sigma}_{uv}\bar{w}_u + \bar{\sigma}_{vv}\bar{w}_v)\right] + \frac{1}{H^3}[u(\bar{\sigma}_{uu}\bar{w}_u + \bar{\sigma}_{uv}\bar{w}_v)$$

$$+ v(\bar{\sigma}_{uv}\bar{w}_u + \bar{\sigma}_{vv}\bar{w}_v)] - \frac{1}{H}\left[\frac{\partial}{\partial u}(\bar{\rho}\overline{h'w'_u} + \bar{\rho}\overline{w'_u w'_u}\bar{w}_u + \overline{w'_u w'_v}\bar{w}_v\right.$$

$$\left. + \bar{e}_o\overline{\rho' w'_u} + \bar{w}_u\bar{w}_u\overline{\rho' w'_u} + \bar{w}_u\bar{w}_v\overline{\rho' w'_v} + \bar{w}_u c_v\overline{\rho' T'}) + \frac{\partial}{\partial v}(\bar{\rho}\overline{h'w'_v}\right.$$

$$\left. + \bar{\rho}\overline{w'_u w'_v}\bar{w}_u + \bar{\rho}\overline{w'_v w'_v}\bar{w}_v + \bar{e}_o\overline{\rho' w'_v} + \bar{w}_u\bar{w}_v\overline{\rho' w'_u} + \bar{w}_v\bar{w}_v\overline{\rho' w'_v} + \bar{w}_v c_v\overline{\rho' T'})\right]$$

$$- \frac{1}{H^3}[u(\bar{\rho}\overline{h'w'_u} + \bar{\rho}\overline{w'_u w'_u}\bar{w}_u + \bar{\rho}\overline{w'_u w'_v}\bar{w}_v + \bar{e}_o\overline{\rho' w'_u} + \bar{w}_u\bar{w}_u\overline{\rho' w'_u}$$

$$+ \bar{w}_u\bar{w}_v\overline{\rho' w'_v} + \bar{w}_u c_v\overline{\rho' T'}) + v(\bar{\rho}\overline{h'w'_v} + \bar{\rho}\overline{w'_u w'_v}\bar{w}_u + \bar{\rho}\overline{w'_v w'_v}\bar{w}_v + \bar{e}_o\overline{\rho' w'_v}$$

$$+ \bar{w}_u\bar{w}_v\overline{\rho' w'_u} + \bar{w}_v\bar{w}_v\overline{\rho' w'_v} + \bar{w}_v c_v\overline{\rho' T'})] \qquad \text{(III-88)}$$

Inspection of the energy equation in both coordinate systems reveals the presence of terms based both on turbulent mass diffusion and turbulent stresses. Two additional types of double-correlation terms can also be identified. One type involves the product $c_v\overline{\rho' T'}$. Based on the time-averaged equation of state,

$$\overline{\rho' T'} = \bar{p}_t / R \tag{III-89}$$

Thus for the double correlation term under consideration,

$$c_v \overline{\rho' T'} = c_v \bar{p}_t / R \tag{III-90}$$

When multiplied by a velocity component, as occurs in Equation (III-86) and (III-88), this first type of double correlation term can be seen to represent a form of turbulent flow work, resulting from the compressibility of the fluid.

The second type of terms represents turbulent energy transfer. In rectangular coordinate these terms are $\bar{\rho}\overline{h' w_x'}$ and $\bar{\rho}\overline{h' w_y'}$, while in parabolic coordinates the corresponding terms are $\bar{\rho}\overline{h' w_u'}$ and $\bar{\rho}\overline{h' w_v'}$. Each of these terms can be seen to represent an exact analogy to a molecular energy transport term. For brevity the following definitions are introduced:

$$\bar{r}_x \equiv \bar{\rho}\overline{h' w_x'} \tag{III-91}$$

$$\bar{r}_y \equiv \bar{\rho}\overline{h' w_y'}$$

$$\bar{r}_u \equiv \bar{\rho}\overline{h' w_u'} \tag{III-93}$$

$$\bar{r}_v \equiv \bar{\rho}\overline{h' w_v'} \tag{III-94}$$

Based on the defining relations for the various turbulent terms, in rectangular the time-averaged energy equation can be written as

$$\frac{\partial(\overline{\rho e}_o)}{\partial t} + \frac{\partial}{\partial x}(\bar{\rho}\bar{e}_o\bar{w}_x) + \frac{\partial}{\partial y}(\bar{\rho}\bar{e}_o\bar{w}_y) = \frac{\partial}{\partial x}[-(\bar{q}_x+\bar{r}_x) + (\bar{\sigma}_{xx}+\bar{\tau}_{xx})\bar{w}_x$$

$$+ (\bar{\sigma}_{xy}+\bar{\tau}_{xy})\bar{w}_y - \bar{e}_o\bar{m}_x - \bar{w}_x(\bar{w}_x\bar{m}_x+\bar{w}_y\bar{m}_y+c_v\bar{p}_t/R)]$$

$$+ \frac{\partial}{\partial y}[-(\bar{q}_y+\bar{r}_y) + (\bar{\sigma}_{xy}+\bar{\tau}_{xy})\bar{w}_x + (\bar{\sigma}_{yy}+\bar{\tau}_{yy})\bar{w}_y - \bar{e}_o\bar{m}_y$$

$$- \bar{w}_y(\bar{w}_x\bar{m}_x+\bar{w}_y\bar{m}_y+c_v\bar{p}_t/R)] \qquad \text{(III-95)}$$

In like fashion in parabolic coordinates,

$$\frac{\partial}{\partial t}(\overline{\rho e}_o) + \frac{1}{H}\left[\frac{\partial}{\partial u}(\bar{\rho}\bar{e}_o\bar{w}_u) + \frac{\partial}{\partial v}(\bar{\rho}\bar{e}_o\bar{w}_v)\right] + \frac{1}{H^3}(u\bar{\rho}\bar{e}_o\bar{w}_u+v\bar{\rho}\bar{e}_o\bar{w}_v)$$

$$= \frac{1}{H}\left\{\frac{\partial}{\partial u}[-(\bar{q}_u+\bar{r}_u) + (\bar{\sigma}_{uu}+\bar{\tau}_{uu})\bar{w}_u + (\bar{\sigma}_{uv}+\bar{\tau}_{uv})\bar{w}_v - \bar{e}_o\bar{m}_u\right.$$

$$- \bar{w}_u(\bar{w}_u\bar{m}_u+\bar{w}_v\bar{m}_v+c_v\bar{p}_t/R)] + \frac{\partial}{\partial v}[-(q_v+\bar{r}_v) + (\bar{\sigma}_{uv}+\bar{\tau}_{uv})\bar{w}_u$$

$$\left. + (\bar{\sigma}_{vv}+\bar{\tau}_{vv})\bar{w}_v - \bar{e}_o\bar{m}_v - \bar{w}_v(\bar{w}_u\bar{m}_u+\bar{w}_v\bar{m}_v+c_v\bar{p}_t/R)]\right\}$$

$$+ \frac{1}{H^3}\left\{u[-(\bar{q}_u+\bar{r}_u) + (\bar{\sigma}_{uu}+\bar{\tau}_{uu})\bar{w}_u + (\bar{\sigma}_{uv}+\bar{\tau}_{uv})\bar{w}_v\right.$$

$$\left. - \bar{e}_o\bar{m}_u - \bar{w}_u(\bar{w}_u\bar{m}_u+\bar{w}_v\bar{m}_v+c_v\bar{p}_t/R)] + v[-(\bar{q}_v+\bar{r}_v)\right.$$

$$+ (\bar{\sigma}_{uv}+\bar{\tau}_{uv})\bar{w}_u + (\bar{\sigma}_{vv}+\bar{\tau}_{vv})\bar{w}_v - \bar{e}_o\bar{m}_v$$

$$- w_v(\bar{w}_u\bar{m}_u+\bar{w}_v\bar{m}_v+c_vp_t/R)]\} \qquad \text{(III-96)}$$

Equations (III-62), (III-71), (III-72), (III-83), (III-84), (III-85), (III-86), (III-95), and (III-96) represent the time-averaged *equations* which form the bases for further development of the analytical model.

Conservation-Law Form

Based on the approach proposed by Lax and Wendroff [62], and also used by others [63,64,65,68,70,72,82], the time-averaged equations for the conservation of mass, momentum, and energy can be written in a simple vector (or matrix) form. For rectangular coordinates the conservation-law form is

$$\frac{\partial A_i}{\partial t} + \frac{\partial B_i}{\partial x} + \frac{\partial C_i}{\partial y} = 0 \qquad \text{(III-97)}$$

where

$$A_i = \begin{bmatrix} \bar{\rho} \\ \overline{\rho w}_x \\ \overline{\rho w}_y \\ \overline{\rho e}_o \end{bmatrix} \qquad \text{(III-98)}$$

$$B_i = \begin{bmatrix} \bar{\rho}\bar{w}_x + \bar{m}_x \\ \bar{\rho}\bar{w}_x\bar{w}_x - \bar{\sigma}_{xx} - \bar{\tau}_{xx} + 2\bar{w}_x\bar{m}_x \\ \bar{\rho}\bar{w}_y\bar{w}_x - \bar{\sigma}_{xy} - \bar{\tau}_{xy} + \bar{w}_y\bar{m}_x + \bar{w}_x\bar{m}_y \\ \bar{\rho}\bar{e}_o\bar{w}_x + \bar{q}_x + \bar{r}_x - (\bar{\sigma}_{xx}+\bar{\tau}_{xx})\bar{w}_x - (\bar{\sigma}_{xy}+\bar{\tau}_{xy})\bar{w}_y + \bar{e}_o\bar{m}_x \\ \qquad + \bar{w}_x(\bar{w}_x\bar{m}_x+\bar{w}_y\bar{m}_y+c_v\bar{p}_t/R) \end{bmatrix} \qquad \text{(III-99)}$$

$$C_i = \begin{bmatrix} \bar{\rho}\bar{w}_y + \bar{m}_y \\ \bar{\rho}\bar{w}_x\bar{w}_y - \bar{\sigma}_{xy} - \bar{\tau}_{xy} + \bar{w}_x\bar{m}_y + \bar{w}_y\bar{m}_x \\ \bar{\rho}\bar{w}_y\bar{w}_y - \bar{\sigma}_{yy} - \bar{\tau}_{yy} + 2\bar{w}_y\bar{m}_y \\ \bar{\rho}\bar{e}_o\bar{w}_y + \bar{q}_y + \bar{r}_y - (\bar{\sigma}_{xx}+\bar{\tau}_{xx})\bar{w}_x - (\bar{\sigma}_{yy}+\bar{\tau}_{yy})\bar{w}_y + \bar{e}_o\bar{m}_y \\ \qquad + \bar{w}_y(\bar{w}_x\bar{m}_x+\bar{w}_y\bar{m}_y+c_v\bar{p}_t/R) \end{bmatrix} \qquad \text{(III-100)}$$

In parabolic coordinates the conservation-law form is

$$\frac{\partial E_i}{\partial t} + \frac{1}{H^2}\frac{\partial(HF_i)}{\partial u} + \frac{1}{H^2}\frac{\partial(HG_i)}{\partial v} + \frac{\Gamma_i}{H^3} = 0 \qquad \text{(III-101)}$$

where

$$E_i = \begin{bmatrix} \bar{\rho} \\ \overline{\rho w}_u \\ \overline{\rho w}_v \\ \overline{\rho e}_o \end{bmatrix} \tag{III-102}$$

$$F_i = \begin{bmatrix} \bar{\rho}\bar{w}_u + \bar{m}_u \\ \bar{\rho}\bar{w}_u\bar{w}_u - \bar{\sigma}_{uu} - \bar{\tau}_{uu} + 2\bar{w}_u\bar{m}_u \\ \bar{\rho}\bar{w}_v\bar{w}_u - \bar{\sigma}_{uv} - \bar{\tau}_{uv} + \bar{w}_u\bar{m}_v + \bar{w}_v\bar{m}_u \\ \bar{\rho}\bar{e}_o\bar{w}_u + \bar{q}_u + \bar{r}_u - (\bar{\sigma}_{uu}+\bar{\tau}_{uu})\bar{w}_u - (\bar{\sigma}_{uv}+\bar{\tau}_{uv})\bar{w}_v + \bar{e}_o\bar{m}_u \\ \qquad + \bar{w}_u(\bar{w}_u\bar{m}_u+\bar{w}_v\bar{m}_v+c_v\bar{p}_t/R) \end{bmatrix} \tag{III-103}$$

$$G_i = \begin{bmatrix} \bar{\rho}\bar{w}_v + \bar{m}_v \\ \bar{\rho}\bar{w}_u\bar{w}_v - \bar{\sigma}_{uv} - \bar{\tau}_{uv} + \bar{w}_u\bar{m}_v + \bar{w}_v\bar{m}_u \\ \bar{\rho}\bar{w}_v\bar{w}_v - \bar{\sigma}_{vv} - \bar{\tau}_{vv} + 2\bar{w}_v\bar{m}_v \\ \bar{\rho}\bar{e}_o\bar{w}_v + \bar{q}_v + \bar{r}_v - (\bar{\sigma}_{uv} + \bar{\tau}_{uv})\bar{w}_u - (\bar{\sigma}_{vv}+\bar{\tau}_{vv})\bar{w}_v + \bar{e}_o\bar{m}_v \\ \qquad + \bar{w}_v(\bar{w}_u+\bar{w}_v\bar{m}_v+c_v\bar{p}_t/R) \end{bmatrix} \tag{III-104}$$

and

$$\Gamma_i = \begin{bmatrix} 0 \\ u(-\bar{\rho}\bar{w}_v\bar{w}_v+\bar{\sigma}_{vv}+\bar{\tau}_{vv}-2\bar{w}_v\bar{m}_v) + v(\bar{\rho}\bar{w}_u\bar{w}_v-\bar{\sigma}_{uv}-\bar{\tau}_{uv}+\bar{w}_u\bar{m}_v+\bar{w}_v\bar{m}_u) \\ u(\bar{\rho}\bar{w}_u\bar{w}_v-\bar{\sigma}_{uv}-\bar{\tau}_{uv}+\bar{w}_u\bar{m}_v+\bar{w}_v\bar{m}_u) + v(-\bar{\rho}\bar{w}_u\bar{w}_u+\bar{\sigma}_{uu}+\bar{\tau}_{uu}-2\bar{w}_u\bar{m}_u) \\ 0 \end{bmatrix} \qquad \text{(III-105)}$$

The numerical technique described in Chapter IV is based on the use of the preceding conservation-law form of the time-averaged equations.

Molecular Transport Models

The momentum and energy equations, as presented in the preceding subsection, are written in terms of viscous stresses $\bar{\sigma}_{ij}$ and molecular heat transfer $\bar{q}_i$. Based on the assumption that the gas is a Newtonian fluid the viscous stresses in rectangular coordinates can be written as

$$\bar{\sigma}_{xx} = -\bar{p}_s + 2\mu \frac{\partial \bar{w}_x}{\partial x} + \lambda\left(\frac{\partial \bar{w}_x}{\partial x} + \frac{\partial \bar{w}_y}{\partial y}\right) \qquad \text{(III-106)}$$

$$\bar{\sigma}_{xy} = \mu \left(\frac{\partial \bar{w}_x}{\partial y} + \frac{\partial \bar{w}_y}{\partial x}\right) \qquad \text{(III-107)}$$

$$\bar{\sigma}_{yy} = -\bar{p}_s + 2\mu \frac{\partial \bar{w}_y}{\partial y} + \lambda \left(\frac{\partial \bar{w}_x}{\partial x} + \frac{\partial \bar{w}_y}{\partial y}\right) \qquad \text{(III-108)}$$

In parabolic coordinates for a Newtonian fluid the viscous stresses are

$$\bar{\sigma}_{uu} = -\bar{p}_s + \frac{2\mu}{H}\left(\frac{\partial \bar{w}_u}{\partial u} + \frac{v\bar{w}_v}{H^2}\right) + \frac{\lambda}{H}\left(\frac{\partial \bar{w}_u}{\partial u} + \frac{\partial \bar{w}_v}{\partial v} + \frac{u\bar{w}_u + v\bar{w}_v}{H^2}\right) \quad \text{(III-109)}$$

$$\bar{\sigma}_{uv} = \frac{\mu}{H}\left(\frac{\partial \bar{w}_v}{\partial u} + \frac{\partial \bar{w}_u}{\partial v} - \frac{u\bar{w}_v + v\bar{w}_u}{H^2}\right) \quad \text{(III-110)}$$

$$\bar{\sigma}_{vv} = -\bar{p}_s + \frac{2\mu}{H}\left(\frac{\partial \bar{w}_v}{\partial v} + \frac{u\bar{w}_u}{H^2}\right) + \frac{\lambda}{H}\left(\frac{\partial \bar{w}_u}{\partial u} + \frac{\partial \bar{w}_v}{\partial v} + \frac{u\bar{w}_u + v\bar{w}_v}{H^2}\right) \quad \text{(III-111)}$$

For molecular heat transfer, based on Fourier's Law in rectangular coordinates,

$$\bar{q}_x = -k\frac{\partial \bar{T}}{\partial x} \quad \text{(III-112)}$$

$$\bar{q}_y = -k\frac{\partial \bar{T}}{\partial y} \quad \text{(III-113)}$$

In parabolic coordinates the relations are

$$\bar{q}_u = -\frac{k}{H}\frac{\partial \bar{T}}{\partial u} \quad \text{(III-114)}$$

$$\bar{q}_v = -\frac{k}{H}\frac{\partial \bar{T}}{\partial v} \quad \text{(III-115)}$$

Equations (III-106) through (III-115) represent the molecular transport models which are incorporated into the overall analytical model.

Turbulent Transport Models

As noted in Chapter II, for the problem under consideration the phenomenological approach to turbulent transport processes appears most suitable. By such a method the turbulent mass diffusion $\bar{m}_i$, turbulent stresses $\bar{\tau}_{ij}$, and turbulent heat transfer $\bar{F}_i$, can be related to components of the density, velocity, and temperature gradients, based on the introduction of eddy mass diffusivity, ϵ_ρ, eddy viscosity ϵ_m, and eddy thermal diffusivity ϵ_h.

The turbulent mass diffusion terms represent a *self-diffusion* process. Thus the eddy mass diffusivity is a *turbulent self-diffusion coefficient* which for simplicity is assumed to be a scalar. By analogy with molecular self-diffusion, based on Fick's Law [93], in rectangular coordinates,

$$\bar{m}_x = -\epsilon_\rho \frac{\partial \bar{\rho}}{\partial x} \qquad \text{(III-116)}$$

$$\bar{m}_y = -\epsilon_\rho \frac{\partial \bar{\rho}}{\partial y} \qquad \text{(III-117)}$$

Likewise in parabolic coordinates,

$$\bar{m}_u = -\frac{\epsilon_\rho}{H} \frac{\partial \bar{\rho}}{\partial u} \qquad \text{(III-118)}$$

$$\bar{m}_v = -\frac{\epsilon_\rho}{H} \frac{\partial \bar{\rho}}{\partial v} \qquad \text{(III-119)}$$

Based on the relation proposed by Boussinseq [23], with the

refinement suggested by Hinze [22], the turbulent stress relations in rectangular coordinates are assumed to be of the form

$$\bar{\tau}_{xx} = -\bar{p}_t + 2\bar{\rho}\epsilon_m \frac{\partial \bar{w}_x}{\partial x} - \frac{2}{3}\bar{\rho}\epsilon_m \left(\frac{\partial \bar{w}_x}{\partial x} + \frac{\partial \bar{w}_y}{\partial y}\right) \qquad \text{(III-120)}$$

$$\bar{\tau}_{xy} = \bar{\rho}\epsilon_m \left(\frac{\partial \bar{w}_x}{\partial y} + \frac{\partial \bar{w}_y}{\partial x}\right) \qquad \text{(III-121)}$$

$$\bar{\tau}_{yy} = -\bar{p}_t + 2\bar{\rho}\epsilon_m \frac{\partial \bar{w}_y}{\partial y} - \frac{2}{3}\bar{\rho}\epsilon_m \left(\frac{\partial \bar{w}_x}{\partial x} + \frac{\partial \bar{w}_y}{\partial y}\right) \qquad \text{(III-122)}$$

In parabolic coordinates the corresponding relations are

$$\bar{\tau}_{uu} = -\bar{p}_t + \frac{2\bar{\rho}\epsilon_m}{H}\left(\frac{\partial \bar{w}_u}{\partial u} + \frac{v\bar{w}_v}{H^2}\right) - \frac{2}{3}\frac{\bar{\rho}\epsilon_m}{H}\left(\frac{\partial \bar{w}_u}{\partial u} + \frac{\partial \bar{w}_v}{\partial v} + \frac{u\bar{w}_u + v\bar{w}_v}{H^2}\right) \qquad \text{(III-123)}$$

$$\bar{\tau}_{uv} = \bar{\rho}\frac{\epsilon_m}{H}\left(\frac{\partial \bar{w}_v}{\partial u} + \frac{\partial \bar{w}_u}{\partial v} - \frac{u\bar{w}_v + v\bar{w}_u}{H^2}\right) \qquad \text{(III-124)}$$

$$\bar{\tau}_{vv} = -\bar{p}_t + 2\frac{\bar{\rho}\epsilon_m}{H}\left(\frac{\partial \bar{w}_v}{\partial v} + \frac{u\bar{w}_u}{H^2}\right) - \frac{2}{3}\frac{\bar{\rho}\epsilon_m}{H}\left(\frac{\partial \bar{w}_u}{\partial u} + \frac{\partial \bar{w}_v}{\partial v} + \frac{u\bar{w}_u + v\bar{w}_v}{H^2}\right) \qquad \text{(III-125)}$$

Notice should be taken that the turbulent normal stresses $\bar{\tau}_{xx}$, $\bar{\tau}_{yy}$, $\bar{\tau}_{uu}$, and $\bar{\tau}_{vv}$, each represent a portion of the kinetic energy of the turbulence. In this regard, although the problem under consideration is two-dimensional, the turbulent kinetic energy is three-dimensional in nature, as noted by the expansion of $\bar{e}_o$ given in Appendix B. Thus for the calculation of the kinetic energy component, $\overline{w'_z w'_z}/2$, the following definition applies

$$\bar{\tau}_{zz} \equiv -\overline{\rho w'_z w'_z} \qquad \text{(III-126)}$$

In rectangular coordinates the relation for $\bar{\tau}_{zz}$ is assumed to be

$$\bar{\tau}_{zz} = -\bar{p}_t - \frac{2}{3}\bar{\rho}\epsilon_m \left(\frac{\partial \bar{w}_x}{\partial x} + \frac{\partial \bar{w}_y}{\partial y}\right) \qquad \text{(III-127)}$$

Likewise in parabolic coordinates

$$\bar{\tau}_{zz} = -\bar{p}_t - \frac{2}{3}\frac{\bar{\rho}\epsilon_m}{H}\left(\frac{\partial \bar{w}_u}{\partial u} + \frac{\partial \bar{w}_v}{\partial v} + \frac{u\bar{w}_u + v\bar{w}_v}{H^2}\right) \qquad \text{(III-128)}$$

The turbulent pressure $\bar{p}_t$ which appears in all expressions for turbulent normal stresses, can be seen to be equal to two-thirds of the kinetic energy of turbulence. Although $\bar{p}_t$ is defined by Equation (III-64) no simple method for directly evaluating the product $\overline{\rho' T'}$ appears to exist. The ratio of the kinetic energy to the absolute value of the turbulent shear stress, however, has been measured for various two-dimensional flow-fields. For each case the ratio appears essentially constant except along lines of symmetry and in laminar sublayers. This ratio for turbulent boundary layers was found to be 3.3 by Klebanoff [94]. For a plane turbulent jet the value 3.75 was obtained by Bradbury [21]. For turbulent flow in a pipe Laufer [44] reported a value of 3.57. Based on these experimentally determined ratios, a simple relation between turbulent pressure and the absolute value of the turbulent shear stress is assumed. In the slot flow,

$$\bar{p}_t = 2.38|\bar{\tau}_{xy}| \qquad \text{(III-129)}$$

For the free-flow region,

$$\bar{p}_t = 2.35|\bar{\tau}_{uv}| \qquad \text{(III-130)}$$

The two preceding relations are assumed to hold except at the wall and along the slot or jet centerline. For the case at the wall the turbulent pressure is zero. In the vicinity of lines of symmetry the turbulent pressure appears to be relatively constant with respect to transverse position [21,44]. Thus the turbulent pressure along the jet or slot axis can be set equal to the value obtained at a neighboring point in the vicinity of the axis.

Notice should be taken that by means of the preceding relations both the turbulent pressure and the turbulent kinetic energy can be calculated. Furthermore such relation, although approximate, always yields positive values for both quantities. This feature is obviously consistent with physical reality.

For the turbulent transport of energy, based on Hinze, for rectangular coordinates

$$\bar{r}_x = -\bar{\rho} c_p \epsilon_h \frac{\partial \bar{T}}{\partial x} \qquad \text{(III-131)}$$

$$\bar{r}_y = -\bar{\rho} c_p \epsilon_h \frac{\partial \bar{T}}{\partial y} \qquad \text{(III-132)}$$

For parabolic coordinates, the relations are

$$\bar{r}_u = -\bar{\rho} c_p \frac{\epsilon_h}{H} \frac{\partial \bar{T}}{\partial u} \qquad \text{(III-133)}$$

$$\bar{r}_v = -\bar{\rho} c_p \frac{\epsilon_h}{H} \frac{\partial \bar{T}}{\partial v} \qquad \text{(III-134)}$$

Comparison of the turbulent stress and heat transfer models with their molecular transport counterparts reveals an exact analogy between the two. Thus the total transport of momentum and energy can be expressed in rectangular coordinates as

$$(\bar{\sigma}_{xx}+\bar{\tau}_{xx}) = -(\bar{p}_s+\bar{p}_t) + 2(\mu+\bar{\rho}\epsilon_m) \frac{\partial \bar{w}_x}{\partial x} + (\lambda - \frac{2\bar{\rho}\epsilon_m}{3})(\frac{\partial \bar{w}_x}{\partial x} + \frac{\partial \bar{w}_y}{\partial y}) \qquad \text{(III-135)}$$

$$(\bar{\sigma}_{xy}+\bar{\tau}_{xy}) = (\mu+\bar{\rho}\epsilon_m)(\frac{\partial \bar{w}_x}{\partial y} + \frac{\partial \bar{w}_y}{\partial x}) \qquad \text{(III-136)}$$

$$(\bar{\sigma}_{yy}+\bar{\tau}_{yy}) = -(\bar{p}_s+\bar{p}_t) + 2(\mu+\bar{\rho}\epsilon_m) \frac{\partial \bar{w}_y}{\partial y} + (\lambda - \frac{2\bar{\rho}\epsilon_m}{3})(\frac{\partial \bar{w}_x}{\partial x} + \frac{\partial \bar{w}_y}{\partial y}) \qquad \text{(III-137)}$$

$$(\bar{q}_x+\bar{r}_x) = -(k+\bar{\rho} c_p \epsilon_q) \frac{\partial \bar{T}}{\partial x} \qquad \text{(III-138)}$$

$$(\bar{q}_y+\bar{r}_y) = -(k+\bar{\rho} c_p \epsilon_q) \frac{\partial \bar{T}}{\partial x} \qquad \text{(III-139)}$$

In parabolic coordinates the total transport expressions are

$$(\bar{\sigma}_{uu}+\bar{\tau}_{uu}) = -(\bar{p}_s+\bar{p}_t) + \frac{2(\mu+\bar{\rho}\epsilon_m)}{H}\left(\frac{\partial \bar{w}_u}{\partial u} + \frac{v\bar{w}_v}{H^2}\right)$$

$$+ \frac{(\lambda-2\bar{\rho}\epsilon_m/3)}{H}\left(\frac{\partial \bar{w}_u}{\partial u} + \frac{\partial \bar{w}_v}{\partial v} + \frac{u\bar{w}_u+v\bar{w}_v}{H^2}\right) \qquad \text{(III-140)}$$

$$(\bar{\sigma}_{uv}+\bar{\tau}_{uv}) = \left(\frac{\mu+\bar{\rho}\epsilon_m}{H}\right)\left(\frac{\partial \bar{w}_v}{\partial u} + \frac{\partial \bar{w}_u}{\partial v} - \frac{u\bar{w}_v+v\bar{w}_u}{H^2}\right) \qquad \text{(III-141)}$$

$$(\bar{\sigma}_{vv}+\bar{\tau}_{vv}) = -(\bar{p}_s+\bar{p}_t) + \frac{2(\mu+\bar{\rho}\epsilon_m)}{H}\left(\frac{\partial \bar{w}_v}{\partial v} + \frac{u\bar{w}_u}{H^2}\right)$$

$$+ \frac{(\lambda-2\bar{\rho}\epsilon_m/3)}{H}\left(\frac{\partial \bar{w}_u}{\partial u} + \frac{\partial \bar{w}_v}{\partial v} + \frac{u\bar{w}_u+v\bar{w}_v}{H^2}\right) \qquad \text{(III-142)}$$

$$(\bar{q}_u+\bar{r}_u) = -\frac{(k+\bar{\rho}c_p\epsilon_h)}{H}\frac{\partial \bar{T}}{\partial u} \qquad \text{(III-143)}$$

$$(\bar{q}_v+\bar{r}_v) = -\frac{(k+\bar{\rho}c_p\epsilon_h)}{H}\frac{\partial \bar{T}}{\partial v} \qquad \text{(III-144)}$$

In general all molecular transport terms are small compared with their turbulent counterparts (except for the normal stresses). In certain regions, however, such as near the wall, the molecular terms dominate and cannot be neglected. Furthermore, there exists the possibility that the analytical model under development may be used for laminar flow as well as for turbulent flow. For these reasons, the molecular terms are retained.

Variation of Molecular Transport Properties

For the variation of molecular viscosity (the first coefficient of viscosity), Sutherland's formula in the form suggest by Van Driest

[37] is used as follows:

$$\mu = \mu_{ref}(T/T_{ref})^{3/2} \frac{1.505T_{ref}}{T + 0.505T_{ref}} \qquad \text{(III-145)}$$

The second coefficient of molecular viscosity presents a peculiar problem. This coefficient is defined as

$$\lambda = -2\mu/3+\mu_B \qquad \text{(III-146)}$$

where μ_B represents the bulk viscosity. For monatomic gases in equilibrium the bulk viscosity is zero [89]. For non-equilibrium processes with gases which are not monatomic, μ_B has been found to be non-zero. For nitrogen at moderate temperatures, Lighthill [95] found μ_B to have a value of 0.8μ. In regions of rarefaction, as well as in shock waves, bulk viscosity can play a significant role [96] and for this reason the assumption is made for the fluid in the current problem

$$\mu_B = 0.8\mu \qquad \text{(III-147)}$$

Notice should be taken that with a nonzero value of bulk viscosity the equilibrium pressure $\bar{p}_s$ is not equal to the mean of the viscous normal stresses. Instead, the latter will be less than $\bar{p}_s$ during rarefaction and greater than $\bar{p}_s$ during compression.

For simplicity in the calculation of other thermophysical properties the Prandtl number, N_{Pr}, is assumed to be a constant. For a

calorically perfect gas the specific heat, c_p, is also constant. Thus the thermal conductivity can be obtained from the relation

$$k = \mu c_p / N_{Pr} \qquad \text{(III-148)}$$

Other thermophysical properties such as kinematic viscosity and thermal diffusivity can be obtained based on their definition, coupled with Equations (III-145) through (III-148).

Variation of Turbulent Transport Properties

Calculation of the turbulent properties is much more involved than calculation of the molecular properties, because the former depend largely on the velocity gradients in the flow and also on the distance from the wall. As noted in Chapter II there exist three types of turbulent flows in the current problem: free jet, boundary layer, and slot. According to the fundamentals of the phenomenological approach for a turbulent boundary layer

$$\epsilon_m = \ell^2 \left| \frac{\partial \bar{w}_x}{\partial y} \right| \qquad \text{(III-149)}$$

The same type of relation can be written for a slot or a free jet. Unfortunately the mixing length is not a constant and no theory of the general variation of this parameter appears to exist. Furthermore, in both jets and slots, terms of the form $|\partial \bar{w}_x / \partial y|$ do not appear to represent the true functions of velocity upon which eddy viscosity depends. An examination of the general variation of eddy viscosity in the three

types of flow under consideration, as experimentally observed [21,44, 94], reveals that the *absolute value of the Laplacian of the magnitude of the velocity* $|\nabla^2\bar{w}|$ exhibits a variation quite similar to that of eddy viscosity. Thus this parameter $|\nabla^2\bar{w}|$ may represent the basis for a more general model for eddy viscosity. Development of such a model, however, is considered beyond the scope of the current study.

For the reasons noted the necessity arises for the use of semi-empirical expressions for the calculation of eddy viscosity in each of the three types of turbulent flow. Once the eddy viscosity is known, calculation of eddy mass diffusivity and eddy thermal diffusivity can be accomplished based on known or measured values for the turbulent Schmidt number and turbulent Prandtl number.

Calculation of Jet Eddy Viscosity

No data for the variation of eddy viscosity in a deflected jet exist, with the possible exception of the results presented by Sawyer [52] and Endo [20]. In each of these two investigations the eddy viscosity along the jet centerline was assumed to vary according to the relation developed by Goertler [20] for a plane jet,

$$(\epsilon_m)_j = 0.0325b|\bar{w}_{jc\ell}-w_\infty| \qquad \text{(III-150)}$$

where $b = 0.130y$.

Neither Sawyer nor Endo assumed a transverse variation of eddy viscosity but both considered that the turbulent shear stress would be affected by the curvature of the jet, and for this reason both investigators

introduced a semi-empirical constant, C, as shown in Equation (II-39). Endo's predicted velocity profile, as already noted, gave good agreement with his experimental data. In Appendix C an analysis of Endo's data is presented. This analysis reveals that, by use of the precise analogy between laminar and turbulent shear stresses in orthogonal curvilinear coordinates, a radial variation of eddy viscosity can be deduced from Endo's results. The variation can be best expressed as a function of the transverse gradient of angular momentum, which is consistent with the observation noted in Chapter II. The relation is

$$(\epsilon_m)_j \approx (\epsilon_m)_{jc\ell}\left\{1 - 0.06\tanh\left\{\frac{1}{\tilde{w}_{jc\ell}}\frac{\partial}{\partial\eta}\left[(R_{jc\ell}+\eta)\tilde{w}_\zeta\right] - 1\right\}\right\} \quad \text{(III-151)}$$

Examination of Equation (III-151) reveals that for a transverse gradient of angular momentum greater than that at the centerline the eddy viscosity is reduced below the centerline value, while for a transverse gradient less than that at the centerline the eddy viscosity is increased. The maximum variation of the eddy viscosity, however, can be seen to be only ±6 per cent. For this reason the assumption is made that with respect to curvature the eddy viscosity remains essentially constant.

In addition to the effects of curvature, the effect of the intermittency of the flow must be considered. Endo's data indicated that the intermittency factor obtained by Bradbury for a plane jet [21] could be applied to curved jets as well. Bradbury's intermittency factor can be represented by the relation

$$\gamma_t = [1 + 0.0596(y/\delta_{1/2})^6]^{-1} \qquad \text{(III-152)}$$

Thus the eddy viscosity at any point in the jet can be expressed as

$$(\epsilon_m)_j = (\epsilon_m)_{jc\ell}[1 + 0.0596(y/\delta_{1/2})^6]^{-1} \qquad \text{(III-153)}$$

The preceding discussion has implied that the variation of eddy viscosity along the centerline of the jet is the same as that for a plane jet. The most precise method of calculating the latter appears to be that developed by Bradbury and Riley [32], which has already been discussed in part in Chapter II. The method utilizes the eddy Reynolds number as the significant dependent variable. Analysis of the tabulated data of Bradbury and Riley reveals that the eddy Reynolds number varies with distance, s, from the jet exit according to the empirical relation

$$(N_{Re})_t = 14.7 + [0.0535 + 0.00159(s-s_o)/\theta_j]^{-1} - \left\{0.0926\ell n\left(\frac{s-s_o}{10\theta_j}\right) + 3.0434\exp\left[\left(\frac{s-s_o-10\theta_j}{30\theta_j}\right)^2\right] - 2.5909\right\} \qquad \text{(III-154)}$$

Although Bradbury and Riley make no suggestion as to a method of calculating s_o (the location of the apparent origin of the jet), a method for determining this distance can be developed by further analysis of the authors' data coupled with a technique developed by Abramovich [14] for calculating the length of the initial region of a plane jet. Based on the tabulated data of the former the centerline velocity of the jet

varies in the main region of the jet according to the empirical relation

$$\frac{w_\infty}{\bar{w}_{jc\ell} - w_\infty} = 0.378\left(\frac{s-s_o}{\theta_j}\right)^{0.5665} \qquad \text{(III-155)}$$

Now at the beginning of the main region of the jet (if the transition region is neglected)

$$w_{jc\ell} = w_{je} \qquad (s=s_H) \qquad \text{(III-156)}$$

where s_H = length of the initial region of the jet.

Then by substitution and rearrangement

$$s_o = s_H - 5.57\theta_j\left(\frac{w_\infty}{w_{je}-w_\infty}\right)^{1.765} \qquad \text{(III-157)}$$

At this point the distance s_o is expressed in terms of s_H, θ, w_∞ and w_{je}. The last three quantities are known or can be calculated. According to Abramovich the distance s_H can be calculated by the semi-empirical relation

$$s_H = b_o/\left\{0.27T_{je}/T_\infty[(A-2B+C) + \right.$$

$$\left. + w_\infty/w_{je}(B-A)]\left(\frac{T_{je}/T_\infty+1}{2}\right)\left[\frac{1 - w_\infty/w_{je}}{1 + (T_{je}/T_\infty)(w_\infty/w_{je})}\right]\right\} \qquad \text{(III-158)}$$

where

$$A = 0.316/\left\{1 + 0.280[(T_{je}/T_\infty)^{3/4} - 1]\right\}$$

$$B = 0.450/\left\{1 + 0.375\left[\left(T_{je}/T_{\infty}\right)^{3/4} - 1\right]\right\}$$

$$C = \ell n(T_{je}/T_{\infty})/(T_{je}/T_{\infty}-1)$$

Thus a means of calculating s_o in terms of known quantities is established. With such a value of s_o for any position s along the jet axis, eddy Reynolds number can be calculated. The assumption is made that for a given velocity distribution the jet half-width $\delta_{1/2}$ and the velocity excess, $(\bar{w}_{jc\ell}-w_{\infty})$, can be calculated. The centerline value of eddy viscosity can then be determined according to the relation

$$(\epsilon_m)_{jc\ell} = |\bar{w}_{jc\ell}-w_{\infty}|\delta_{1/2}/(N_{Re})_t \qquad \text{(III-159)}$$

Calculation of Boundary Layer Eddy Viscosity

As previously noted, for the calculation of eddy viscosity the boundary layer is divided into two regions. In the inner region a simplified form of Equation (II-32) is used as follows:

$$(\epsilon_m)_{b\ell i} = 0.16y^2\left|\frac{\partial w}{\partial x} + \frac{\partial w}{\partial y}\right| \qquad \text{(III-160)}$$

Use of this simpler relation, which is the basis for the more complex relation [41], appears justified because the exponential term, which is dropped, is only of significance in the laminar sublayer. The latter is not of primary interest in the current study and no grid points in the numerical solution lie within this small portion of the inner region.

For the outer region the eddy viscosity is calculated according to the relation

$$(\epsilon_m)_{b\ell o} = 0.0081\delta_{b\ell}^2\left|\frac{\partial w}{\partial x} + \frac{\partial w}{\partial y}\right|[1 + 5.5(y/\delta_{b\ell})^6]^{-1} \qquad \text{(III-161)}$$

This equation is based on an analysis of the mixing length data presented by Maise and McDonald [39]. For purposes of the current study Equation (III-161) is simpler to use than Equation (II-33) because the former involves the boundary layer thickness $\delta_{b\ell}$ as opposed to the momentum thickness.

Based on an analysis of Equations (III-160) and (III-161), coupled with the logic used by Cebeci, Smith, and Wang [39] to determine the boundary between the inner and outer regions, the following relations are assumed to hold:

$$(\epsilon_m)_{b\ell} = \begin{cases} (\epsilon_m)_{b\ell i} & (0 \le uv \le 0.225\delta_{b\ell}) \qquad \text{(III-162a)} \\ (\epsilon_m)_{b\ell o} & (uv > 0.225\delta_{b\ell}) \qquad \text{(III-162b)} \end{cases}$$

Calculation of Slot Eddy Viscosity

For flow in the slot the relation developed by Hinze [22] is assumed to hold. Thus in the coordinate systems for the slot Equation (II-35) becomes

$$(\epsilon_m)_s = \frac{2\bar{\sigma}_w}{\bar{\rho} b_w} |x - x_{sc\ell}| \Big/ \left|\frac{\partial \bar{w}_y}{\partial x}\right| \qquad \text{(III-163)}$$

Calculation of $(\epsilon_m)_s$ by the preceding relation appears to be a more realistic approach than by using Equation (II-34), because the results are more consistent with experimental data for eddy viscosity along the slot centerline. Along the centerline, with Equation (III-163) the evaluation of an indeterminate expression is required but this simply involves the reciprocal of $\partial^2 \bar{w}_y / \partial x^2$.

General Logic for Calculation of Eddy Viscosity

By means of the relations developed in the three preceding subsections, values of the eddy viscosity can be calculated for the jet, boundary layer, and slot. A fundamental problem arises with regard to the determination of which expression is most applicable at a particular point, especially in the free flow region. Based on a careful examination of the manner in which each relation predicts eddy viscosity, coupled with an appreciation for the general nature of turbulence, the following expressions are used

$$\epsilon_m = \begin{cases} (\epsilon_m)_s \quad (x_{\ell es} \le x \le x_{tes}, y_s \le y \le 0) & \text{(III-164a)} \\ (\epsilon_m)_s \quad (u=0,\ v_{tes} \le v \le v_{\ell es}) & \text{(III-164b)} \\ (\epsilon_m)_j + (\epsilon_m)_{b\ell}\left\{1-\exp\left\{-0.693\left[s_v(u, v_{c\ell}, v)/(\delta_{1/2})_d\right]^7\right\}\right\} \quad (u>o, v<v_{c\ell}) & \text{(III-164c)} \\ (\epsilon_m)_j + (\epsilon_m)_{b\ell}\left\{1-\exp\left\{-0.693\left[s_v(u, v_{c\ell}, v)/(\delta_{1/2})_u\right]^7\right\}\right\} \quad (u>o, v \ge v_{c\ell}) & \text{(III-164d)} \end{cases}$$

where

$s_v(u, v_{c\ell}, v)$ = transverse distance from jet centerline to point (u,v) as defined in Appendix D.

$(\delta_{1/2})_d$ = jet half-width on downstream side of jet.

$(\delta_{1/2})_u$ = jet half-width on upstream side of jet.

Calculation of Eddy Mass Diffusivity and Eddy Thermal Diffusivity

For turbulent flow the turbulent Schmidt number $(N_{Sc})_t$ is defined as

$$(N_{Sc})_t \equiv \epsilon_m/\epsilon_\rho \tag{III-165}$$

Likewise the turbulent Prandtl number $(N_{Pr})_t$ is defined as

$$(N_{Pr})_t \equiv \epsilon_m/\epsilon_h \tag{III-166}$$

Based on Hinze [22] the assumption is made that

$$(N_{Sc})_t = (N_{Pr})_t \tag{III-167}$$

Furthermore, based on the results of Chapter II the assumption is made that

$$(N_{Pr})_t = \begin{cases} 0.57 \text{ (for the free-flow region)} & \text{(III-168a)} \\ 0.75 \text{ (for the slot-flow region)} & \text{(III-168b)} \end{cases}$$

Then the eddy mass diffusivity can be calculated by the relation

$$\epsilon_\rho = \epsilon_m/(N_{Sc})_t \qquad \text{(III-169)}$$

Likewise the eddy thermal diffusivity is determined by the relation

$$\epsilon_h = \epsilon_m/(N_{Pr})_t \qquad \text{(III-170)}$$

Boundary Conditions

Essential to the analytical model is the proper establishment of the appropriate boundary conditions. For compressible flow over any solid surface this point is of special significance because there is considerable variance of opinion as to the proper method for setting up such conditions [73,82,84]. In the discussion which follows the methods employed for establishing the boundary conditions are the result of a combination of theory and practical considerations, the latter based on past experience.

Free Flow Region

Along the upstream and downstream physical boundaries, free stream conditions are assumed to exist. Thus

$$\left.\begin{aligned} \bar{\rho} &= \rho_\infty \\ \bar{w}_u &= w_\infty u/H \\ \bar{w}_v &= -w_\infty v/H \\ \bar{T} &= T_\infty \\ \bar{p} &= p_\infty \end{aligned}\right\} \begin{aligned} &(v=v_\infty,\ 0\le u\le u_\infty) \\ &\qquad \text{and} \\ &(u=u_\infty,\ 0\le v\le v_\infty) \end{aligned} \qquad \text{(III-171)}$$

Because of the nature of parabolic coordinates, boundary conditions along the fourth physical boundary, referred to in the statement of the problem, are also accounted for by the preceding equation.

The plane in which the flat plate lies can be divided into six subdivisions in parabolic coordinates. In the first subdivision, which lies upstream of the plate, the boundary conditions are

$$\left.\begin{aligned} \frac{\partial \bar{\rho}}{\partial u} &= 0 \\ \bar{w}_u &= 0 \\ \frac{\partial \bar{w}_v}{\partial u} &= 0 \\ \frac{\partial \bar{T}}{\partial u} &= 0 \end{aligned}\right\} \quad (u=0,\ v_{\ell ep}<v<v_\infty) \qquad \text{(III-172)}$$

These conditions are based on the assumption that the flow upstream of the plate is symmetrical with respect to the streamline lying along the u_1-parabola.

For the second subdivision, which extends from the leading edge of the plate to the leading edge of the jet, the no-slip condition holds. Thus

$$\left.\begin{aligned} w_u &= 0 \\ w_v &= 0 \end{aligned}\right\} \quad (u=0,\ v_{\ell es}\leq v\leq v_{\ell ep}) \qquad \text{(III-173)}$$

In addition to these relations for the velocity components, some boundary condition must be established for temperature and density (or pressure). One approach to establishing the necessary conditions is to apply the continuity and energy equations, with the no-slip condition taken into account, and with the heat flux $\bar{q}_u$ at the wall set equal to zero, representing an adiabatic wall. Herewith, the resulting equations can be written

$$\frac{\partial E_i}{\partial t} + \frac{1}{H^2}\left[\frac{\partial (HF_i)}{\partial u} + \frac{\partial (HG_i)}{\partial v}\right] = 0 \quad (u=0,\ v_{\ell es} \leq v \leq v_{\ell ep}) \quad (i=1,4) \qquad \text{(III-174)}$$

Equation (III-174) is solved only for E_1 and E_4, with the definitions of E_1, E_4, F_1, F_4, G_1, and G_4 given by Equations (III-102), (III-103), and (III-104).

A suitable and workable alternate approach, especially adapted for use with numerical techniques involving non-uniform grid systems, is based on the calculation of pressure and temperature in lieu of density and temperature. For pressure the assumption is made that the pressure at a point on the surface is a simple function of the flow properties of the fluid in the immediate vicinity of that point. The functional relation which is assumed to hold is

$$\bar{p} = \left[\int_0^{u^+} \bar{p}_{o(v^-)}\,du + \int_0^{u^+} \bar{p}_{o(v^+)}\,du + \int_{v^-}^{v^+} \bar{p}_{o(u^+)}\,dv\right]/(2\Delta u + 2\Delta v)$$

$$(u=0,\ v_{\ell es} \leq v \leq v_{\ell ep}) \qquad \text{(III-175)}$$

where

$$\bar{P}_{o(v^-)} = \bar{P}_s + \bar{P}_t + \bar{\rho}\bar{w}_v|\bar{w}_v|/2 \quad (u=0,\ v^-=v-\Delta v)$$

$$\bar{P}_{o(v^+)} = \bar{P}_s + \bar{P}_t - \bar{\rho}\bar{w}_v|\bar{w}_v|/2 \quad (u=0,\ v^+=v+\Delta v)$$

$$\bar{P}_{o(u^+)} = \bar{P}_s + \bar{P}_t - \bar{\rho}\bar{w}_u|\bar{w}_u|/2 \quad (u^+=\Delta u,\ v=v)$$

For the calculation of temperature, the adiabatic wall boundary conditions as originally posed in Chapter I is modified to allow the wall to possess thermal capacitance because of advantages covered in subsequent discussion. During the transient phase of the problem the wall exchanges heat with the fluid, but as steady-state is approached the adiabatic boundary condition is closely approximated. An energy balance, based on a control volume involving both the plate and the fluid, results in the following relation for the temperature at the wall:

$$\frac{\partial}{\partial t}(E_4+\rho_w c_w \bar{T}) + \frac{1}{H^2}\left\{\frac{\partial[H(F_4+q_{uw})]}{\partial u} + \frac{\partial[H(G_4+q_{vw})]}{\partial v}\right\} = 0 \qquad \text{(III-176)}$$

where

ρ_w = density of wall.

c_w = heat capacity of the wall.

q_{uw} = u-component of heat flux in the wall.

q_{vw} = v-component of heat flux in the wall.

A detailed discussion of the development of this version of the temperature boundary condition is presented in Appendix E. The inclusion of the thermal capacitance of the wall can be seen to have a damping effect on the variation of the fluid temperature at the wall.

The slot exit plane comprises the third subdivision in which boundary conditions must be established. The boundary conditions in this region are based on the continuity of flow properties between the slot and the free stream. Thus

$$\begin{bmatrix} \bar{\rho} \\ \bar{w}_u \\ \bar{w}_v \\ \bar{T} \end{bmatrix}_{(u=0,\ v_{tes} \le v \le v_{les})} = \begin{bmatrix} \bar{\rho} \\ \bar{w}_y \\ -\bar{w}_x \\ \bar{T} \end{bmatrix}_{(y=0,\ x_{les} \le x \le x_{tes})} \qquad \text{(III-177)}$$

In the fourth subdivision, which extends from the trailing edge of the slot to the origin, the boundary conditions are the same as in the second subdivision. By the no-slip requirement,

$$\left.\begin{aligned} w_u &= 0 \\ w_v &= 0 \end{aligned}\right\} \quad (u=0,\ 0 \le v \le v_{tes}) \qquad \text{(III-178)}$$

Based on the use of the continuity and energy equations, with the no-slip condition and the adiabatic wall accounted for as before, the density and temperature at wall can be calculated by the relation

$$\frac{\partial E_i}{\partial t} + \frac{1}{H^2}\left[\frac{\partial (HF_i)}{\partial u} + \frac{\partial (HG_i)}{\partial v}\right] = 0 \quad (u=0,\ 0 \le v \le v_{tes})\ (i=1,4) \qquad \text{(III-179)}$$

The alternate approach, for pressure and temperature relations, are

likewise the same as previously presented for the second subdivision. Thus

$$\bar{p} = \left[\int_{o}^{u^+} \bar{p}_{o(v^-)}du + \int_{o}^{u^+} \bar{p}_{o(v^+)}du + \int_{v^-}^{v^+} \bar{p}_{o(u^+)}dv\right]/(2\Delta u+2\Delta v)$$

$$(u=0,\ 0\le v\le v_{tes}) \qquad \text{(III-180)}$$

and

$$\frac{\partial}{\partial t}(E_4+\rho_w c_w \bar{T}) + \frac{1}{H^2}\left\{\frac{\partial[H(F_4+q_{uw})]}{\partial u} + \frac{\partial[H(G_4+q_{vw})]}{\partial v}\right\} = 0$$

$$(u=0,\ 0\le v\le v_{tes}) \qquad \text{(III-181)}$$

The fifth subdivision extends downstream from the origin to the trailing edge of the plate. The no-slip conditions are

$$\left.\begin{aligned} w_u &= 0 \\ w_v &= 0 \end{aligned}\right\} \quad (0\le u\le u_{tep},\ v=0) \qquad \text{(III-182)}$$

For the calculation of density and temperature, the continuity and energy equations can be applied at the wall as before with the following results:

$$\frac{\partial E_i}{\partial t} + \frac{1}{H^2}\left\{\frac{\partial(HF_i)}{\partial u} + \frac{\partial(HG_i)}{\partial v}\right\} = 0 \quad (0\le u\le u_{tep},\ v=0) \quad (i=1,4) \qquad \text{(III-183)}$$

By the second approach the equations for pressure and temperature are

$$\bar{p} = \left[\int_{o}^{v^+} \bar{p}_{o(u^-)}dv + \int_{o}^{v^+} \bar{p}_{o}(u^+)dv + \int_{u^-}^{u^+} \bar{p}_{o}(v^+)du\right]/(2\Delta u+2\Delta v)$$

$$(0\leq u\leq u_{tep},\ v=0) \quad \text{(III-184)}$$

where

$$\bar{p}_{o(u^-)} = \bar{p}_s + \bar{p}_t + \bar{\rho}\bar{w}_u|\bar{w}_u|/2 \quad (u^-=u-\Delta u,\ v=0)$$

$$\bar{p}_{o(u^+)} = \bar{p}_s + \bar{p}_t - \bar{\rho}\bar{w}_u|\bar{w}_u|/2 \quad (u^+=u+\Delta u,\ v=0)$$

$$\bar{p}_{o(v^+)} = \bar{p}_s + \bar{p}_t - \bar{\rho}\bar{w}_v|\bar{w}_v|/2 \quad (u=u,\ v=\Delta v)$$

and

$$\frac{\partial(E_4+\rho_w c_w \bar{T})}{\partial t} + \frac{1}{H^2}\left\{\frac{\partial[H(F_4+q_{uw})]}{\partial u} + \frac{\partial[H(G_4+q_{vw})]}{\partial v}\right\} = 0$$

$$(0\leq u\leq u_{tep},\ v=0) \quad \text{(III-185)}$$

For the sixth subdivision, which extends downstream from the trailing edge of the plate, the boundary conditions are

$$\left.\begin{aligned} \frac{\partial\bar{\rho}}{\partial v} &= 0 \\ \bar{w}_v &= 0 \\ \frac{\partial\bar{w}_u}{\partial v} &= 0 \\ \frac{\partial\bar{T}}{\partial v} &= 0 \end{aligned}\right\} \quad (v=0,\ u_{tep}\leq u\leq u_\infty) \qquad \text{(III-186)}$$

As with the first subdivision the preceding relations are based on the assumption that flow downstream of the plate is symmetrical with respect to the streamline lying along the v_1-parabola.

Slot Flow Region

As noted in the statement of the problem in Chapter I, the assumption is made that the entrance plane to the slot flow region is located a considerable distance upstream (in the negative y-direction) of the slot inlet. The flow entering the system across this plane is assumed to be uniform and isentropically related to a specified set of stagnation conditions (T_{jo},p_{jo},ρ_{jo}). Furthermore the mass flow rate across this plane is equal to the mass flow rate across a plane located just downstream of the slot inlet. Based on the preceding assumptions the upstream boundary conditions can be expressed as

$$\left.\begin{aligned} \bar{\rho}\bar{w}_y b_w &= \left(\int_{x_{\ell es}}^{x_{tes}} \bar{\rho}\bar{w}_y dx\right)_{y=y_s} \\ \bar{w}_x &= 0 \\ \bar{T} &= T_{jo} - \bar{w}_y^2/(2c_p) \\ \bar{\rho} &= \rho_{jo}(\bar{T}/T_{jo})^{1/\gamma-1} \end{aligned}\right\} (x_{\ell es} \le x \le x_{tes},\ y=-y_s) \qquad \text{(III-187)}$$

The preceding relations for $\bar{\rho}$, $\bar{w}_y$ and $\bar{T}$ are implicit in form and must be solved by iteration.

For the two walls of the slot the same conditions as described along the surface of the plate are assumed to exist. Thus in rectangular coordinates, for the velocity boundary conditions along the walls,

$$\left.\begin{aligned} w_x &= 0 \\ w_y &= 0 \end{aligned}\right\} \quad (x=x_{les},x_{tes};\ y_s\le y\le 0) \qquad \text{(III-188)}$$

As before there are two approaches to establish the remaining two boundary conditions. First by the use of the continuity and energy equations, with the no-slip and adiabatic conditions applied,

$$\frac{\partial A_i}{\partial t} + \frac{\partial B_i}{\partial x} + \frac{\partial C_i}{\partial y} = 0 \quad (x=x_{les},x_{tes};\ y_s\le y\le 0)\ (i=1,4) \qquad \text{(III-189)}$$

Equation (III-189) is solved only for A_1 and A_4, with the definitions for A_1, A_4, B_1, B_4, C_1, and C_4 given by Equations (III-98), (III-99), and (III-100). By the second approach for pressure along the leading slot wall,

$$\bar{p} = \left[\int_{x_{les}}^{x^+} \bar{p}_{o(y^-)}dx + \int_{x_{les}}^{x^+} \bar{p}_{o(y^+)}dx + \int_{y^-}^{y^+} \bar{p}_{o(x^+)}dy\right]/(2\Delta x+2\Delta y)$$

$$(x=x_{les},\ y_s\le y\le 0) \qquad \text{(III-190)}$$

where

$$\bar{p}_{o(y^-)} = \bar{p}_s + \bar{p}_t + \bar{\rho}\bar{w}_y|\bar{w}_y|/2 \quad (x=x_{les},\ y^-=y-\Delta y)$$

$$\bar{p}_{o(y^+)} = \bar{p}_s + \bar{p}_t - \bar{\rho}\bar{w}_y|\bar{w}_y|/2 \quad (x-x_{les},\ y^+=y+\Delta y)$$

$$\bar{p}_{o(x^+)} = \bar{p}_s + \bar{p}_t - \bar{\rho}\bar{w}_x|\bar{w}_x|/2 \quad (x^+=x_{les}+\Delta x,\ y=y)$$

For pressure along the trailing slot wall by the second approach,

$$\bar{p} = \left[\int_{x^-}^{x_{tes}} \bar{p}_{o(y^-)}dx + \int_{x^-}^{x_{tes}} \bar{p}_{o(y^+)}dx + \int_{y^-}^{y^+} \bar{p}_{o(x^-)}dy\right]/(2\Delta x+2\Delta y)$$

$$(x=x_{tes},\ y_s \le y \le 0) \qquad \text{(III-191)}$$

where

$$\bar{p}_{o(y^-)} = \bar{p}_s + \bar{p}_t + \bar{\rho}\bar{w}_y|\bar{w}_y|/2 \quad (x=x_{tes},\ y^-=y-\Delta y)$$

$$\bar{p}_{o(y^+)} = \bar{p}_s + \bar{p}_t - \bar{\rho}\bar{w}_y|\bar{w}_y|/2 \quad (x=x_{tes},\ y^+=y+\Delta y)$$

$$\bar{p}_{o(x^-)} = \bar{p}_s + \bar{p}_t + \bar{\rho}\bar{w}_x|\bar{w}_x|/2 \quad (x=x_{tes}-\Delta x,\ y=y)$$

For temperature along both walls based on the second approach,

$$\frac{\partial(A_4+\rho_w c_w \bar{T})}{\partial t} + \frac{\partial(B_4+q_{xw})}{\partial x} + \frac{\partial(C_4+q_{yw})}{\partial y} = 0$$

$$(x=x_{\ell es}, x_{tes};\ y_s \le y \le 0) \qquad \text{(III-192)}$$

where

q_{xw} = x-component of heat flux in the wall.

q_{yw} = y-component of heat flux in the wall.

In the slot exit plane the boundary conditions are, as previously noted under the free flow region boundary conditions, simply the requirement for continuity of the flow properties. In effect the conservation equations must be satisfied for both rectangular and parabolic coordinates. This is facilitated by the simple manner in which the two

coordinate systems join together in this plane, as noted in prior discussion of the coordinate systems.

Initial Conditions

Because a transient approach is used in the solution of the governing equations, initial conditions must be established for all flow properties at all points within both flow regions, including along all physical boundaries. There are two fundamental methods for setting up the initial conditions. In the first method the initial conditions are selected in such a manner that the transient portion of the solution represents the actual buildup of the flow phenomena. The second method involves setting up initial conditions which are as close to the final steady-state solution as possible. For this second method the transient approach to the solution is simply an efficient relaxation scheme.

Several different sets of initial conditions can be developed based on the first method. The simplest of these involves a plate in a stationary free stream with stationary gas in the slot. The pressure and temperature are everywhere uniform except along the entrance plane to the slot flow region. In this plane jet stagnation conditions exist. At time zero the plate begins to accelerate in the negative x-direction. This acceleration continues until the free stream velocity is reached. Meanwhile the pressure difference at the upstream end of the slot produces flow in the positive y-direction. As the flow proceeds through the slot, the jet emerges into the free stream and is deflected.

A more advanced set of initial conditions, based on the first method, would involve steady-state flow over the plate with the final

free stream velocity and the slot containing stationary gas. Another set would consist of a fully developed plane jet in a quiescent ambient environment, with the latter commencing a uniform acceleration at time zero. An extreme case would involve a fully developed slot flow emerging into a fully developed free stream at time zero.

These various sets of initial conditions, based on the first method, have a fundamental appeal for two reasons. First, they are simple to set up. Second, they provide the investigator with an opportunity to gain insight into the physical phenomena which occur during the production of the jet. At the same time they suffer from at least one serious drawback: length of computation time to reach steady-state conditions. Furthermore, they may lead, during the transient buildup, to complex flow patterns, involving discontinuities, which represent severe convergence tests for any numerical technique. If such a flow condition is encountered after considerable computation time, and if as a result the numerical technique diverges, the entire computation process is essentially lost.

The second method lacks the basic appeal of the first and also demands considerable knowledge of the general pattern of the steady-state solution. At the same time it should in general require significantly less computation time. The likelihood of encountering extreme flow phenomena, such shocks and rarefactions, is somewhat reduced, except in the case when such phenomena actually exist in the steady-state solution. For these reasons the second method appears most suitable for the current problem.

In establishing an initial approximation for the final solution, the assumption is made that the velocity distribution in the vicinity of the jet centerline resembles that for a turbulent plane jet as developed by Goertler [30]. This assumption is consistent with the results of Endo [20]. A second assumption is made that elsewhere in the free flow region the flow pattern is a simple combination of turbulent flow over a flat plate and the induced flow surrounding a jet. Finally, the flow in the slot is assumed to be fully developed and unaffected by the free stream. The resulting initial conditions, which represent the starting point for the computational process, are presented in Appendix F.

CHAPTER IV

NUMERICAL TECHNIQUE

For the problem under study with the analytical model developed in the preceding chapter, only a numerical solution is feasible at the present time. There are a number of important steps necessary in the formulation of the numerical technique. The first step is the establishment of a grid system for the region of interest. Once the grid is set up, finite-difference approximations for all spatial derivatives can be derived. In addition, based on the grid system, interpolation and numerical integration procedures can be established. By means of the finite-difference approximations for the spatial derivatives, the solution can be marched forward in time based on the use of one of the numerical procedures discussed in Chapter II. Such procedures are generally applicable only to interior grid points (points which do not lie along a physical boundary), and thus special procedures must be established at boundary grid points to advance the solution forward in time. Each numerical procedure is characterized by certain stability and convergence criteria. These must be carefully established and conformed with. The final step in the development of the numerical technique involves the development of a digital computer program, which incorporates all the features of the numerical process developed in the preceding steps into an accurate, efficient, computational procedure. Each of the steps noted is dealt with in a subsequent portion of this chapter.

Grid System

Because two different coordinate systems are used, two separate but compatible, grid systems are required. For the slot flow region an ordinary rectangular grid system is established as shown in Figure 5. The subscript m is used to represent incrementation in the x-direction while n is used for incrementation in the y-direction. There are M x-grid lines and N y-grid lines. The x-increments are equal and the following relations hold:

$$x_m = x_{\ell es} + (m-1)\Delta x \qquad \text{(IV-1)}$$

where

$$\Delta x = b_w/(M-1) \qquad \text{(IV-2)}$$

For the y-increments the first and last are different from the increments in the slot. The y-grid coordinates relations are as follows:

$$\left.\begin{aligned} y_1 &= -10L_s \\ y_n &= -L_s + (n-1.5)L_s/(N-2.5) \quad (2\leq n\leq N-1) \\ y_N &= u_2 v_{c\ell} \end{aligned}\right\} \qquad \text{(IV-3)}$$

The parabolic grid system for the free flow region is shown in Figure 6. The subscript j is used to represent incrementation in the u-direction while k is used for the v-direction. By definition the

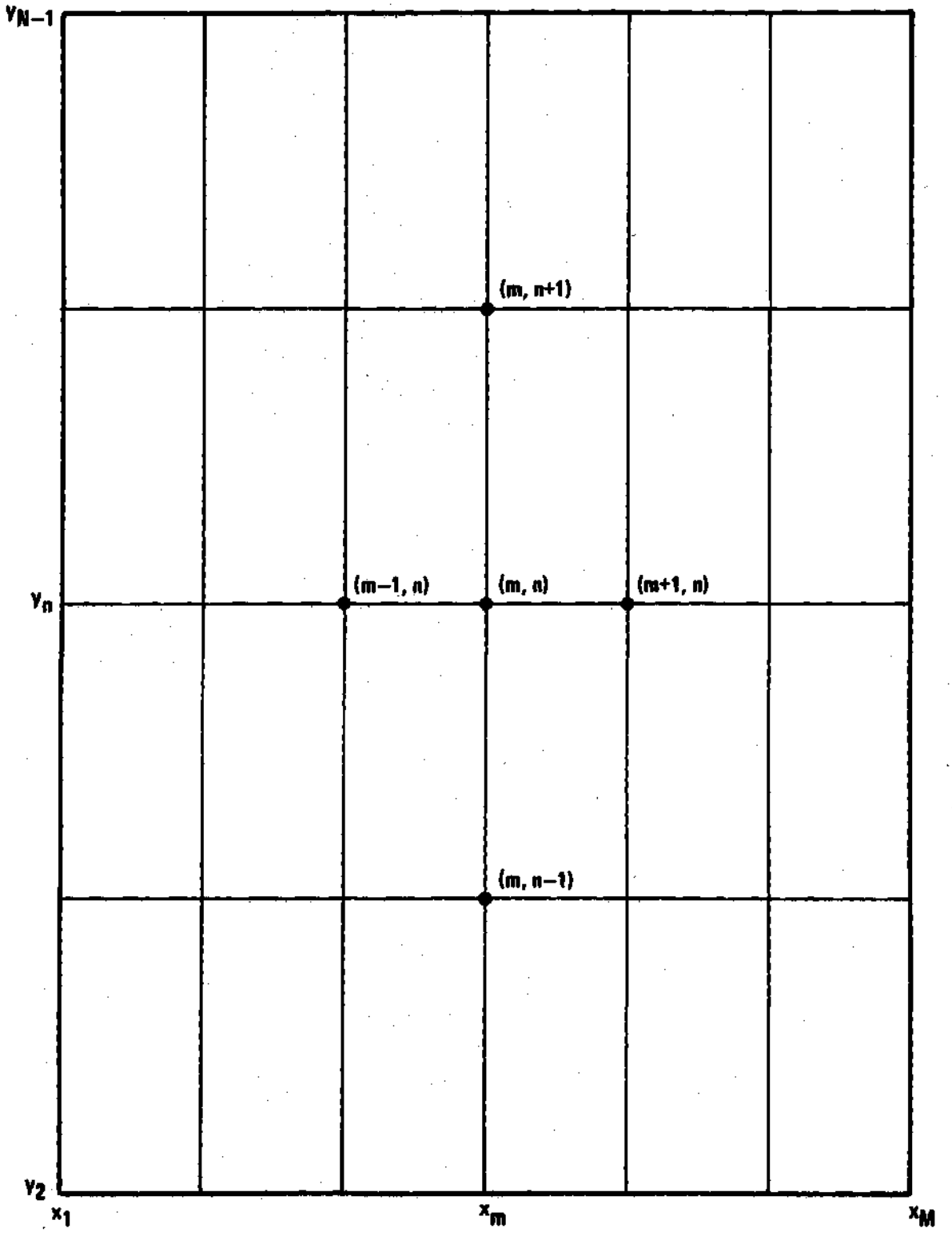

Figure 5. Rectangular Grid System

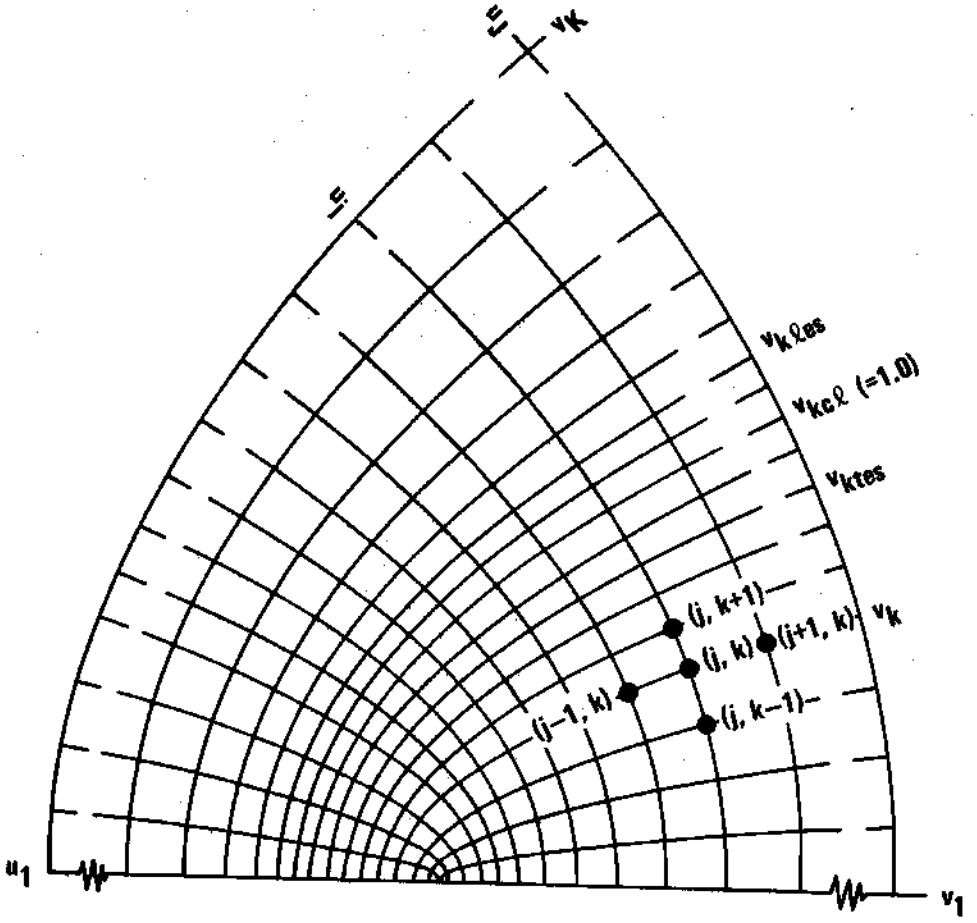

Figure 6. Parabolic Grid System

increments Δu_j and Δv_k are defined as

$$\Delta u_j \equiv u_{j+1} - u_j \tag{IV-4}$$

$$\Delta v_k \equiv v_{k+1} - v_k \tag{IV-5}$$

There are *J* u-increments and *K* v-increments. Notice should be taken that the number of v-parabolas from the origin to the trailing edge of the slot is designated as *ktes*. From the origin to the approximate jet centerline the number of v-parabolas is *kcl*. Likewise, *kles* is the number from the origin to the leading edge of the slot, and *klep* is the number from the origin to the leading edge of the plate. There are two v-parabolas (v_K and v_{K-1}) upstream of the plate. The number of u-parabolas from the origin to the trailing edge of the plate is *jtep*, and there are two u-parabolas (u_J and u_{J-1}) downstream of the plate. The following relations are used to establish the v-grid lines:

$$\left.\begin{aligned}
v_1 &= 0 \\
v_k &= v_{k-1} + \sqrt{-2(x_{sc\ell}+b_o+\Delta x)/(ktes-2)} \quad (2\le k\le ktes-1) \\
v_k &= \sqrt{v_{k-1}^2+2\Delta x} \quad (ktes\le k\le k\ell es) \\
v_k &= \sqrt{v_{k-1}^2+2C_1^{k-k\ell e}\Delta x} \quad (k\ell es+1\le k\le K-2) \\
v_{k-1} &= 2v_{K-2}-v_{K-3} \\
v_k &= 10v_{K-1}
\end{aligned}\right\} \tag{IV-6}$$

where the constant C_1 is determined by the relation

$$x_{\ell ep} + 0.5v^2_{k\ell es} + \sum_{k=k\ell e+1}^{K-2} C_1^{k-k\ell es}\Delta x + C_1^{K-1-k\ell es}\Delta x/2 = 0 \qquad \text{(IV-7)}$$

For the u-grid lines the relations are

$$\left.\begin{aligned} u_j &= v_j && (0\le j\le ktes)\\ u_j &= \sqrt{u^2_{j-1} + 2C_2^{j-ktes}\Delta x} && (ktes+1\le j\le J-2)\\ u_{J-1} &= 2u_{J-2} - u_{J-3}\\ u_J &= 10u_{J-1} \end{aligned}\right\} \qquad \text{(IV-8)}$$

when the constant C_2 is determined by the relation

$$x_{tep} - 0.5u^2_{ktes} - \sum_{j=kte+1}^{J-2} C_2^{j-ktes}\Delta x - C_2^{J-1-ktes}\Delta x/2 = 0 \qquad \text{(IV-9)}$$

The parabolic grid system can be seen to mesh exactly with the rectangular grid system in the slot exit plane. In this plane the following relation holds:

$$k = k\ell es + 1 - m \quad (j=1,\ kte\le k\le k\ell e,\ 1\le m\le M,\ n=N-1) \qquad \text{(IV-10)}$$

Finite-Difference Approximations for Spatial Derivatives

There exist a considerable number of methods for approximating a derivative by means of a finite difference [71,97]. The accuracy of

the approximation is usually established by means of a Taylor series expansion. Experience generally indicates that finite difference equations of second-order accuracy are desirable for fluid dynamic problems [69,71]. For the case of variable grid increments, as shown in Appendix G, the partial derivative $\partial f/\partial u$ can be approximated with second-order accuracy by the relation $\delta_u(f)$ where

$$\delta_u(f)_{j,k} \equiv \frac{\frac{\Delta u_{j-1}}{\Delta u_j}(f_{j+1,k}-f_{j,k}) + \frac{\Delta u_j}{\Delta u_{j-1}}(f_{j,k}-f_{j-1,k})}{\Delta u_{j-1} + \Delta u_j} \quad \text{(IV-11)}$$

In similar manner the derivatives $\partial f/\partial v$, $\partial f/\partial x$ and $\partial f/\partial y$ can be approximated with second-order accuracy by $\delta_v(f)$, $\delta_x(f)$ and $\delta_y(f)$, respectively, as follows:

$$\delta_v(f)_{j,k} \equiv \frac{\frac{\Delta v_{k-1}}{\Delta v_k}(f_{j,k+1}-f_{j,k}) + \frac{\Delta v_k}{\Delta v_{k-1}}(f_{j,k}-f_{j,k-1})}{\Delta v_{k-1} + \Delta v_k} \quad \text{(IV-12)}$$

$$\delta_x(f)_{m,n} \equiv \frac{f_{m+1,n} - f_{m-1,n}}{2\Delta x} \quad \text{(IV-13)}$$

$$\delta_y(f)_{m,n} \equiv \frac{\left(\frac{y_n-y_{n-1}}{y_{n+1}-y_n}\right)(f_{m,n+1}-f_{m,n}) + \left(\frac{y_{n+1}-y_n}{y_n-y_{n-1}}\right)(f_{m,n}-f_{m,n-1})}{y_{n+1} - y_{n-1}} \quad \text{(IV-14)}$$

Under certain conditions the use of first-order approximation is desirable. Backward differences for these cases are

$$\delta_u^-(f)_{j,k} \equiv \frac{f_{j,k} - f_{j-1,k}}{\Delta u_{j-1}} \qquad \text{(IV-15)}$$

$$\delta_v^-(f)_{j,k} \equiv \frac{f_{j,k} - f_{j,k-1}}{\Delta v_{k-1}} \qquad \text{(IV-16)}$$

$$\delta_x^-(f)_{m,n} \equiv \frac{f_{m,n} - f_{m-1,n}}{\Delta x} \qquad \text{(IV-17)}$$

$$\delta_y^-(f)_{m,n} \equiv \frac{f_{m,n} - f_{m,n-1}}{y_n - y_{n-1}} \qquad \text{(IV-18)}$$

Similarly, forward differences are defined as:

$$\delta_u^+(f)_{j,k} \equiv \frac{f_{j+1,k} - f_{j,k}}{\Delta u_j} \qquad \text{(IV-19)}$$

$$\delta_v^+(f)_{j,k} \equiv \frac{f_{j,k+1} - f_{j,k}}{\Delta v_k} \qquad \text{(IV-20)}$$

$$\delta_x^+(f)_{m,n} \equiv \frac{f_{m+1,n} - f_{m,n}}{\Delta x} \qquad \text{(IV-21)}$$

$$\delta_y^+(f)_{m,n} \equiv \frac{f_{m,n+1} - f_{m,n}}{y_{n+1} - y_n} \qquad \text{(IV-22)}$$

Notice should be taken that Equations (IV-11) through (IV-14) do not apply at the plate or slot wall. (j=1, k=1, m=1, or m=M.) For these cases, as shown in Appendix G, the partial derivatives $\partial f/\partial u$, $\partial f/\partial v$, and $\partial f/\partial x$ can be approximated by $\delta_{uw}(f)$, $\delta_{vw}(f)$ and $\delta_{xw}(f)$ with second-order accuracy as follows:

$$\delta_{uw}(f)_{1,k} \equiv -\frac{(2\Delta u_1+\Delta u_2)}{(\Delta u_1+\Delta u_2)\Delta u_1} f_{1,k} + \frac{(\Delta u_1+\Delta u_2)}{\Delta u_1 \Delta u_2} f_{2,k} - \frac{\Delta u_1}{(\Delta u_1+\Delta u_2)} f_{3,k} \qquad \text{(IV-23)}$$

$$\delta_{vw}(f)_{j,1} \equiv -\frac{(2\Delta v_1+\Delta v_2)}{(\Delta v_1+\Delta v_2)\Delta v_1} f_{j,1} + \frac{(\Delta v_1+\Delta v_2)}{\Delta v_1 \Delta v_2} f_{j,2} - \frac{\Delta v_1}{(\Delta v_1+\Delta v_2)\Delta v_2} f_{j,3} \qquad \text{(IV-24)}$$

$$\delta_{xw}(f)_{1,n} \equiv -\frac{3}{2\Delta x} f_{1,n} + \frac{2}{\Delta x} f_{2,n} - \frac{1}{2\Delta x} f_{3,n} \qquad \text{(IV-25)}$$

$$\delta_{xw}(f)_{M,n} \equiv \frac{3}{2\Delta x} f_{M,n} - \frac{2}{\Delta x} f_{M-1,n} + \frac{1}{2\Delta x} f_{M-2,n} \qquad \text{(IV-26)}$$

Interpolation and Numerical Integration Procedures

As noted in Appendix G the central finite-difference equations already presented can be shown to represent exactly the slope of a parabola passing through three adjacent points. For consistency it is therefore desirable to use parabolas both for interpolation and integration.

For interpolation the resulting functions are

$$f(u) \equiv \frac{f_{j-1,k}(u_j-u)(u_{j+1}-u)}{(u_j-u_{j-1})(u_{j+1}-u_{j-1})} + \frac{f_{j,k}(u_{j-1}-u)(u_{j+1}-u)}{(u_{j-1}-u_j)(u_{j+1}-u_j)} + \frac{f_{j+1,k}(u_{j-1}-u)(u_j-u)}{(u_{j-1}-u_{j+1})(u_j-u_{j+1})} \quad (u_{j-1}<u<u_{j+1}) \qquad \text{(IV-27)}$$

$$f(v) \equiv \frac{f_{j,k-1}(v_k-v)(v_{k+1}-v)}{(v_k-v_{k-1})(v_{k+1}-v_{k-1})} + \frac{f_{j,k}(v_{k-1}-v)(v_{k+1}-v)}{(v_{k-1}-v_k)(v_{k+1}-v_k)}$$

$$+ \frac{f_{j,k+1}(v_{k-1}-v)(v_k-v)}{(v_{k-1}-v_{k+1})(v_k-v_{k+1})} \quad (v_{k-1}<v<v_{k+1}) \qquad \text{(IV-28)}$$

$$f(x) \equiv \frac{f_{m-1,n}(x_m-x)(x_{m+1}-x)}{(x_m-x_{m-1})(x_{m+1}-x_{m-1})} + \frac{f_{m,n}(x_{m-1}-x)(x_{m+1}-x)}{(x_{m-1}-x_m)(x_{m+1}-x_m)}$$

$$+ \frac{f_{m+1,n}(x_{m-1}-x)(x_m-x)}{(x_{m-1}-x_{m+1})(x_m-x_{m+1})} \quad (x_{m-1}<x<x_{m+1}) \qquad \text{(IV-29)}$$

$$f(y) = \frac{f_{m,n-1}(y_n-y)(y_{n+1}-y)}{(y_n-y_{n-1})(y_{n+1}-y_{n-1})} + \frac{f_{m,n}(y_{n-1}-y)(y_{n+1}-y)}{(y_{n-1}-y_n)(y_{n+1}-y_n)}$$

$$+ \frac{f_{m,n+1}(y_{n-1}-y)(y_n-y)}{(y_{n-1}-y_{n+1})(y_n-y_{n+1})} \quad (y_{n-1}<y<y_{n+1}) \qquad \text{(IV-30)}$$

The four preceding relations are equivalent to Lagrangian interpolation polynomials.

For numerical integration, Simpson's rule corresponds to integration along parabolic curves. Integration of f(u) over the interval (u_{j1},u_{j2}) is thus approximated as follows:

$$\int_{u_{j1}}^{u_{j2}} \approx \sum_{j=j1+1}^{j2-1} g_j \quad (j=j1+1,j1+3,j1+5,\ldots,j2-1) \qquad \text{(IV-31)}$$

where

$$g_j = \frac{f_{j-1}(\Delta u_{j-1}+\Delta u_j)(2\Delta u_{j-1}-\Delta u_j)}{6\Delta u_{j-1}} + \frac{f_j(\Delta u_{j-1}+\Delta u_j)^3}{6\Delta u_{j-1}\Delta u_j}$$

$$+ \frac{f_{j+1}(\Delta u_{j-1}+\Delta u_j)(2\Delta u_j-\Delta u_{j-1})}{6\Delta u_j}$$

Likewise the integral of f(v) over the interval (v_{k1},v_{k2}) can be approximated as

$$\int_{v_{k2}}^{v_{k1}} f dv \approx \sum_{k=k1-1}^{k2-1} g_k \quad (k=k1+1,k1+3,k1+5,\ldots,k2-1) \qquad \text{(IV-32)}$$

where

$$g_k = \frac{f_{k-1}(\Delta v_{k-1}+\Delta v_k)(2\Delta v_{k-1}-\Delta v_k)}{6\Delta v_{k-1}} + \frac{f_k(\Delta v_{k-1}+\Delta v_k)^3}{6\Delta v_{k-1}\ v_k}$$

$$+ \frac{f_{k+1}(\Delta v_{k-1}+\Delta v_k)(2\Delta v_k-\Delta v_{k-1})}{6\Delta v_k}$$

The integral of f(x) over the interval (x_{m1},x_{m2}) is

$$\int_{x_{m1}}^{x_{m2}} f dx \approx \sum_{m=m1+1}^{m2-1} g_m \quad (m=m1+1,m1+3,m1+5,\ldots,m2-1) \qquad \text{(IV-33)}$$

where

$$g_m = \frac{\Delta x}{3}(f_{m-1}+f_m+f_{m+1})$$

Integration of f(y) over the interval (y_{n1},y_{n2}) is approximated as

$$\int_{y_{n1}}^{y_{n2}} f\,dy \approx \sum_{n=n1+1}^{n2-1} g_n \qquad (n=n1+1,n1+3,n1+5,\ldots,n2-1) \qquad \text{(IV-34)}$$

where

$$g_n = \frac{f_{n-1}(y_{n+1}-y_{n-1})(2y_{n-1}+3y_n-y_{n+1})}{6(y_n-y_{n-1})} + \frac{f_n(y_{n+1}-y_{n-1})^3}{6(y_n-y_{n-1})(y_{n+1}-y_n)}$$

$$+ \frac{f_{n+1}(y_{n+1}-y_{n-1})(y_{n-1}-3y_n+2y_{n+1})}{6(y_{n+1}-y_n)}$$

Time-Marching Procedures for Interior Points

As discussed in the literature survey there exist a number of approaches to the numerical solution of transient, multi-dimensional fluid dynamic problems. For compressible fluid flow the most promising appear to be the Lax-Wendroff technique (with its numerous variations) and the Rusanov technique. The latter is simpler but the former is more accurate. Based on the comparative performance of the two techniques as reported by Skoglund, Cole and Staiano [82], coupled with the current opinion of various investigators [58,98,99], some version of the Lax-Wendroff would appear most suitable for the current problem. Furthermore, the two-step version is apparently simpler and more practical than the one-step version.

In its original form, as described by Richtmyer [64] the two-step Lax-Wendroff technique produces the following finite-difference equation at the interior points (j,k) in the free flow region for the time step &:

$$E^{\ell+1}_{i,j,k} = \frac{1}{4}\left(E^{\ell}_{i,j-1,k}+E^{\ell}_{i,j,k-1}+E^{\ell}_{i,j+1,k}+E^{\ell}_{i,j,k+1}\right) - \Delta t[\delta_u(HF^{\ell}_i)_{j,k}$$

$$+ \delta_v(HG^{\ell}_i)_{j,k} + \Gamma^{\ell}_{i,j,k}/H_{j,k}]/H^2_{j,k} \qquad \text{(IV-35a)}$$

$$E^{\ell+2}_{i,j,k} = E^{\ell}_{i,j,k} - 2\Delta t[\delta_u(HF^{\ell+1}_i)_{j,k} + \delta_v(HG^{\ell+1}_i)_{j,k}$$

$$+ \Gamma^{\ell+1}_{i,j,k}/H_{j,k}]/H^2_{j,k} \qquad \text{(IV-35b)}$$

Likewise for the slot flow region at interior points (m,n) and time step ℓ

$$A^{\ell+1}_{i,m,n} = \frac{1}{4}\left(A^{\ell}_{i,m-1,n}+A^{\ell}_{i,m,n-1}+A^{\ell}_{i,m+1,n}+A^{\ell}_{i,m,n+1}\right)$$

$$- \Delta t[\delta_x(B^{\ell}_i)_{m,n} + \delta_y(C^{\ell}_i)_{m,n}] \qquad \text{(IV-36a)}$$

$$A^{\ell+2}_{i,m,n} = A^{\ell}_{i,m,n} - 2\Delta t[\delta_x(B^{\ell+1}_i)_{m,n} + \delta_y(C^{\ell+1}_i)_{m,n}] \qquad \text{(IV-36b)}$$

Experience reveals that the preceding equations, which are based on central finite differences for all spatial derivatives, are not especially suited for viscous, turbulent flow. This situation results in part from the fact that the quantities F_i, B_i, G_i and C_i contain first partial derivatives, which for second-order accuracy should be evaluated by central finite differences. These same quantities (F_i, G_i, B_i, and C_i) appear in first partial derivatives, which are also approximated by central finite differences. Thus for the point (j,k)

the variation of E_i with time depends upon the 13 points (j-2,k), (j-1,k), (j,k), (j+1,k), (j+2,k), (j,k-2), (j,k-1), (j,k+1), (j,k+2), (j-1,k-1), (j-1,k+1), (j+1,k-1), and (j+1,k+1). A similar set of 13 points influence the temporal variation of A_i at point (m,n). Although a precise explanation is not available, experience indicates that utilization of this set of 13 points tends to produce wavy patterns in pressure and density in the vicinity of regions of rapid compression or expansion.

Based on the work of MacCormack [85] and Lomax [86], the use of a numerical scheme which involves alternating backward and forward differences appears superior to the original two-step method for reducing the tendency toward wavy patterns in pressure. Such an approach involves only 9 points instead of 13. For the current problem in the free flow region the following two sets of two-step equations represent an adaptation of this version of the Lax-Wendroff method.

$$E^{\ell+1}_{i,j,k} = E^{\ell}_{i,j,k} - \Delta t[\delta^{+}_{u}(H^{-}F^{\ell}_{i})_{j,k} + \delta^{+}_{v}(H^{-}G^{\ell}_{i})_{j,k} + {}^{-}\Gamma^{\ell}_{i,j,k}/H_{j,k}]/H^{2}_{j,k} \qquad \text{(IV-37a)}$$

$$E^{\ell+2}_{i,j,k} = \frac{1}{2}\{E^{\ell}_{i,j,k} + E^{\ell+1}_{i,j,k} - \Delta t[\delta^{-}_{u}(H^{+}F^{\ell+1}_{i})_{j,k} + \delta^{-}_{v}(H^{+}G^{\ell+1}_{i})_{j,k} + {}^{+}\Gamma^{\ell+1}_{i,j,k}/H_{j,k}]/H^{2}_{j,k}\} \qquad \text{(IV-37b)}$$

$$E_{i,j,k}^{\ell+3} = E_{i,j,k}^{\ell+2} - \Delta t[\delta_u^-(H^+F_i^{\ell+2})_{j,k} + \delta_v^-(H^+G_i^{\ell+2})_{j,k} + {}^+\Gamma_{i,j,k}^{\ell+2}/H_{j,k}]/H_{j,k}^2 \qquad \text{(IV-37c)}$$

$$E_{i,j,k}^{+4} = \frac{1}{2}\{E_{i,j,k}^{\ell+2} + E_{i,j,k}^{\ell+3} - \Delta t[\delta_u^+(H^-F_i^{\ell+3})_{j,k} + \delta_v(H^-G_i^{\ell+3})_{j,k} + {}^-\Gamma_{i,j,k}^{\ell+3}/H_{j,k}]/H_{j,k}^2\} \qquad \text{(IV-37d)}$$

The use of the signs + and - as superscripts preceding the terms, F_i, G_i, and Γ_i indicates the direction (forward or backward) of the finite differences which are used to approximate all partial derivatives contained within the superscripted term. For the slot flow region the corresponding equations are

$$A_{i,m,n}^{\ell+1} = A_{i,m,n}^{\ell} - \Delta t[\delta_x^+({}^-B_i^{\ell})_{m,n} + \delta_y^+({}^-C_i^{\ell})_{m,n}] \qquad \text{(IV-38a)}$$

$$A_{i,m,n}^{+2} = \frac{1}{2}\{A_{i,m,n}^{\ell} + A_{i,m,n}^{\ell+1} - \Delta t[\delta_x({}^+B_i^{\ell+1})_{m,n} + \delta_y^-(-C_i^{\ell+1})_{m,n}]\} \qquad \text{(IV-38b)}$$

$$A_{i,m,n}^{\ell+3} = A_{i,m,n}^{\ell+2} - \Delta t[\delta_x^-({}^+B_i^{\ell+2})_{m,n} + \delta_y^-({}^+C_i^{\ell+2})_{m,n}] \qquad \text{(IV-38c)}$$

$$A_{i,m,n}^{\ell+4} = \frac{1}{2}\{A_{i,m,n}^{\ell+2} + A_{i,m,n}^{\ell+3} - \Delta t[\delta_x^+({}^-B_i^{\ell+3})_{m,n} + \delta_y^+({}^-C_i^{\ell+3})_{m,n}]\} \qquad \text{(IV-38d)}$$

As before the use of + or - as a superscript preceding B_i and C_i indicates the direction of the finite differences.

Time Marching Procedures for Boundary Points

The time-marching procedures for boundary points must be capable of satisfying the boundary conditions previously discussed in Chapter III while generating values of the five flow variables as a function of time.

Free Flow Region

Along the upstream and downstream boundary parabolas (v_K and u_J) in the free flow field the boundary points possess constant flow properties as given by Equation (III-171). Thus no time-marching process is involved for these points.

In the plane of the plate, in the first subdivision discussed in the boundary conditions, the flow processes symmetry as indicated by Equations (III-172). If these equations are substituted into the general governing equation, a simplified set of transient equations is produced. The latter can be readily solved by the general time-marching procedure discussed in the preceding subsection.

Along the surface of the plate in the second subdivision, in accordance with Equation (III-171)

$$\left.\begin{aligned}(w_u)_{1,k} &= 0\\ (w_v)_{1,k} &= 0\end{aligned}\right\} \quad (k\ell es \le k \le k\ell ep) \qquad \text{(IV-39)}$$

As already noted there are two approaches for solving for density (or pressure) and temperature. The first approach involves using the simplified Equation (III-174). The latter can be readily incorporated into

the general time-marching technique. The second approach involves calculation of pressure and temperature at the surface according to Equations (III-175) and (III-176). In finite-difference form Equation (III-175) becomes

$$\bar{p}^{\ell+1}_{1,k} = \left\{[(\bar{p}_o)^{\ell}_{1,k-1} + (\bar{p}_o)^{\ell}_{1,k+1}]\Delta u_i + (\bar{p}_o)^{\ell}_{2,k}(\Delta v_{k-1}+\Delta v_k)\right\}/(2\Delta u_1 + \Delta v_{k-1}+\Delta v_k) \quad (k\ell es \le k \le k\ell ep) \qquad \text{(IV-40)}$$

where

$$(\bar{p}_o)^{\ell}_{1,k-1} = (\bar{p}_s)^{\ell}_{1,k-1} + (\bar{p}_t)^{\ell}_{1,k-1} + \bar{\rho}^{\ell}_{1,k-1}(\bar{w}_v)^{\ell}_{1,k-1}|(\bar{w}_v)^{\ell}_{1,k-1}|/2$$

$$(\bar{p}_o)^{\ell}_{1,k+1} = (\bar{p}_s)^{\ell}_{1,k+1} + (\bar{p}_t)^{\ell}_{1,k+1} - \bar{\rho}^{\ell}_{1,k+1}(\bar{w}_v)^{\ell}_{1,k+1}|(\bar{w}_v)^{\ell}_{1,k+1}|/2$$

$$(\bar{p}_o)^{\ell}_{2,k} = (\bar{p}_s)^{\ell}_{2,k} + (\bar{p}_t)^{\ell}_{2,k} - \bar{\rho}^{\ell}_{2,k}(\bar{w}_u)^{\ell}_{2,k}|(\bar{w}_u)_{2,k}|/2$$

The finite-difference version of Equation (III-176) can be solved by the same technique as used for the interior points.

The equations for the boundary points in the third subdivision (the slot exit plane) are the simple identities

$$\left.\begin{aligned}
\bar{\rho}^{\ell}_{1,k} &= \bar{\rho}^{\ell}_{N-1,k\ell es+1-k} \\
(\bar{w}_u)^{\ell}_{1,k} &= (\bar{w}_y)^{\ell}_{N-1,k\ell es+1-k} \\
(\bar{w}_v)^{\ell}_{1,k} &= (\bar{w}_x)^{\ell}_{N-1,k\ell es+1-k} \\
\bar{T}^{\ell}_{1,k} &= \bar{T}^{\ell}_{N-1,k\ell es+1-k}
\end{aligned}\right\} (ktes<k<k\ell es) \qquad \text{(IV-41)}$$

In the fourth subdivision ($1 \le k \le ktes$) as indicated by Equations (III-178) through (III-181) the situation is identical to that for the second subdivision and the numerical treatment of the two approaches is the same.

For the fifth subdivision, based on Equation (III-182) the velocity is zero. Thus

$$\left.\begin{aligned}
(\bar{w}_u)_{j,1} &= 0 \\
(\bar{w}_v)_{j,1} &= 0
\end{aligned}\right\} (1 \le j \le jtep) \qquad \text{(IV-42)}$$

As before there exist two approaches for establishing the remainder of the boundary conditions. The first of these based on Equation (III-183) can be simply incorporated into the overall numerical procedure for the interior points. For the calculation of pressure by the second approach, by means of Equation (III-184),

$$\bar{p}^{\ell+1}_{j,1} = \left\{[\bar{p}_o)^{\ell}_{j-1,1} + (\bar{p}_o)^{\ell}_{j+1,1}]\Delta v_1 + (\bar{p}_o)^{\ell}_{j,2}\ (\Delta u_{j-1} + \Delta u_j)\right\}/(2\Delta v_1 + \Delta u_{j-1} + \Delta u_j) \quad (1 \le j \le jtep) \qquad \text{(IV-43)}$$

where

$$(\bar{p}_o)^{\ell}_{j-1,1} = (\bar{p}_s)^{\ell}_{j-1,1} + (\bar{p}_t)^{\ell}_{j-1,1} + \bar{\rho}^{\ell}_{j-1,1}(\bar{w}_u)_{j-1,1}|(\bar{w}_u)^{\ell}_{j-1,1}|/2$$

$$(\bar{p}_o)^{\ell}_{j+1,1} = (\bar{p}_s)^{\ell}_{j+1,1} + (\bar{p}_t)^{\ell}_{j+1,1} - \bar{\rho}^{\ell}_{j+1,1}(\bar{w}_u)^{\ell}_{j+1,1}|(\bar{w}_u)^{\ell}_{j+1,1}|/2$$

$$(\bar{p}_o)^{\ell}_{j,2} = (\bar{p}_s)^{\ell}_{j,2} + (\bar{p}_t)^{\ell}_{j,2} - \bar{\rho}^{\ell}_{j,2}(\bar{w}_v)^{\ell}_{j,2}|(\bar{w}_v)_{j,2}|/2$$

Calculation of temperature based on a finite difference version of Equation (III-185) can be incorporated into the overall numerical scheme for interior points.

In the sixth subdivision of the plane of the plate, Equation (III-186) represents symmetry analogous to that in the first subdivision. By following the same procedure as used in latter case, the general numerical technique can be utilized for solution of flow properties at boundary points in the sixth subdivision.

Slot Flow Region

For boundary points in the entrance plane to the slot flow region, based on Equation (III-187) the following relations apply:

$$\left.\begin{aligned}
&\bar{\rho}^{\ell+1}_{m,1}(\bar{w}_y)^{\ell+1}_{m,1}b_w = \sum_{m=2}^{M-1} g_m \quad (m=2,4,\ldots,M-1)\\
&(\bar{w}_x)^{\ell+1}_{m,1} = 0\\
&\bar{T}^{\ell+1}_{m,1} = T_{jo} - [(\bar{w}_y)^{\ell+1}_{m,1}]^2/(2c_\rho)\\
&\bar{\rho}^{\ell+1}_{m,1} = \rho_{jo}(\bar{T}^{\ell+1}_{m,1}/T_{jo})^{1/(\gamma-1)}
\end{aligned}\right\} \quad (1\le m\le M,\ n=1) \qquad \text{(IV-44)}$$

where

$$g_m = \frac{\Delta x}{3}\left[\bar{\rho}^{\ell}_{2,m-1}(\bar{w}_y)^{\ell}_{2,m-1} + 4\bar{\rho}^{\ell}_{2,m}(\bar{w}_y)_{2,m} + \bar{\rho}^{\ell}_{2,m+1}(\bar{w}_y)^{\ell}_{2,m+1}\right]$$

The first, third, and fourth relations are simultaneously solved by use of the Newton-Raphson method [100].

Along the slot walls as along the surface of the plate the no-slip condition represented by Equation (III-188) yields

$$\left.\begin{aligned}
(\bar{w}_x)^{\ell}_{1,n} &= 0\\
(\bar{w}_y)^{\ell}_{1,n} &= 0
\end{aligned}\right\} \quad (2\le n\le N-1) \qquad \text{(IV-45)}$$

and

$$\left.\begin{aligned}
(\bar{w}_x)^{\ell}_{M,n} &= 0\\
(\bar{w}_y)^{\ell}_{M,n} &= 0
\end{aligned}\right\} \quad (2\le n\le N-1) \qquad \text{(IV-46)}$$

The first approach for calculating density and temperature in accordance with Equation (III-189) can be solved by the same time-marching procedure used for the interior points of the slot flow. The second approach involves calculation of pressure and temperature. For the former, the finite-difference approximations of Equations (III-190) and (III-191) for the two walls are

$$\bar{p}^{\ell+1}_{1,n} = \left\{\left[(\bar{p}_o)^{\ell}_{1,n-1} + (\bar{p}_o)^{\ell}_{1,n+1}\right]\Delta x + (\bar{p}_o)^{\ell}_{2,n}(y_{n+1}-y_{n-1})\right\}/(2\Delta x + y_{n+1}-y_{n-1}) \quad (2\le n\le N-1) \tag{IV-47}$$

and

$$\bar{p}^{\ell+1}_{M,n} = \left\{\left[(\bar{p}_o)^{\ell}_{M,n-1} + (\bar{p}_o)^{\ell}_{M,n+1}\right]\Delta x + (\bar{p}_o)^{\ell}_{M-1,n}(y_{n+1}-y_{n-1})\right\}/(2\Delta x + y_{n+1}-y_{n-1}) \quad (2\le n\le N-1) \tag{IV-48}$$

where

$$(\bar{p}_o)^{\ell}_{1,n-1} = (\bar{p}_s)^{\ell}_{1,n-1} + (\bar{p}_t)^{\ell}_{1,n-1} + \bar{\rho}^{\ell}_{1,n-1}(\bar{w}_y)_{1,n-1}|(\bar{w}_y)^{\ell}_{1,n-1}|/2$$

$$(\bar{p}_o)^{\ell}_{1,n+1} = (\bar{p}_s)^{\ell}_{1,n+1} + (\bar{p}_t)^{\ell}_{1,n+1} - \bar{\rho}^{\ell}_{1,n+1}(\bar{w}_y)^{\ell}_{1,n+1}|(\bar{w}_y)^{\ell}_{1,n+1}|/2$$

$$(\bar{p}_o)^{\ell}_{2,n} = (\bar{p}_s)^{\ell}_{2,n} + (\bar{p}_t)^{\ell}_{2,n} - \bar{\rho}^{\ell}_{2,n}(\bar{w}_x)_{2,n}|(\bar{w}_x)^{\ell}_{2,n}|/2$$

$$(\bar{p}_o)^{\ell}_{M,n-1} = (\bar{p}_s)^{\ell}_{M,n-1} + (\bar{p}_t)^{\ell}_{M,n-1} + \bar{\rho}^{\ell}_{M,n-1}(\bar{w}_y)^{\ell}_{M,n-1}|(\bar{w}_y)^{\ell}_{M,n-1}|/2$$

$$(\bar{p}_o)^{\ell}_{M,n+1} = (\bar{p}_s)^{\ell}_{M,n+1} + (\bar{p}_t)^{\ell}_{M,n+1} - \bar{\rho}^{\ell}_{M,n+1}(\bar{w}_y)^{\ell}_{M,n+1}|(\bar{w}_y)^{\ell}_{M,n+1}|/2$$

$$(\bar{p}_o)^{\ell}_{M-1,n} = (\bar{p}_s)^{\ell}_{M-1,n} + (\bar{p}_t)^{\ell}_{M-1,n} + \bar{\rho}^{\ell}_{M-1,n}(\bar{w}_x)^{\ell}_{M-1,n}|(\bar{w}_x)^{\ell}_{M-1,n}|/2$$

For the calculation of temperature by the second approach the finite-difference version of Equation (III-192) can be solved as before using the general time-marching procedures for interior points in the slot flow.

For the points lying in the exit plane of the slot, the governing equations are the same as for interior points, Equation (III-97). Thus the general time-marching procedure for interior points applies. In order to permit both forward and backward differences, as well as central differences in the y-direction at these points, however, the need arises for an auxiliary set of rectangular grid points which actually lie in the free flow region at y_N. Values for all flow properties at this last set of points are obtained by interpolation of property values obtained in the free flow region.

Stability and Convergence Considerations

As pointed out in Chapter II stability and convergence criteria for two-dimensional compressible inviscid flow are relatively well established. For viscous flow the implicit relation, Equation (II-44) developed by Thommen [66] for the one-dimensional case in the absence of heat conduction appears to be the most advanced expression. Extension of this relation to include two dimensions and turbulent transport phenomena appears to be quite difficult, as observed by Walker and

Zumwalt [101]. Furthermore, the resulting expression is quite likely to be implicit in form, thus requiring iteration at each time step to determine the size of the next time step. To avoid introduction of such additional complexities to the numerical technique, the standard inviscid stability criterion is used. For parabolic coordinates this criterion is

$$\Delta t^{\ell}_{j,k} \leq \left\{ [|(\bar{w}_u)^{\ell}_{j,k}| + \bar{a}^{\ell}_{j,k}]/(\Delta u_j H_{j,k}) \right.$$

$$\left. + [|(\bar{w}_v)^{\ell}_{j,k}| + \bar{a}^{\ell}_{j,k}]/(\Delta v_k H_{j,k}) \right\}^{-1} \qquad \text{(IV-49)}$$

where

$$\bar{a}^{\ell}_{j,k} = (\gamma R \bar{T}^{\ell}_{j,k})^{1/2}$$

For rectangular coordinates,

$$\Delta t^{\ell}_{m,n} \leq \left\{ [|(\bar{w}_x)^{\ell}_{m,n}| + \bar{a}^{\ell}_{m,n}]/\Delta x \right.$$

$$\left. + [|(\bar{w}_y)^{\ell}_{m,n}| + \bar{a}^{\ell}_{m,n}]/(y_{n+1}-y_n) \right\}^{-1} \qquad \text{(IV-50)}$$

In order to use the same time step at all grid points it is necessary to determine the minimum value of $\Delta t^{\ell}_{j,k}$ and likewise the minimum value of $\Delta t^{\ell}_{m,n}$. The smaller of the two is then used as the time step for all grid points. Notice should be taken that, with either the Lax-Wendroff method or MacCormack's variation of that method, the use of a nonuniform

grid, coupled with the use of a time step, established in the manner just described, produces a signal speed in the numerical process which may be considerably greater than the speed of sound in the corresponding physical system.

For linear equations convergence can be established by means of Lax's Equivalence Theorem [71]. Such a theorem states that stability is the necessary and sufficient condition for convergence if the initial value problem is properly posed with a finite-difference approximation which satisfies the consistency condition. The latter requires that the truncation error approach zero as the time and space increments are reduced to zero.

The current problem, however, is non-linear and no precise criteria for convergence appears to exist. The fundamental question as to whether or not the Navier-Stokes equations, with boundary conditions and initial conditions, are well-posed currently cannot be answered [73]. According to a general theorem by Strang [102] for non-linear equations, for a solution which is "sufficiently smooth," convergence will occur if a consistent non-linear finite-difference operator is used whose first linear variation is stable in the L_2 norm (defined by the Parseval relation [71]). The preceding theorem, however, as noted by Richtmyer and Morton, does not take into account the effect of boundary conditions and thus cannot be taken as a general criterion for convergence.

Although no precise method of establishing convergence appears practical, it should be noted that several different numerical methods similar to the method under consideration have been shown to be

consistent and stable for linearized fluid dynamic problems [71,73]. As indicated in the literature survey, considerable success has been achieved in obtaining physically reasonable results with the technique applied to non-linear fluid dynamic problems. Based on these considerations the assumptions are made that the problem is "well posed" and that convergence occurs with the numerical technique described.

Digital Computer Program

The numerical procedure outlined in the preceding section forms the basis for a digital computer program entitled DEFJET. The program, written in FORTRAN V for the UNIVAC 1108 digital computer consists of a main routine, 46 subroutines and 6 function subprograms. A description of each part of the program is provided in Appendix H along with a flow chart of the major segments.

The program DEFJET has a capacity for 961 grid points (31 by 31) in the free flow region and 121 (11 by 11) in the slot flow region. The rate of computation, with all grid points used, is approximately 10 time steps per minute on the UNIVAC 1108. As the solution is marched out in time, the program periodically provides an output on magnetic tape of all essential flow variables.

Computer Graphics

Because of the considerable quantity of output, the use of computer graphics is essential for efficient presentation of the numerical results. The rapid, accurate graphical display of the data is useful both in diagnosing problem areas in the numerical technique and in the

efficient interpretation of the final solution. Three programs, entitled MNPLOT, VECTOR and AUXPLT, designed for use with the UNIVAC 1108 computer and the CalComp Plotter, provide the necessary graphics capability. All three are designed to use as input data the output of DEFJET on magnetic tape. All plots produced by the programs are automatically sized to fit on 8-1/2 by 11-inch pages with allowance made for standard margins.

The program MNPLOT generates contour plots of eight different flow variables (two velocity components, density, temperature, pressure, speed, stream function and eddy viscosity) for both the free flow and slot flow regions. The program possesses a "magnification" feature which permits enlarged graphical presentation of any desired portion of either flow region. The number of contour lines can be varied and each contour line is labeled with its magnitude.

The program VECTOR is designed to provide a visual indication of the magnitude and direction of the fluid velocity at each grid point in both flow regions. This is achieved by drawing at each point an arrow the length and orientation of which corresponds to the time-averaged fluid velocity vector. Each grid point is marked by a small dot, thus clearly indicating the origin of each arrow. The program possesses the same "magnification" feature as MNPLOT, and in addition has the capability of leaving out arrows along specified grid lines to reduce plotting clutter. Provision is made for comparison with experimental data.

For conventional graphical plots, the program AUXPLT is used. Basically AUXPLT is capable of producing a standard graph with one flow

variable as the ordinate and one spatial variable as the abscissa. A plot can be generated of any one of the eight flow variables previously mentioned, along any specified segment of any designated u, v, x or y-grid line. As with VECTOR, the program contains a provision for presenting experimental data for purposes of comparison or correlation.

CHAPTER V

DISCUSSION OF RESULTS

The analytical model described in Chapter III combined with the numerical technique discussed in Chapter IV provide a means of obtaining a solution to the problem of the two-dimensional deflected jet. In order to specify the problem 13 primary parameters must be assigned values. These parameters are:

1. Free stream velocity, $\hat{w}_\infty$.
2. Free stream pressure, $\hat{\rho}_\infty$.
3. Free stream temperature, $\hat{T}_\infty$.
4. Jet stagnation pressure, $\hat{\rho}_{jo}$.
5. Jet stagnation temperature, $\hat{T}_{jo}$.
6. Specific gas constant, $\hat{R}$.
7. Specific heat of gas at constant pressure, $\hat{c}_p$.
8. Reference value of first coefficient of viscosity, $\hat{\mu}_{ref}$.
9. Prandtl number of gas, Pr.
10. Distance upstream from slot centerline to leading edge of plate, $\hat{L}_{up}$.
11. Distance downstream from slot centerline to trailing edge of plate, $\hat{L}_{dp}$.
12. Slot width, $\hat{b}_w$.
13. Slot length, $\hat{L}_s$.

The general flow pattern may vary significantly depending upon these primary input parameters.

In order to demonstrate in a meaningful manner the validity and accuracy of the numerical solution, the primary input parameters should be assigned values which match actual test conditions for which experimental data exist. By such an approach, a valid comparison between numerical predictions and experimental results is possible. The literature survey in Chapter II suggests two experimental studies for this purpose, Ivanov [8], and Heyser and Maurer [13]. These two studies represent the basis for the selection of input parameters for two test cases.

In the first two subsections which follow, the solutions obtained for the test cases are compared with the corresponding experimental data. Based on an analysis of these test cases a more precise understanding of the general flow pattern can be obtained. A discussion of important features of the flow is provided in the third subsection. In the process of developing the analytical model and the numerical technique, certain significant concepts relative to turbulent compressible flow have evolved. These concepts are described in the final subsection of this chapter.

Test Case No. 1
(Low Subsonic Jet/Low Subsonic Free Stream)

In Table IV of his book [8], Ivanov presents the result of 18 different tests involving two-dimensional deflected jets. Based on certain considerations regarding the spacing and total number of parabolic grid points, the sixth test in this table was selected for purposes of comparison. The appropriate values of the 13 test parameters are provided in Table 1.

Table 1. Input Parameters for Test Case No. 1

Parameters	Value
Free stream velocity, $\hat{w}_\infty$	12.63 ft/sec
Free stream pressure, $\hat{\rho}_\infty$	2116.2 lb_f/ft^2
Free stream temperature, $\hat{T}_\infty$	538.2°R
Jet stagnation pressure, $\hat{\rho}_{jo}$	2120.8 lb_f/ft^2 *
Jet stagnation temperature, $\hat{T}_{jo}$	543.9°R *
Specific gas constant, $\hat{R}$	.0686 $BTU/lb_m/°R$
Specific heat of gas at constant pressure, $\hat{c}_p$	.2402 $BTU/lb_m/°R$
Reference value of first coefficient of viscosity, $\hat{\mu}_{ref}$	9.724 10^{-6} $lb_m/(ft\ sec)$
Prandtl number of gas, Pr	.72
Distance upstream from slot centerline to leading edge of plate, $\hat{L}_{up}$	1.0499 ft
Distance downstream from slot centerline to trailing edge of plate, $\hat{L}_{dp}$	3.0513 ft
Slot width, $\hat{b}_w$	.02625 ft
Slot length, $\hat{L}_s$	.643 ft

*These stagnation properties produce an isentropic jet exit velocity $\hat{w}_{je}$ of 63.7 ft/sec, along with an isentropic jet exit temperature $\hat{T}_{je}$ of 543.6°R.

Analysis of Test Conditions

The stagnation pressure of the jet, as shown in the table, is seen to be only slightly greater than that of the free stream. The resulting jet velocity is approximately 64 feet per second, which represents low subsonic flow. The free stream and jet temperatures are essentially the same and thus heat transfer is not a dominant feature of the flow.

In order to establish the applicability of the analytical model, the necessity arises for determining whether or not the slot flow, the boundary layer, and the jet are all turbulent for the specified input conditions. This point can be established by calculation of the appropriate Reynolds numbers.

Normally, turbulent flow occurs in slots where the Reynolds number ($2\hat{\rho}_s\hat{w}_s\hat{b}_w/\hat{\mu}_s$) exceeds 10,000 [42]. For the case under consideration, with the temperature and velocity given in Table 1, the slot Reynolds number is approximately 21,000. Thus the slot flow falls in the turbulent range.

For plane jets, if the jet exit Reynolds number ($\hat{\rho}_{je}\hat{w}_{je}\hat{b}_w/\hat{\mu}_{je}$) exceeds 30, the jet is generally turbulent [103]. It can be seen that in the current case the jet exit Reynolds number is equal to one-half of the slot Reynolds number and therefore has a value of ~10,500. This would strongly indicate a turbulent jet.

If a turbulent boundary layer is to exist, the plate Reynolds number in the vicinity of the jet exit ($\hat{\rho}_\infty\hat{w}_\infty\hat{L}_{up}/\hat{\mu}_\infty$) should be greater than 5×10^5, unless some tripping device is used, or free-stream

turbulence is present [29]. Based on the conditions given in the table, the plate Reynolds number is approximately 8×10^4. This would not be sufficient for a turbulent boundary layer except for the fact that Ivanov's test apparatus included a screen at the leading edge of the plate, which produced free-stream turbulence.* Based on the preceding point it appears reasonable to assume that the boundary layer is turbulent in the vicinity of the jet exit.

Predicted Flow Pattern

Based on the input values given in Table 1, by means of the program DEFJET, a transient numerical solution for Test Case No. 1 was carried out for 4154 time steps, representing approximately seven hours of Univac-1108 computation time. The resulting flow pattern at this point was plotted by means of the programs VECTOR and MNPLOT. Two sets of plots were developed. The first set covered the region bounded by the four parabolas u_5, u_{25}, v_1, and v_{25} and was designed to provide an overall view of the flow pattern, excluding the region in the immediate vicinity of the jet exit. The second set, covering the region bounded by the parabolas u_1, u_{13}, v_1, and v_{25}, was designed to present an enlarged view of the flow pattern near the jet exit.

Notice should be taken that all figures are presented in dimensionless form. Each dimensionless quantity has been previously defined in the second section of Chapter III. Of special significance is the quantity dimensionless time. As already noted, one unit of such time

---

*In addition, examination of Figure 9 of Ivanov's book reveals that the frame of the screen acted as a tripping device.

represents the physical time required for a particle traveling at the isentropic jet exit velocity to travel twice the distance along the x-axis from the origin to the slot centerline. For Test Case No. 1 the total elapsed dimensionless time was 0.711, corresponding to approximately 3 milliseconds. While this time period appears small, a signal moving at the speed of sound could, in such a span of time, travel a distance of roughly 3.3 feet. Inspection of the values of $\hat{L}_{up}$ and $\hat{L}_{dp}$, as given in Table 1, reveals that the elapsed time was sufficient for the presence of the jet to be felt over the entire length of the plate.

The grid system for the overall view is presented in Figure 7. To avoid crowding, only every other v-parabola is shown. The close spacing of the latter on either side of v_{cl} is a result of the relatively narrow slot used by Ivanov, coupled with the need for maximum resolution of the jet velocity profile. In all figures concerned with the overall view, the same scale is used. It is important to recall that the centerline of the slot is at $x \approx -0.5$.

The fluid velocity vectors, as shown in Figure 8, provide an overall indication of the flow pattern. To reduce clutter, velocity vectors have been plotted only at every second u-parabola. The predicted velocity profiles can be seen to resemble the exponential distribution observed by Reichardt [27] in his experiments for turbulent plane jets. The non-uniform spacing of the v-parabolas, however, tends to obscure portions of some of the predicted profiles. Of special interest is the upstream behavior of the free stream. Such behavior displays very little deviation from the normal pattern occurring in

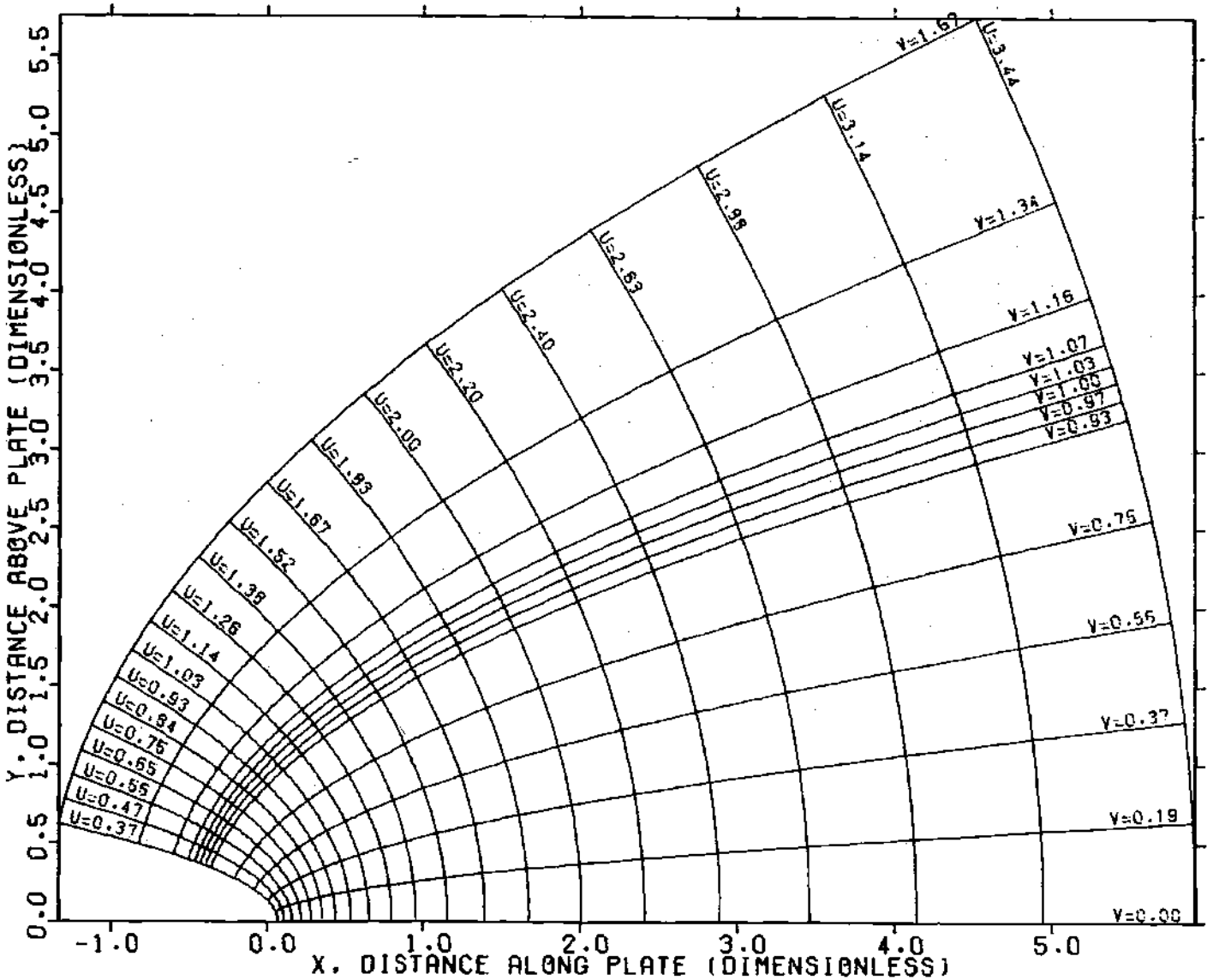

Figure 7. Parabolic Grid System for the Free Flow, Overall View, Low Subsonic Jet/Low Subsonic Free Stream (Test Case No. 1)

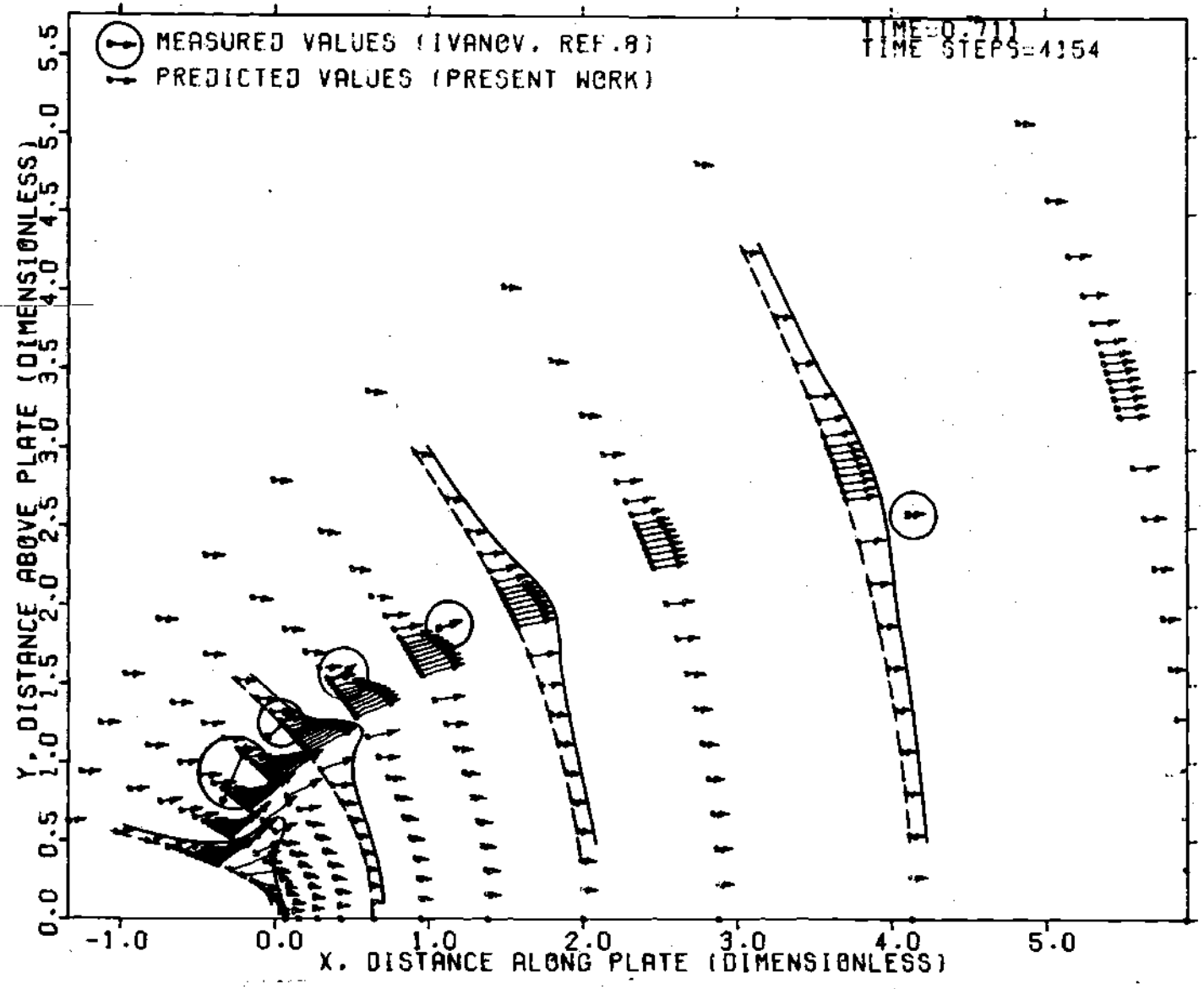

Figure 8. Fluid Velocity in the Free Flow, Overall View, Low Subsonic Jet/Low Subsonic Free Stream (Test Case No. 1)

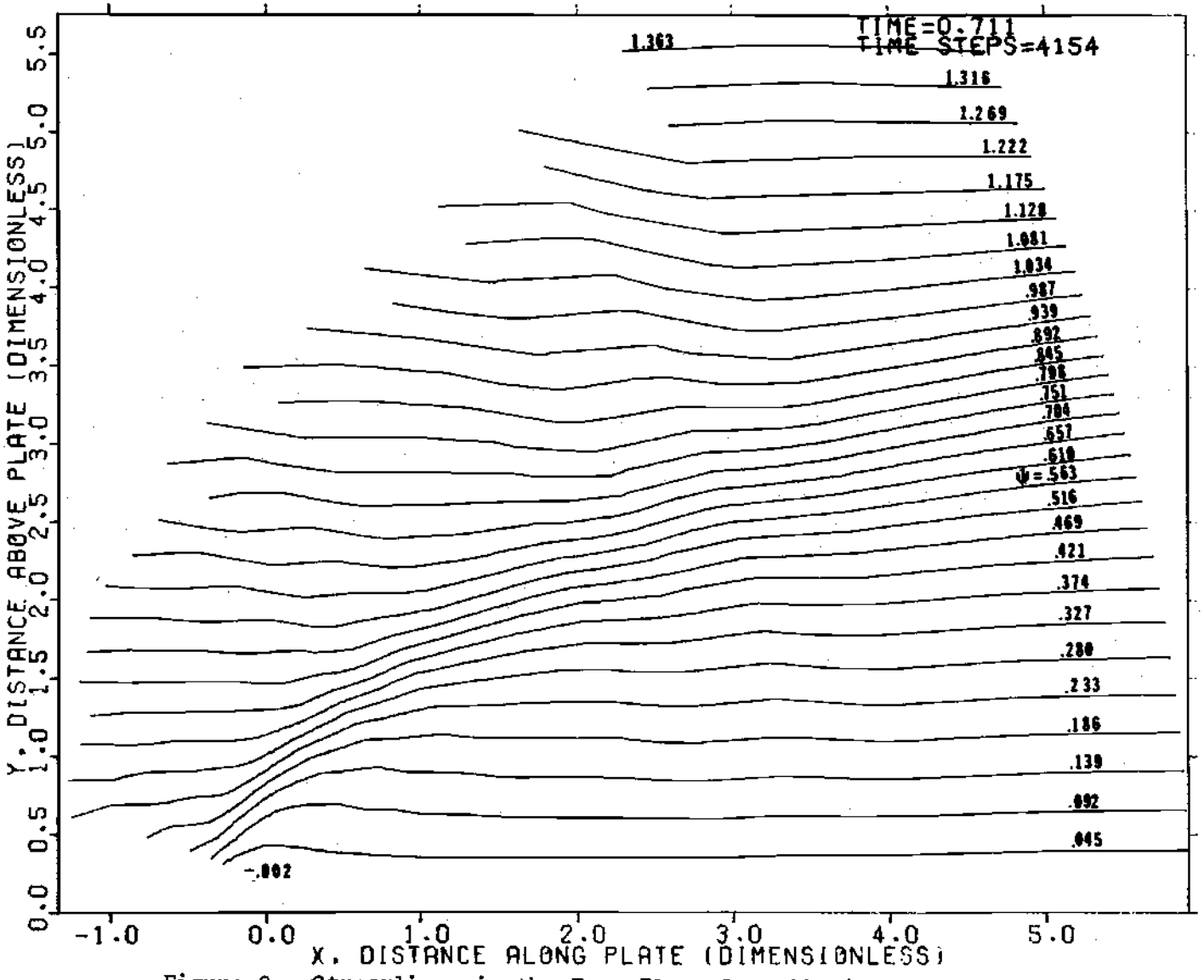

Figure 9. Streamlines in the Free Flow, Overall View, Low Subsonic Jet/Low Subsonic Free Stream (Test Case No. 1)

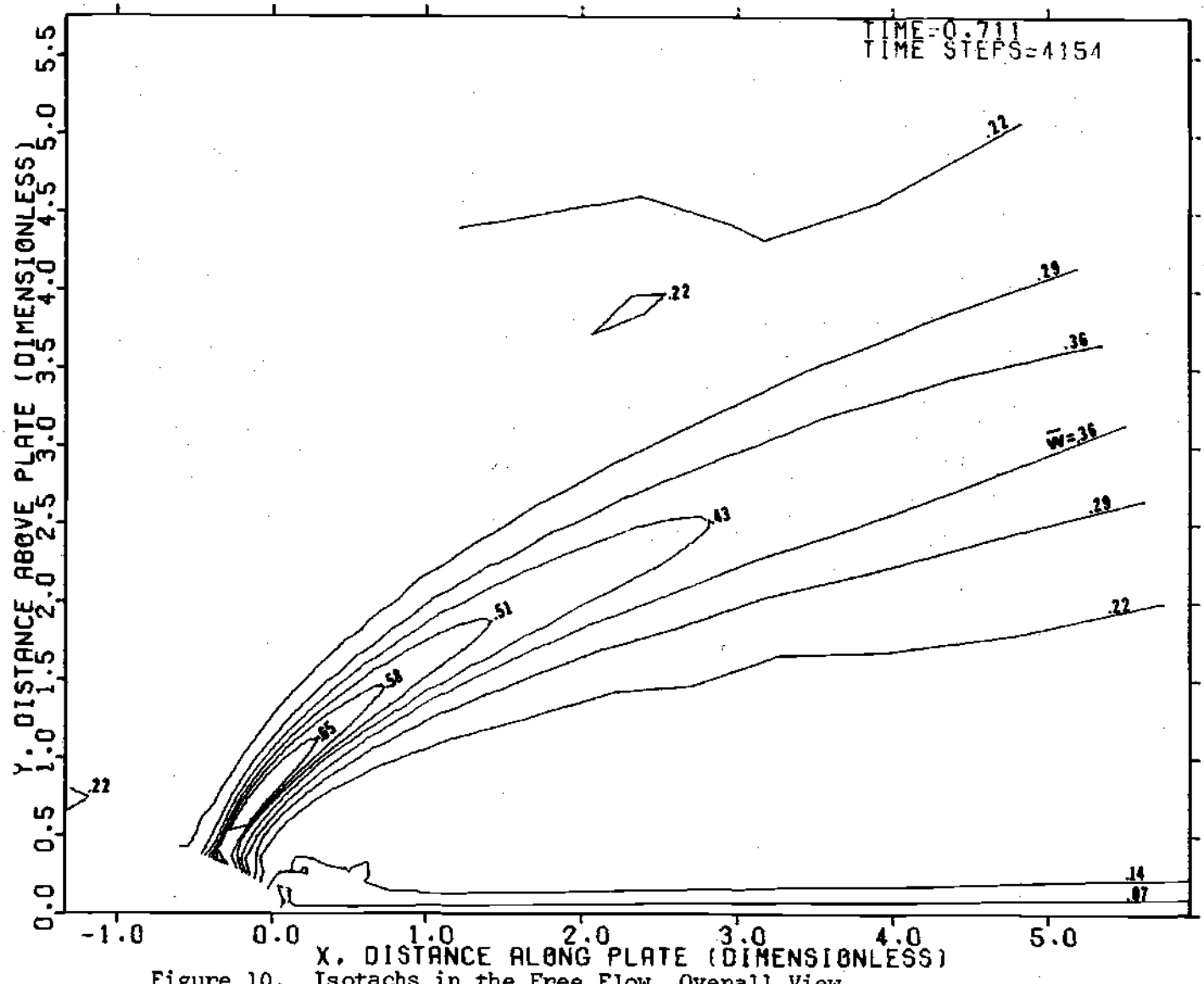

Figure 10. Isotachs in the Free Flow, Overall View,
Low Subsonic Jet/Low Subsonic Free Stream (Test Case No. 1)

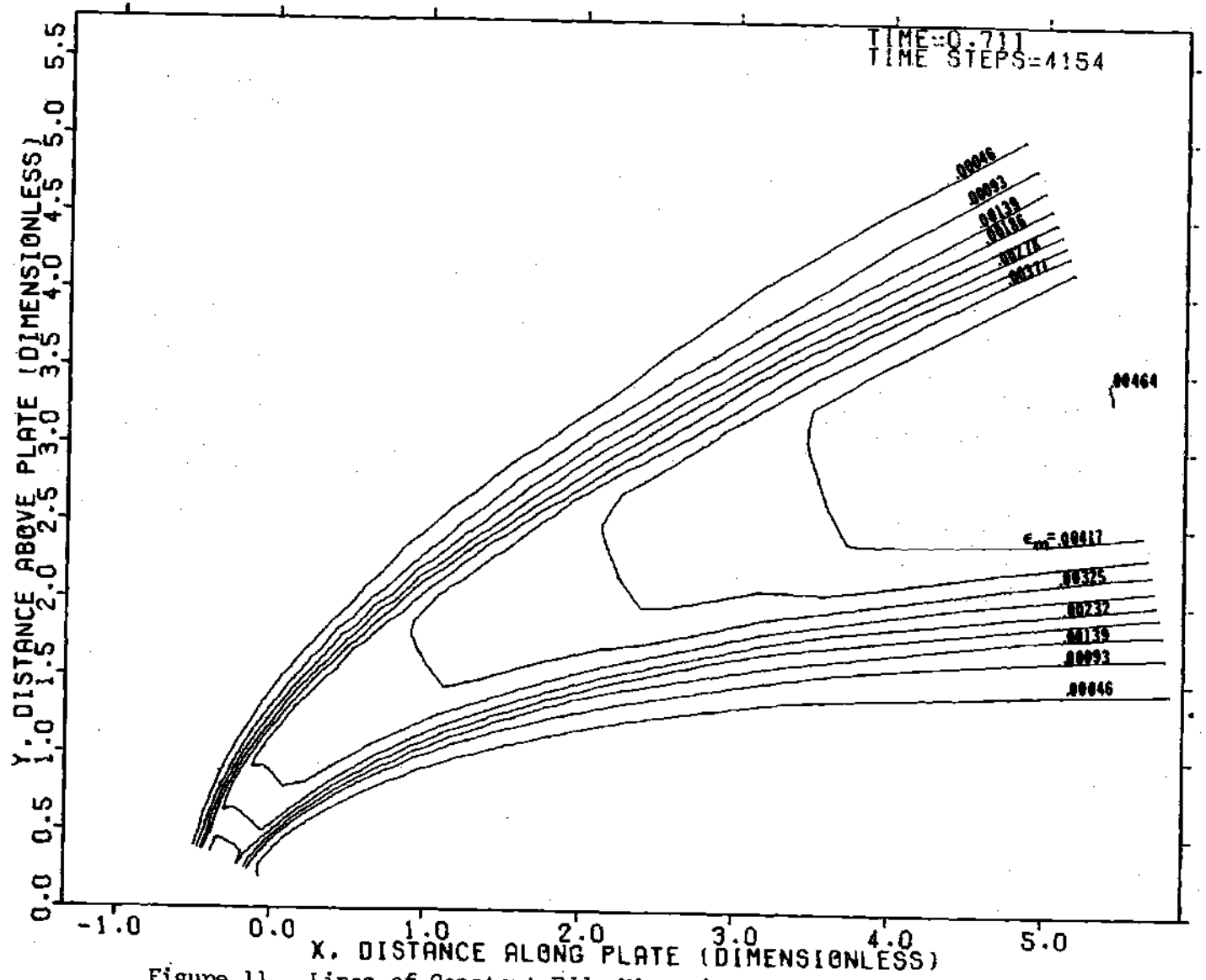

Figure 11. Lines of Constant Eddy Viscosity in the Free Flow, Overall View, Low Subsonic Jet/Low Subsonic Free Stream (Test Case No. 1)

viscosity along the jet centerline generally increases with distance downstream. The transverse variation of eddy viscosity results primarily from the intermittency factor.

For the enlarged view of the free flow region in the vicinity of the jet exit, the grid system is displayed by Figure 12. As before only every other v-parabola is drawn. The four subsequent figures concerned with the enlarged view for Test Case No. 1 conform to the scale of this grid.

The flow pattern produced by the velocity vectors for the enlarged view is shown in Figure 13. The jet velocity profiles can be observed as before but again the spacing of the v-parabolas blots out portions of the profile. Upstream of the jet near the plate the free stream slows down and then begins to turn in the direction of the jet. No boundary layer separation is observed. To the right of the jet exit a recirculation region forms, as expected. The flow appears to reattach to the plate in the vicinity of the origin of the coordinate system.

Figure 14 presents a plot of streamline in the enlarged view. The streamlines originating within the jet are quite evident as is the downstream recirculation region. As before, comparison of the fluid velocity plot and the streamlines indicates that the latter pass through the jet.

Isotachs for the enlarged view are provided in Figure 15. Again a decay in the jet centerline velocity can be observed as well as the usual transverse variation. Certain asymmetrical patterns are noted in

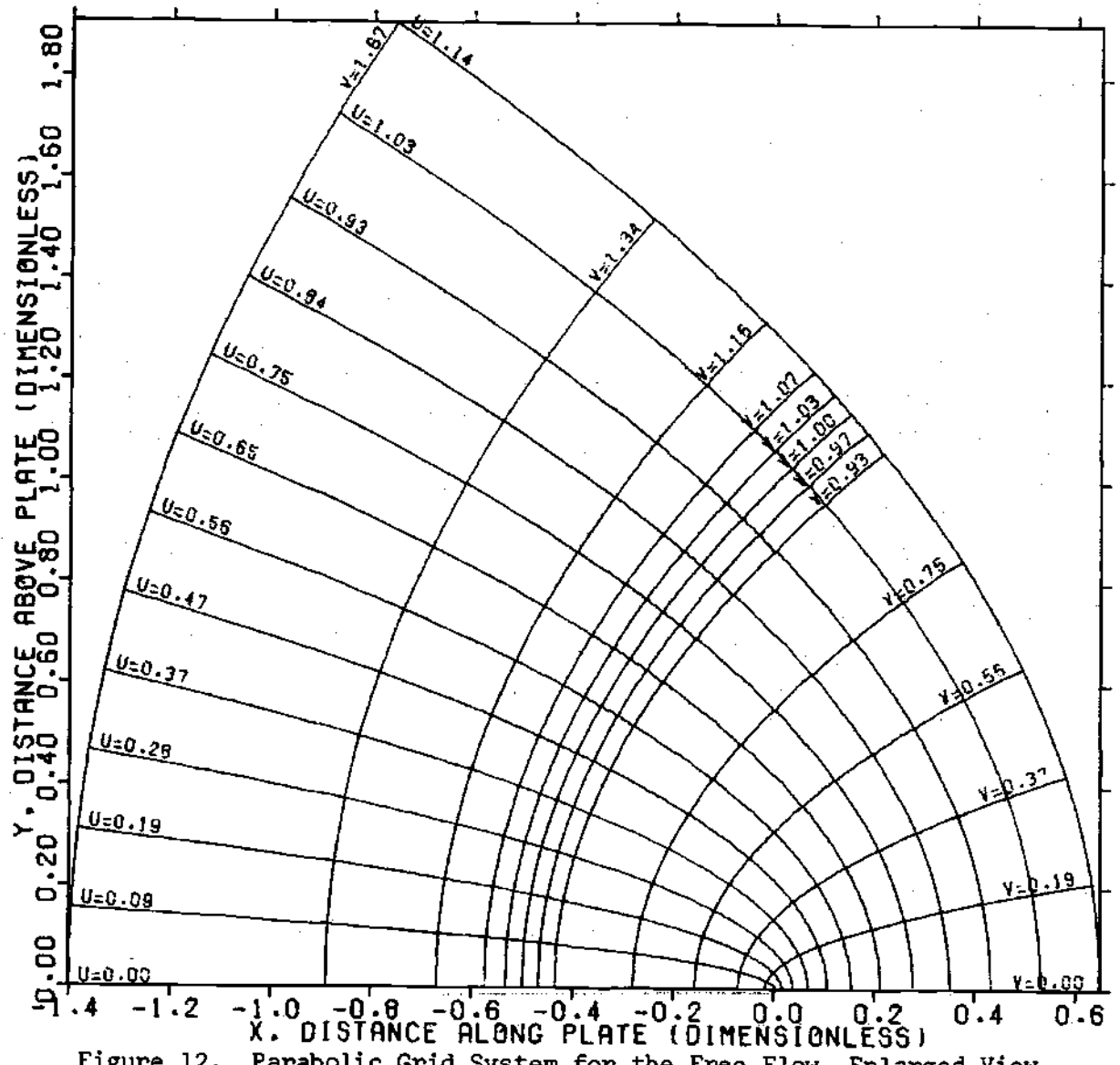

Figure 12. Parabolic Grid System for the Free Flow, Enlarged View, Low Subsonic Jet/Low Subsonic Free Stream (Test Case No. 1)

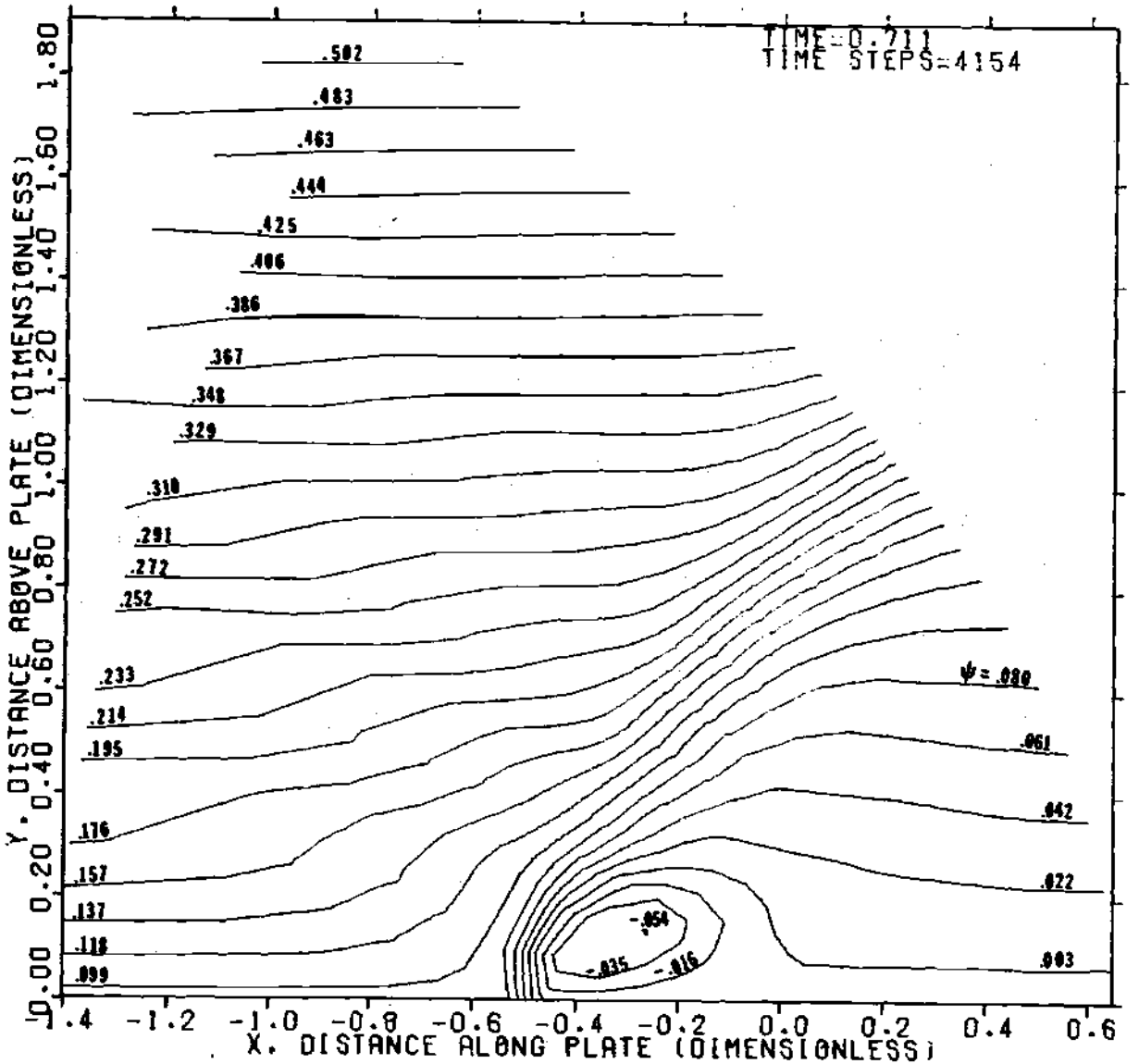

Figure 14. Streamlines in the Free Flow, Enlarged View, Low Subsonic Jet/Low Subsonic Free Stream (Test Case No. 1)

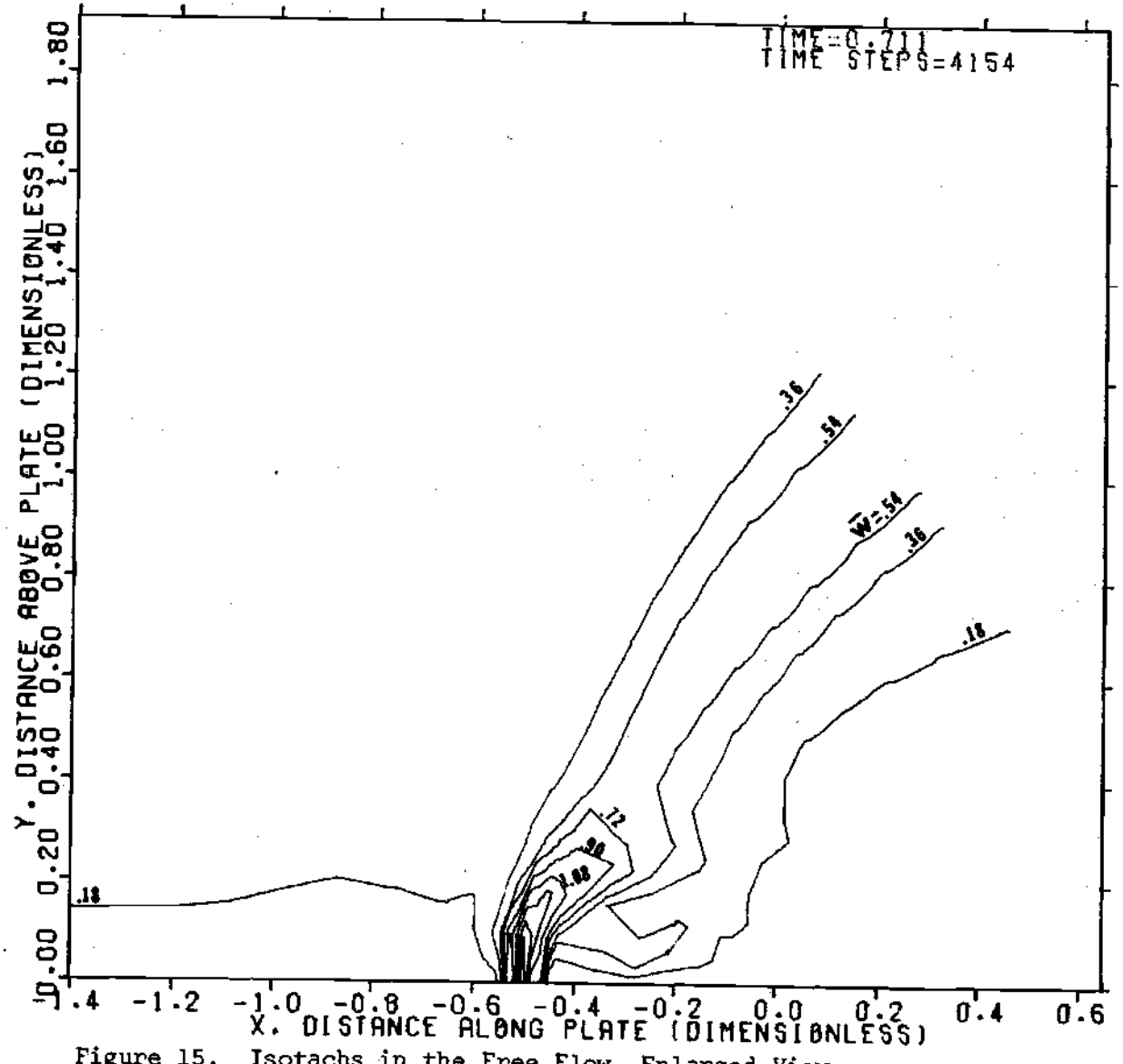

Figure 15. Isotachs in the Free Flow, Enlarged View, Low Subsonic Jet/Low Subsonic Free Stream (Test Case No. 1)

the immediate proximity of the jet exit. The isotach contours in the recirculation region appear somewhat erratic, most likely due to the plotting program. The presence of a boundary layer upstream of the jet is indicated by the isotach w=0.18 which is roughly parallel to the plate to the left of the jet.

The contour plot of eddy viscosity in the enlarged view, as shown in Figure 16, is quite complex. The jet centerline eddy viscosity increases rapidly with distance downstream, in the immediate proximity of the jet exit, reaching a local maximum after a short distance. Next the centerline eddy viscosity begins to decrease until a minimum is reached. Beyond this point the eddy viscosity increases with distance downstream. On either side of the mouth of the slot, local peaks in the eddy viscosity are observed. These reflect the large velocity gradients existing in these two regions.

Although the numerical solution (in the free flow region) at the end of 4154 time steps was generally smooth, stable, and changing relatively slowly with time, true steady-state conditions were not achieved. Furthermore as the numerical solution was marched out in time beyond approximately 3000 time steps, the flow pattern in the slot displayed signs of instability. The pattern was characterized by a gradual pressure buildup in the slot entrance plane and a physically unrealistic peak in the velocity along the slot centerline. Limitations in computer availability, coupled with the apparent numerical problems developing in the slot, precluded devoting more computation time to Test Case No. 1.

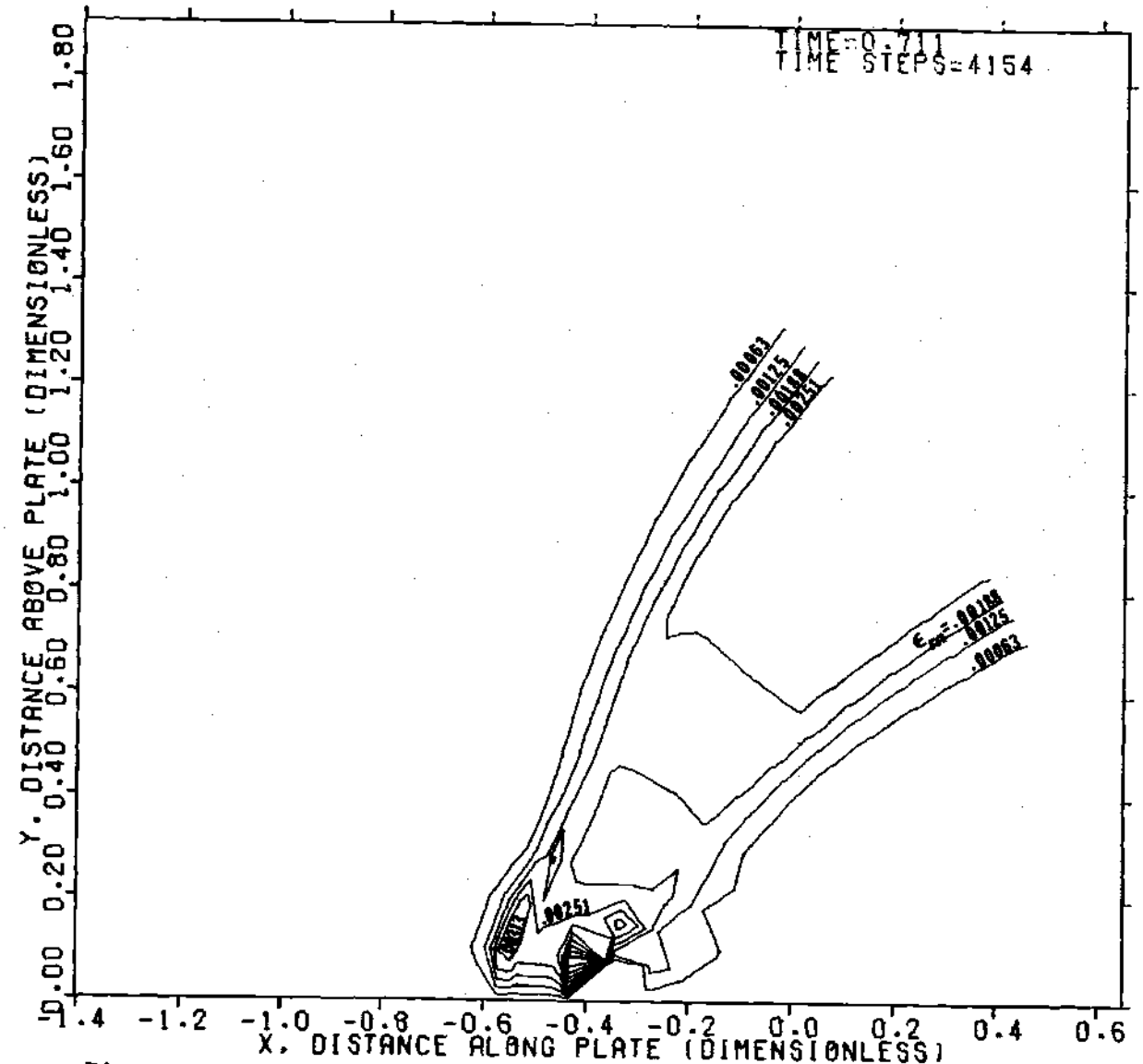

Figure 16. Lines of Constant Eddy Viscosity in the Free Flow, Enlarged View Low Subsonic Jet/Low Subsonic Free Stream (Test Case No. 1)

Comparison with Experimental Data

The jet centerline velocities, as measured and located at five different points by Ivanov, are indicated in Figures 8 and 13. The measured jet centerline velocities are observed to decay more rapidly with distance downstream than those predicted.

With regard to the location of the jet centerline, Figure 17 provides a comparison between the predicted centerline and that observed by Ivanov. Also included in the figure are the jet trajectories produced by the equations proposed by various investigators [3,5,7,14,16, 17]. Inspection of Figure 17 reveals that the predicted trajectory initially drifts to the right of the experimental data. Further downstream, however, the two paths cross and beyond this point the predicted curve lies to the left of the measured values. The jet path, predicted by the analytical model, displays better agreement than obtained by the relations proposed by Davis [3], Taylor [7], Abramovich [14], and Ackerberg [17]. The relations proposed by Ivanov [5] (to fit his own experimental data), and by Vizel and Mostinskii [16] (also to fit that same data), both appear to produce better agreement with the experimental data prior to the point where the paths cross. Beyond this point the path predicted by the analytical model is in slightly better agreement with the measured curve.

It is of interest to point out that although the predicted jet centerline initially coincided with the curve of Vizel and Mostinskii, as time progressed in the computation process the predicted curve gradually shifted to the right of its initial position. This shift was most

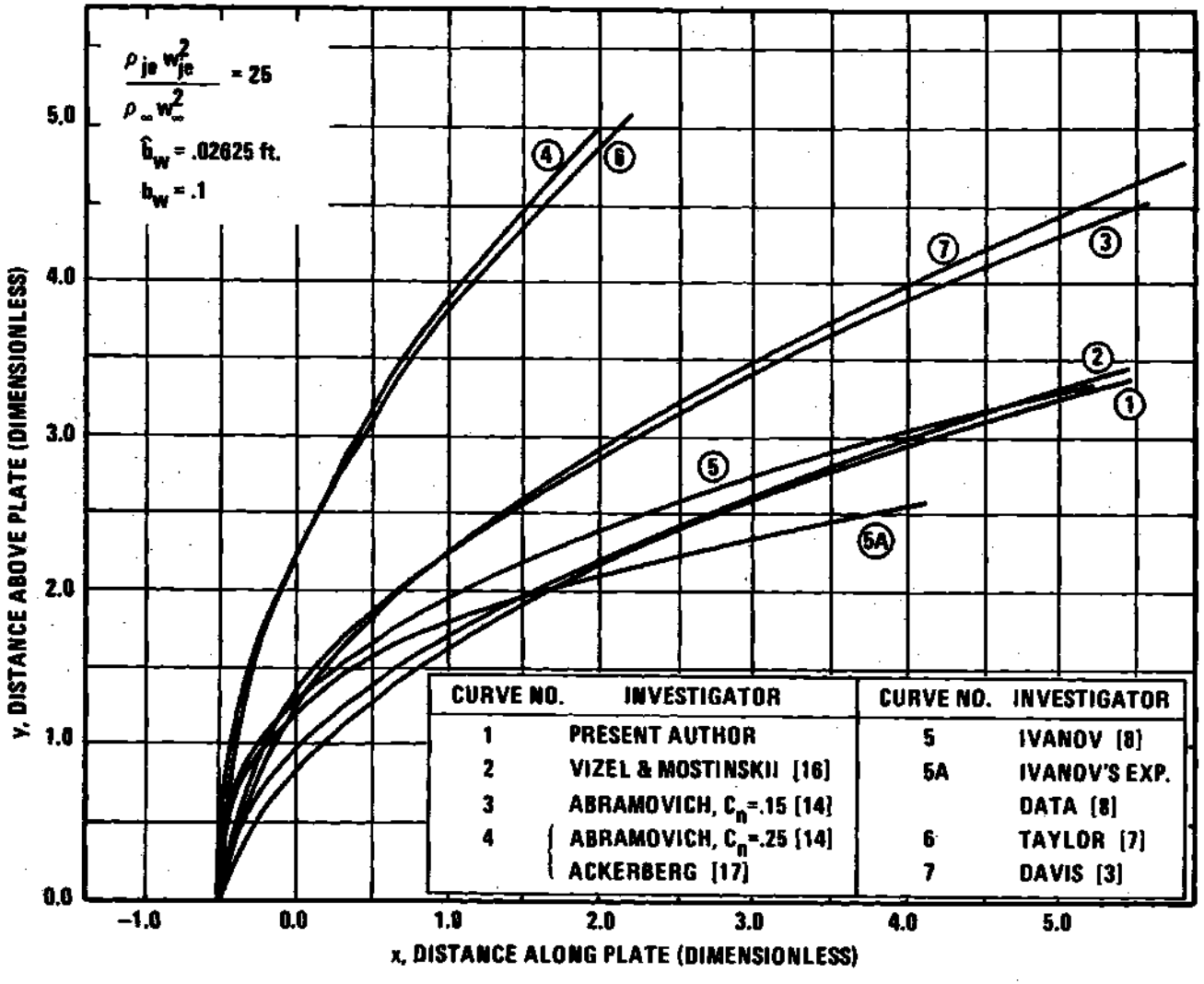

Figure 17. Measured and Predicted Jet Paths,
Low Subsonic Jet/Low Subsonic Free Stream (Test Case No. 1)

pronounced just downstream of the recirculation region. A very slow drift to the right was still present in that part of the curve beyond x~1.0 at the time the computation process was ended.

Aside from the fact already noted that the numerical solution did not achieve a steady-state condition, there exists another explanation for the differences between the observations and the predictions. Ivanov's jet used for Test Case No. 1 had a breadth-to-width ratio of only 5.0, which appears somewhat small for producing a two-dimensional jet. The presence of three-dimensional effects in the experiment thus may have produced some distortion in the results. Certainly the jet centerline velocity decays more rapidly in a three-dimensional jet, due to the fact that the jet is diffusing momentum in three dimensions as opposed to two. It would appear therefore that the predicted jet centerline velocities are quite reasonable and the agreement with the experimental data is certainly satisfactory.

Test Case No. 2
(Transonic Jet/High Subsonic Free Stream)

Heyser and Maurer [13] presented the results of four tests involving a choked plane jet exhausting into a subsonic free stream.* The first of these four tests was selected for purposes of comparison. Table 2 contains the corresponding values of the 13 test parameters based on analysis of the figure already noted, coupled with direct contact with Maurer [104,105].

---

*See Figure 25(a) of their report [13].

Table 2. Input Parameters for Test Case No. 2

Parameter	Value
Free stream velocity, $\hat{w}_\infty$	896.3 ft/sec
Free stream pressure, $\hat{p}_\infty$	2115.8 lb_f/ft^2
Free stream temperature, $\hat{T}_\infty$	451.6°R
Jet stagnation pressure, $\hat{p}_{jo}$	16397.4 lb_f/ft^2 *
Jet stagnation temperature, $\hat{T}_{jo}$	518.4°R *
Specific gas constant, $\hat{R}$	.686 $BTU/lb_m/°R$
Specific heat of gas at constant pressure, $\hat{c}_p$	.2401 $BTU/lb_m/°R$
Reference value of first coefficient of viscosity, $\hat{\mu}_{ref}$	9.724 10^{-6} $lb_m/(ft\ sec)$
Prandtl number of gas, Pr	.72
Distance upstream from slot centerline to leading edge of plate, $\hat{L}_{up}$	.3281 ft
Distance downstream from slot centerline to trailing edge of plate, $\hat{L}_{dp}$	.3609 ft
Slot width, $\hat{b}_w$	.003281 ft
Slot length, $\hat{L}_s$	.016405 ft

*These stagnation properties produce an isentropic jet exit velocity $\hat{w}_{je}$ of 1,020 ft/sec, along with an isentropic jet exit temperature $\hat{T}_{je}$ of 432.0°R.

Analysis of Test Conditions

The existence of choked flow is clearly indicated by the ratio of $\hat{\rho}_{jo}/\hat{\rho}_{\infty}$, which has a value of 7.73. The slot and jet exit velocity should be sonic, while the free stream is high subsonic (M_{∞}=0.86). As with Test Case No. 1, the free-stream temperature and the jet temperature are essentially equal and thus heat transfer is not of primary importance.

To establish the validity of the assumption of turbulent flow in the slot, jet and boundary layer, calculation of the three corresponding Reynolds numbers is necessary. For the slot, the Reynolds number ($2\hat{\rho}_s\hat{w}_s\hat{b}_w/\hat{\mu}_s$) is 2.4×10^5, which is considerably above the lower limit, 10^4, for turbulent flow. As previously noted, turbulent jets normally are produced with Reynolds numbers ($\hat{\rho}_{je}\hat{w}_{je}\hat{b}_w/\hat{\mu}_{je}$) above 30, and thus the jet should be turbulent with a Reynolds number of $\sim1.2\times10^5$.

The plate Reynolds number in the vicinity of the jet exit ($\hat{\rho}_{\infty}\hat{w}_{\infty}\hat{L}_{up}/\hat{\mu}_{\infty}$) is approximately 2.9×10^6. This value is sufficiently greater than the standard value of 5×10^5 to justify the assumption of a turbulent boundary layer. In addition notice should be taken that the free stream in the experiment by Heyser and Maurer was generated by means of flow exhausting from a nozzle. The diameter of the nozzle is not given but it appears that this diameter is of the same order of magnitude as the plate length.* With such a diameter the nozzle Reynolds number ($\hat{\rho}\hat{w}\hat{D}/\hat{\mu}$) would be $\sim6\times10^6$. Round jets are normally turbulent for

*See Figures 16a and 16b of Reference 13.

Reynolds numbers above 80 [103]. Thus the boundary layer produced by the test conditions would be turbulent.

Predicted Flow Pattern

A transient numerical solution for Test Case No. 2 was carried out for 3536 time steps by means of the program DEFJET. The plotting programs MNPLOT, VECTOR, and AUXPLT were utilized to plot the flow patterns which resulted. As with Test Case No. 1, two sets of plots were generated. The first set representing an overall view (excluding the region in the immediate vicinity of the jet exit) covered the region bounded by the parabolas u_{10}, u_{22}, v_1, and v_{20}. An enlarged view of the flow in the vicinity of the jet exit was provided by the second set. The latter covered the area of which the boundaries were u_1, u_{14}, v_1, and v_{19}.

Figure 18 presents the grid system for the overall view. Because of the relatively wide slot used by Heyser and Maurer, as compared with that used by Ivanov, close spacing of the v-parabolas on either side of $v_{c\ell}$ is unnecessary. As before, all figures relating to the overall view for Test Case No. 2 have the same scale as used in Figure 18.

As with Test Case No. 1 notice should be taken that all figures are presented in dimensionless form with the definition of each dimensionless quantity appearing in the second section of Chapter III. With regard to dimensionless time, it should be noted that one unit of this quantity represents the physical time required for a particle moving at the isentropic jet exit velocity to travel twice the distance along the x-axis from the origin to the slot centerline. For Test Case No. 2

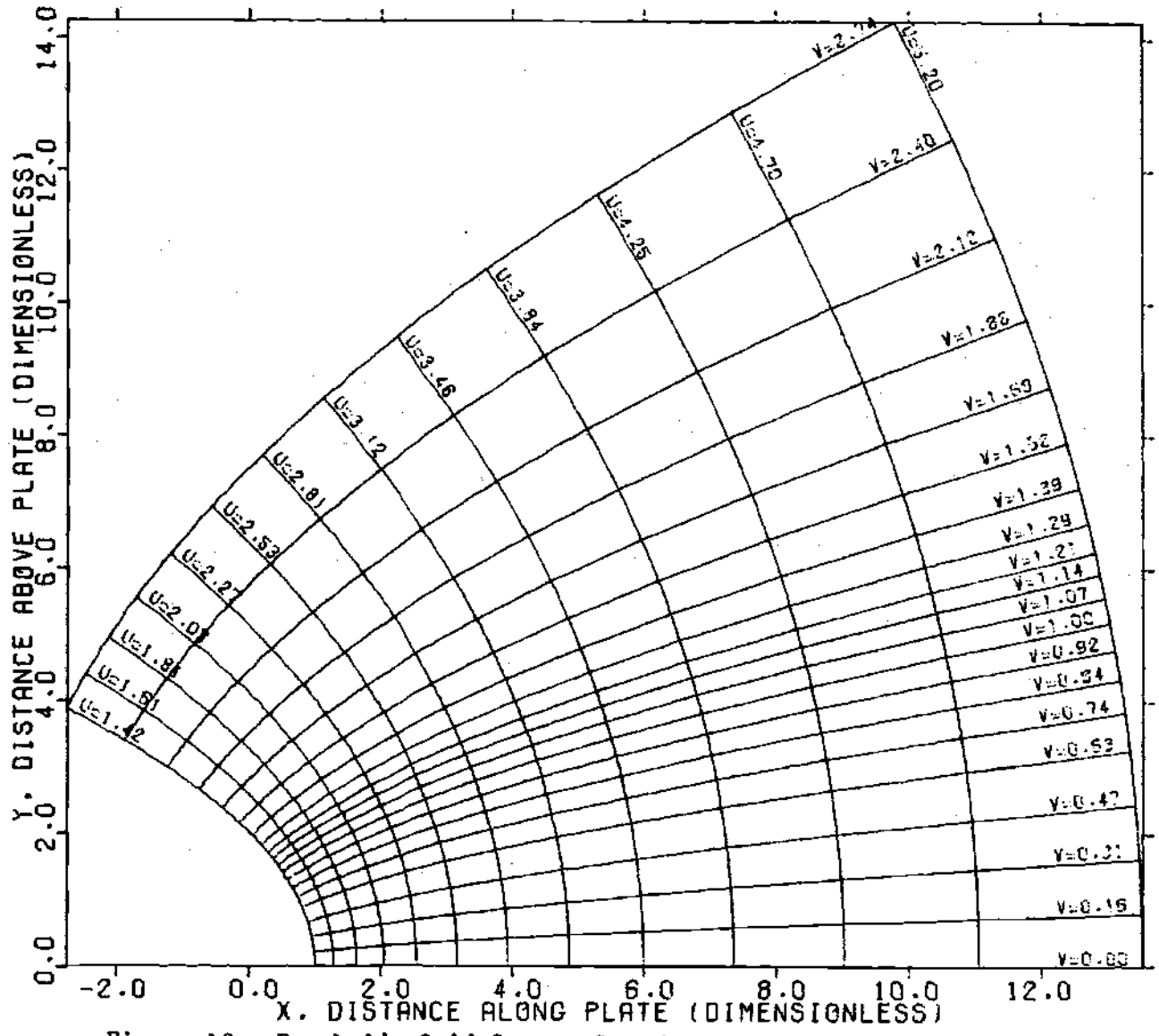

Figure 18. Parabolic Grid System for the Free Flow, Overall View, Transonic Jet/High Subsonic Free Stream (Test Case No. 2)

the total elapsed dimensionless time was 10.641, representing approximately 76 microseconds. During this time period a signal traveling at the speed of sound could travel ~0.076 feet and thus cover approximately 25 per cent of the plate.

The overall flow pattern based on the fluid velocity vectors is presented in Figure 19. The jet velocity profiles are observed to resemble those for a turbulent plane jet as observed by Reichardt [27]. The lower portions of these same profiles indicate the presence of a sizeable recirculation region downstream of the jet adjacent to the plate.

The jet is observed to disperse more rapidly in Test Case No. 2 than was observed in Test Case No. 1. This can be attributed in part to the fact that for the second case the ratio of jet exit velocity to the free stream velocity (~1.14) is much smaller than for the first case (~5.05). Thus, based on the velocity vectors it is difficult to identify the jet in Test Case No. 2 beyond the parabola u=4.25. Of special interest in the overall view is the extent to which the free stream is disrupted by the jet. It appears that the influence of the latter is felt further upstream than was observed in Test Case No. 1.

Downstream of the jet there appears to be no shielded region, except for the recirculation region itself. The jet is seen to attach to the wall in the vicinity of x=6.0, which is considerably further downstream than was observed in Test Case No. 1. A wall jet is produced beyond this point.

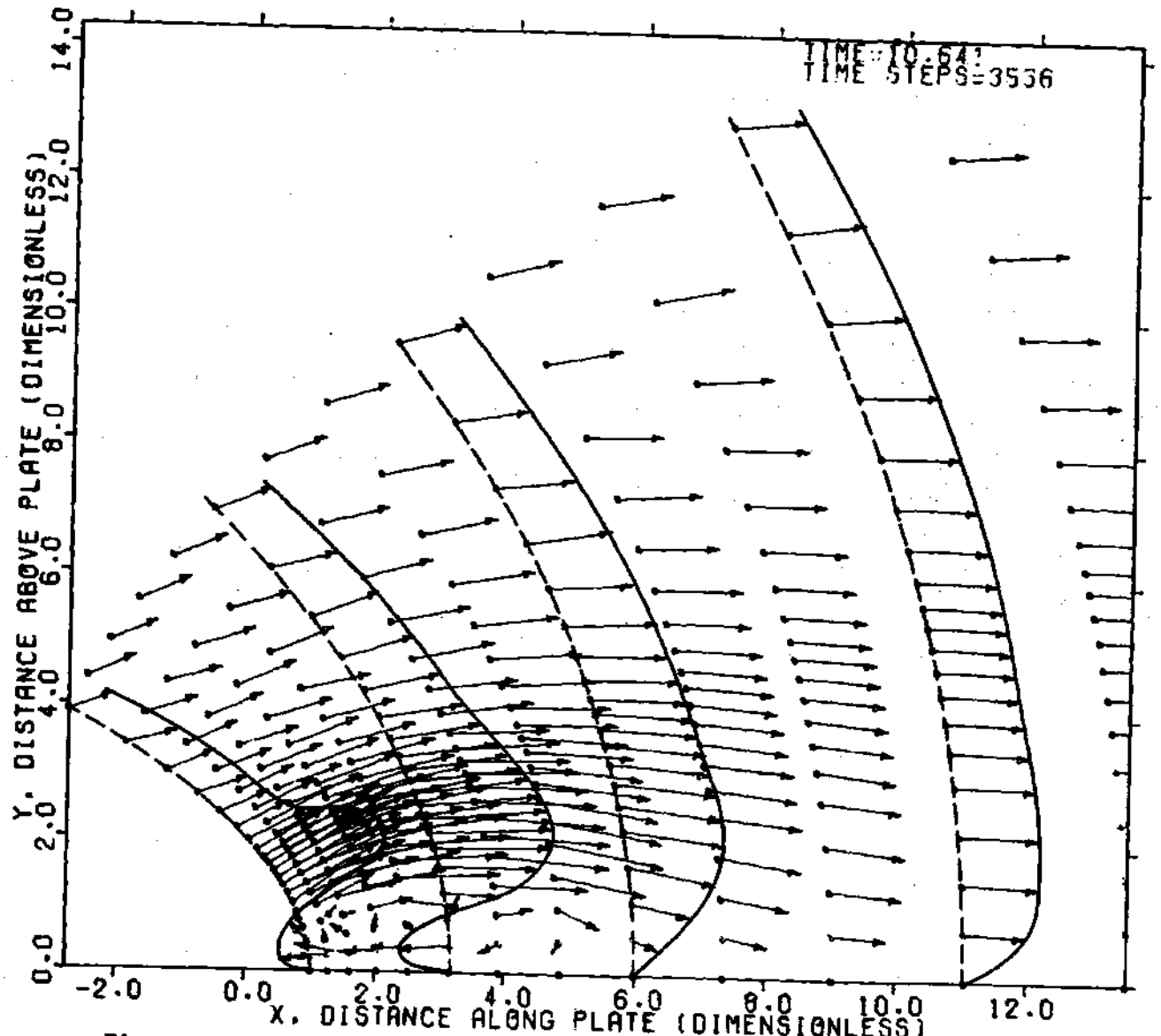

Figure 19. Fluid Velocity in the Free Flow, Overall View, Transonic Jet/High Subsonic Free Stream (Test Case No. 2)

Another item of interest in the figure is the indication of a normal shock wave in the vicinity of the parabola u=3.84. Although the free stream velocity is subsonic and the jet exit velocity is only sonic, because of the jet being underexpanded, supersonic flow occurs in a portion of the flow field. The normal shock marks the downstream limit of the supersonic flow region. All flow beyond this shock is subsonic.

The pattern of streamlines for the overall view, as shown in Figure 20, is quite similar to that produced by the velocity vectors in the preceding figure. Only slight penetration of the jet by the streamlines can be detected. In general the streamlines appear to conform to the path of the jet. The overall pattern gives the impression of arcs of concentric circles. A series of waves are located along these arcs, but the precise significance of these waves is not clear. Consistent with the observations made based on the velocity vector patterns, the deflection of the streamlines upstream of the jet indicates that the influence of the latter is felt further upstream than was observed in Test Case No. 1.

Isotachs are presented in Figure 21. A local maximum within the supersonic core is observed along the jet centerline at u=3.12. The decay of the jet centerline velocity can be observed downstream of this point. A transverse variation is likewise indicated. The normal shock previously noted can be seen to lie generally between the isotachs w=1.19 and w=1.04. The sawtooth pattern of the latter is believed to be related to the presence of the shock.

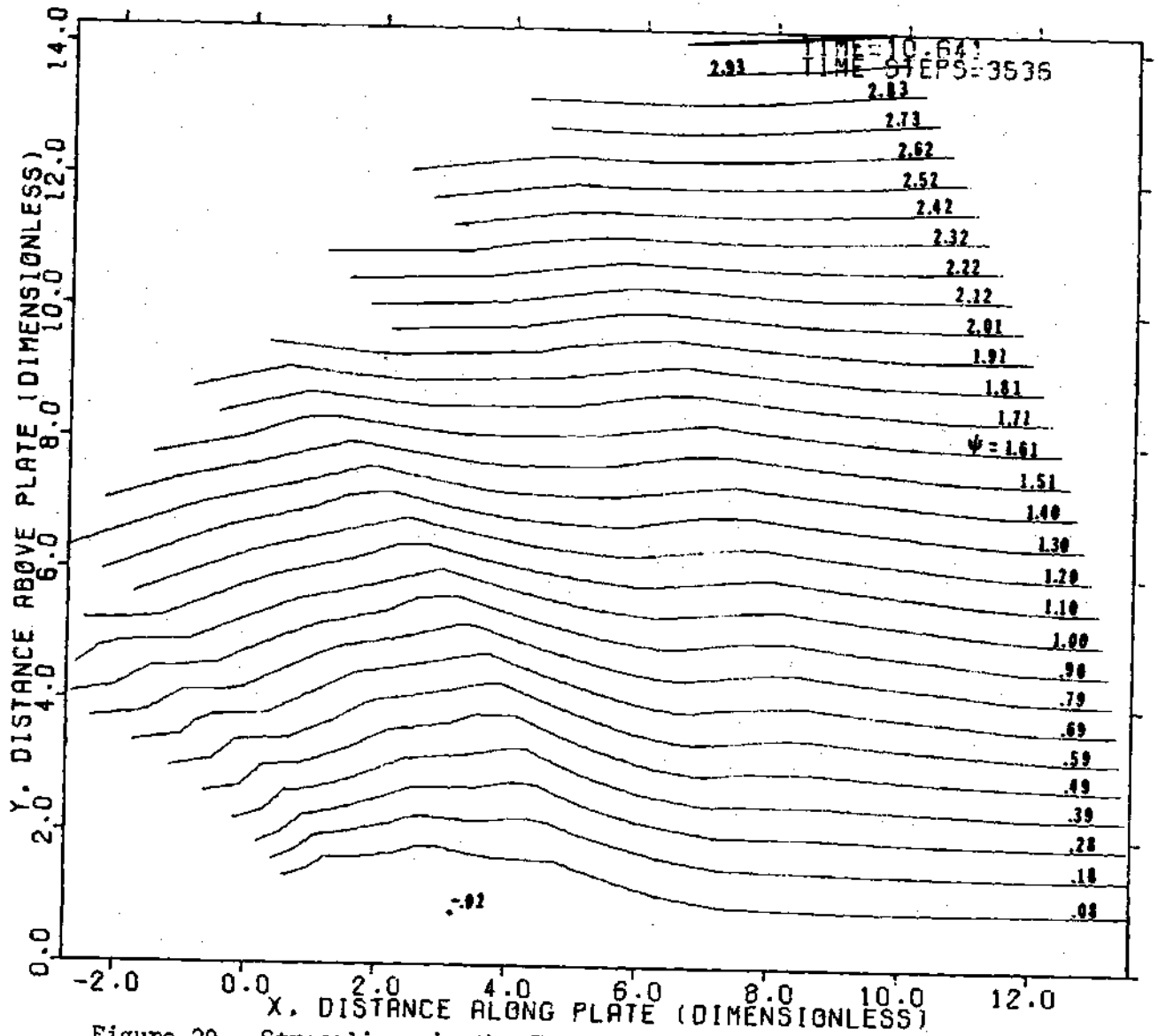

Figure 20. Streamlines in the Free Flow, Overall View, Transonic Jet/High Subsonic Free Stream (Test Case No. 2)

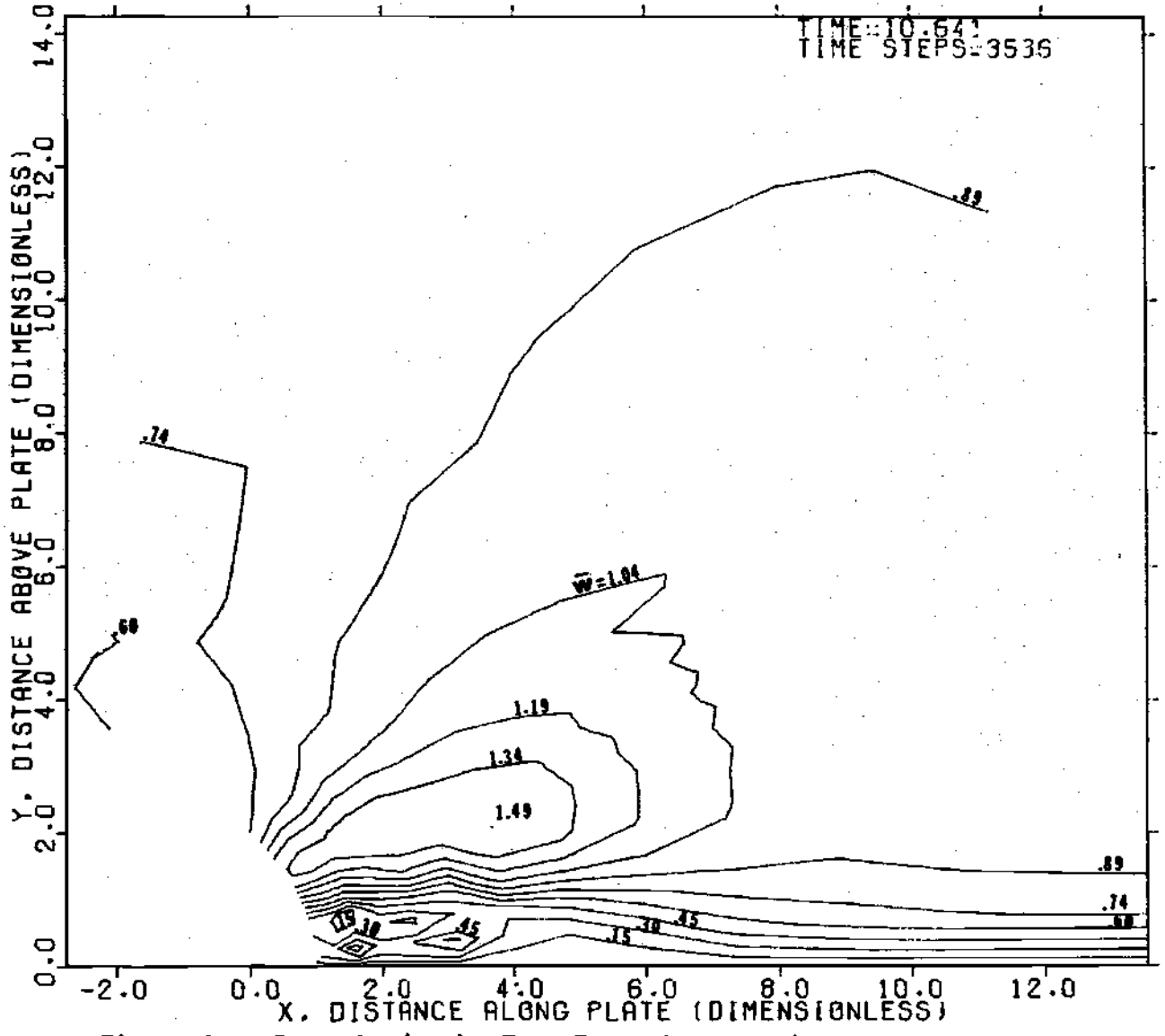

Figure 21. Isotachs in the Free Flow, Overall View,
Transonic Jet/High Subsonic Free Stream (Test Case No. 2)

Lines of constant eddy viscosity, which are plotted in Figure 22, indicate considerable asymmetry with respect to the jet centerline. This implies that the jet half-velocity width $\delta_{1/2}$ for the convex side of the jet is much greater than on the concave side. The variation of jet centerline eddy viscosity with distance downstream differs considerably from the general case for a plane jet. In the region covered by the overall view, the centerline eddy viscosity is observed to initially increase until a local maximum is reached at u=2.81. Further downstream the centerline value decreases out to u=4.25. Beyond this point $(\epsilon_m)_{jc\ell}$ increases with distance downstream. In the vicinity of the minimum the contours form a hump-like pattern.

Because compressibility effects are more significant in Test Case No. 2, considerable benefit can be derived from the study of isobars, which are shown in Figure 23 for the overall view. The pattern which is observed is somewhat erratic, but careful examination reveals that the isobars tend to fan out away from the jet. The region on the convex side of the jet contains high pressure isobars while on the concave side low pressure isobars are encountered. The recirculation region downstream of the jet, as expected, is a region of low pressure. The normal shock is observed to lie between the isobars p=0.14 and p=0.16. The sawtooth pattern, observed with the isotachs, is again present.

The grid system for the enlarged view of Test Case No. 2 is presented in Figure 24. As already noted the relatively wide slot used by Heyser and Maurer permits a more uniform spacing of the v-parabolas. The scale of all subsequent figures, relating to the enlarged view, is the same as that shown in Figure 24.

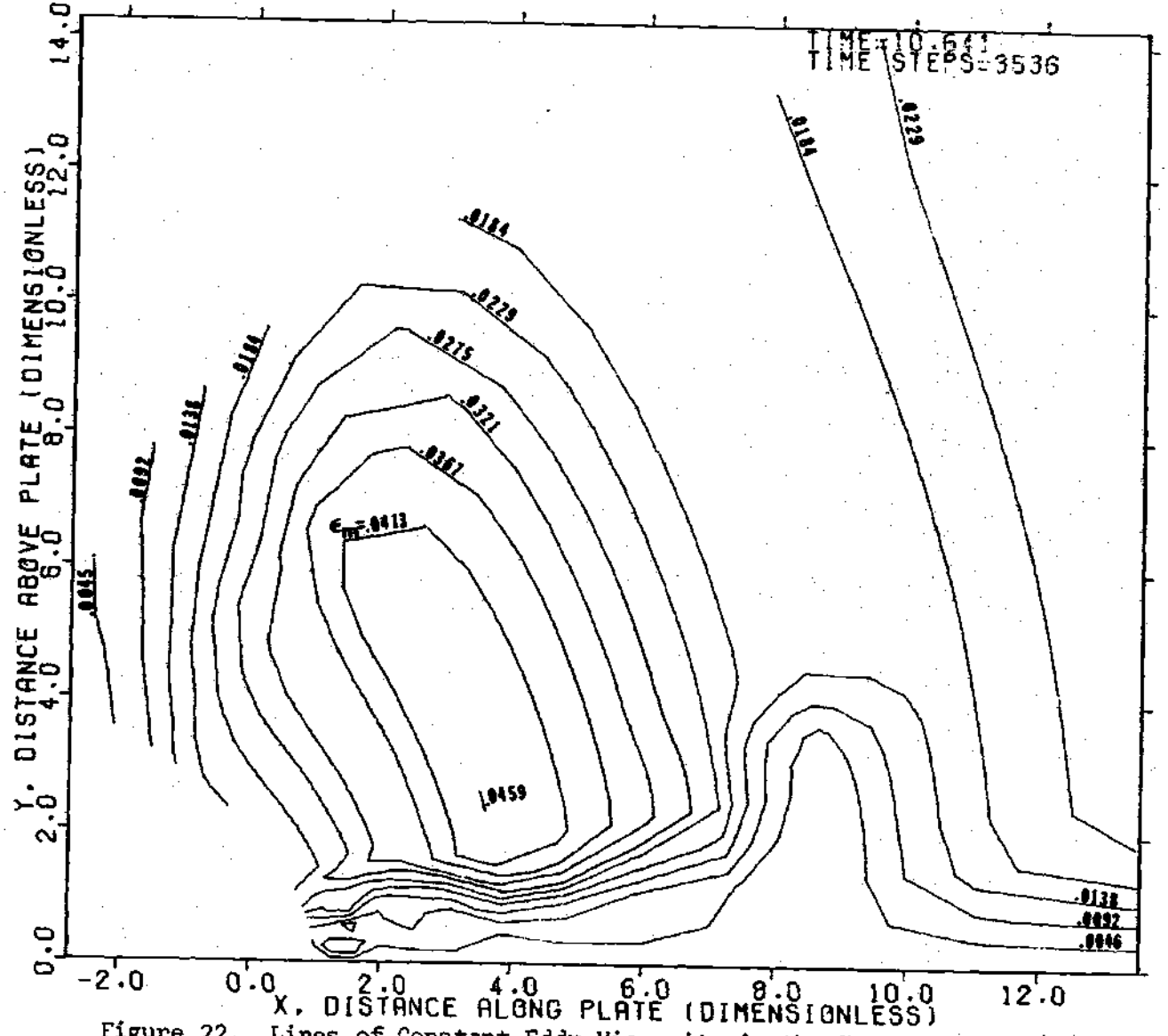

Figure 22. Lines of Constant Eddy Viscosity in the Free Flow, Overall View, Transonic Jet/High Subsonic Free Stream (Test Case No. 2)

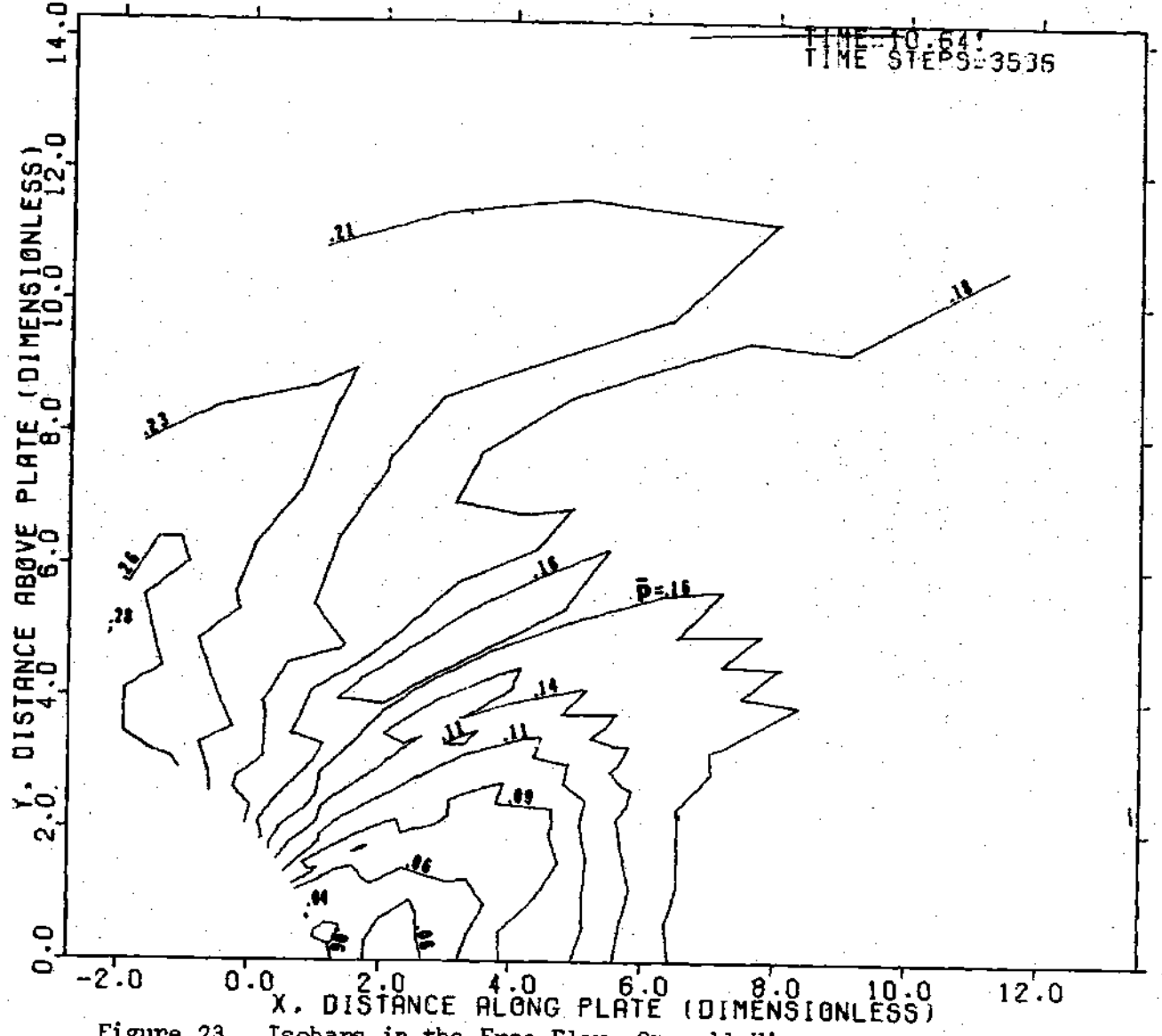

Figure 23. Isobars in the Free Flow, Overall View, Transonic Jet/High Subsonic Free Stream (Test Case No. 2)

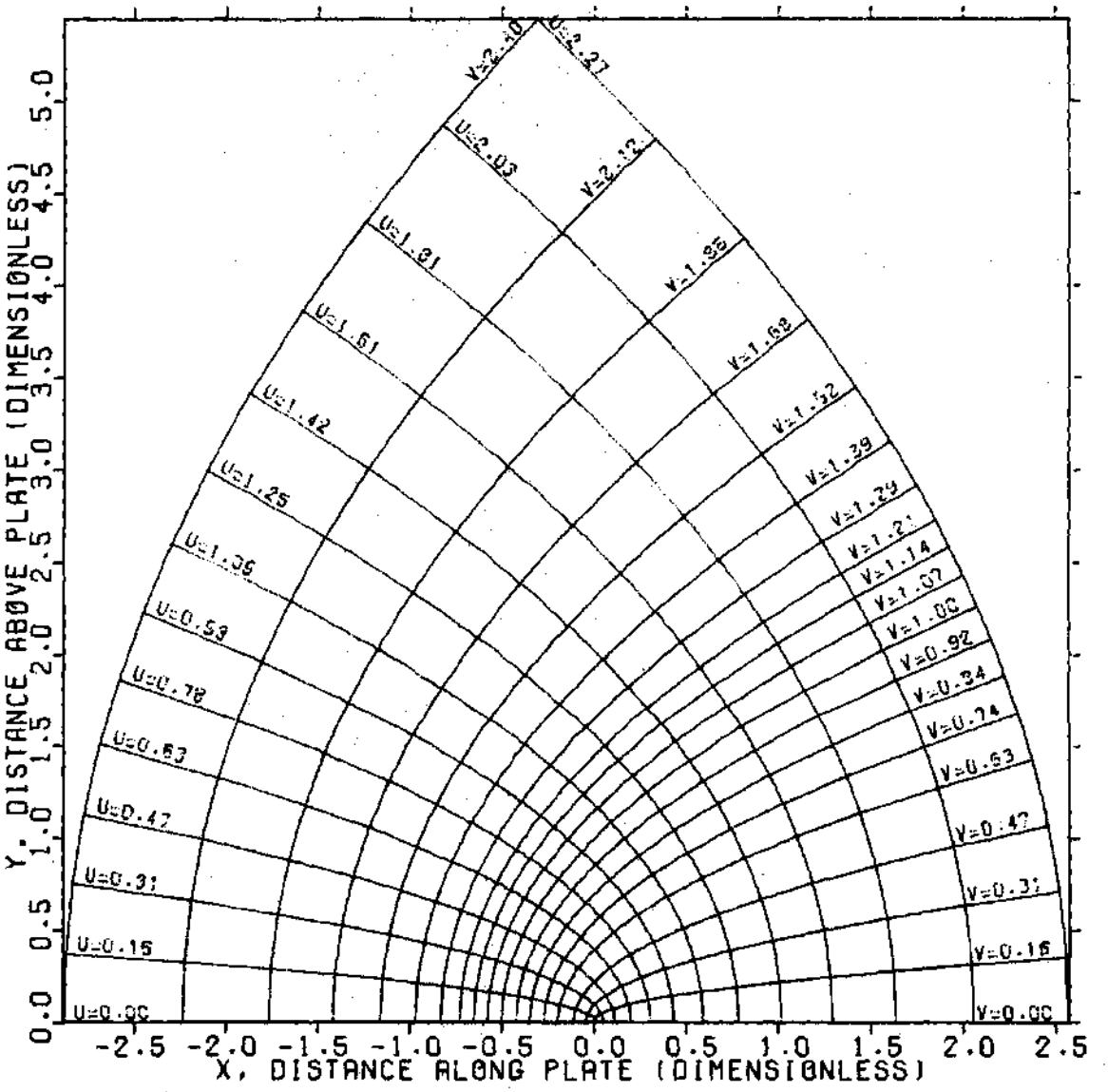

Figure 24. Parabolic Grid System for the Free Flow, Enlarged View, Transonic Jet/High Subsonic Free Stream (Test Case No. 2)

A number of interesting features are contained in Figure 25, which presents a plot of velocity vectors. As before the jet velocity profiles are visible. The jet centerline appears to lie to the right of $v_{c\ell}$. Upstream of the jet, boundary layer separation is observed in the vicinity of x=-3.0. A weak separation vortex, rotating clockwise is clearly visible. Between this vortex and the leading edge of the jet the flow is observed to first turn toward the plate and then, closer to the jet, to turn away from the plate. The result is essentially a "U-turn" which never seems to close into a counter-clockwise vortex. Downstream of the jet exit, near the plate, a portion of the recirculation region can be observed.

Streamlines for the enlarged view, as shown in Figure 26, clearly outline the jet flow pattern, and, as in the overall view, closely resemble the pattern produced by the velocity vectors. One exception to the general resemblance occurs in the region of boundary layer separation. Here the streamline ψ=0.27 passes through the region when the separation vortex lies, without producing a closed loop. This difference in the two patterns possibly results from mass diffusion which is taken into account in the streamlines, but not in the velocity vectors. The "U-turn" which the flow makes between the separation region and the leading edge of the jet is clearly visible.

The contour plot of isotachs for the enlarged view is presented in Figure 27. The jet centerline velocity is seen to initially increase as the underexpanded gas accelerates, producing a supersonic core. A local maximum is reached at u=0.93. Further downstream the centerline

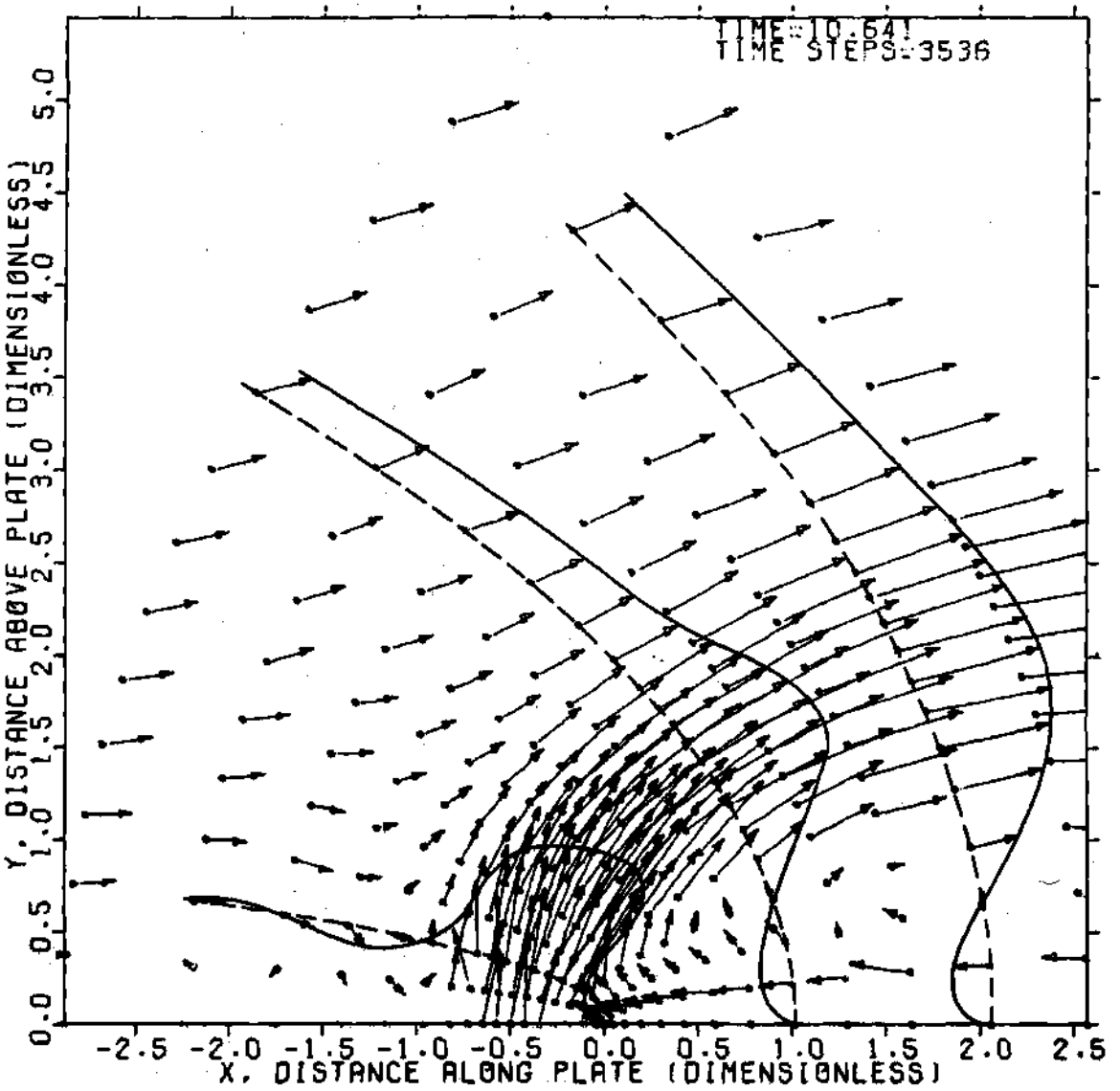

Figure 25. Fluid Velocity in the Free Flow, Enlarged View, Transonic Jet/High Subsonic Free Stream (Test Case No. 2)

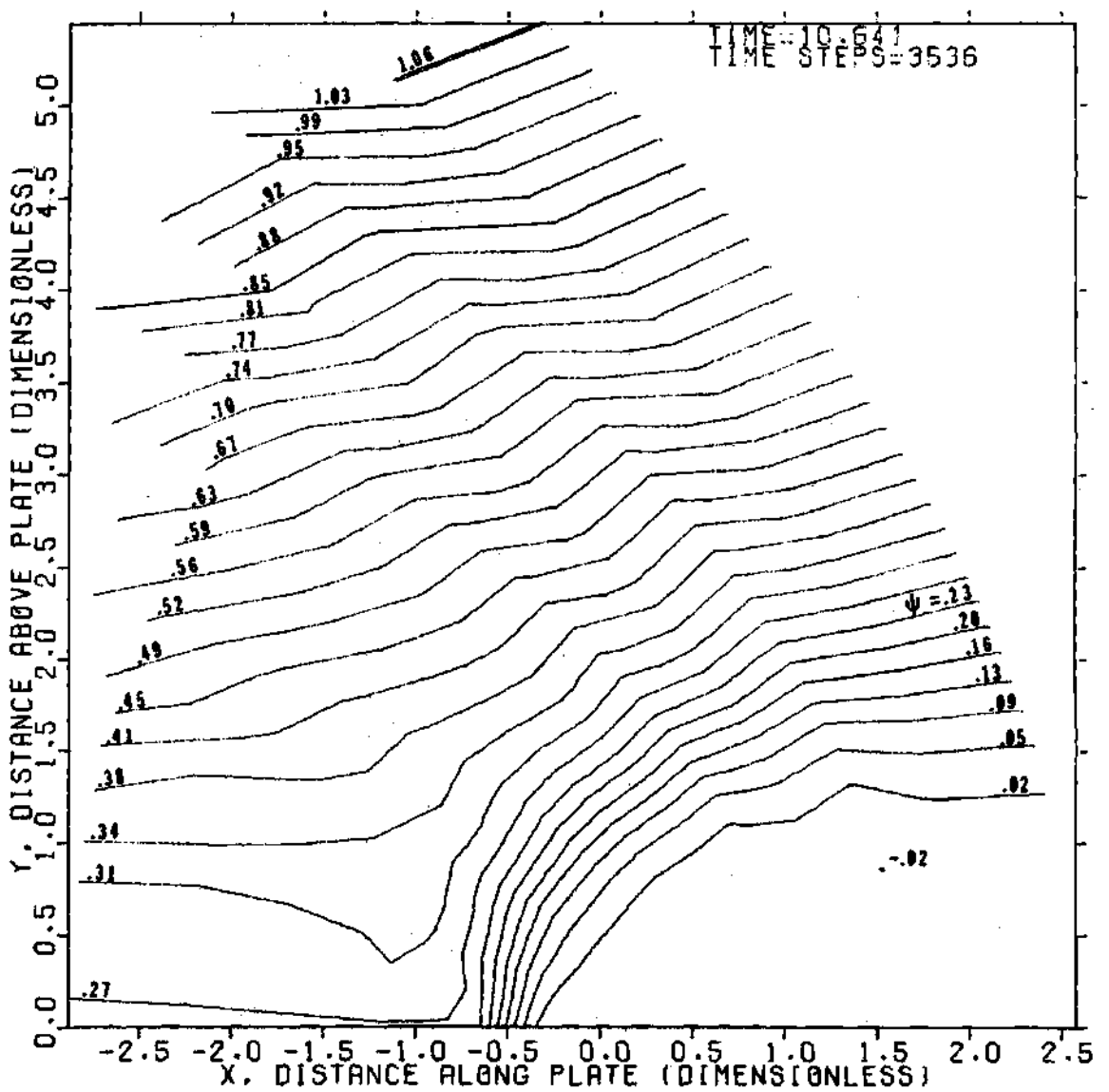

Figure 26. Streamlines in the Free Flow, Enlarged View, Transonic Jet/High Subsonic Free Stream (Test Case No. 2)

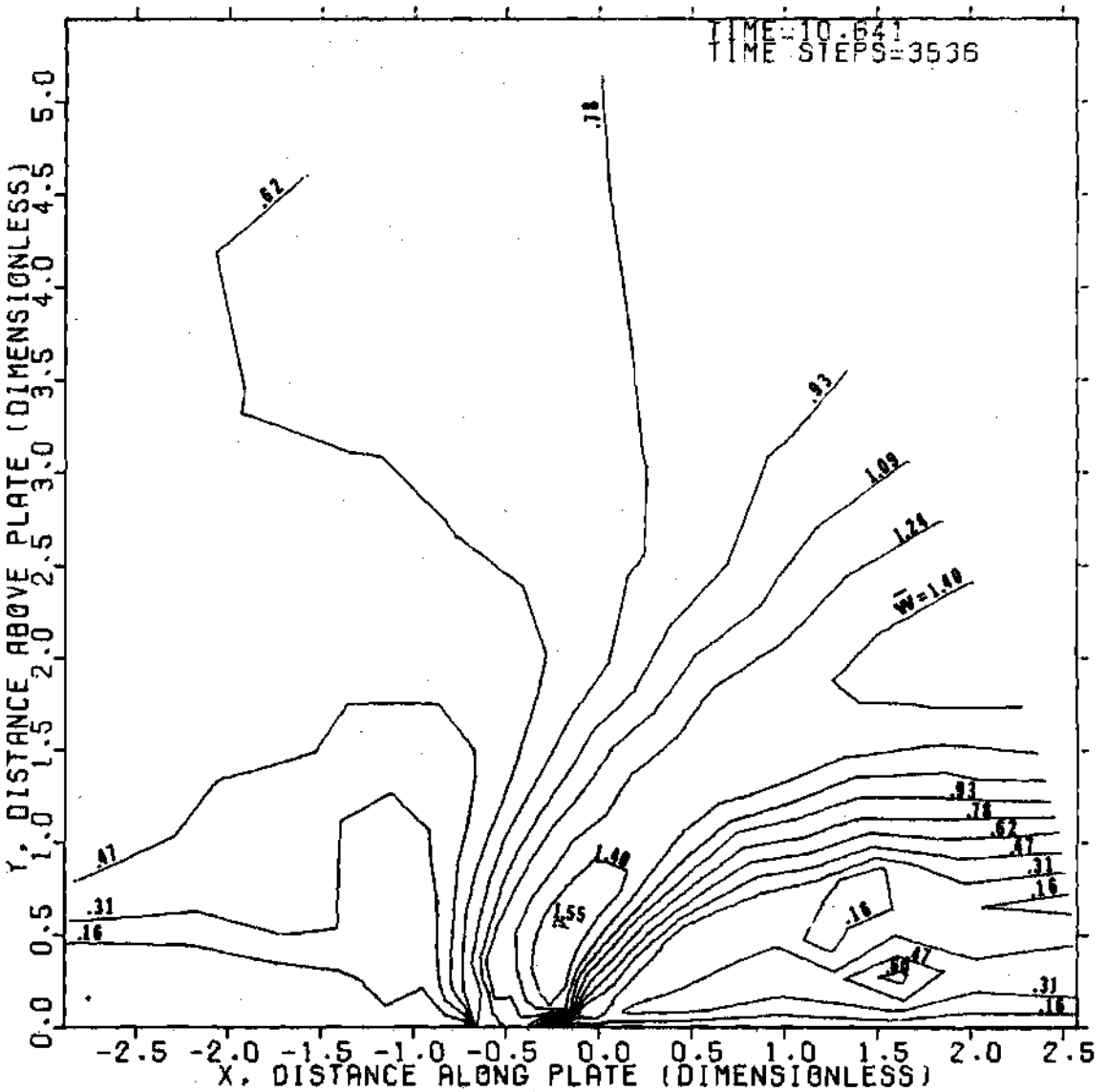

Figure 27. Isotachs in the Free Flow, Enlarged View, Transonic Jet/High Subsonic Free Stream (Test Case No. 2)

velocity first decreases out to u=1.61 and then begins to increase. The transverse variation of the jet speed generally conforms to the expected pattern.

Lines of constant eddy viscosity for the enlarged view are shown in Figure 28. The pattern is quite complex. The jet centerline eddy viscosity first increases until a value of .0167 is reached in the vicinity of u=0.47. The centerline value then appears to remain essentially constant until u=0.93. Beyond this point, the value of centerline eddy viscosity increases with distance downstream. As with Test Case No. 1, two local maxima occur, one on either side of the jet exit. The local maxima result from the large velocity gradients which exist in these areas. The asymmetric pattern with respect to the jet centerline which was noted in the overall view, is again clearly indicated.

Isobars for the enlarged view, as shown in Figure 29, indicate the presence of a sharp pressure gradient in the vicinity of the jet exit. This is to be expected due to the rapid expansion of the jet as it emerges into the lower pressure free stream. As with the overall view, the isobars appear to fan out from the jet with the higher pressure region corresponding to the convex side of the jet, and the lower pressure to the concave side. The recirculation region is seen to contain the point of minimum pressure.

The predicted flow pattern at the end of 3536 time steps, while stable and reasonably smooth, had not reached a true steady-state condition. As in Test Case No. 1, the flow in the slot, as time progressed, began to display physically unrealistic features. These

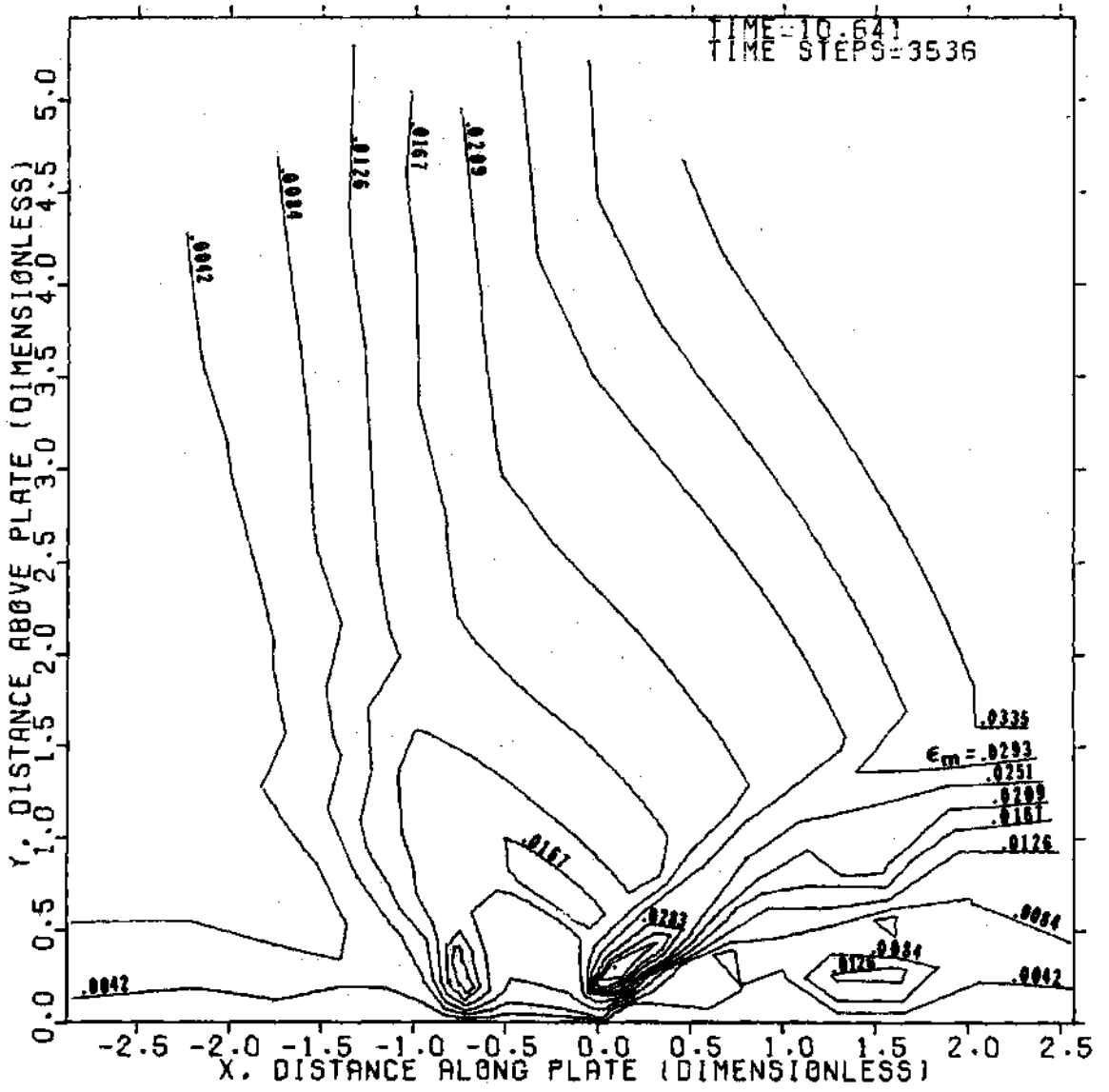

Figure 28. Lines of Constant Eddy Viscosity in the Free Flow, Enlarged View, Transonic Jet/High Subsonic Free Stream (Test Case No. 2)

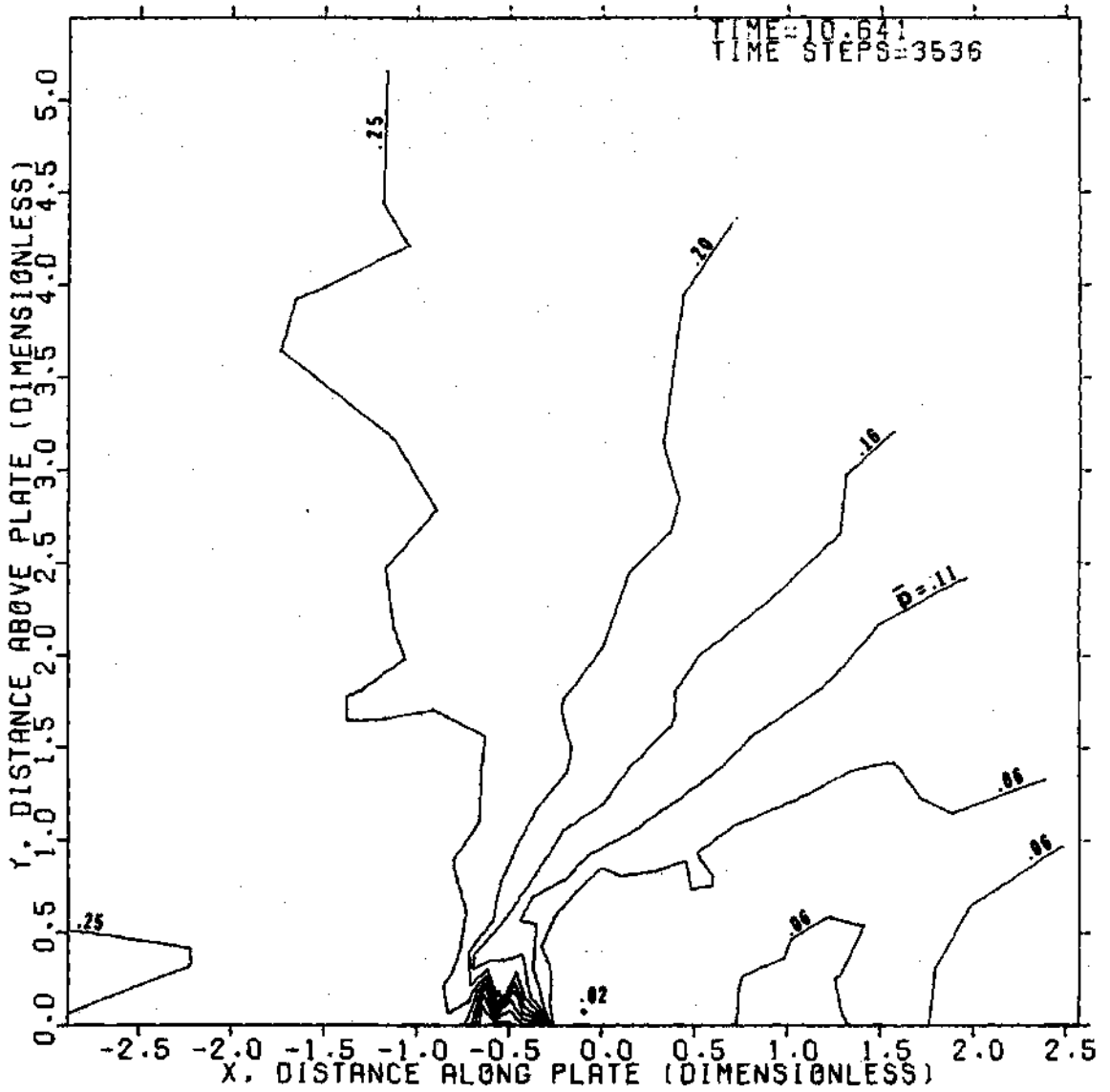

Figure 29. Isobars in the Free Flow, Enlarged View, Transonic Jet/High Subsonic Free Stream (Test Case No. 2)

included a pressure decrease upstream and a gradual reduction of the flow in the slot.

Comparison with Experimental Data

As noted in Chapter II, the experimental data obtained by Heyser and Maurer consisted primarily of pressure measurements along the flat plate. The measured values corresponding to Test Case No. 2 are shown in Figure 30 along with the predicted pressure distribution. A number of differences between the two distributions are immediately evident. The predicted distribution is more extreme in its range and appears more jagged. The measured distribution indicates that the influence of the jet extends a greater distance both upstream and downstream.

The observed difference can be explained to a certain extent by several factors. First, the predicted pressure peak at $x \approx -4.0$ actually represents a moving pressure pulse which is being propagated upstream along the plate. This pulse does not have any true physical significance but instead was produced by the initial conditions to the problem. Given sufficient time it apparently would continue to move upstream, gradually weakening with distance.

The second predicted pressure peak, occurring at $x = -1.0$, coincides with the point of boundary layer reattachment just upstream of the jet. This peak appears stationary and stable and appears to act as a sign of boundary layer separation. Although the measured distribution upstream of the jet contains no such peak, it is interesting to note that a number of the other test runs, carried out by Heyser and Maurer with higher pressure ratios (p_{j_o}/p_∞), did contain a "hump" or "plateau" in the same region where the predicted peak occurs.

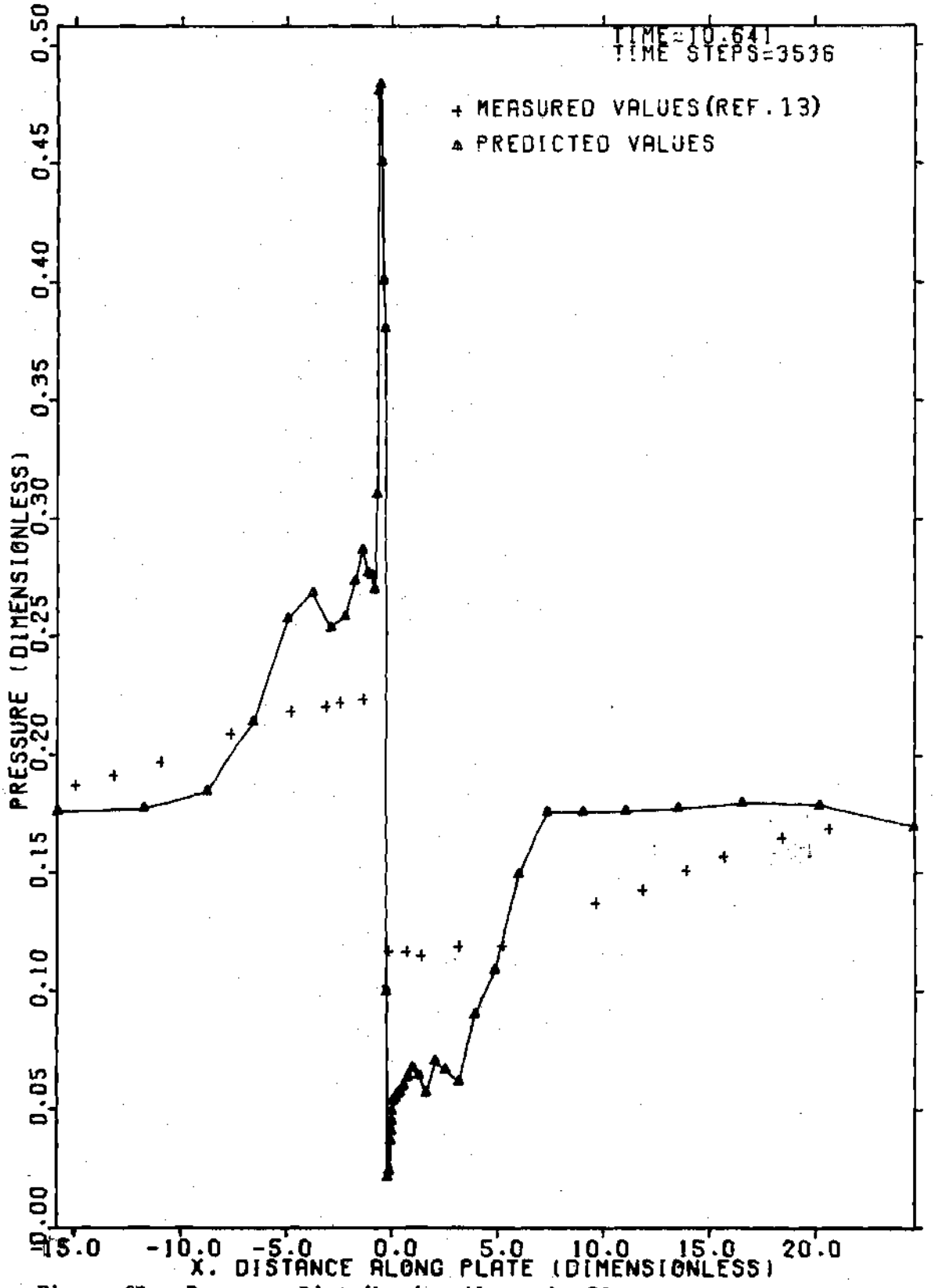

Figure 30. Pressure Distribution Along the Plate, Transonic Jet/High Subsonic Free Stream (Test Case No. 2)

The third predicted pressure peak is simply the pressure maximum in the vicinity of the jet centerline. Such a pressure distribution in the jet exit plane results from the jet being underexpanded. Notice should be taken that Heyser and Maurer took no pressure measurements in this region.

Downstream of the jet exit, the predicted region of low pressure is seen to involve lower pressures than those measured. The difference between the minimum values of measured and predicted pressure is due at least in part to the presence of three-dimensional effects present in the actual experiments, as noted by Maurer [105]. These effects, which would also be present on the upstream side of the jet, would tend to reduce the degree of rarefaction in the recirculation region.

A sharp pressure gradient is predicted in the vicinity of $x = 6.0$, while the measured distribution displays no such variation. The predicted gradient results from the presence of the normal shock, which as already discussed, is predicted to occur in the jet along the parabola $u = 3.84$. The absence of such a pattern from the measured data is difficult to explain because the schlieren photograph presented by Heyser and Maurer clearly indicates a normal shock in the same general region as that predicted.* Apparently the actual shock, present in the experiment, did not extend as near the surface as does the predicted shock.

The preceding discussion provides a partial explanation to the differences between the measured and predicted pressure distributions. In addition to the points noted the fact that a true steady-state

---

*See Figure 18 of Reference 13.

solution was not obtained in 3536 time steps may be quite significant. Additional time would certainly have eliminated the first pressure peak, representing a pressure pulse moving upstream. The remainder of the predicted distribution, however, apparently would experience relatively small changes with additional time. The normal shock possibly would move slightly further downstream, but there was no indication that this shock would disappear or move out of the picture.

Although Heyser and Maurer did not obtain experimental data which would permit location of the jet centerline, some benefit can be derived by comparing the jet path predicted by the analytical model with that predicted by the equations of various investigators [3,7,14,16,17]. Such a comparison is provided in Figure 31. The jet trajectory as predicted by the analytical model is seen to originate slightly to the right of the slot centerline. This resulted from the asymmetry of the velocity profile at the slot exit. All of the jet paths produced by the various investigators display greater penetration than the path predicted by the analytical model, but all of the former are based on data involving jets and free streams of much lower velocities than those involved in the tests of Heyser and Maurer.

Important Features of Deflected Jets

The two test cases for which numerical results have been generated provide valuable insight into the general nature of deflected jets. Of course, the two cases alone are not sufficient to permit forming broad generalizations. At the same time certain significant

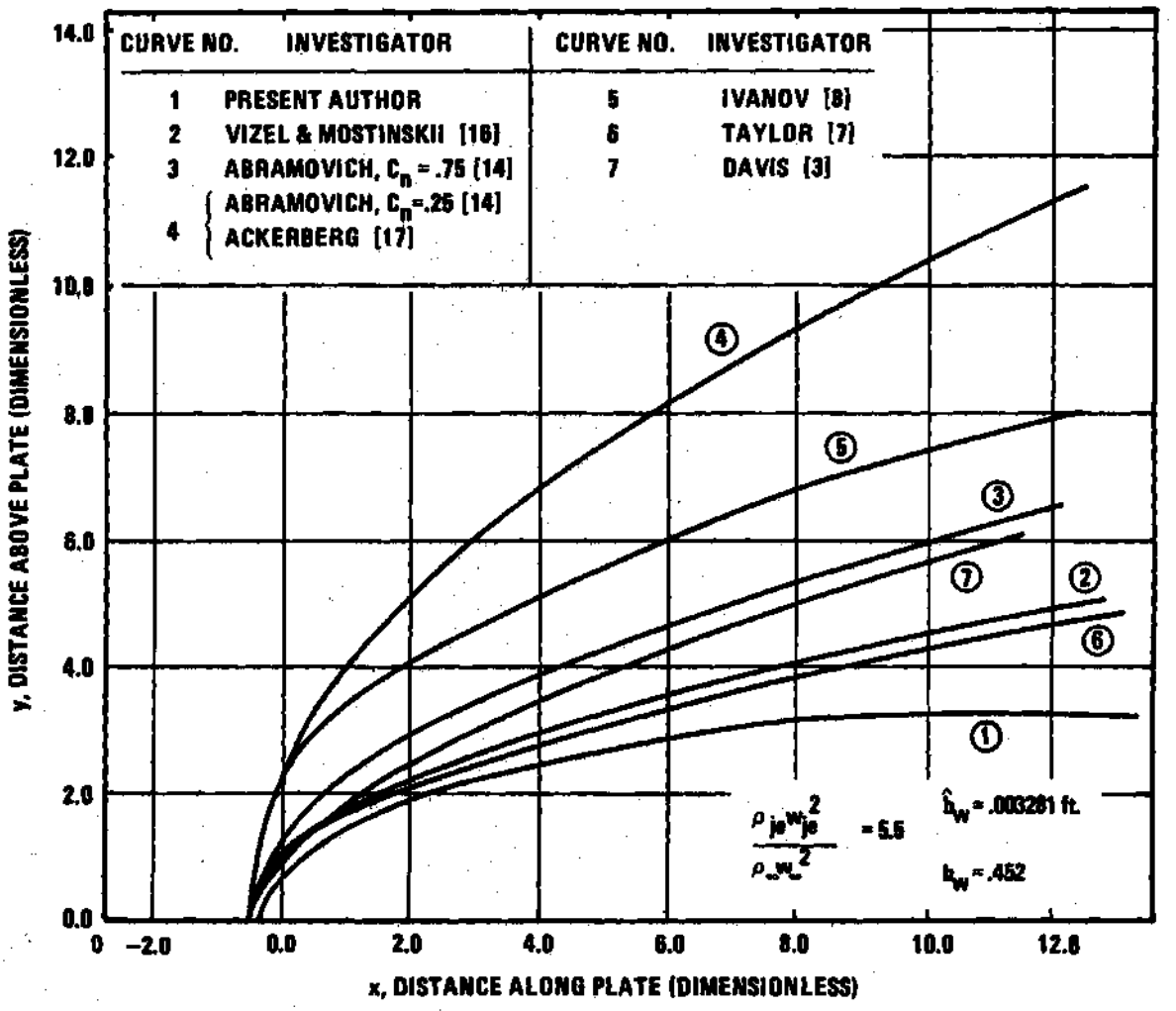

Figure 31. Predicted Jet Paths, Transonic Jet/High Subsonic Free Stream (Test Case No. 2)

features of deflected jets which have not been previously noted are suggested by the predicted flow pattern and are worthy of discussion.

Perhaps the most significant feature of the low velocity case (Test Case No. 1) is the observation that streamlines originating in the free stream, upstream of the jet, actually traversed the latter. Thus at least part of the fluid in the sizable shielded region, downstream of the jet, appears to come from the free stream as shown in Figures 9 and 14. Although the jet appears to penetrate out into the free stream for a significant distance the fluid leaving the slot actually penetrates a much shorter distance before curving back and flowing along the plate. In essence, based on the streamline pattern, the jet appears to represent a step-like process in which momentum transport continues for a greater distance than does mass transport.

There exists at least one significant argument which tends to refute the possibility of the streamlines from the free stream traversing the jet in the manner predicted for Test Case No. 1. In order for such traverse to occur, the net amount of kinetic energy transferred across the streamlines must be of the same order of magnitude as that of the jet as it leaves the slot. The amount of kinetic energy at the jet exit is relatively large and it is difficult to conceive of such a quantity of kinetic energy being transported across streamlines. This transverse transport of kinetic energy may be attributed in part to the large shear stresses associated with turbulent flow processes, but there is some doubt that turbulence alone can explain such transport. Furthermore, turbulent processes are inherently dissipative in nature, and

thus it is difficult to envision the transport process persisting so far out into the free stream in the manner predicted.

If turbulent transport is not sufficient to account for the transverse transport of kinetic energy, the implication is that an imbalance exists between the transport of kinetic energy along the streamlines and the transport across the streamlines. Such an imbalance would produce large time rates of change of kinetic energy at points along the streamlines. These large time derivatives would in turn indicate that the numerical computational process was far from the true steady-state solution.

If the preceding line of thought is continued the possibility that the computational process is far from the steady-state solution leads to the conclusion that the predicted flow patterns as presented may be more representative of the initial conditions or some intermediate transient case than the steady-state solution. In an attempt to shed some light on this point, the patterns of streamlines generated at various times during the computational process for Test Case No. 1 are presented in Figures 32 through 36.

The pattern of the streamlines, based on the initial conditions as given in Appendix F, is shown in Figure 32. No recirculation region is present but study of the velocity vectors for the initial time period indicates that streamlines originating upstream of the jet pass through the jet in the initial pattern. At this juncture it is important to note that the streamlines as presented are based on integrated mass flow rates and not on the actual direction of the velocity vectors.

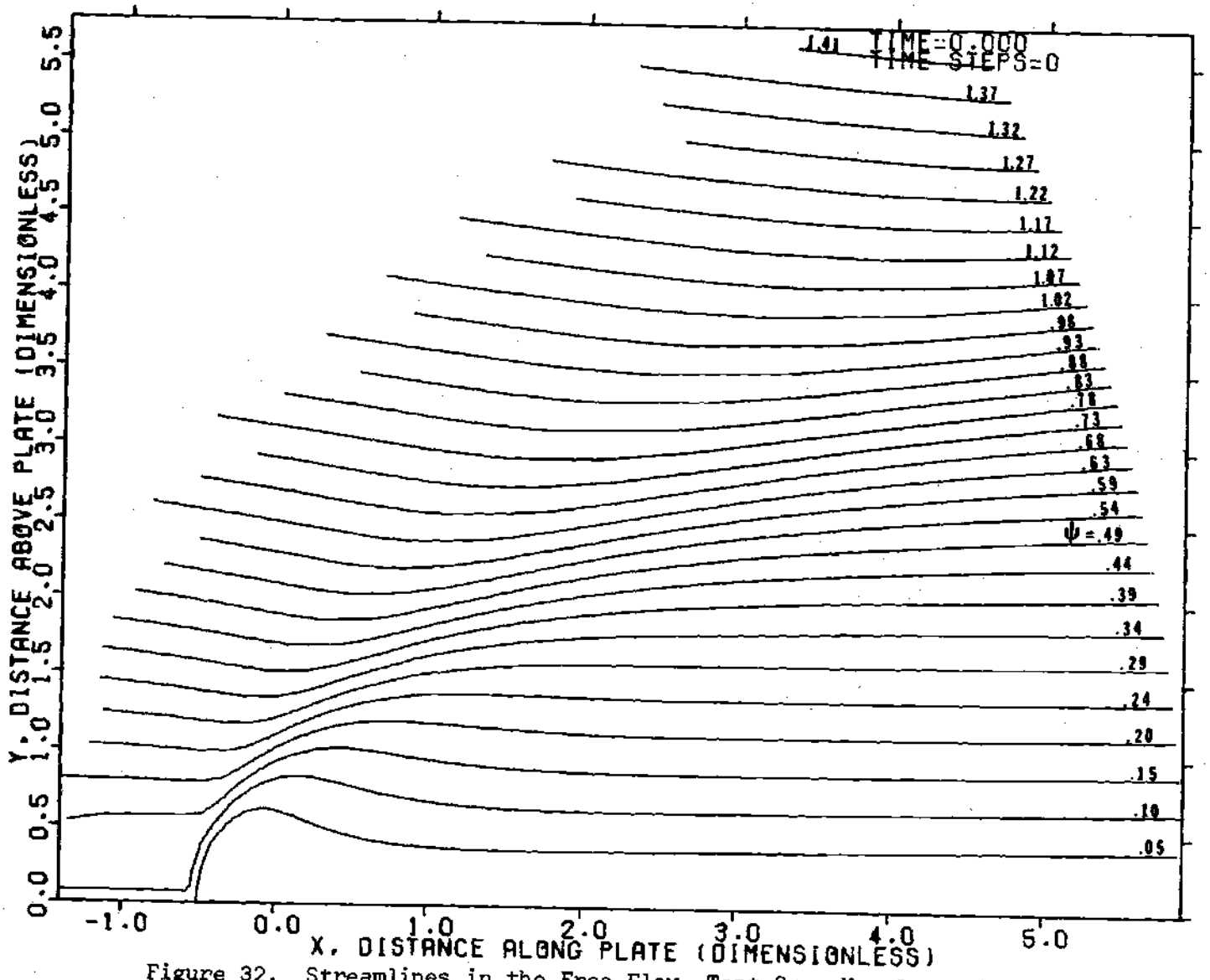

Figure 32. Streamlines in the Free Flow, Test Case No. 1 at Time Zero

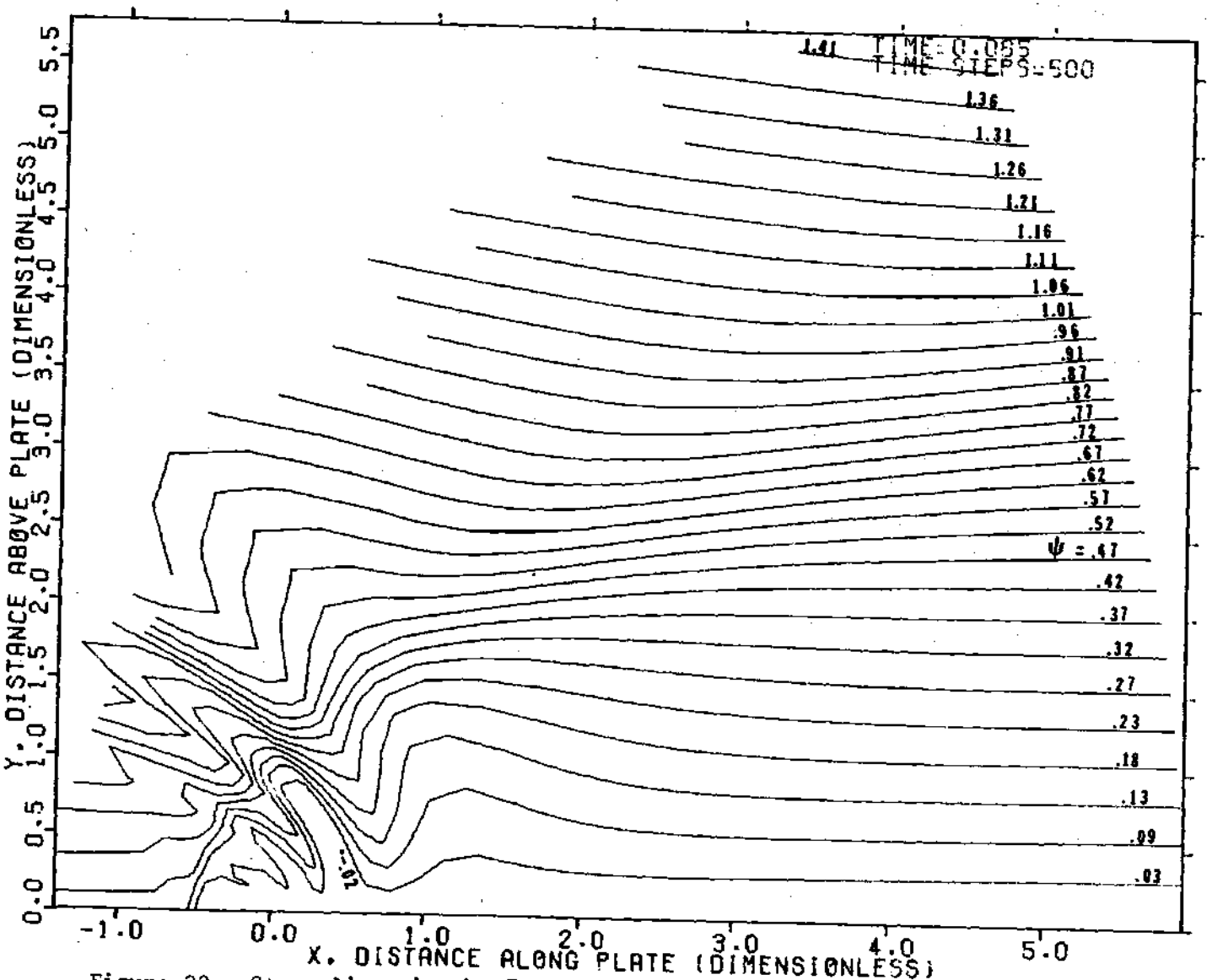

Figure 33. Streamlines in the Free Flow, Test Case No. 1 after 500 Time Steps

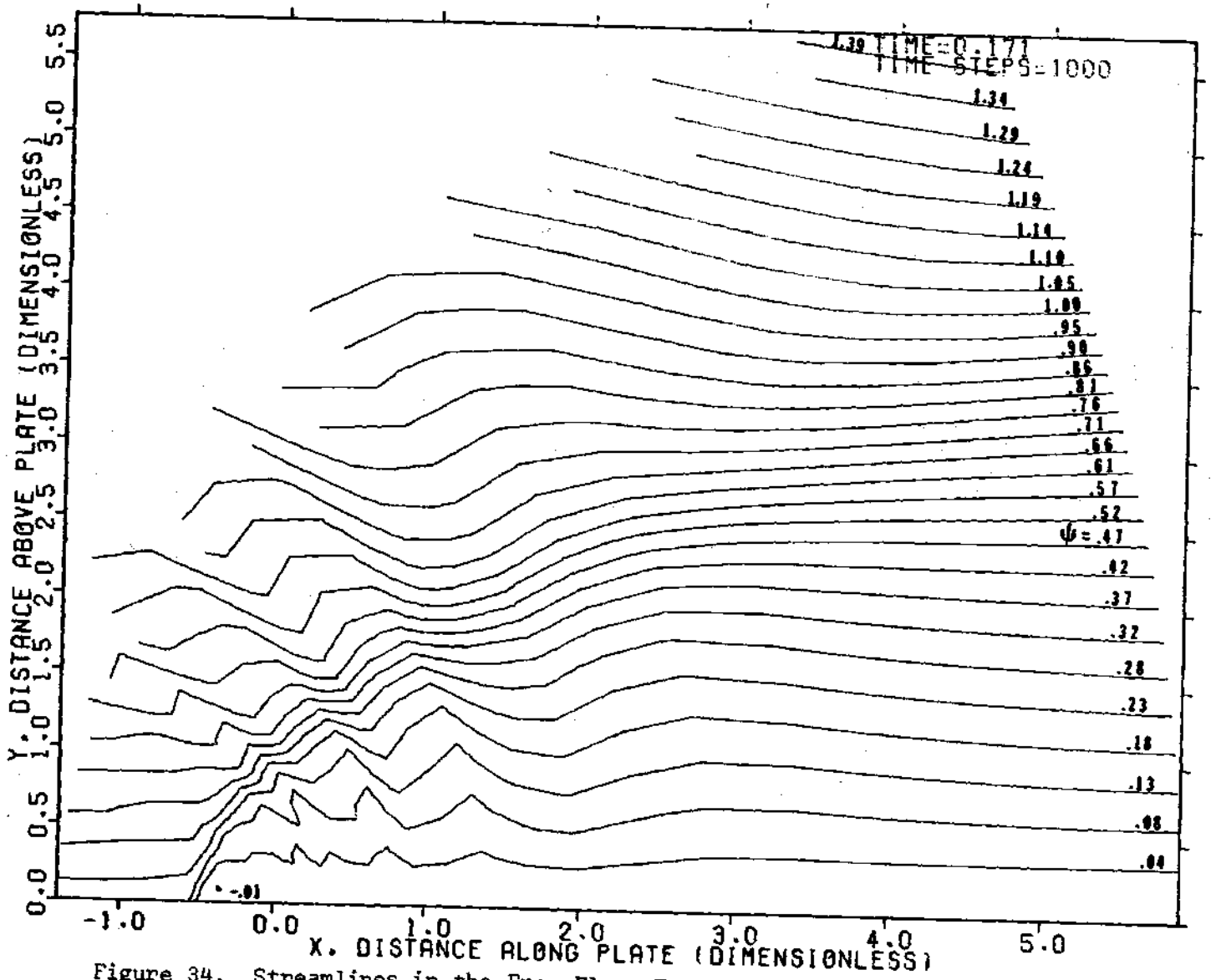

Figure 34. Streamlines in the Free Flow, Test Case No. 1 after 1000 Time Steps

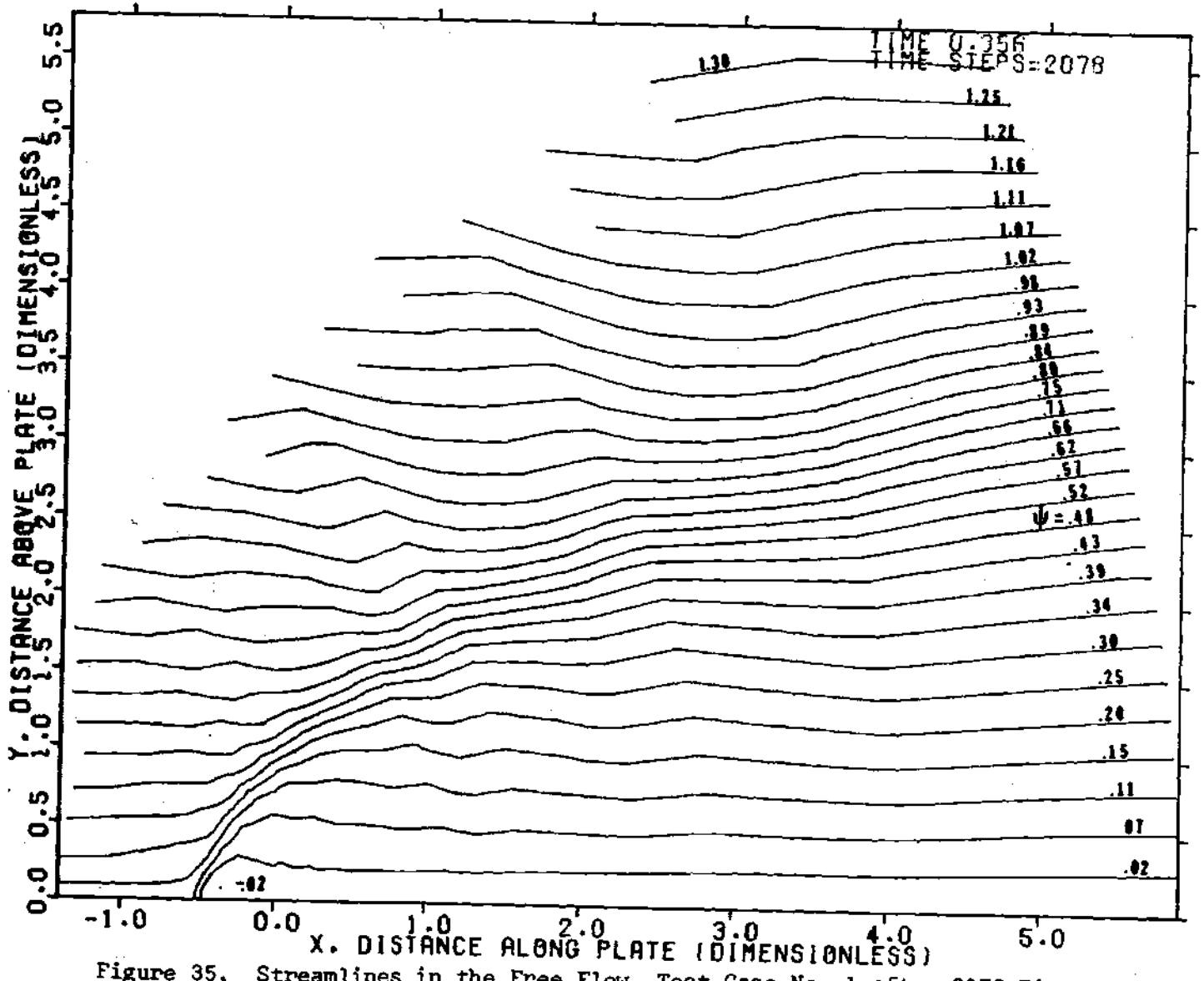

Figure 35. Streamlines in the Free Flow, Test Case No. 1 after 2078 Time Steps

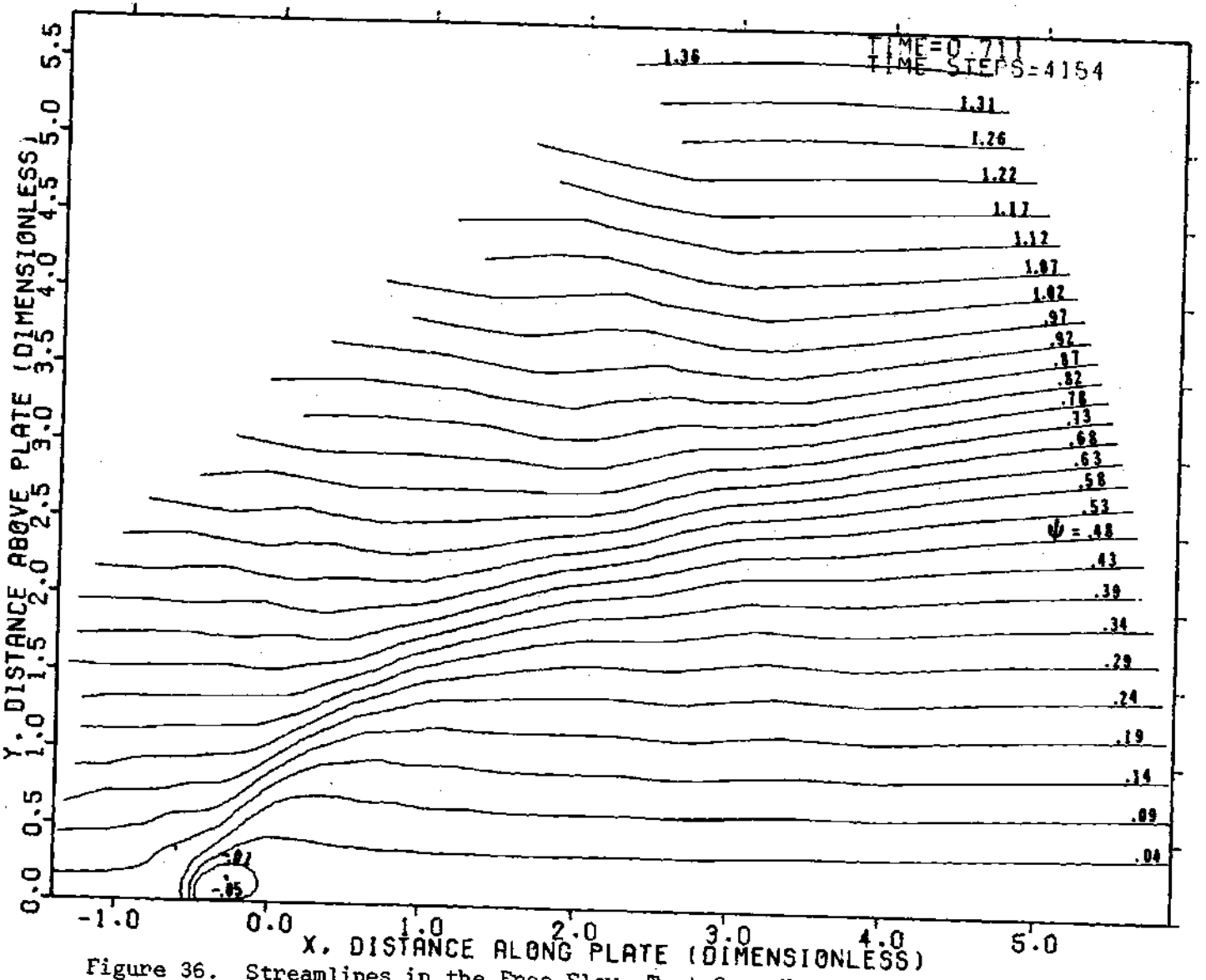

Figure 36. Streamlines in the Free Flow, Test Case No. 1 after 4154 Time Steps

Thus initially the streamlines may not (and actually do not) coincide with the direction of the velocity vectors.

Figure 33 presents the pattern of the flow after 500 time steps. The streamlines exhibit an erratic wavy pattern which is not fully understood. Apparently the initial conditions introduce disturbances into the flow, which as time progresses, cause the streamlines to behave in this manner.

After 1000 time steps the pattern of the streamlines is shown in Figure 34. The wavy pattern is still present but has by this time proceeded further downstream while becoming reduced in amplitude. Although not plotted in the figure a small recirculation region is present adjacent to the plate just downstream of the jet.

Figure 35 presents the flow pattern after 2078 time steps. The wavy pattern observed in the previous two figures has moved still further downstream but is much reduced in amplitude. The recirculation region previously noted is still present and has grown slightly stronger.

The final flow pattern after 4154 time steps is presented in Figure 36, which is essentially a compilation of Figures 9 and 14. The wavy pattern appears to have spread downstream beyond the limits of the figure and is scarcely detectable. The recirculation region has grown larger and is now clearly visible. Except for the growth of this recirculation region the flow pattern at this time resembles that shown in Figure 35, which represents the flow more than 2000 time steps earlier. Notice should be taken, however, that if the recirculation region continues to grow it could conceivably produce significant changes in the flow pattern at a later time.

The erratic wavy pattern of the streamlines which develops after approximately 500 timesteps, and the subsequent smoothing out of this pattern would tend to indicate that the final flow pattern as presented is more than a small perturbation of the initial conditions. On the other hand, the former still displays considerable resemblance to the latter. Thus, in spite of the fact that the pattern is changing extremely slowly at the final time, the sequence of events does not conclusively prove that the final pattern is very close to the steady-state solution.

At this time there appears to be no simple method of explaining the questions which have been raised by the preceding argument. A simplified analysis, which tends to support the validity of the final flow pattern is presented in Appendix I. Notice should be taken however that this analysis contains certain crucial assumptions which may be subject to question, and thus such analysis cannot be interpreted as conclusive proof of the validity of the final predicted flow pattern for Test Case No. 1.

With regard to streamlines from the free stream passing through the jet, another question, which appears significant is concerned with the downstream boundary conditions. As given by Equation (III-171) these downstream conditions are inherently based on the assumption that the flow far downstream of the jet behaves as if the jet were absent. It might be argued that such boundary conditions conceivably could force the streamlines to pass through the jet in the manner predicted in Test Case No. 1.

In considering the preceding question it is important to take note of the magnitude of the distance in Test Case No. 1 between the slot and the downstream parabola u_∞ or u_J. This distance is $\sim 10^4\ b_w$ or $\sim 100\ L_{dp}$, which physically represents about 300 feet. It would seem unlikely that any disturbance produced by the jet could physically persist for this distance, and thus the flow should closely resemble the flow which would occur in the absence of the jet. At the same time, from a mathematical standpoint a *close resemblance* may not be sufficiently precise for defining boundary conditions. If such is the case, one alternative is to cause u_∞ to approach infinity. Examination of the central finite difference model as given by Equation (IV-11) reveals that this alternative is equivalent to using a backward difference model in the u-direction along the parabola u_{J-1}. The end result would thus be a set of "free" or "floating" interior points along this parabola. For subsonic flow the existence of such "floating" grid points would appear to be incompatible with the governing equations, which become elliptical under steady-state conditions.

Based on the preceding discussion there appears to be no simple answer to the question of the influence of the downstream boundary conditions on the behavior of the streamlines in the jet. Further study of this point appears warranted.

For the high-velocity underexpanded jet (Test Case No. 2) involving a velocity ratio (w_{je}/w_∞) of 1.14, the traverse of the jet by the streamlines is not apparent. The absence of any real shielded region, in contrast to the presence of the latter for the low speed

case, is also of interest. Finally, the existence of a region, between the separation vortex and the jet exit, in which the flow appears to make a "U-turn" is significant. As noted in Figure 2, the preconceived general flow pattern contained a counter-clockwise vortex in this area. Careful study of possible flow patterns in the region indicates that the "U-turn" is physically more realistic than the vortex.

With regard to the jet centerline the results indicate that for both low-speed and high-speed flow a parabola is indeed a good approximation of the jet path. In general, the parabola $v_{c\ell}$ based on Equation (III-18) appears to lie to the left of the predicted jet centerline, especially in the initial portion of the jet.

The fact that the jet centerline appeared to be closely approximated by a parabola lends strong support to the original decision to use parabolic coordinates. Analysis of the two test cases reveals that in order to obtain the same resolution of the flow field in rectangular coordinates approximately twice as many grid points would have been necessary. Such a number of grid points would have caused the program to exceed the core storage of the UNIVAC 1108 and would have necessitated the use of overlay storage. Although the parabolic equations contain roughly 50 per cent more terms than their rectangular counterparts it can be readily seen that the use of twice as many grid points with the rectangular equations would require more computation time. Furthermore, access time requirements associated with the use of overlay storage would further increase the computation time.

Observations Concerning Numerical Computation of Turbulent Compressible Flow

The numerical solutions obtained were the result of a considerable amount of experimentation with a number of different approaches. Numerous variations of the initial conditions, boundary conditions, and time-marching techniques were investigated. The ground rules for neglecting time-averaged turbulent terms were revised several times. Practical considerations, associated with the requirement for large amounts of computer time, proved to be of considerable importance. All of this experience has proved most valuable in gaining a better understanding of compressible turbulent flow and the proper technique for obtaining numerical solutions of such flow.

Initial Conditions

With regard to initial conditions both approaches described in Chapter III were attempted. The first approach, involving simple, physically realistic initial conditions invariably resulted in one of two problems. If the jet and the free stream were allowed to build up slowly, excessive computation time became a problem. On the other hand if more extreme initial conditions were used, strong shock waves or blast waves were produced by the interaction. Such waves proved to be too much for the numerical technique to handle, with regions of extreme rarefaction occurring behind such blast waves in the recirculation region downstream of the jet.

The second approach to the initial conditions, although ultimately successful, was not without problems. Considerable effort was necessary to avoid initial flow patterns which would represent the

presence of excessive momentum or energy within the jet. The fact that both test cases involved jets whose temperatures were close to that of the free stream reduced this problem so far as excess energy was concerned. For other cases, involving hot jets, however, the need arises for a careful review of the initial conditions.

Boundary Conditions

Both approaches to the boundary conditions were tested. The approach involving use of the conservation-law form of the governing equations for density and temperature, with the no-slip and adiabatic conditions at the wall taken into account, resulted in three problems: First, negative densities and pressures in the vicinity of the corners of the slot exit were encountered. The explanation of this development lies in the fact that density, by the continuity equation, must continuously decrease with time at any point on the wall above which the normal component of velocity is always directed away from the surface. Thus negative values for density can be produced and these in turn, by the equation of state, produce negative pressures.

The second problem involved a physically unacceptable symmetrical distortion of the temperature and density distribution on the surface in the vicinity of the origin. Due to the extreme curvature of the parabolas in this region, the finite difference approximations to the spatial derivatives produced cumulative errors in the time-marching technique, which caused the distortion.

The use of a simple adiabatic wall boundary condition produced the third problem. With this condition considerable instability in the

wall temperature was encountered. The wall temperature displayed rapid fluctuations with respect to time, resulting from oscillations in the flow properties in the gas immediately above it. These variations in temperature at the wall in turn produced pressure fluctuations which strongly affected the flow velocities at points above the surface. The latter would in turn produce more variations in the flow properties in the gas resulting in additional temperature fluctuations at the wall. The process tended to become unstable and in some cases led to divergence.

The use of the second approach to the boundary conditions successfully eliminated all three problems noted. The density and pressure at the corner points remained at physically acceptable levels; the distortion about the origin essentially disappeared; and the temperature at the wall was no longer characterized by strong fluctuations. The success of the second approach can be attributed to three basic features of the model used. First, the manner in which pressure was calculated at the wall instead of density eliminated the problem with the corner points and the density distortion in the vicinity of the origin. The temperature distortion about the latter was removed by allowing heat flow along the surface of the wall through the solid wall material (which was assumed to be a metal). Finally the presence of the wall thermal capacitance, as expected, acted as a strong damping device for the temperature fluctuations.

Time-Marching Technique and Mass Diffusion

The initial choice for a numerical technique was the original Lax-Wendroff two-step method as given by Equations (IV-35) and (IV-36). With such an approach wavy patterns in the pressure and density distributions, in the vicinity of shock waves or regions of rarefaction, were invariably encountered, which in turn produced divergence. In an effort to reduce the wavy patterns, artificial viscosity in the form used by Lapidus [72] was introduced. The resulting flow appeared stable but the use of an empirical stabilizing parameter, such as artificial viscosity, appeared inconsistent with the objectives of the study.

At this point two significant observations were made. First the magnitude of the artificial viscosity was roughly the same as that of the calculated values of eddy viscosity. Second, the introduction of an artificial viscosity term in the continuity equation proved especially beneficial in reducing the wavy patterns already noted. This second point implied the existence of *mass diffusion*. Re-examination of the ground rules for neglecting time-averaged turbulent terms led to the conclusion that there was no real justification for dropping double-correlation terms involving ρ'. Other investigators appear to have neglected [35] or somehow combined such terms with other quantities [37 and 41] in such a way as to mask their presence; and *these terms initially had been neglected in the current study*. A careful analysis of these double correlation terms revealed that, as already discussed in Chapter III they represent turbulent mass self-diffusion.

When introduced into the conservation law form of the governing equations, with the Lax-Wendroff two-step method, without artificial

viscosity, the general stability of the numerical procedure was improved as compared with the original approach. The technique, however, was still not as stable as when artificial viscosity was used. Study of this difference in stability revealed that the artificial viscosity terms were introduced in such a way as to involve only nine grid points for numerical calculations while the turbulent mass diffusion as well as the momentum diffusion (stresses), and energy diffusion terms in the Lax-Wendroff two-step method involved 13 grid points.

By changing from the original Lax-Wendroff method to the special version of MacCormack's approach, as given by Equations (IV-37) and (IV-38), without the use of artificial viscosity, stability was achieved which was essentially equivalent to that obtained when such a parameter was employed. All numerical results which have been described were obtained by this numerical procedure, which is discussed in Chapter IV, *without the use of artificial viscosity*. This sequence of events strongly implies three items: First, *artificial viscosity is simply an empirical version of eddy viscosity*. Second, *turbulent mass diffusion is significant in turbulent compressible flow and cannot be truly neglected*. Third, *in the numerical computation of diffusion terms the number of grid points involved should be limited to the point in question and the eight points (in two dimensions) surrounding that point*.

Notice should be taken that most of the problems with the first approaches to both the initial conditions and the boundary conditions were encountered while using the original Lax-Wendroff two-step method without mass diffusion or artificial viscosity. The possibility exists

that the use of the variation of MacCormack's method might in itself eliminate some of these problems. Time and budgetary limitations precluded investigation of this point.

Computation Time

A significant problem is computational fluid dynamics is the requirement for large amounts of computation time. As previously noted for Test Case No. 1 the computation time involved ~7 hours on the Univac 1108 Computer. Based on the fact that 949 grid points were involved, it can be seen that each point required roughly 7×10^{-3} hours or 25 seconds of computation time. The actual elapsed time in Test Case No. 1 was ~3 milliseconds. Thus the ratio of computation time per point to elapsed time for this case was $\sim8\times10^{3}$.

For Test Case No. 2 the computation time was ~6 hours, which for 949 grid points represents approximately 6×10^{-3} hours or 22 seconds per point. The actual elapsed time was ~76 microseconds. The ratio of computation time per point to real time can thus be seen to be $\sim3\times10^{5}$.

A comparison of the ratio of computation time per point to real time for the two cases reveals that a larger ratio was involved in the second case. This larger ratio can be attributed to the fact that Test Case No. 2 involved greater fluid velocities and smaller model dimensions than were involved in Test Case No. 1. Thus the physical time, associated with each computational time step in accordance with Equation (IV-49), was smaller for Test Case No. 2 than for Test Case No. 1.

Aside from the relative magnitude of the two ratios, their absolute magnitude (compared with some ideal ratio, such as unity) provides

some indication of the difficulties associated with numerical computations involving turbulent compressible flow. Reduction of these ratios appears to be an area which merits considerable study.

CHAPTER VI

CONCLUSIONS

In order to present the conclusions in an orderly manner, as in Chapter II, it is desirable to subdivide subsequent discussion into three parts as follows:

1. deflected jets,
2. turbulent flow characteristics, and
3. computational fluid dynamics.

Before proceeding with such discussion, however, several general comments are in order. First, the basic fact must be recognized that a steady-state solution to the problem has not been fully achieved. Second, there exist within the analytical model a number of assumptions and approximations, the validity of which is still not completely established. In this regard, determination of the optimum combination of such assumptions and approximations is most important. The preceding comments combine to yield the additional point that the work as reported represents only the first step in a series of studies aimed at the problem under consideration.

Deflected Jets

The numerical solutions for the two test cases, while never reaching a true steady-state, nevertheless provide the basis for a number of conclusions regarding the behavior of two-dimensional,

compressible, turbulent deflected jets. A basic conclusion, which is consistent with previous observations, is that the jet centerline appears to closely resemble a parabola. Immediately upstream of the jet exit, along the plate, the pressure exceeds the free stream value, while downstream of the jet exit near the plate the reverse is true. In the latter region a recirculation pattern occurs.

Consistent with several prior studies, for certain ratios of jet exit velocity to free stream velocity, streamlines originating in the free stream upstream of the jet appear to traverse the jet, crossing the centerline and entering the shielded region downstream of the recirculation zone. The fluid velocity in the shielded region for such a case is less than that of the jet or the free stream, but at least a portion of this fluid originates in the free stream. Notice should be taken that this concept of the jet being traversed in the manner described conflicts with a basic argument regarding the relative magnitude of the transport of kinetic energy across streamlines compared with such transport along streamlines. There exists the distinct possibility that the traverse phenomenon as described may be only transient in nature. In the final steady-state it may disappear or be significantly reduced.

For cases involving sonic, underexpanded jets, boundary layer separation along the plate upstream of the jet is likely to occur. If such does occur, between the region of separation and the jet, the flow appears to reattach to the plate. The result in this region is a "U-turn" pattern.

Turbulent Flow Characteristic

The experience, gained in formulating the analytical model and analyzing the numerical results obtained, has produced an improved understanding of certain features of turbulent flow, when treated from the phenomenological standpoint. First, in all coordinate systems, for each stress component or component of heat flux in laminar flow there exists an exact counterpart in turbulent flow. In addition, however, for turbulent compressible flow, turbulent mass self-diffusion is present, for which the laminar counterpart is not obvious. Such mass diffusion introduces additional terms into the time-averaged equations governing turbulent flow.

With regard to eddy viscosity, the general conclusion is that such a parameter represents a useful tool in the solution of turbulent flow problems even when boundary layer approximations are not applicable. The mixing length theorem, however, is generally inadequate for the calculation of eddy viscosity, and there exists a need for a more general theory, possibly based on the second spatial derivatives of velocity as opposed to first derivatives.

The effect of curvature of the flow on the magnitude of the eddy viscosity appears to be relatively small for the case considered. Such an effect, however, can be best explained in terms of the radial gradient of angular momentum. Positive values of the latter tend to reduce the eddy viscosity while the reverse is true for negative values.

A simple approximate relation between the magnitude of the turbulent shear stress and the turbulent pressure appears to provide a

means of calculating the latter and also calculating the kinetic energy of turbulence.

Computational Fluid Dynamics

As already discussed in Chapter V, a number of different versions of the numerical technique and the associated boundary and initial conditions were investigated. The experience derived from such investigations, coupled with an analysis of the numerical results, permit the formulation of several conclusions.

First, the variation of MacCormack's version of the original Lax-Wendroff two-step method, as described in Chapter IV, appears the most promising method available for solving two-dimensional turbulent flow problems. This method possesses second-order accuracy as compared with the first-order accuracy of Rusanov's method as used by Bauer [35]. There is no apparent requirement for the use of artificial viscosity as required by the original Lax-Wendroff two-step method in the vicinity of shocks or regions of rarefaction. The fact that the numerical approach as presented is superior to the original Lax-Wendroff technique results from the manner in which second partial derivatives are evaluated by the latter. The conservation-law form of the governing equations appears to contribute to the problem which arises when the Lax-Wendroff two-step method is used. The only other method which appears to have been applied to turbulent flow without the usual boundary layer approximations is that reported by Trulio [70], and there is not sufficient information available on Trulio's method to allow a valid comparison.

The use of artificial viscosity for stabilizing numerical techniques appears to represent an empirical approximation to the more physically acceptable concept of eddy viscosity, along with eddy mass and thermal diffusivity. Such a conclusion in turn implies that *some of the instabilities associated with computational fluid dynamics may actually represent or be related to the physical instabilities characteristic of turbulent flow.*

For the specific problem of two-dimensional deflected jets the use of parabolic coordinates appears quite promising. Certain problems, however, pertaining to non-uniform grid spacing and the large curvature of the grid lines in the vicinity of the origin, still remain.

The final methods used for calculating flow properties at boundary points along the wall appear quite promising. Further investigations of the effect of mass diffusion on the boundary-point flow properties may reveal, however, that the reduced versions of the governing equations are sufficient for these same calculations.

The boundary conditions, used at the entrance to the slot flow region to describe flow entering that region, appear to be in need of modification. The current form apparently was the cause of the numerical problems occurring in the slot flow. It is evident that disturbances produced by the interaction of the jet and the free stream are propagated up the slot and thus the approach to the problem, which involved solving the flow in the slot as well as in the free stream, appears correct.

The large amount of computation time required to obtain meaningful numerical results emphasizes the importance of the initial conditions. To reduce the computation time, initial conditions, which are closer to the final steady-state solution, must be used. Such conditions may be of necessity quite complex in form, but the results presented in the current study should provide some basis for establishing better initial conditions.

CHAPTER VII

RECOMMENDATIONS

For purposes of organization the recommendations are divided into three parts in the same manner as in Chapters II and VI.

Deflected Jets

Additional computation time should be devoted to the two test cases which have been presented. A number of additional test runs with the existing program, DEFJET (or some modified version of it), should be carried out to permit a more complete understanding of the flow patterns which occur under test conditions different from those studied. Special attention should be given to test conditions involving a supersonic free stream and/or a supersonic jet.

Experimental studies should be carried to provide more complete measurement of the entire flow field associated with two-dimensional turbulent deflected jets. Special effort should be directed toward confirming (or rebutting) the existence of the several flow phenomena which have been predicted but which have not been previously detected.

Turbulent Flow Characteristics

The variation of eddy viscosity as previously measured in boundary layers, jets, wakes, and ducts should be studied with the goal of developing a more general method of predicting this parameter. In this regard the original mixing length theory should be carefully examined

to determine how it could be modified or generalized to yield more realistic values for eddy viscosity. In addition, experimental studies of turbulent curved flow should be carried out to provide a more complete understanding of the effect of curvature on eddy viscosity.

The effects of turbulent mass self-diffusion in turbulent compressible flow should be studied both analytically and experimentally. A better understanding as to why such terms appear to have no laminar counterparts should be developed.

A rigorous analysis of the approximate relationship between turbulent shear stress and turbulent pressure should be performed. A more precise expression, which relates these two quantities in an invariant manner, should be derived.

Computational Fluid Dynamics

The current program, DEFJET, should be subjected to several modifications in an effort to determine whether or not it can be improved. Such modifications would include a return to the reduced governing equations (with mass diffusion accounted for) as a means of calculating flow properties at the boundary points. The boundary conditions at the entrance to the slot flow region should be examined and appropriate changes to these conditions should be made to eliminate the numerical problems encountered in the slot flow.

Special attention should be given to the use of governing equations in some form other than the conservation-law form. Such a form should be designed to cause the variation of flow properties with time

at a particular grid point in the numerical solution to depend only upon the eight surrounding grid points as well as the point itself.

APPENDICES

APPENDIX A

CALCULATIONS OF THE ISENTROPIC JET EXIT CONDITIONS

As noted in Chapter III, the isentropic jet exit velocity $\hat{w}_{je}$ is the characteristic velocity for the nondimensionalization procedure. Calculation of this parameter can be accomplished by one-dimensional compressible flow analysis [92], neglecting the effect of the free stream velocity.

The jet exit Mach number for unchoked flow is

$$(N_{Ma})_{je} = \left[\left(\frac{\hat{p}_{jo}}{\hat{p}_{\infty}}\right)^{\frac{\gamma-1}{\gamma}} - 1\right]\left(\frac{2}{\gamma-1}\right)^{1/2} \quad \left[\frac{\hat{p}_{\infty}}{\hat{p}_{jo}} > \left(\frac{2}{\gamma+1}\right)^{\frac{\gamma}{\gamma-1}}\right] \tag{A-1a}$$

For choked flow,

$$(N_{Ma})_{je} = 1 \quad \left[\frac{\hat{p}_{\infty}}{\hat{p}_{jo}} \leq \left(\frac{2}{\gamma+1}\right)^{\frac{\gamma}{\gamma-1}}\right] \tag{A-1b}$$

Now

$$\hat{T}_{je} = \hat{T}_{jo} \Big/ \left[1 + \frac{\gamma-1}{2}(N_{Ma})^2_{je}\right] \tag{A-2}$$

Then

$$\hat{w}_{je} = (N_{Ma})_{je}\sqrt{\gamma \hat{R} \hat{T}_{je}} \tag{A-3}$$

The items $\hat{p}_{jo}$, $\hat{p}_{\infty}$, $\hat{T}_{jo}$, $\hat{R}$ and γ are all input items or can be derived from the latter. Thus the isentropic jet exit velocity $\hat{w}_{je}$ can be determined based on a given set of values for the input items.

The characteristic density of the flow, as also noted in Chapter III, is the isentropic jet exit density $\hat{\rho}_{je}$. By means of one-dimensional isentropic compressible flow analysis, this density can be expressed as a function of jet exit Mach number as follows:

$$\hat{\rho}_{je} = \hat{\rho}_{jo}\left[1 + \frac{\gamma-1}{2}(N_{Ma})^2_{je}\right]^{\frac{-1}{\gamma-1}} \qquad \text{(A-4)}$$

All terms on the right-hand side of Equation (A-4) can be derived in terms of input items.

APPENDIX B

DEVELOPMENT OF THE TIME-AVERAGED EQUATIONS GOVERNING TURBULENT FLOW

The equation of state and the equations governing the instantaneous conservation of mass, momentum, and energy are presented in Chapter III. As noted in that chapter each flow property is assumed to consist of a time-averaged component and a fluctuating component. In certain cases the sum or product of two flow properties is treated in this manner also. This special treatment of certain sums or products is desirable for the sake of brevity, but a complete understanding of such special terms is necessary before the time-averaged equations can be developed.

Expansion of Terms Containing Products and Sums

The first term to be considered is the stagnation internal energy e_o. Based on the definition of e_o, for rectangular coordinates this term can be expanded as follows:

$$e_o = c_v(\bar{T}+T') + [(\bar{w}_x+w_x')^2 + (\bar{w}_y+w_y')^2 + (w_z')^2]/2$$

$$= c_v\bar{T} + c_vT' + (\bar{w}_x^2+2\bar{w}_xw_x'+w_x'w_x'+\bar{w}_y^2+2\bar{w}_yw_y'+w_y'w_y'+w_z'w_z')/2 \qquad \text{(B-1)}$$

Application of the basic rules for time-averaging to the preceding relation yields

$$\bar{e}_o = c_v\bar{T} + (\bar{w}_x^2+\overline{w'_x w'_x}+\bar{w}_y^2+\overline{w'_y w'_y}+\overline{w'_z w'_z})/2 \qquad \text{(B-2)}$$

This in turn implies

$$e'_o = c_v T' + \bar{w}_x w'_x + \bar{w}_y w'_y \qquad \text{(B-3)}$$

For parabolic coordinates a similar procedure yields

$$\bar{e}_o = c_v\bar{T} + (\bar{w}_u^2+\overline{w'_u w'_u}+\bar{w}_v^2+\overline{w'_v w'_u}+\overline{w'_z w'_z})/2 \qquad \text{(B-4)}$$

and

$$e'_o = c_v T' + \bar{w}_u w'_u + \bar{w}_v w'_v \qquad \text{(B-5)}$$

The development of the terms involving a mass flux (the product of density and a velocity component) is relatively straightforward. For rectangular coordinates in the x-direction,

$$\rho w_x = (\bar{\rho}+\rho')(\bar{w}_x+w'_x)$$

$$= \bar{\rho}\bar{w}_x + \bar{\rho}w'_x + \rho'\bar{w}_x + \rho'w'_x \qquad \text{(B-6)}$$

Time-averaging yields

$$\overline{(\rho w_x)} = \bar{\rho}\bar{w}_x + \overline{\rho' w'_x} \qquad \text{(B-7)}$$

This implies

$$(\rho w_x)' = \bar{\rho} w_x' + \rho' \bar{w}_x \tag{B-8}$$

In similar fashion for the y-direction,

$$\overline{(\rho w_y)} = \bar{\rho} \bar{w}_y + \overline{\rho' w_y'} \tag{B-9}$$

and

$$(\rho w_y)' = \bar{\rho} w_y' + \rho' \bar{w}_y \tag{B-10}$$

Likewise in parabolic coordinates for the u-direction

$$\overline{(\rho w_u)} = \bar{\rho} \bar{w}_u + \overline{\rho' w_u'} \tag{B-11}$$

and

$$(\rho w_u)' = \bar{\rho} w_u' + \rho' \bar{w}_u \tag{B-12}$$

In the v-direction,

$$\overline{(\rho w_v)} = \bar{\rho} \bar{w}_v + \overline{\rho' w_v'} \tag{B-13}$$

and

$$(\rho w_v)' = \bar{\rho} w_v' + \rho' \bar{w}_v \tag{B-14}$$

The term ρe_o in rectangular coordinates can be expanded as follows:

$$\rho e_o = (\bar{\rho}+\rho')(\bar{e}_o+e_o')$$

$$= \bar{\rho}\bar{e}_o + \bar{\rho}e_o' + \rho'\bar{e}_o + \rho'e_o' \qquad \text{(B-15)}$$

Time-averaging yields the result

$$\overline{(\rho e_o)} = \bar{\rho}\bar{e}_o + \overline{\rho'e_o'}$$

$$= \bar{\rho}[c_v\bar{T} + (\bar{w}_x^2+\overline{w_x'w_x'}+\bar{w}_y^2+\overline{w_y'w_y'}+\overline{w_z'w_z'})/2]$$

$$+ c_v\overline{\rho'T'} + \bar{w}_x\overline{\rho'w_x'} + \bar{w}_y\overline{\rho'w_y'} \qquad \text{(B-16)}$$

Thus

$$(\rho e_o)' = \bar{\rho}e_o' + \rho'\bar{e}_o$$

$$= \bar{\rho}(c_vT'+\bar{w}_xw_x'+\bar{w}_yw_y') + \rho'[c_v\bar{T} + (\bar{w}_x^2$$

$$+\overline{w_x'w_x'}+\bar{w}_y^2+\overline{w_y'w_y'}+\overline{w_z'w_z'})/2] \qquad \text{(B-17)}$$

In like manner for parabolic coordinates, analysis of the same product ρe_o reveals

$$\overline{(\rho e_o)} = \bar{\rho}\bar{e}_o + \overline{\rho' e_o'}$$

$$= \bar{\rho}[c_v\bar{T} + (\bar{w}_u^2 + \overline{w_u'w_u'} + \bar{w}_v^2 + \overline{w_v'w_v'} + \overline{w_z'w_z'})/2]$$

$$+ c_v\overline{\rho'T'} + \bar{w}_u\overline{\rho'w_u'} + \bar{w}_v\overline{\rho'w_v'} \qquad \text{(B-18)}$$

and

$$(\rho e_o)' = \bar{\rho}e_o' + \rho'\bar{e}_o$$

$$= \bar{\rho}(c_vT' + \bar{w}_u w_u' + \bar{w}_v w_v') + \rho'[c_v\bar{T} + (\bar{w}_u^2$$

$$+ \overline{w_u'w_u'} + \bar{w}_v^2 + \overline{w_v'w_v'} + \overline{w_z'w_z'})/2] \qquad \text{(B-19)}$$

Examination of those preceding expressions, involving the time-averaging of products, reveals that all triple correlation terms occur in the fluctuating portion of the product. Thus in the time-averaged equation such triple correlations will be averaged out. This is equivalent to the usual practice of neglecting triple correlation terms.

Rules for Neglecting Terms

Before proceeding with the development of time-averaged equations certain ground rules for dropping or neglecting terms need to be established. Because of the current lack of complete understanding of turbulent compressible flow, retention of all time-averaged terms is desirable.

Certain terms, associated with fluctuations in the molecular transport processes, however, appear to be negligible based on order-of-magnitude considerations. Thus the double correlation terms $\overline{\sigma'_{xy}w'_x}$, $\overline{\sigma'_{xy}w'_y}$, $\overline{\sigma'_{uv}w'_u}$, and $\overline{\sigma'_{uv}w'_v}$ are neglected. The double correlation terms involving the normal stresses must be given careful attention because the pressure fluctuation p' is contained within such terms. In order to retain p' while neglecting the viscous portion of the fluctuation in the normal stress, the following approximations are used

$$\overline{w'_x\sigma'_{xx}} = \overline{w'_xp'} \tag{B-20}$$

$$\overline{w'_y\sigma'_{yy}} = \overline{w'_yp'} \tag{B-21}$$

$$\overline{w'_u\sigma'_{uu}} = \overline{w'_up'} \tag{B-22}$$

$$\overline{w'_v\sigma'_{vv}} = \overline{w'_vp'} \tag{B-23}$$

In addition to the double-correlation terms involving fluctuations of the viscous stresses, certain other double correlation terms appear negligible. These are the terms $\overline{w'_xw'_z}$, $\overline{w'_yw'_z}$, $\overline{w'_uw'_z}$, and $\overline{w'_vw'_z}$, which, for two-dimensional flows, should be identically zero according to Bousinesq's relation and therefore are neglected.

As already noted the method of time-averaging products is equivalent to neglecting certain triple-correlation terms ($\overline{\rho'w'_xw'_x}$, $\overline{\rho'w'_yw'_y}$, $\overline{\rho'w'_uw'_u}$, and $\overline{\rho'w'_vw'_v}$). For consistency all other triple correlation terms ($\overline{\rho'w'_xw'_y}$, $\overline{\rho'w'_uw'_v}$, $\overline{\rho'T'w'_u}$ and $\overline{\rho'T'w'_v}$) are likewise neglected.

Time-Averaged Equation of State

For an ideal gas, the instantaneous equation-of-state, Equation (III-49) can be expressed as follows:

$$p = R(\bar{\rho}+\rho')(\bar{T}+T')$$

$$= R(\bar{\rho}\bar{T}+\bar{\rho}T'+\rho'\bar{T}+\overline{\rho'T'}) \qquad \text{(B-24)}$$

Thus the time-averaged equation of state is

$$\bar{p} = R(\bar{\rho}\bar{T}+\overline{\rho'T'}) \qquad \text{(B-25)}$$

This implies

$$p' = R(\bar{\rho}T'+\rho'\bar{T}) \qquad \text{(B-26)}$$

Time-Averaged Continuity Equation

The instantaneous continuity equation in rectangular coordinates, Equation (III-50), can be expanded as follows:

$$\frac{\partial(\bar{\rho}+\rho')}{\partial t} + \frac{\partial[(\bar{\rho}+\rho')(\bar{w}_x+w_x')]}{\partial x} + \frac{\partial[(\bar{\rho}+\rho')(\bar{w}_y+w_y')]}{\partial y} = 0 \qquad \text{(B-27)}$$

Time-averaging yields

$$\frac{\partial\bar{\rho}}{\partial t} + \frac{\partial(\bar{\rho}\bar{w}_x)}{\partial x} + \frac{\partial(\overline{\rho'w_x'})}{\partial x} + \frac{\partial(\bar{\rho}\bar{w}_y)}{\partial y} + \frac{\partial(\overline{\rho'w_y'})}{\partial y} = 0 \qquad \text{(B-28)}$$

In parabolic coordinates expansion of the instantaneous continuity equation, Equation (III-51), results in the following:

$$\frac{\partial(\bar{\rho}+\rho')}{\partial t} + \frac{1}{H}\frac{\partial}{\partial u}[(\bar{\rho}+\rho')(\bar{w}_u+w_u')] + \frac{1}{H}\frac{\partial}{\partial v}[(\bar{\rho}+\rho')(\bar{w}_v+w_v')]$$

$$+ \frac{1}{H^3}[(\bar{\rho}+\rho')(\bar{w}_u+w_u')u + (\bar{\rho}+\rho')(\bar{w}_v+w_v')v] = 0 \qquad \text{(B-29)}$$

The time-averaged equation is thus

$$\frac{\partial\bar{\rho}}{\partial t} + \frac{1}{H}\frac{\partial}{\partial u}(\bar{\rho}\bar{w}_u+\overline{\rho' w_u'}) + \frac{1}{H}\frac{\partial}{\partial v}(\bar{\rho}\bar{w}_v+\overline{\rho' w_v'})$$

$$+ \frac{1}{H^3}[(\bar{\rho}\bar{w}_u+\overline{\rho' w_u'})u + (\bar{\rho}\bar{w}_v+\overline{\rho' w_v'})v] = 0 \qquad \text{(B-30)}$$

Time-Averaged Momentum Equations

In rectangular coordinates the x-momentum equation, Equation (III-56), can be expanded as follows:

$$\frac{\partial[(\overline{\rho w_x}) + (\rho w_x)']}{\partial t} + \frac{\partial}{\partial x}\{[(\overline{\rho w_x})+(\rho w_x)'](\bar{w}_x+w_x')\} + \frac{\partial}{\partial y}\{[(\overline{\rho w_x})$$

$$+ (\rho w_x)'](\bar{w}_y+w_y')\} = \frac{\partial}{\partial x}(\bar{\sigma}_{xx}+\sigma'_{xx}) + \frac{\partial}{\partial y}(\bar{\sigma}_{xy}+\sigma'_{xy}) \qquad \text{(B-31)}$$

The time-averaged equation is thus

$$\frac{\partial(\overline{\rho w_x})}{\partial t} + \frac{\partial}{\partial x}[(\overline{\rho w_x})\bar{w}_x + \overline{(\rho w_x)' w_x'}] + \frac{\partial}{\partial y}[(\overline{\rho w_x})\bar{w}_y + \overline{(\rho w_x)' w_y'}]$$

$$= \frac{\partial}{\partial x}\bar{\sigma}_{xx} + \frac{\partial}{\partial y}\bar{\sigma}_{xy} \qquad \text{(B-32)}$$

Based on relations for $(\overline{\rho w_x})$ and $(\rho w_x)'$ previously given by Equation (B-7) and (B-8),

$$\frac{\partial(\overline{\rho w_x})}{\partial t} + \frac{\partial}{\partial x}(\bar{\rho}\bar{w}_x\bar{w}_x + \overline{\rho' w_x' \bar{w}_x} + \overline{\rho' \bar{w}_x w_x'} + \bar{\rho}\overline{w_x' w_x'}) + \frac{\partial}{\partial y}(\bar{\rho}\bar{w}_x\bar{w}_y$$

$$+\overline{\rho' w_x' \bar{w}_y} + \overline{\rho' \bar{w}_x w_y'} + \bar{\rho}\ \overline{w_x' w_y'}) = \frac{\partial}{\partial x}\bar{\sigma}_{xx} + \frac{\partial}{\partial y}\bar{\sigma}_{xy} \qquad \text{(B-33)}$$

Rearrangement yields the final form for the time-averaged x-momentum equation as follows:

$$\frac{\partial(\overline{\rho w_x})}{\partial t} + \frac{\partial}{\partial x}(\bar{\rho}\bar{w}_x\bar{w}_x) + \frac{\partial}{\partial y}(\bar{\rho}\bar{w}_x\bar{w}_y) = \frac{\partial\bar{\sigma}_{xx}}{\partial x} + \frac{\partial\bar{\sigma}_{xy}}{\partial y} - \frac{\partial}{\partial x}(\bar{\rho}\overline{w_x' w_x'} + 2\bar{w}_x\overline{\rho' w_x'})$$

$$- \frac{\partial}{\partial y}(\bar{\rho}\overline{w_x' w_y'} + \bar{w}_x\overline{\rho' w_y'} + \bar{w}_y\overline{\rho' w_x'}) \qquad \text{(B-34)}$$

In an analogous fashion, based on an expansion of Equation (III-57), the time-averaged y-momentum equation is

$$\frac{\partial(\overline{\rho w_y})}{\partial t} + \frac{\partial}{\partial x}(\bar{\rho}\bar{w}_y\bar{w}_x) + \frac{\partial}{\partial y}(\bar{\rho}\bar{w}_y\bar{w}_y) = \frac{\partial\bar{\sigma}_{xy}}{\partial x} + \frac{\partial\bar{\sigma}_{yy}}{\partial y} - \frac{\partial}{\partial x}(\bar{\rho}\overline{w_x' w_y'}$$

$$+\bar{w}_y\overline{\rho' w_x'} + \bar{w}_x\overline{\rho' w_y'}) - \frac{\partial}{\partial y}(\bar{\rho}\overline{w_y' w_y'} + 2\bar{w}_y\overline{\rho' w_y'}) \qquad \text{(B-35)}$$

In parabolic coordinates the instantaneous u-momentum equation, Equation (III-58), can be expanded as follows:

$$\frac{\partial[(\rho w_u) + (\rho w_u)']}{\partial t} + \frac{1}{H}\frac{\partial}{\partial u}\left\{[(\overline{\rho w_u})+(\rho w_u)'](\bar{w}_u+w_u')\right\} + \frac{1}{H}\frac{\partial}{\partial v}\left\{[(\overline{\rho w_u})\right.$$

$$\left. + (\rho w_u)'](\bar{w}_v+w_v')\right\} + \frac{1}{H^3}\left\{u[(\overline{\rho w_u})+(\rho w_u)'](\bar{w}_u+w_u')+2v[(\overline{\rho w_u})\right.$$

$$\left.+(\rho w_u)'](\bar{w}_v+w_v') - u[(\overline{\rho w_v})+(\rho w_v)'](\bar{w}_v+w_v')\right\} = \frac{1}{H}\left[\frac{\partial}{\partial u}(\bar{\sigma}_{uu}+\sigma'_{uu})\right.$$

$$\left. + \frac{\partial}{\partial v}(\bar{\sigma}_{uv}+\sigma'_{uv})\right] + \frac{1}{H^3}[u(\bar{\sigma}_{uu}+\sigma'_{uu})$$

$$+2v(\bar{\sigma}_{uv}+\sigma'_{uv})-u(\bar{\sigma}_{vv}+\sigma'_{vv})] \qquad \text{(B-36)}$$

Time-averaging of the preceding equation produces

$$\frac{\partial(\overline{\rho w_u})}{\partial t} + \frac{1}{H}\frac{\partial}{\partial u}[(\overline{\rho w_u})\bar{w}_u+\overline{(\rho w_u)'w_u'}] + \frac{1}{H}\frac{\partial}{\partial v}[(\overline{\rho w_u})\bar{w}_v$$

$$+\overline{(\rho w_u)'w_v'}] + \frac{1}{H^3}\left\{u[(\overline{\rho w_u})\bar{w}_u+\overline{(\rho w_u)'w_u'}] + 2v[(\overline{\rho w_u})\bar{w}_v\right.$$

$$\left. + \overline{(\rho w_u)'w_v'}] - u[(\overline{\rho w_v})\bar{w}_v+\overline{(\rho w_u)'w_v'}]\right\}$$

$$= \frac{1}{H}\left(\frac{\partial\bar{\sigma}_{uu}}{\partial u} + \frac{\partial\sigma_{uv}}{\partial v}\right) + \frac{1}{H^3}(u\bar{\sigma}_{uu}+2v\bar{\sigma}_{uv}-u\bar{\sigma}_{vv}) \qquad \text{(B-37)}$$

Rearrangement of Equation (B-37) and use of the definitions of (ρw_u) and $(\rho w_u)'$, as given by Equations (B-11) and (B-12), results in the final version of the time-averaged u-momentum equation,

$$\frac{\partial(\overline{\rho w_u})}{\partial t} + \frac{1}{H}\frac{\partial}{\partial u}(\bar{\rho}\bar{w}_u\bar{w}_u) + \frac{1}{H}\frac{\partial}{\partial v}(\bar{\rho}\bar{w}_u\bar{w}_v) + \frac{1}{H^3}(u\bar{\rho}\bar{w}_u\bar{w}_u$$

$$+ 2v\bar{\rho}\bar{w}_u\bar{w}_v - u\bar{\rho}\bar{w}_v\bar{w}_v) = \frac{1}{H}\left(\frac{\partial\bar{\sigma}_{uu}}{\partial u} + \frac{\partial\bar{\sigma}_{uv}}{\partial v}\right) + \frac{1}{H^3}(u\bar{\sigma}_{uu} + 2v\bar{\sigma}_{uv} - u\bar{\sigma}_{vv})$$

$$- \frac{1}{H}\left[\frac{\partial}{\partial u}(\bar{\rho}\overline{w_u'w_u'} + 2\bar{w}_u\overline{\rho' w_u'}) + \frac{\partial}{\partial v}(\bar{\rho}\overline{w_u'w_v'} + \bar{w}_u\overline{\rho' w_v'} + \bar{w}_v\overline{\rho' w_u'})\right]$$

$$- \frac{1}{H^3}\left[u(\bar{\rho}\overline{w_u'w_u'} + 2\bar{w}_u\overline{\rho' w_u'}) + 2v(\bar{\rho}\overline{w_u'w_v'} + \bar{w}_u\overline{\rho' w_v'} + \bar{w}_v\overline{\rho' w_u'}\right.$$

$$\left. - u(\bar{\rho}\overline{w_v'w_v'} + 2\bar{w}_v\overline{\rho' w_v'})\right] \qquad \text{(B-38)}$$

Development of the time-averaged v-momentum equation is based upon an expansion of Equation (III-59) and proceeds in a similar manner to that used for the u-momentum equation. The result is

$$\frac{\partial(\overline{\rho w_v})}{\partial t} + \frac{1}{H}\frac{\partial}{\partial u}(\bar{\rho}\bar{w}_v\bar{w}_u) + \frac{1}{H}\frac{\partial}{\partial v}(\bar{\rho}\bar{w}_v\bar{w}_v) + \frac{1}{H^3}(-v\bar{\rho}\bar{w}_u\bar{w}_u + 2u\bar{\rho}\bar{w}_v\bar{w}_u + v\bar{\rho}\bar{w}_v\bar{w}_v)$$

$$= \frac{1}{H}\left(\frac{\partial\bar{\sigma}_{uv}}{\partial u} + \frac{\partial\bar{\sigma}_{vv}}{\partial v}\right) + \frac{1}{H^3}(-v\bar{\sigma}_{uu} + 2u\bar{\sigma}_{uv} + v\bar{\sigma}_{vv})$$

$$- \frac{1}{H}\left[\frac{\partial}{\partial u}(\bar{\rho}\overline{w_u'w_v'} + \bar{w}_u\overline{\rho' w_v'} + \bar{w}_v\overline{\rho' w_u'}) + \frac{\partial}{\partial v}(\bar{\rho}\overline{w_v'w_v'} + 2\bar{w}_v\overline{\rho' w_v'})\right]$$

$$- \frac{1}{H^3}\left[-v(\bar{\rho}\overline{w_u'w_u'} + 2\bar{w}_u\overline{\rho' w_u'}) + 2u(\bar{\rho}\overline{w_u'w_v'} + \bar{w}_u\overline{\rho' w_v'} + \bar{w}_v\overline{\rho' w_u'})\right.$$

$$\left. + v(\bar{\rho}\overline{w_v'w_v'} + 2\bar{w}_v\overline{\rho' w_v'})\right] \qquad \text{(B-39)}$$

Time-Averaged Energy Equation

In rectangular coordinates the instantaneous energy equation, Equation (III-60), can be expanded as follows:

$$\frac{\partial}{\partial t}\left[\overline{(\rho e_o)}+(\rho e_o)'\right] + \frac{\partial}{\partial x}\left\{\left[\overline{(\rho e_o)}+(\rho e_o)'\right](\bar{w}_x+w_x')\right\} + \frac{\partial}{\partial y}\left\{\left[\overline{(\rho e_o)}\right.\right.$$

$$\left.\left. + (\rho e_o)'\right](\bar{w}_y+w_y')\right\} = -\frac{\partial}{\partial x}(\bar{q}_x+q_x') - \frac{\partial}{\partial y}(\bar{q}_y+q_y')$$

$$+ \frac{\partial}{\partial x}\left[(\bar{\sigma}_{xx}+\sigma'_{xx})(\bar{w}_x+w_x')+(\bar{\sigma}_{xy}+\sigma'_{xy})(\bar{w}_y+w_y')\right]$$

$$+ \frac{\partial}{\partial y}\left[(\bar{\sigma}_{xy}+\sigma'_{xy})(\bar{w}_x+w_x')+(\bar{\sigma}_{yy}+\sigma'_{yy})(\bar{w}_y+w_y')\right] \qquad \text{(B-40)}$$

Time-averaging results in

$$\frac{\partial\overline{(\rho e_o)}}{\partial t} + \frac{\partial}{\partial x}\left[\overline{(\rho e_o)}\bar{w}_x+\overline{(\rho e_o)'w_x'}\right] + \frac{\partial}{\partial y}\left[\overline{(\rho e_o)}\bar{w}_y+\overline{(\rho e_o)'w_y'}\right]$$

$$= -\frac{\partial}{\partial x}\bar{q}_x - \frac{\partial}{\partial y}\bar{q}_y + \frac{\partial}{\partial x}\left(\bar{\sigma}_{xx}\bar{w}_x+\overline{\sigma'_{xx}w'_x}+\bar{\sigma}_{xy}\bar{w}_y+\overline{\sigma'_{xy}w'_y}\right)$$

$$+ \frac{\partial}{\partial y}\left(\bar{\sigma}_{xy}\bar{w}_x+\overline{\sigma'_{xy}w'_x}+\bar{\sigma}_{yy}\bar{w}_y+\overline{\sigma'_{yy}w'_y}\right) \qquad \text{(B-41)}$$

Based on the defining relations for (ρe_o) and $(\rho e_o)'$ as given by Equations (B-16) and (B-17), and on the previously-mentioned simplifying assumptions relating to double correlation terms containing viscous stresses, Equation (B-41) can be written as

$$\frac{\partial(\overline{\rho e_o})}{\partial t} + \frac{\partial}{\partial x}\left[(\bar{\rho}\bar{e}_o+\overline{\rho' e_o'})\bar{w}_x+\bar{e}_o\overline{\rho' w_x'}+\bar{\rho}\overline{e_o' w_x'}\right] + \frac{\partial}{\partial y}\left[(\bar{\rho}\bar{e}_o+\overline{\rho' e_o'})\bar{w}_y\right.$$

$$\left. + \bar{e}_o\overline{\rho' w_y'}+\bar{\rho}\overline{e_o' w_y'}\right] = -\frac{\partial}{\partial x}\bar{q}_x - \frac{\partial}{\partial y}\bar{q}_y + \frac{\partial}{\partial x}(\bar{\sigma}_{xx}\bar{w}_x$$

$$+ p'w_x'+\bar{\sigma}_{xy}\bar{w}_y) + \frac{\partial}{\partial y}(\bar{\sigma}_{xy}\bar{w}_x+\bar{\sigma}_{yy}\bar{w}_y+p'w_y') \qquad \text{(B-42)}$$

Rearrangement and use of the definition of e_o' as given by Equation (B-3), produces

$$\frac{\partial(\overline{\rho e_o})}{\partial t} + \frac{\partial}{\partial x}(\bar{\rho}\bar{e}_o\bar{w}_x) + \frac{\partial}{\partial y}(\bar{\rho}\bar{e}_o\bar{w}_y) = -\frac{\partial\bar{q}_x}{\partial x} - \frac{\partial q_y}{\partial y} + \frac{\partial}{\partial x}(\bar{\sigma}_{xx}\bar{w}_x$$

$$+p'w_x'+\bar{\sigma}_{xy}\bar{w}_y) + \frac{\partial}{\partial y}(\bar{\sigma}_{xy}\bar{w}_x+\bar{\sigma}_{yy}\bar{w}_y+p'w_y') - \frac{\partial}{\partial x}\left[(c_v\overline{\rho' T'}+\bar{w}_x\overline{\rho' w_x'}\right.$$

$$+\bar{w}_y\overline{\rho' w_y'})\bar{w}_x+\bar{e}_o\overline{\rho' w_x'}+\bar{\rho}(c_v\overline{T' w_x'}+\bar{w}_x\overline{w_x' w_x'}$$

$$\left.+\bar{w}_y\overline{w_y' w_x'})\right] - \frac{\partial}{\partial y}\left[(c_v\overline{\rho' T'}+\bar{w}_x\overline{\rho' w_x'}+\bar{w}_y\overline{\rho' w_y'})\bar{w}_y\right.$$

$$\left.+\bar{e}_o\overline{\rho' w_y'}+ (c_v\overline{T' w_y'}+\bar{w}_x\overline{w_x' w_y'}+\bar{w}_y\overline{w_y' w_y'})\right] \qquad \text{(B-43)}$$

It is convenient to introduce the relation

$$h' \equiv c_v T' + p'/\bar{\rho} \qquad \text{(B-44)}$$

Use of this relation produces the time-averaged energy equation in the final form,

$$\frac{\partial(\overline{\rho e_o})}{\partial t} + \frac{\partial}{\partial x}(\bar{\rho}\bar{e}_o\bar{w}_x) + \frac{\partial}{\partial y}(\bar{\rho}\bar{e}_o\bar{w}_y) = -\frac{\partial \bar{q}_x}{\partial x} - \frac{\partial \bar{q}_y}{\partial y}$$

$$+ \frac{\partial}{\partial x}(\bar{\sigma}_{xx}\bar{w}_x+\bar{\sigma}_{xy}\bar{w}_y) + \frac{\partial}{\partial y}(\bar{\sigma}_{xy}\bar{w}_x+\bar{\sigma}_{yy}\bar{w}_y) - \frac{\partial}{\partial v}[(c_v\overline{\rho'T'}$$

$$+\bar{w}_x\overline{\rho'w'_x}+\bar{w}_y\overline{\rho'w'_y})\bar{w}_x+\bar{e}_o\overline{\rho'w'_x}+\rho(\overline{h'w'_x}+\bar{w}_x\overline{w'_xw'_x}+\bar{w}_y\overline{w'_yw'_x})]$$

$$- \frac{\partial}{\partial y}[(c_v\overline{\rho'T'}+\bar{w}_x\overline{\rho'w'_x}+\bar{w}_y\overline{\rho'w'_y})\bar{w}_y+\bar{e}_o\overline{\rho'w'_y}$$

$$+\bar{\rho}(\overline{h'w'_y}+\bar{w}_x\overline{w'_xw'_y}+\bar{w}_y\overline{w'_yw'_y})] \qquad \text{(B-45)}$$

In parabolic coordinates the instantaneous energy equation, Equation (III-61) can be expanded as follows:

$$\frac{\partial}{\partial t}[(\overline{\rho e_o})+(\rho e_o)'] + \frac{1}{H}\frac{\partial}{\partial u}\{[(\overline{\rho e_o})+(\rho e_o)'](\bar{w}_u+w'_u)\} + \frac{1}{H}\frac{\partial}{\partial v}\{[(\overline{\rho e_o})$$

$$+ (\rho e_o)'](\bar{w}_v+w'_v)\} + \frac{1}{H^3}\{u[(\overline{\rho e_o})+(\rho e_o)'](\bar{w}_u+w'_u)$$

$$+ v[(\overline{\rho e_o})+(\rho e_o)'](\bar{w}_u+w'_u)\} = -\frac{1}{H}[\frac{\partial}{\partial u}(\bar{q}_u+q'_u) + \frac{\partial}{\partial v}(\bar{q}_v+q'_v)]$$

$$- \frac{1}{H^3}[u(\bar{q}_u+q'_u)+v(\bar{q}_v+q'_v)] + \frac{1}{H}\{\frac{\partial}{\partial u}[(\bar{\sigma}_{uu}+\sigma'_{uu})(\bar{w}_u+w'_u)$$

$$+ (\bar{\sigma}_{uv}+\sigma'_{uv})(\bar{w}_v+w'_v) + \frac{\partial}{\partial v}[(\bar{\sigma}_{uv}+\sigma'_{uv})(\bar{w}_u+w'_u) + (\bar{\sigma}_{vv}+\sigma'_{uv})(\bar{w}_v+w'_v)]\}$$

$$+ \frac{1}{H^3}\left[u(\bar{\sigma}_{uu}+\sigma'_{uu})(\bar{w}_u+w'_u)+u(\bar{\sigma}_{uv}+\sigma'_{uv})(\bar{w}_v+w'_v)\right.$$

$$\left.+ v(\bar{\sigma}_{uv}+\sigma'_{uv})(\bar{w}_u+w'_u)+v(\bar{\sigma}_{vv}+\sigma'_{vv})(\bar{w}_v+w'_v)\right] \qquad \text{(B-46)}$$

Time-averaging produces

$$\frac{\partial(\overline{\rho e_o})}{\partial t} + \frac{1}{H}\frac{\partial}{\partial u}\left[(\overline{\rho e_o})\bar{w}_u+\overline{(\rho e_o)'w'_u}\right] + \frac{1}{H}\frac{\partial}{\partial v}\left[(\overline{\rho e_o})\bar{w}_v+\overline{(\rho e_o)'w'_v}\right]$$

$$+ \frac{1}{H^3}\left\{u\left[(\overline{\rho e_o})\bar{w}_u+\overline{(\rho e_o)'w'_u}\right]+v\left[(\overline{\rho e_o})\bar{w}_u+\overline{(\rho e_o)'w'_u}\right]\right\}$$

$$= -\frac{1}{H}\left(\frac{\partial \bar{q}_u}{\partial u}+\frac{\partial \bar{q}_v}{\partial v}\right) - \frac{1}{H^3}\left(u\bar{q}_u+v\bar{q}_v\right) + \frac{1}{H}\left[\frac{\partial}{\partial u}\left(\bar{\sigma}_{uu}\bar{w}_u+\overline{\sigma'_{uu}w'_u}\right.\right.$$

$$\left.+\bar{\sigma}_{uv}\bar{w}_v+\overline{\sigma'_{uv}w'_v}\right) + \frac{\partial}{\partial v}\left(\bar{\sigma}_{uv}\bar{w}_u+\overline{\sigma'_{uv}w'_u}+\bar{\sigma}_{vv}\bar{w}_v+\overline{\sigma'_{vv}w'_v}\right)\Big]$$

$$+ \frac{1}{H^3}\left[u\left(\bar{\sigma}_{uu}\bar{w}_u+\overline{\sigma'_{uu}w'_u}+\bar{\sigma}_{uv}\bar{w}_v+\overline{\sigma'_{uv}w'_v}\right)+v\left(\bar{\sigma}_{uv}\bar{w}_u\right.\right.$$

$$\left.\left.+\overline{\sigma'_{uv}w'_u}+\bar{\sigma}_{vv}\bar{w}_v+\overline{\sigma'_{vv}w'_v}\right)\right] \qquad \text{(B-47)}$$

If the relations for $(\overline{\rho e_o})$ and $(\rho e_o)'$, as given by Equations (B-18) and (B-19), are introduced into Equation (B-47), along with the simplifying assumptions pertaining to the viscous stress fluctuations in the double-correlation terms, the result is

$$\frac{\partial(\overline{\rho e_o})}{\partial t} + \frac{1}{H}\frac{\partial}{\partial u}\left[(\bar{\rho}\bar{e}_o+\overline{\rho' e'_o})\bar{w}_u+\bar{e}_o\overline{\rho' w'_u}+\bar{\rho}\overline{e'_o w'_u}\right] + \frac{1}{H}\frac{\partial}{\partial v}\left[(\bar{\rho}\bar{e}_o\right.$$

$$+\overline{\rho' e_o'})\bar{w}_v+\bar{e}_o\overline{\rho' w_v'}+\bar{\rho}\overline{e_o' w_v'}] + \frac{1}{H}\{u[(\bar{\rho}\bar{e}_o+\overline{\rho' e_o'})\bar{w}_u+\bar{e}_o\overline{\rho' w_u'}+\bar{\rho}\overline{e_o' w_u'}]$$

$$+ v[(\bar{\rho}\bar{e}_o+\overline{\rho' e_o'})\bar{w}_v+\bar{e}_o\overline{\rho' w_v'}+\bar{\rho}\overline{e_o' w_u'}]\} = -\frac{1}{H}\left(\frac{\partial \bar{q}_u}{\partial u}+\frac{\partial \bar{q}_v}{\partial v}\right)$$

$$-\frac{1}{H^3}(u\bar{q}_u+v\bar{q}_v) + \frac{1}{H}\left[\frac{\partial}{\partial u}(\bar{\sigma}_{uu}\bar{w}_u+\rho' w_u'+\bar{\sigma}_{uv}\bar{w}_v) + \frac{\partial}{\partial v}(\bar{\sigma}_{uv}\bar{w}_u+\bar{\sigma}_{vv}\bar{w}_v\right.$$

$$\left.+\rho' w_v')\right] + \frac{1}{H^3}[u(\bar{\sigma}_{uu}\bar{w}_u+\rho' w_u'+\bar{\sigma}_{uv}\bar{w}_v)+v(\bar{\sigma}_{uv}\bar{w}_u+\bar{\sigma}_{vv}\bar{w}_v+\rho' w_v')] \qquad \text{(B-48)}$$

Based on the definitions for e_o' and h' as given by Equations (B-5) and (B-44), Equation (B-48) can be written as

$$\frac{\partial(\overline{\rho e_o})}{\partial t} + \frac{1}{H}\left[\frac{\partial}{\partial u}(\bar{\rho}\bar{e}_o\bar{w}_u) + \frac{\partial}{\partial v}(\bar{\rho}\bar{e}_o\bar{w}_v)\right] + \frac{1}{H^3}(u\bar{\rho}\bar{e}_o\bar{w}_u+v\bar{\rho}\bar{e}_o\bar{w}_v)$$

$$= -\frac{1}{H}\left(\frac{\partial \bar{q}_u}{\partial u}+\frac{\partial \bar{q}_v}{\partial v}\right) - \frac{1}{H^3}(u\bar{q}_u+v\bar{q}_v) + \frac{1}{H}\left[\frac{\partial}{\partial u}(\bar{\sigma}_{uu}\bar{w}_u+\bar{\sigma}_{uv}\bar{w}_v)\right.$$

$$\left.+\frac{\partial}{\partial v}(\bar{\sigma}_{uv}\bar{w}_u+\bar{\sigma}_{vv}\bar{w}_v)\right] + \frac{1}{H^3}[u(\bar{\sigma}_{uu}\bar{w}_u+\bar{\sigma}_{uv}\bar{w}_v)+v(\bar{\sigma}_{uv}\bar{w}_u$$

$$+\bar{\sigma}_{vv}\bar{w}_v)] - \frac{1}{H}\frac{\partial}{\partial u}[(c_v\overline{\rho' T'}+\bar{w}_u\overline{\rho' w_u'}+\bar{w}_v\overline{\rho' w_v'})\bar{w}_u+\bar{e}_o\overline{\rho' w_u'}$$

$$+\bar{\rho}(\overline{h' w_u'}+\bar{w}_u\overline{w_u' w_u'}+\bar{w}_v\overline{w_v' w_u'})] - \frac{1}{H}\frac{\partial}{\partial v}[(c_v\overline{\rho' T'}+\bar{w}_u\overline{\rho' w_u'}$$

$$+\bar{w}_v\overline{\rho' w_v'})\bar{w}_v+\bar{e}_o\overline{\rho' w_v'}+\bar{\rho}(\overline{h' w_v'}+\bar{w}_u\overline{w_u' w_v'}+\bar{w}_v\overline{w_v' w_v'})]$$

$$-\frac{1}{H^3}\{u[(c_v\overline{\rho' T'}+\bar{w}_u\overline{\rho' w_u'}+\bar{w}_v\overline{\rho' w_v'})\bar{w}_u+\bar{e}_o\overline{\rho' w_u'}+\bar{\rho}(\overline{h' w_u'}$$

$$+\bar{w}_u\overline{w'_u w'_u}+\bar{w}_v\overline{w'_v w'_u})]+v[(c_v\overline{\rho' T'}+\bar{w}_u\overline{\rho' w'_u}+\bar{w}_v\overline{\rho' w'_v})\bar{w}_v$$

$$+\bar{e}_o\overline{\rho' w'_v}+\bar{\rho}(\overline{h' w'_v}+\bar{w}_u\overline{w'_u w'_v}+\bar{w}_v\overline{w'_v w'_v})]\Big\} \qquad \text{(B-49)}$$

APPENDIX C

TRANSVERSE VARIATION OF EDDY VISCOSITY

The only available experimental data, which appears to provide any indication of the variation of eddy viscosity in a deflected jet is that of Endo [20]. As previously noted in Chapter II, and as confirmed by personal contact [106] and [107] Endo assumed no transverse variation of eddy viscosity in his analytical model, but he adopted Sawyer's relation [50] for the turbulent shear stress in the form

$$\bar{\tau}_{\eta\zeta} = \bar{\rho}(\epsilon_m)_{jc\ell}\left(\frac{\partial \bar{w}_\zeta}{\partial \eta} - C\,\frac{\bar{w}_\zeta}{R_{jc\ell}}\right) \tag{C-1}$$

For purposes of comparison, it is important to note that in general curvilinear coordinates the stress-strain relation for viscous stresses is

$$\sigma_{\eta\zeta} = \mu\left(\frac{R_{jc\ell}}{R_{jc\ell}+\eta}\,\frac{\partial w_\eta}{\partial \eta} + \frac{\partial w_\zeta}{\partial \eta} - \frac{w_\zeta}{R_{jc\ell}+\eta}\right) \tag{C-2}$$

If the relation proposed by Boussinesq [23] is assumed to hold in all coordinate systems for turbulent stresses, then

$$\bar{\tau}_{\eta\zeta} = \bar{\rho}(\epsilon_m)_j\left(\frac{R_{jc\ell}}{R_{jc\ell}+\eta}\,\frac{\partial \bar{w}_\eta}{\partial \zeta} + \frac{\partial \bar{w}_\zeta}{\partial \eta} - \frac{\bar{w}_\zeta}{R_{jc\ell}+\eta}\right) \tag{C-3}$$

Now by order of magnitude considerations,

$$\left|\frac{\partial \bar{w}_\eta}{\partial \zeta}\right| << \left|\frac{\partial \bar{w}_\zeta}{\partial \eta}\right| \tag{C-4}$$

and

$$\left|\frac{\bar{w}_\zeta}{R_{jc\ell}+\eta}\right| \sim \left|\frac{\partial \bar{w}_\zeta}{\partial \eta}\right| \tag{C-5}$$

Thus, if $\partial \bar{w}_\eta / \partial \zeta$ is neglected,

$$\bar{\tau}_{\eta\zeta} = \bar{\rho}(\epsilon_m)_j\left(\frac{\partial \bar{w}_\zeta}{\partial \eta} - \frac{\bar{w}_\zeta}{R_{jc\ell}+\eta}\right) \tag{C-6}$$

A combination of Equations (C-1) and (C-6) produces

$$\bar{\rho}(\epsilon_m)_j\left(\frac{\partial \bar{w}_\zeta}{\partial \eta} - \frac{\bar{w}_\zeta}{R_{jc\ell}+\eta}\right) = \bar{\rho}(\epsilon_m)_{jc\ell}\left(\frac{\partial \bar{w}_\zeta}{\partial \eta} - C\,\frac{w_\zeta}{R_{jc\ell}}\right) \tag{C-7}$$

Rearrangement yields

$$\frac{(\epsilon_m)_j}{(\epsilon_m)_{jc\ell}} = \left(\frac{\partial \bar{w}_\zeta}{\partial \eta} - C\,\frac{\bar{w}_\zeta}{R_{jc\ell}}\right)\Big/\left(\frac{\partial \bar{w}_\zeta}{\partial \eta} - \frac{\bar{w}_\zeta}{R_{jc\ell}+\eta}\right) \tag{C-8}$$

The analytical model utilized by Endo produced velocity profiles in good agreement with his experimental data, as noted in Chapter II. In addition Endo provided experimental data for the radius of curvature of the deflected jet. Thus by use of a combination of both his analytical and experimental data, the dimensionless ratio $(\epsilon_m)_j/(\epsilon_m)_{jc\ell}$ can be evaluated in terms of the right-hand side of Equation (C-8). This

in effect provides an indication of the transverse variation of eddy viscosity. For such variation to be meaningful, however, it must be expressed as a function of the most pertinent independent variable. Based on the results of various studies [49,51,53,54,55] as discussed in Chapter II, the dimensionless ratio $\partial[(R_{jc\ell}+\eta)\bar{w}_\zeta]/\partial\eta\cdot(1/\bar{w}_{jc\ell})$, produced by dividing the radial gradient of angular momentum by the jet centerline velocity, appears the most appropriate independent variable. This parameter can also be evaluated based on the results of Endo.

A preliminary evaluation of the right-hand side of Equation (C-8) as a function of the dimensionless radial gradient of angular momentum, at several different axial positions, reveals that the former parameter increases with a decreasing radial gradient of angular momentum. This functional relationship can be described approximately by the relation

$$(\epsilon_m)_j \approx (e_m)_{jc\ell}\left\{1-0.06\tanh\left\{\frac{1}{\bar{w}_{jc\ell}}\frac{\partial[(R_{jc\ell}+\eta)\bar{w}_\zeta]}{\partial\eta}-1\right\}\right\} \qquad \text{(C-9)}$$

The variation of eddy viscosity is consistent with the basic stability criterion set forth by Rayleigh [50] if the concept of *flow instability* is considered equivalent to *turbulence intensity*.

APPENDIX D

CALCULATION OF DISTANCE ALONG A PARABOLA

As noted in Chapter III the centerline of the jet resembles a parabola, and for this reason parabolic coordinates are used in the free flow region. The necessity arises for calculating distances along the jet axis, downstream from the jet exit, and distances transverse to the jet axis, in order to determine certain basic jet parameters. For simplicity these distances are assumed to lie along either a u-parabola or a v-parabola. There is thus a need for developing a relation for calculating the distance s along a specified parabola between two specific points.

For the case of distance along a v_k-parabola

$$dx = u\,du$$

$$dy = v_k\,du$$

$$ds = \sqrt{dx^2+dy^2}$$

$$= \sqrt{u^2+v_k^2}\;du$$

Then between the points (u_{j1},v_k) and (u_{j2},v_k) the distance is

$$s = \int_{u_{j1}}^{u_{j2}} \sqrt{u^2+v_k^2}\, du$$

$$= \frac{1}{2}\left[u_{j2}\sqrt{u_{j2}^2+v_k^2} - u_{j1}\sqrt{u_{j1}^2+v_k^2} + v_k^2 \ell n\left(\frac{u_{j2} + \sqrt{u_{j2}^2+v_k^2}}{u_{j1} + \sqrt{u_{j1}^2+v_k^2}}\right)\right] \quad (D\text{-}1)$$

For brevity it is convenient to represent this distance with the following notation:

$$s_u(v_k,u_{j1},u_{j2}) \equiv \left|\int_{u_{j1}}^{u_{j2}} \sqrt{u^2+v_k}\, du\right| \quad (D\text{-}2)$$

In like fashion, for the distance along a u_j-parabola,

$$dx = -vdv$$

$$dy = u_j dv$$

$$ds = \sqrt{dx^2+dy^2}$$

$$= \sqrt{u_j^2+v^2}\, dv$$

Then between the points (u_j,u_{k1}) and (u_j,v_{k2}) the distance is

$$s = \int_{v_{k1}}^{v_{k2}} \sqrt{u_{j1}^2+v^2}\, dv$$

$$= \frac{1}{2}\left[v_{k2}\sqrt{u_j^2+v_{k2}^2} - v_{k1}\sqrt{u_j^2+v_{k1}^2} + u_j \ell n\left(\frac{v_{k2} + \sqrt{u_j^2+v_{k2}^2}}{v_{k1} + \sqrt{u_j^2+v_{k1}^2}}\right)\right] \quad (D\text{-}3)$$

As before this distance is represented by the following notation:

$$s_v(u_j, v_{k1}, v_{k2}) \equiv \left| \int_{v_{k1}}^{v_{k2}} \sqrt{u_j^2+v^2}\, dv \right| \quad (D\text{-}4)$$

APPENDIX E

ENERGY BOUNDARY CONDITION AT AN INSULATED WALL WITH THERMAL CAPACITANCE

For the sake of brevity the analytical development which follows is presented in rectangular coordinates. The results obtained, however, can be readily applied to parabolic coordinates as well.

The control volume at the surface of the wall, as shown in Figure 37, is formed in such a manner as to include equal volumes of fluid and solid. As noted in the figure the left face of the solid is insulated and thus an adiabatic condition is assumed to hold along this face. This implies

$$q_{xw} - \frac{\partial q_{xw}}{\partial x} \frac{\Delta x}{2} = 0 \qquad \text{(E-1)}$$

The energy fluxes across the remaining faces are indicated in the figure. Notice that at the interface of the solid and the fluid

$$q_{xw} = B_4 \qquad \text{(E-2)}$$

The total energy of the control volume is

$$E_4 \frac{\Delta x}{2} \Delta y + \rho_w c_w T \frac{\Delta x}{2} \Delta y = (E_4 + \rho_w c_w T) \frac{\Delta x}{2} \Delta y \qquad \text{(E-3)}$$

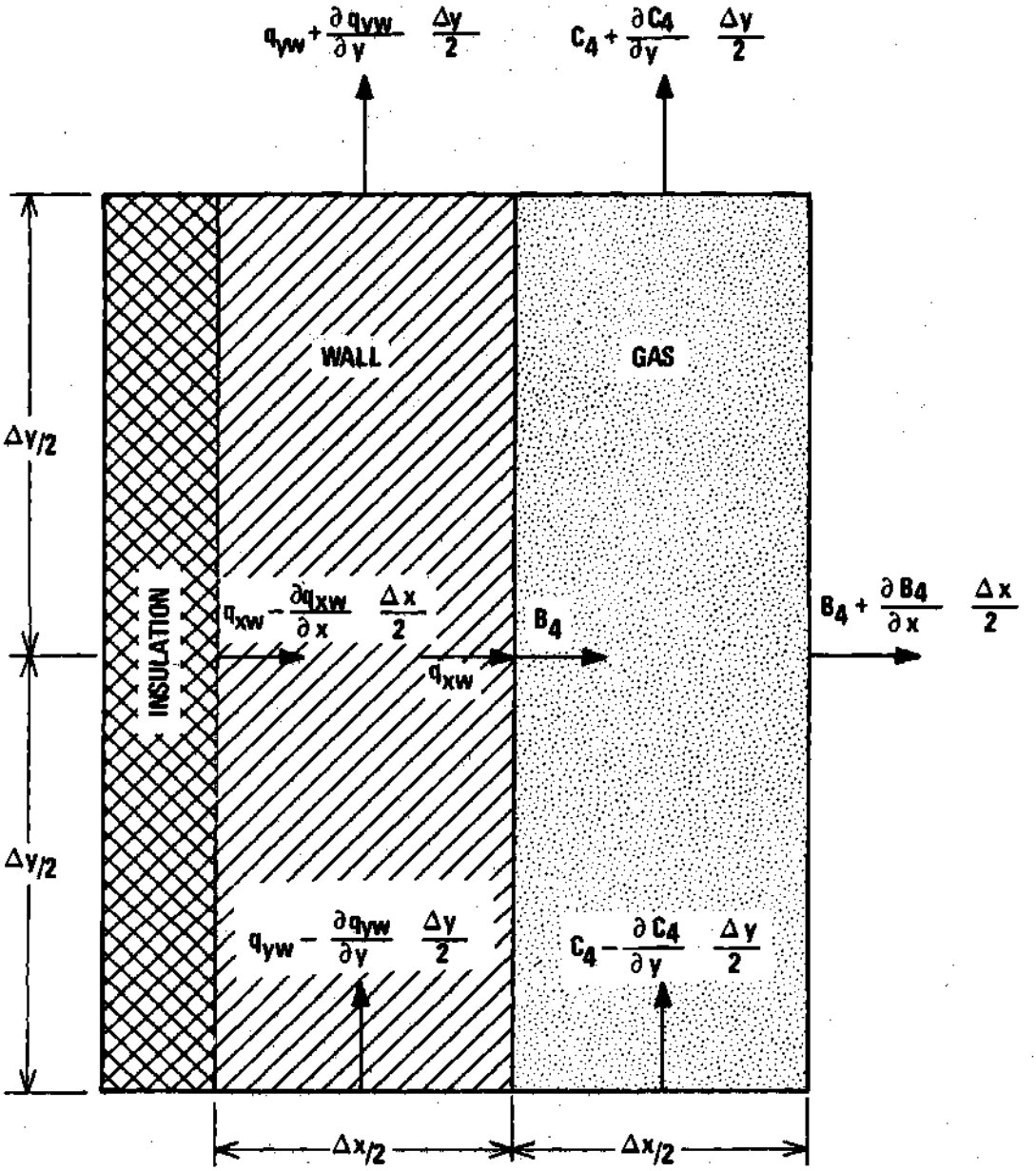

Figure 37. Control Volume at the Surface of the Wall

Based on the fundamental concept of conservation of energy, the time-rate of change of the total energy equals the net energy transport. Thus

$$\frac{\partial}{\partial t}(E_4+\rho_w c_w T)\frac{\Delta x}{2}\Delta y = (q_{yw} - \frac{\partial q_{yw}}{\partial y}\frac{\Delta y}{2} - q_{yw} - \frac{\partial q_{yw}}{\partial y}\frac{\Delta y}{2})\frac{\Delta x}{2} + (C_4 - \frac{\partial C_y}{\partial y}\frac{\Delta y}{2} - C_4 - \frac{\partial C_4}{\partial y}\frac{\Delta y}{2})\frac{\Delta x}{2} + (q_{xw} - \frac{\partial q_{xw}}{\partial x}\frac{\Delta x}{2} - B_4 - \frac{\partial B_4}{\partial x}\frac{\Delta x}{2})\Delta y \qquad (E-4)$$

Division by $\Delta x \Delta y/2$ and simplification yield

$$\frac{\partial}{\partial t}(E_4+\rho_w c_w T) = -(\frac{\partial C_4}{\partial y} + \frac{\partial q_{yw}}{\partial y} + \frac{\partial B_4}{\partial x} + \frac{\partial q_{xw}}{\partial x}) \qquad (E-5)$$

This is the equation governing conservation of energy at the surface of an insulated wall with thermal capacitance.

APPENDIX F

CALCULATION OF INITIAL CONDITIONS

Based on the three assumptions presented in the discussion of the initial conditions in Chapter III, a set of initial values can be assigned to all points in the free flow and slot flow regions.

Free Flow Region

For convenience and brevity certain terms are introduced as follows:

$T_{\infty o}$ = $T_\infty + w_\infty^2/(2c_p)$

σ = spreading coefficient (=7.67)

s_{HA} = $13.5b_o/1.82$

$s_u(v_k,u_{j1},u_{j2})$ = distance along v_k-parabola from u_{j2} to u_{j2} (see Appendix D).

$s_v(u_j,v_{k1},v_{k2})$ = distance along u_j-parabola from v_{k1} to v_{k2} (see Appendix D).

S = $\sqrt{s_{HA}/s_u(v_{c\ell},u_1,u)}$

η = $\sigma s_v(u,v_{c\ell},v)(v-v_{c\ell})/[|v-v_{c\ell}|s_u(v_{c\ell},u_1,u)]$

Z = $-13.5[s_v(u,v_{c\ell},v)-b_o]/s_u(v_{c\ell},u_1,u)$

x_p = $.5(u^2-v^2) + L_{up} + .5$

$$y_p = uv$$

$$(N_{Re})_x = \frac{\rho_\infty w_\infty x_p}{T_\infty}$$

$$\delta_{b\ell} = .37\, x_p (N_{Re})_x^{-.2}$$

$$(\bar{w}_u)_{b\ell} = \begin{cases} 0.99 w_\infty \; u/H \; (y_p/\delta_{b\ell})^{1/7} & (y_p \le \delta_{b\ell}) \\ w_\infty \; u/H \; \{0.99 + 0.01 \exp[-0.001/(y_p/\delta_{b\ell} - 1)]\} & (y_p > \delta_{b\ell}) \end{cases}$$

$$(\bar{w}_v)_{b\ell} = \begin{cases} 0.99 w_\infty \; v/H \; (y_p/\delta_{b\ell})^{1/7} & (y_p \le \delta_{b\ell}) \\ -w_\infty \; v/H \; \{.99 + .01 \exp[-0.001/(y_p/\delta_{b\ell} - 1)]\} & (y_p > \delta_{b\ell}) \end{cases}$$

$$(\bar{w}_v)_{i1} = -[w_{je} - (\bar{w}_u)_{b\ell}] \exp(-Z^2)/(27\pi)$$

$$(\bar{w}_v)_{i2} = [w_{je} - (\bar{w}_u)_{b\ell}][2\eta(1-\tanh^2\eta) - \tanh\eta] S/(2\sigma)$$

$$(\bar{w}_v)_{i3} = -[w_{je} - (\bar{w}_u)_{b\ell} \tanh^2 u] \exp(-Z^2)/(27\sqrt{\pi})$$

Upstream of the plate, along the v_∞-parabola the initial conditions are

$$\left.\begin{aligned} \bar{\rho} &= \rho_\infty \\ \bar{w}_u &= w_\infty \; u/H \\ \bar{w}_v &= -w_\infty \; v_\infty/H \\ \bar{T} &= T_\infty \end{aligned}\right\} \quad (0 \le u \le u_\infty, \; v = v_\infty) \qquad \text{(F-1)}$$

Downstream of the plate, along the u_∞-parabola the initial conditions are, in like fashion,

$$\left.\begin{aligned} \bar{\rho} &= \rho_\infty \\ \bar{w}_u &= w_\infty u_\infty / H \\ \bar{w}_v &= -w_\infty v / H \\ \bar{T} &= T_\infty \end{aligned}\right\} (u=u_\infty,\ 0\le v\le v_\infty) \qquad \text{(F-2)}$$

Along the u_l-parabola in the plane of the plate the following initial conditions are assumed:

$$\left.\begin{aligned} \bar{\rho} = \rho_\infty \Big\{ & 1+1.5\Big\{\tanh[s_v(u_l,v_{c\ell},v)/b_o](v-v_{c\ell})/|v-v_{c\ell}| \\ & - \tanh[s_v(u_l,v_{c\ell},v)/bw](v-v_{c\ell})/|v-v_{c\ell}|\Big\}\Big\}/(RT) \\ & + (\rho_{je}-\rho_\infty)\Big\{1-\tanh[s_v(u_l,v_{c\ell},v)/b_o]\Big\} \\ \bar{w}_u &= 0 \\ \bar{w}_v &= 0 \\ \bar{T} &= T_{\infty o} \end{aligned}\right\} (u=u_l,\ v_l\le v\le v_{les}) \qquad \text{(F-3a)}$$

$$\left.\begin{aligned}
\bar{\rho} &= p_{je}/(RT) \\
\bar{w}_u &= w_{je}\left[\left|\left(b_o - \left|-0.5v^2+.5\right|\right)\right|/b_o\right]^{1/7} \\
\bar{w}_v &= 0 \\
\bar{T} &= T_{jo} - \bar{w}^2/(2/c_p)
\end{aligned}\right\} \quad (u=u_l,\ v_{tes}\le v\le v_{les}) \qquad \text{(F-3b)}$$

$$\left.\begin{aligned}
\bar{\rho} &= p_\infty\Big\{1+1.5\Big\{\tanh[s_v(u_l,v_{cl},v)/b_o](v-v_{cl})/|v-v_{cl}| \\
&\quad - \tanh[s_v(u_l,v_{cl},v)/b_w](v-v_{cl})/|v-v_{cl}|\Big\}\Big\}/(RT) \\
&\quad + (\rho_{je}-\rho_\infty)\left\{1-\tanh^2[s_v(u,v_{cl},v)/b_o]\right\} \\
\bar{w}_u &= 0 \\
\bar{w}_v &= 0 \\
\bar{T} &= T_{\infty o}
\end{aligned}\right\} \quad (u=u_l,\ v_{les}\le v\le v_{lep}) \qquad \text{(F-3c)}$$

$$\left.\begin{aligned}
\bar{\rho} &= \rho_\infty \\
\bar{w}_u &\simeq 0 \\
\bar{w}_v &= -w_\infty \\
\bar{T} &= T_\infty
\end{aligned}\right\} \quad (u=u_l,\ v_{lep}<v<v_\infty) \qquad \text{(F-3d)}$$

Along the v_1-parabola a similar set of conditions are assumed as follows:

$$\left.\begin{aligned}
\bar{\rho} &= p_\infty\Big\{1+1.5\Big\{\tanh[s_v(u,v_{c\ell},v_1)/b_o](v_1-v_{c\ell})/|v_1-v_{c\ell}| \\
&\quad - \tanh[s_v(u,v_{c\ell},v_1)/b_w](v_1-v_{c\ell})/|v_1-v_{c\ell}|\Big\}\Big\}/(RT) \\
&\quad + (\rho_{je}-\rho_\infty)\Big\{1-\tanh^2[s_v(u,v_{c\ell},v_1)/b_o]\Big\}u_2/(2u) \\
\bar{w}_u &= 0 \\
\bar{w}_v &= 0 \\
\bar{T} &= T_{\infty o}
\end{aligned}\right\} (u_1 \le u \le u_{tep},\ v=v_1) \qquad \text{(F-4a)}$$

$$\left.\begin{aligned}
\bar{\rho} &= \rho_\infty \\
\bar{w}_u &= w_\infty \\
\bar{w}_v &= 0 \\
\bar{T} &= T_\infty
\end{aligned}\right\} (u_{tep} < u < u_\infty,\ v=v_1) \qquad \text{(F-4b)}$$

For the calculation of initial values of velocity components for all interior points in the free flow region, the latter is divided into four subregions. In the first subregion,

$$\left.\begin{aligned}\bar{w}_u &= [w_{je}+(\bar{w}_u)_{b\ell}]/2 + [w_{je}-(\bar{w}_u)_{b\ell}]\mathrm{erf}(Z)/2 \\ \bar{w}_v &= [(w_v)_{i1}+(\bar{w}_v)_{b\ell}]/2 + [(\bar{w}_v)_{i1}-(\bar{w}_v)_{b\ell}]\mathrm{erf}(Z)/2\end{aligned}\right\} \quad [v_{c\ell}\le v<v_\infty,\ s_u(v_{c\ell},u_1,u)<S_{HA}] \qquad \text{(F-5a)}$$

In the second subregion,

$$\left.\begin{aligned}\bar{w}_u &= (\bar{w}_u)_{b\ell} + [w_{je}-(\bar{w}_u)_{b\ell}](1-\tanh^2\eta)S \\ \bar{w}_v &= (\bar{w}_v)_{b\ell}\tanh^2\eta + (\bar{w}_v)_{i2}(1-\tanh^2\eta)\end{aligned}\right\} \quad [v_{c\ell}\le v<v_\infty,\ s_u(v_{c\ell},u_1,u)\ge S_{HA}] \qquad \text{(F-5b)}$$

In the third subregion,

$$\left.\begin{aligned}\bar{w}_u &= [w_{je}+(\bar{w}_u)_{b\ell}\tanh^2 u]/2 \\ &\quad + [w_{je}-(\bar{w}_u)_{b\ell}\tanh^2 u]\mathrm{erf}(Z)/2 \\ \bar{w}_v &= -[(\bar{w}_v)_{i3}+(\bar{w}_v)_{b\ell}\tanh^2 u]/2 \\ &\quad + [(\bar{w}_v)_{i3}-(\bar{w}_v)_{b\ell}\tanh^2 u]\mathrm{erf}(Z)/2\end{aligned}\right\} \quad [v_1<v<v_{c\ell},\ s_u(v_{c\ell},u_1,u)<S_{HA}] \qquad \text{(F-5c)}$$

In the fourth subregion,

$$\left.\begin{aligned}\bar{w}_u &= (\bar{w}_u)_{b\ell}\tanh^2 u + [w_{je}-(\bar{w}_u)_{b\ell}\tanh^2 u](1-\tanh^2\eta)S \\ \bar{w}_v &= (w_v)_{b\ell}\tanh^2 u + [w_{je}-(\bar{w}_u)_{b\ell}\tanh^2 u][2\eta(1 \\ &\qquad -\tanh^2\eta)-\tanh^2\ ]S/(2\sigma)\end{aligned}\right\} \quad [v_1<v<v_{c\ell},\ s_u(v_{c\ell},u_1,u)>S_{HA}) \qquad \text{(F-5d)}$$

For the initial temperature of all interior points in the free flow region the following relations are assumed to hold:

$$\bar{T} = \begin{cases} T_{\infty o} - \bar{w}^2/(2c_p) & [s_u(v_{c\ell},u_1,u)<S_{HA},\ v_1<v<v_{tes}] \quad \text{(F-6a)} \\ T_{jo} - \bar{w}^2/(2c_p) & [s_u(v_{c\ell},u_1,u)<S_{HA},\ v_{tes}\le v\le v_{\ell es}] \quad \text{(F-6b)} \\ T_{\infty o} - \bar{w}^2/(2cp) & [s_u(v_{c\ell},u_1,u)<S_{HA},\ v_{\ell es}<v<v_\infty] \quad \text{(F-6c)} \\ T_{\infty o} - \bar{w}^2/(2c_p) + (T_{jo}-T_{\infty o})(1-\tanh^2\eta)S & [s_u(v_{c\ell},u_1,u)\ge S_{HA},\ v_1<v<v_\infty] \quad \text{(F-6d)} \end{cases}$$

The initial density for all interior points is assumed as follows:

$$\bar{\rho} = \rho_\infty\ 1+1.5\{\tanh[s_v(u,v_{c\ell},v)/b_o](v-v_{c\ell})/|v-v_{c\ell}| - \tanh[s_v(u,v_{c\ell},v)/b_w](v-v_{c\ell})/|v-v_{c\ell}|\}u_2/(2u)\ /(RT) + (\rho_{je}-\rho_\infty)\{1-\tanh^2[s_v(u,v_{c\ell},v)/b_o]\}u_2/(2u) \quad (u_1<u<u_\infty,\ v_1<v<v_\infty) \quad \text{(F-7)}$$

Slot Flow Region

The initial conditions for the flow in the slot are considerably simpler than those for the free flow region. The following relationships are assumed:

$$
\left.
\begin{aligned}
\bar{\rho} &= p_{je}/(R\bar{T}) \\
\bar{w}_x &= 0 \\
\bar{w}_y &= w_{je}\left[\left|(b_o-|x+.5|)\right|/b_o\right]^{1/7} \\
\bar{T} &= T_{jo} - \bar{w}^2/(2c_p)
\end{aligned}
\right\}
\qquad (x_{les} \le x \le x_{tes},\ y_{-\infty} < y < 0) \qquad \text{(F-8)}
$$

APPENDIX G

FINITE-DIFFERENCE EQUATIONS

The Taylor series expansion for the function, $f_{j+1,k}$[= $f(u_j+\Delta u_j, v_k)$] about the point (j,k) is

$$f_{j+1,k} = f_{j,k} + \Delta u_j \left(\frac{\partial f}{\partial u}\right)_{j,k} + \frac{\Delta^2 u_j}{2}\left(\frac{\partial^2 f}{\partial u^2}\right)_{j,k} + O(\Delta^3 u_j) \qquad \text{(G-1)}$$

Likewise the expansion for the function $f_{j-1,k}$ is

$$f_{j-1,k} = f_{j,k} - \Delta u_{j-1}\left(\frac{\partial f}{\partial u}\right)_j + \frac{\Delta^2 u_{j-1}}{2}\left(\frac{\partial^2 f}{\partial u^2}\right)_{j,k} + O(\Delta^3 u_{j-1}) \qquad \text{(G-2)}$$

If Equation (G-2) is multiplied by $\Delta^2 u_j/\Delta^2 u_{j-1}$ and then subtracted from Equation (G-1), the result is

$$f_{j+1,k} - \frac{\Delta^2 u_j}{\Delta^2 u_{j-1}} f_{j-1,k} = f_{j,k} - \left(\frac{\Delta^2 u_j}{\Delta^2 u_{j-1}}\right) f_{j,k} + \Delta u_j \left(\frac{\partial f}{\partial u}\right)_{j,k} + \left(\frac{\Delta^2 u_j}{\Delta^2 u_{j-1}}\right)\left(\frac{\partial f}{\partial u}\right)_{j,k} + O(\Delta^3 u) \qquad \text{(G-3)}$$

Rearrangement yields

$$\left(\frac{\partial f}{\partial u}\right)_{j,k} = \frac{f_{j+1,k} - f_{j,k} + (\Delta^2 u_j/\Delta^2 u_{j-1})(f_{j,k} - f_{j-1,k})}{\Delta u_j + \Delta^2 u_j/\Delta u_{j-1}}$$

$$= \frac{(\Delta u_{j-1}/\Delta u_j)(f_{j+1}-f_j) + (\Delta u_j/\Delta u_{j-1})(f_{j,k}-f_{j-1,k})}{\Delta u_{j-1} + \Delta u_j} \qquad \text{(G-4)}$$

Equation (G-4) can be seen to represent a second-order approximation of the partial derivative $\partial f/\partial u)_{j,k}$. Analysis based on Crandall [97] also reveals that the preceding finite-difference approximation equals the slope of a parabola at point $(u_j, f_{j,k})$ passing through the three points $(u_{j-1}, f_{j-1,k})$, $(u_j, f_{j,k})$ and $(u_{j+1}, f_{j+1,k})$.

In certain cases such as at the wall where j=1, expansions can only be carried out in the positive direction. For such a case the Taylor series expansion for the function $f_{j+2,k}$ about the point (j,k) is useful as follows:

$$f_{j+2,k} = f_{j,k} + (\Delta u_j + \Delta u_{j+1}) \frac{\partial f}{\partial u})_{j,k} + \frac{(\Delta u_j + \Delta u_{j+1})^2}{2} \frac{\partial^2 f}{\partial u^2})_{j,k} + O[(\Delta u_j + \Delta u_{j+1})^3] \qquad \text{(G-5)}$$

Multiplication of Equation (G-1) by $(\Delta u_j + \Delta u_{j+1})^2/\Delta^2 u_j$ and subtraction of the result from Equation (G-5) produce

$$f_{j+2,k} - [(\Delta u_j + \Delta u_{j+1})^2/\Delta^2 u_j] f_{j+1,k} = f_{j,k} - [(\Delta u_j + \Delta u_{j+1})^2/\Delta^2 u_j] f_{j,k} + (\Delta u_j + \Delta u_{j+1}) \frac{\partial f}{\partial u})_{j,k} - [(\Delta u_j + \Delta u_{j+1})^2/\Delta^2 u_j] \frac{\partial f}{\partial u})_{j,k} + O(\Delta^3 u) \qquad \text{(G-6)}$$

By rearranging, the following second-order approximation is obtained:

$$\left(\frac{\partial f}{\partial u}\right)_{j,k} \approx \frac{(f_{j+2,k}-f_{j,k}) - [(\Delta u_j+\Delta u_{j+1})^2/\Delta^2 u_j](f_{j+1,k}-f_{j,k})}{\Delta u_j + \Delta u_{j+1} - (\Delta u_j+\Delta u_{j+1})^2/\Delta u_j}$$

$$= \frac{-(2\Delta u_j+\Delta u_{j+1})}{(\Delta u_j+\Delta u_{j+1})\Delta u_j} f_{j,k} + \frac{\Delta u_j + \Delta u_{j+1}}{\Delta u_j \Delta u_{j+1}} f_{j+1,k}$$

$$- \frac{\Delta u_j}{\Delta u_{j+1}(\Delta u_j+\Delta u_{j+1})} f_{j+2,k} \qquad \text{(G-7)}$$

As before it can be shown that this finite difference approximation equals the slope of a parabola at point $(u_j, f_{j,k})$ passing through the three points, $(u_j, f_{j,k})$, $(u_{j+1}, f_{j+1,k})$, and $(u_{j+2}, f_{j+2,k})$.

APPENDIX H

DESCRIPTION OF DIGITAL COMPUTER PROGRAM

General Characteristics

The numerical technique described in Chapter IV is incorporated into a digital computer program entitled DEFJET. The program consists of the main routine (also entitled DEFJET), 46 subroutines and six function sub-programs, and is written in FORTRAN V for the UNIVAC 1108 digital computer. Because of its length, no source listing is included. Subsequent portions of this appendix, however, provide a description of (1) subroutines and function, (2) program terminology, (3) all input items, (4) all output items, and (5) the general logic of the program.

Subroutines and Function Subprograms

In Table 3 the subroutines are arranged in alphabetical order, with the exception that the main routine is listed first. For each subroutine, all other subroutines or subprograms, which call up the particular subroutine or are called up by it, are listed in alphabetical order in the table. The purpose of each subroutine is also given. Table 4 provides similar information for each function subprogram.

Program Terminology

Throughout the program, in general, the same terminology is used. This terminology is designed to resemble as closely as possible the

terminology of the analytical model and the numerical method. Table 5 provides a listing in alphabetical order of the most important FORTRAN variables. For each variable the units are indicated along with the corresponding symbol (if any) from the analytical model, or, where no symbol is assigned, the appropriate definition.

Input Items

The 30 input items are contained on seven cards. Table 6 contains the format for each card along with the names of each input item. Notice should be taken that these input items are made up of the 13 primary input parameters plus 17 auxiliary items. Certain of the latter specify the number of grid lines in each region or subregion of the flow, and also indicate the starting, stopping, and printing times for the computation. Others specify quantities such as $(N_{Pr})_t$ and C_∞ which are constants. Still others provide the thermophysical property data for the plate.

Output Items

The output of DEFJET is entirely dimensionless and is printed in non-formatted form on magnetic tape. The initial output includes a listing of the grid lines in both the parabolic and rectangular coordinate systems. The dimensionless time (TIME) and the time-step (NSTEP) are next printed out, followed by the values of the eight primary flow properties for each point in the free flow region and the slot flow region. For the former the eight properties are WU(J,K), WV(J,K), T(J,K), P(J,K), RHO(J,K), EV(J,K), PSI(J,K) and W(J,K). The eight

properties for the slot flow region are WX(M,N), WY(M,N), TXY(M,N), PXY(M,N), RHOXY(M,N), EVXY(M,N), PSIXY(M,N), and WXY(M,N).

Computer Logic

The basic logic for the subroutines DEFJET, LW1 and LW2 are presented in Figures 38, 39, and 40. By utilization of these flow charts in conjunction with Tables 3 and 4, the general organization and operation of the program can be understood.

Table 3. Subroutines of DEFJET

Subroutine	Called By	Calls Up	Purpose
DEFJET		DENS1, DENS2, DMSL, DTMIN, EDVIS, EDVIXY, EV3CL, GRID, INCOND, INPUT, JETENT, JETEX1, JETEX2, LW1, LW2, MASDIF, OUTPUT, PRESS, SIMP, SPEED1, SPEED2, TEMPUV, TEMPXY, TURBF, TURBS, VELGRA, VIS2, VISJV, VIXSY	Acts as main "driver" program. For flow logic see Figure 38.
BIMX(IEQ)	LW1, LW2		Calculates B(M,N) for all points in the slow flow.
CINX(IEQ)	LW1, LW2		Calculates C(M,N) for all points in the slot flow.
DELBL	INCOND		Calculates boundary layer thickness, DEL.
DENS1	DEFJET		Calculates RHO(J,K) and RHOXY(M,N) during first numerical step (LWSTEP=1).
DENS2	DEFJET		Calculates RHO(J,K) and RHOXY(M,N) during second numerical step (LWSTEP-2).
DESIG (I, L1,L2,FF, DM,DP)	FD1, FD1W, INTUV, INTXY		For a given designation I, at point (L1,L2), along the coordinate L, establishes values for FF(1), FF(2), FF(3), and values for the backward (DM) and forward (DP) space increments.
DMSL	DEFJET		Calculates WJS, RHOJS and XLS. From these dimensional parameters, combined with input parameters, calculates dimensionless parameters.
DTMIN	DEFJET		Calculates maximum time step DT, based on stability criteria.
EDVIS	DEFJET, INCOND	SV, FD1	Calculates eddy viscosity in the boundary layer EVBL, and eddy viscosity in the jet EVJ. Establishes effective eddy viscosity EV(J,K) for all points in free flow region.
EDVIXY	DEFJET, INCOND		Calculates eddy viscosity EVXY(M,N) in the slot.
EV3CL	DEFJET, INCOND	JETVEL, SIMP, SU	Calculate eddy viscosity along jet centerline, EVCL(J).
FIJX(IEQ)	LW1, LW2		Calculates F(J,K) for all points in the free flow for a given value of IEQ.
GAMM(IEQ)	LW1, LW2		Calculates GAM(J,K) for all points in the free flow for a given value for IEQ.
GIKX(IEQ)	LW1, LW2		Calculates G(J,K) for all points in the free flow for a given value of IEQ.
GRID	DEFJET	ATANH, METFAC	Calculates values for grid lines U(J), V(K), X(M), and Y(N).
INCOND (ISTART, NSTEP, TIME)	DEFJET	DELBL, EDVIS, EDVIXY, EV3CL, INTUV, MASDIF, SU, SV, TURBF, TURBS, VELGRA, VIS2, VISUV, VISXY	Calculates initial conditions for all points in free flow and slot flow for ISTART=0. For ISTART<0, reads output tape from previous run and restarts program.
INPUT	DEFJET		Reads seven basic data cards discussed in Table 6.
INTER1 (F1, F2,F3,F,X1, X2,X3,X)	WBC1, WBC2		Given the function values of F1, F2, and F3 corresponding to the points X1, X2, and X3, determines the value of the function F for point X by parabolic interpolation.

Table 3. Subroutines of DEFJET (Continued)

Subroutine	Called by	Calls Up	Purpose
INTMAX (F1, F2,F3,FMAX, X1,X2,X3, XFMAX)	JETVEL		Given the function values F1, F2, and F3 corresponding to the points X1, X2 and X3, calculates the maximum value of the function FMAX and its location XFMAX, based on parabolic interpolation.
INTUV (I, XM,YN,FF)	INCOND, JETEX1, JETEX2		By means of double parabolic interpolation determines the value, FF, of the parameter designated by I, for the point in the free flow with rectangular coordinates XM, YN.
IP1 (IEQ)	LW1		For the first numerical step (LWSTEP=1), calculates E1(IEQ,1,KM1) and E1(IEQ,JM1,1) for a given value of IEQ.
IP2 (IEQ)	LW2		For the second numerical step (LWSTEP=2), calculates E2(IEQ,1,KM1) and E2(IEQ,JM1,1) for a given value of IEQ.
JETENT (NSTEP)	DEFJET	SIMP	Calculates the flow properties along the slot entrance line (N=1).
JETEX1	DEFJET	INTUV	For the first numerical step calculates E1(IEQ, 1,K) in the slot exit plane (KTE<K<KLE) and A1(IEQ,M,MMAX) for IEQ=1,2,3 and 4.
JETEX2	DEFJET	INTUV	For the second numerical step calculates E2 (IEQ,1,K) in the slot exit plane (KTE<K<KLE) and A2(IEQ,M,MMAX) for IEQ=1,2,3 and 4.
JETVEL	EV3CL	INTMAX, SU, SV	Calculates WMAX(J), B1S2U(J), and B1S2D(J).
LW1	DEFJET	BIMX, CINX, FD1, FIJK, GAMM, GIKX, IP1, WBC1	Calculates E1(IEQ,J,K) for all points in the free flow except J=1, J=JMAX, K=1, or K=KMAX. Calculates A1(IEQ,M,N) for all points in the slot flow except M=1, M=MMAX, N=1, or N=NMAX. For flow logic see Figure 39.
LW2	DEFJET	BIMX, CINX, FD1, FIJK, GAMM, GIKX, IP2, WBC2	Calculates E2(IEQ,J,K) for all points in the free flow except J=1, J=JMAX, K=1, or K=KMAX. Calculates A2 (IEQ,M,N) for all points in the slot flow except M=1, M=MMAX, N=1, or N=NMAX. For flow logic see Figure 40.
MASDIF	DEFJET, INCOND	FD1	Calculates XMU(J,K) and XMV(J,K) for all points in the free flow and XMX(M,N) and XMY(M,N) for all points in the slot flow.
METFAC	GRID		Calculates H(J,K) for all points in the free flow.
OUTPUT (NSTEP, TIME)	DEFJET	STFN, STFNXY	For all points in both the free flow and the slot flow, generates an output tape of the eight basic flow properties at specified time interval (IPRINT).
PRESS	DEFJET		Calculates P(J,K) for all points in free flow and PXY(M,N) for all points in the slot flow.
SPEED1	DEFJET		For the first numerical step calculates WU(J,K), WV(J,K) and W(J,K) for all points in the free flow and calculates WX(M,N),WY(M,N), and WXY(M,N) for all points in the slot flow.
SPEED2	DEFJET		For the second numerical step calculates WU(J,K), WV(J,K), and W(J,K) for all points in the free flow, and calculates WX(M,N), WY(M,N) and WXY(M,N) for all points in the slot flow.

Table 3. Subroutines of DEFJET (Continued)

Subroutine	Called by	Calls Up	Purpose
STFN	OUTPUT	SV	Calculates PSI(J,K) for all points in the free flow.
STFNXY	OUTPUT		Calculates PSIXY(M,N) for all points in the slot flow.
TEMPUV	DEFJET		Calculates T(J,K) for all points in the free flow.
TEMPXY	DEFJET		Calculates TXY(M,N) for all points in the slot flow.
TURBF	DEFJET, INCOND	FD1, FD1W	Calculates the total stresses and total heat fluxes for all points in the free flow.
TURBS	DEFJET, INCOND	FD1, FD1W	Calculates the total stresses and total heat fluxes for all points in the slot flow.
VELGRA	DEFJET, INCOND	FD1W	Calculates the derivatives of the velocity components, with respect to the coordinate normal to the wall, for all wall points.
VIS2	DEFJET, INCOND		Calculates the second coefficient of viscosity for all points in the free flow and slot flow.
VISUV	DEFJET, INCOND		Calculates the first coefficient of viscosity for all points in the free flow.
VISXY	DEFJET, INCOND		Calculates the first coefficient of viscosity for all points in the slot flow.
WBC1(IEQ)	LW1	FD1, FD1W, INTER1	For a given value of IEQ during the first numerical step calculates E1(IEQ,J,K) for all wall points in the free flow and A1(IEQ,M,N) for all wall points in the slot flow.
WBC2(IEQ)	LW2	FD1, FD1W, INTER1	For a given value of IEQ during the second numerical step calculates E2(IEQ,J,K) for all wall points in the free flow and A2(IEQ,J,K) for all wall points in the slot flow.

Table 4. Function Subprograms of DEFJET

Function	Called By	Calls Up	Purpose
ATANH(ARG)	GRID		Calculates inverse hyperbolic tangent of ARG.
FD1(I,L1,L2,L)	EDVIS, FD1W, LW1, LW2, MASDIF, TURBF TURBS, WBC1, WBC2	DESIG, FD1W	Calculates the finite difference approximation of the derivative of the parameter designated by I at the point (L1,L2) with respect to the space coordinate designated by L. If IDIREC=1, a backward difference is used. If IDIREC=2, a forward difference is used.
FD1W(I,L1,L2,L)	FD1, TURBF, TURBS, VELGRA, WBC1, WBC2	DESIG	Calculates the finite difference approximation of the derivative of the parameter designated by I, at the wall point, (L1,L2) with respect to the space coordinate designated by L (which is normal to the wall at the point involved).
SIMP(NS,H,Y)	DEFJET, EV3CL, JETENT		Carries out numerical integration of the function, Y, with NS the number of intervals, each equal to H.
SU(VK,U1,U2)	EV3CL, INCOND, JETVEL		Calculates the distance along the parabola V(K) from U1 to U2.
SV(UJ,V1,V2)	EDVIS, INCOND, JETVEL, STFN		Calculates the distance along the parabola U(J) from V1 to V2.

Table 5. Important FORTRAN Variables

FORTRAN Name	Units	Symbol/Definition
A1(IEQ,M,N)		$A^{\ell+1}_{i,m,n}$
A2(IEQ,M,N)		$A^{\ell+2}_{i,m,n}$
B(M,N)		$B_{i,m,n}$
B1S2D(J)		$\delta_{1/2}$ for downstream side of jet at u_j
B1S2U(J)		$\delta_{1/2}$ for upstream side of jet at u_j
BWS	ft	$\hat{b}_w$
C(M,N)		$C_{i,m,n}$
CAMB		C_∞
CPS	BTU/(lb_m°R)	$\hat{c}_p$
CVS	BTU/(lb_m°R)	$\hat{c}_v$
CVMS	BTU/(lb_m°R)	$\hat{c}_w$
DEL		$\delta_{b\ell}$
DT		Δt
E1(IEQ,J,K)		$E^{\ell+1}_{i,j,k}$
E2(IEQ,J,K)		$E^{\ell+2}_{i,j,k}$
EV(J,K)		ϵ_m at point (j,k) in the free flow
EVBL		$(\epsilon_m)_{b\ell}$ based on calculations for a turbulent boundary layer

Table 5. Important FORTRAN Variables (Continued)

FORTRAN Name	Units	Symbol/Definition
EVCL(J)		$(\epsilon_m)_{jc\ell}$
EVJ		$(\epsilon_m)_j$ based on calculations for a plane turbulent jet
EVXY(M,N)		ϵ_m at a point (m,n) in the slot flow
F(J,K)		$F_{i,j,k}$
G(J,K)		$G_{i,j,k}$
GAM(J,K)		$\Gamma_{i,j,k}$
H(J,K)		$H_{j,k}$
I		a general designator used to specify a particular flow property
IDIREC		a designator used to specify the use of backward finite differences (IDIREC=1) or forward finite difference (IDIREC=2)
IEQ		i (used to indicate component of A_i, B_i, C_i, E_i, F_i, G_i and Γ_i)
IPRINT		the number of computational steps between outputs
ISTART		the computational step at which the numerical procedure is to commence
J		j
JMAX		J

Table 5. Important FORTRAN Variables (Continued)

FORTRAN Name	Units	Symbol/Definition
JMI		J-1
JTEP		jtep
K		k
KLEP		klep
KMAX		K
KMI		K-1
KTE		ktes
L		a general designator used to specify a particular direction or coordinate
M		m
MMAX		M
MM1		M-1
N		n
NMAX		N
NM1		N-1
P(J,K)		p at point (j,k) in the free flow
PAMBS	lb_f/ft^2	$\hat{p}_\infty$
PJOS	lb_f/ft^2	$\hat{p}_{jo}$

Table 5. Important FORTRAN Variables (Continued)

FORTRAN Name	Units	Symbol/Definition
PR		N_{Pr}
PRTF		$(N_{Pr})_t$ for free flow
PRTS		$(N_{Pr})_t$ for slot flow
PSI(J,K)		ψ at point (j,k) in the free flow
PSIXY(M,N)		ψ at point (m,n) in the slot flow
PXY(M,N)		p at point (m,n) in the slot flow
RHO(J,K)		ρ at point (j,k) in the free flow
RHOJS	lb_m/ft^3	$\hat{\rho}_{jo}$
RHOMS	lb_m/ft^3	$\hat{\rho}_w$
RHOXY(M,N)		ρ at point (m,n) in the slot flow
RS	$BTU/(lb_m\,^oR)$	$\hat{R}$
SLS	ft	$\hat{L}_s$
T(J,K)		T at point (j,k) in the free flow
TAMBS	^oR	$\hat{T}_\infty$
TIME		t
TIMEND		t at which program is to terminate
TJOS	^oR	$\hat{T}_{jo}$
TXY(M,N)		T at point (m,n) in the slot flow
U(J)		u_j
V(K)		v_k
VISC(J,K)		μ at point (j,k) in the free flow

Table 5. Important FORTRAN Variables (Continued)

FORTRAN Name	Units	Symbol/Definition
VISCAS	$lb_m/(ft\ sec)$	$\hat{\mu}_{ref}$
VISCXY(M,N)		μ at point (m,n) in the slot flow
W(J,K)		w at point (j,k) in the free flow
WAMBS	ft/sec	$\hat{w}_\infty$
WJS	ft/sec	$\hat{w}_{je}$
WMAX(J)		$w_{jc\ell}$ at u_j
WU(J,K)		w_u at point (j,k) in the free flow
WV(J,K)		w_v at point (j,k) in the free flow
WX(M,N)		w_x at point (m,n) in the slot flow
WXY(M,N)		w at point (m,n) in the slot flow
WY(M,N)		w_y at point (m,n) in the slot flow
X(M)		x_m
XKMS	BTU/(ft hr°R)	$\hat{k}_w$
XLPDS	ft	$\hat{L}_{dp}$
XLPUS	ft	$\hat{L}_{up}$
XLS	ft	$\hat{L}$
Y(N)		y_n

Table 6. Input Data for DEFJET

Card No.	Format	Items
1	(6F10.0)	PAMBS, PJOS, TAMBS, TJOS, WAMBS
2	(7E10.0)	CPS, CVS, RS, VISCAS
3	(6F10.0)	PR, PRTF, PRTS, CAMB
4	(6F10.0)	BWS, SLS, XLPUS, XLPDS
5	(6F10.0)	RHOMS, CVMS, XKMS
6	(12I5)	JMAX, JTEP, KMAX, KLEP, KTE, MMAX, NMAX
7	(2I10,F10.0)	ISTART, IPRINT, TIMEND

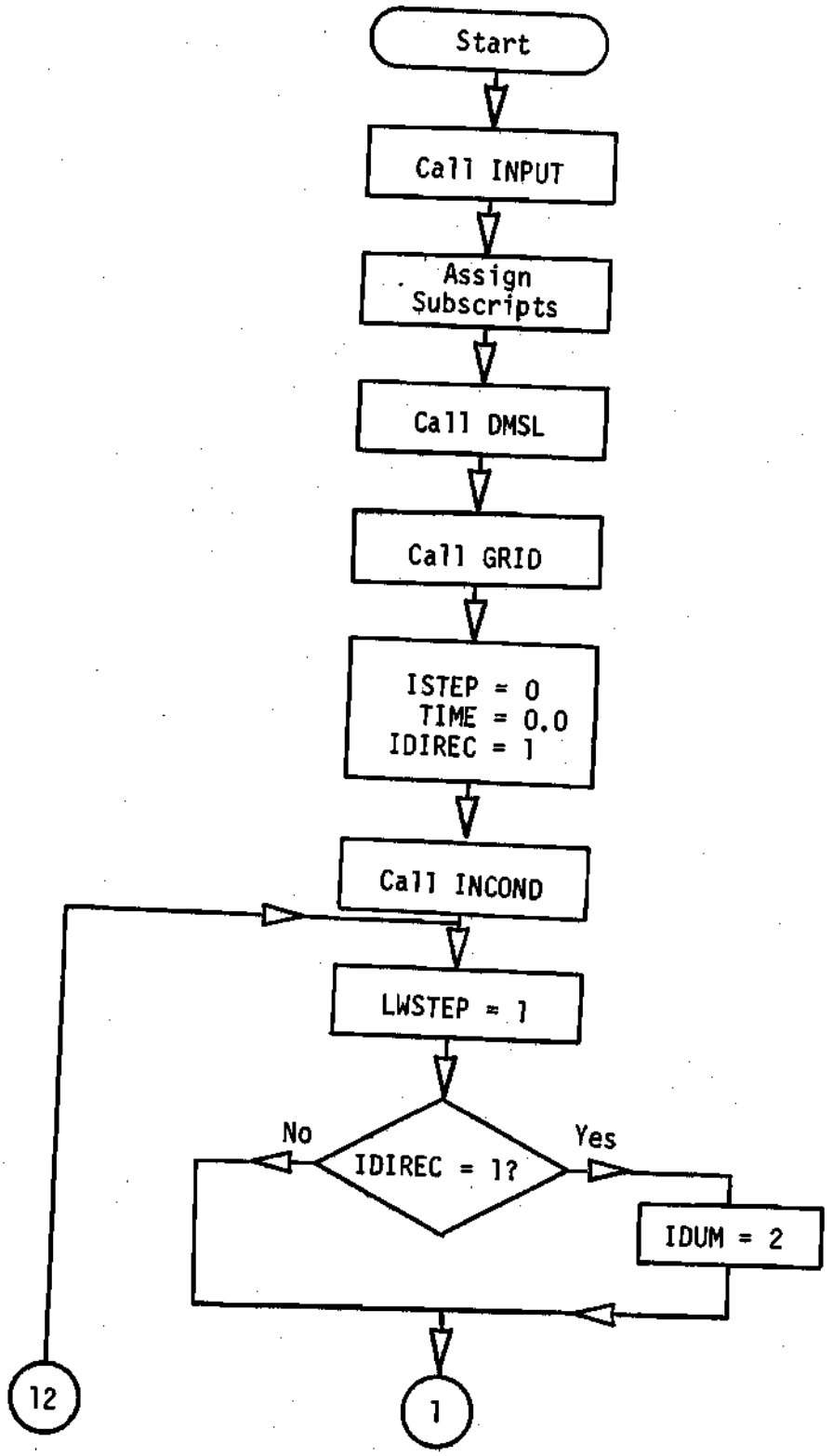

Figure 38. Flow Chart of the Main Routine, DEFJET

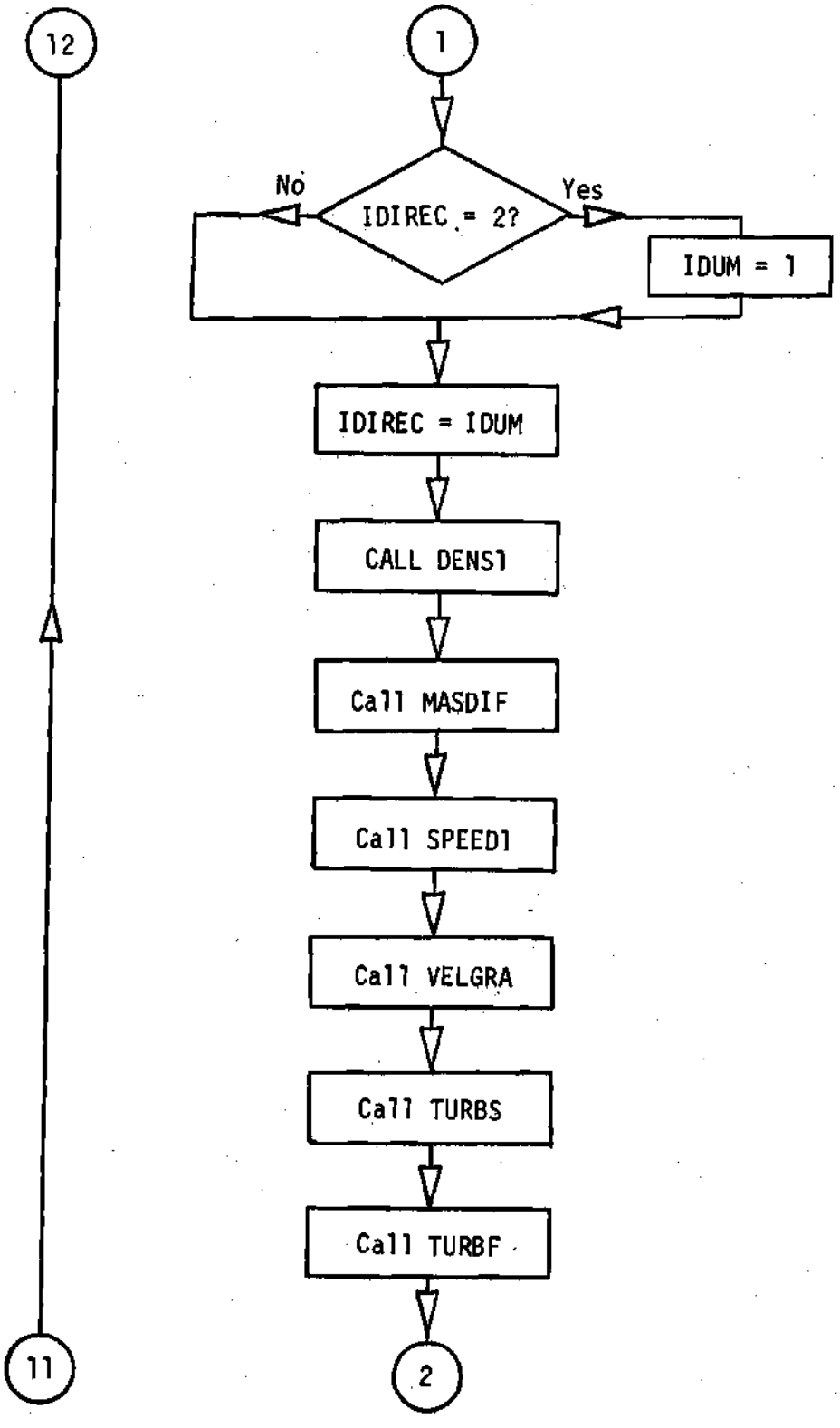

Figure 38. Flow Chart of the Main Routine, DEFJET (Continued)

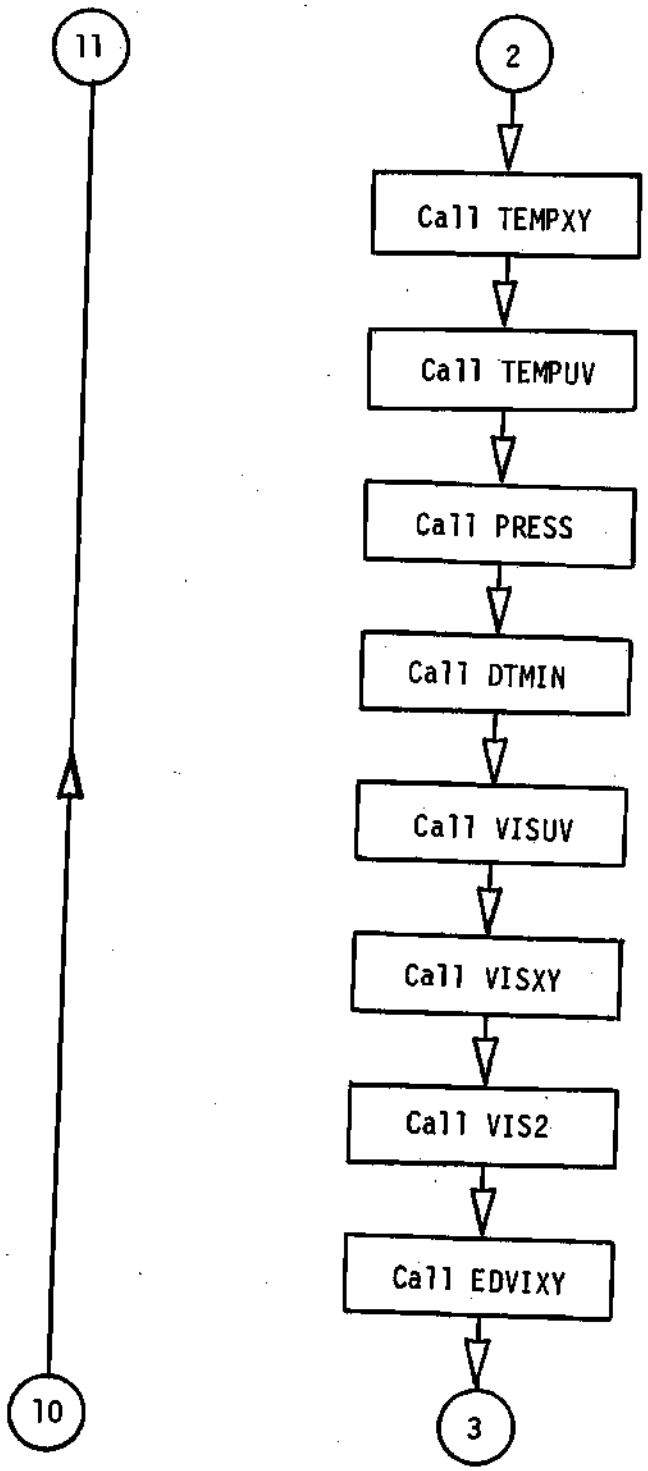

Figure 38. Flow Chart of the Main Routine, DEFJET (Continued)

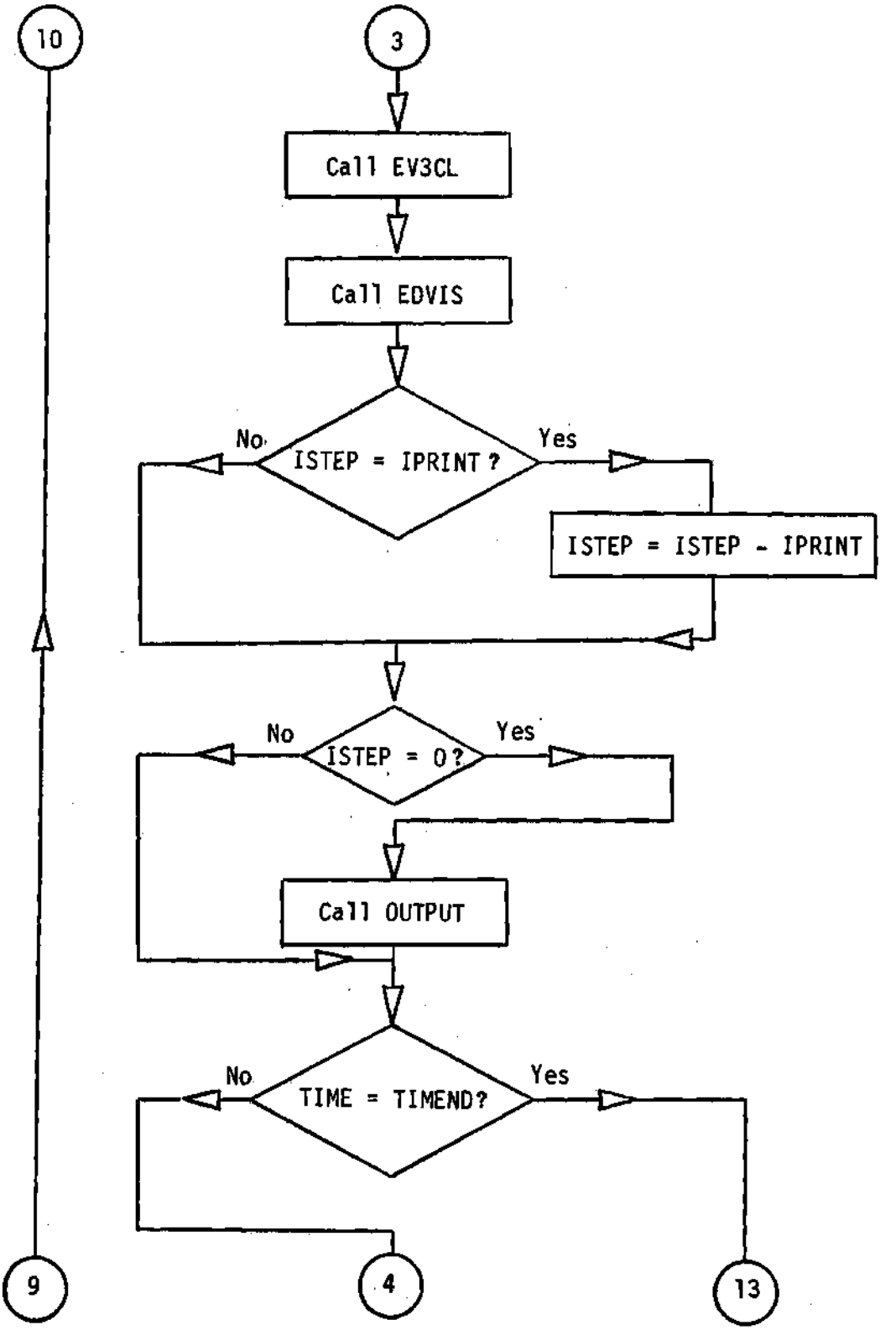

Figure 38. Flow Chart of the Main Routine, DEFJET (Continued)

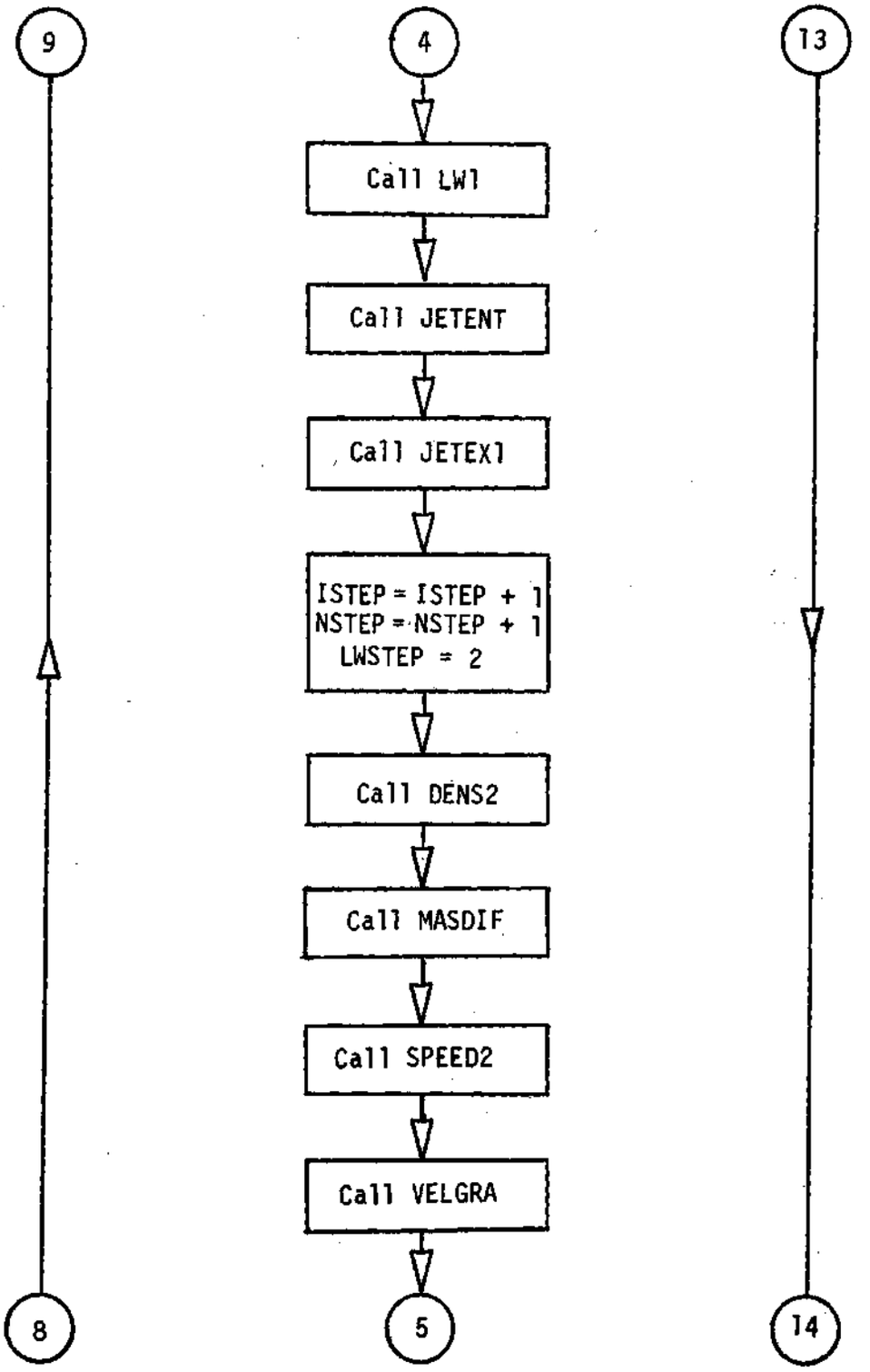

Figure 38. Flow Chart of the Main Routine, DEFJET (Continued)

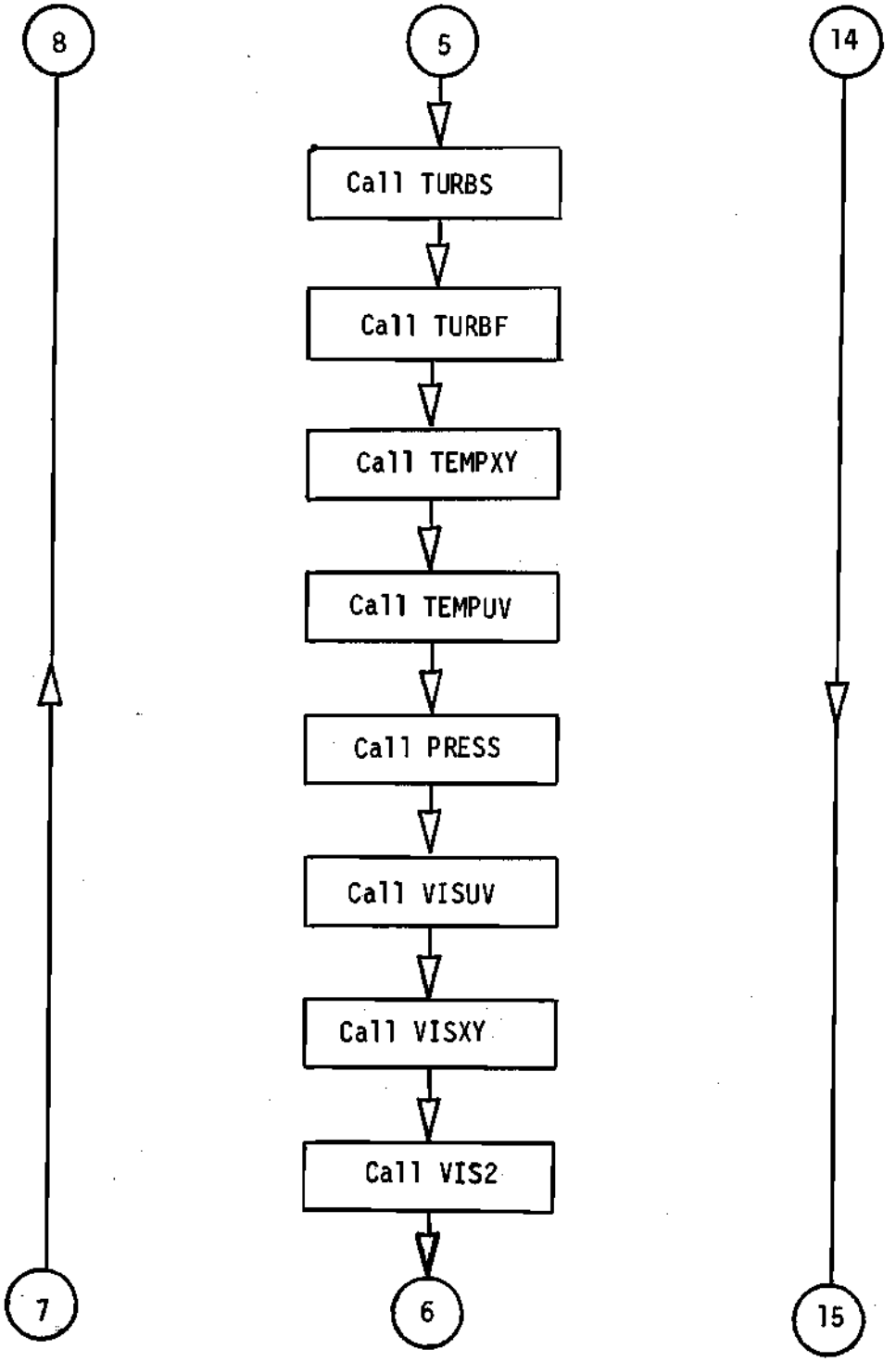

Figure 38. Flow Chart of the Main Routine, DEFJET (Continued)

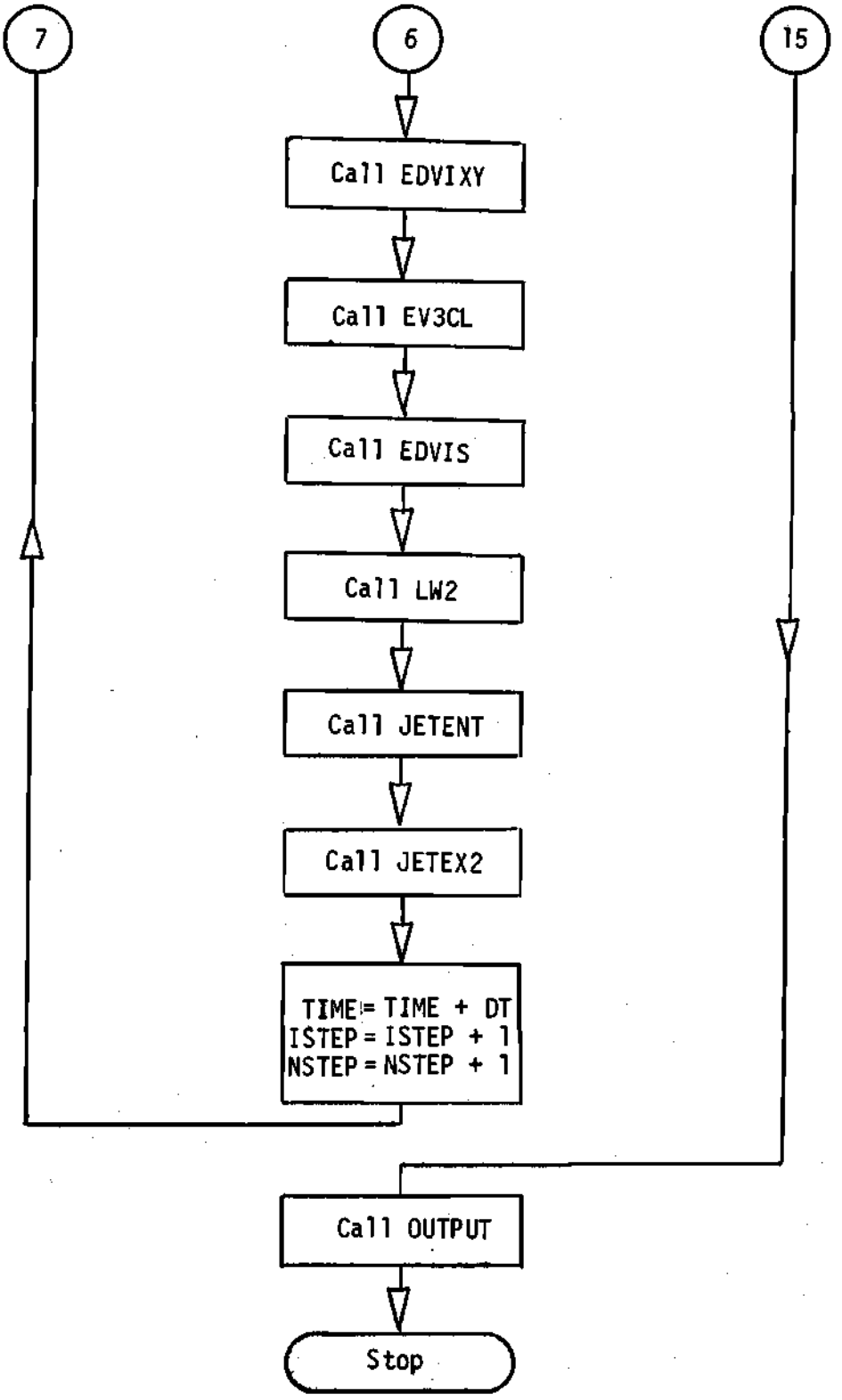

Figure 38. Flow Chart of the Main Routine, DEFJET (Continued)

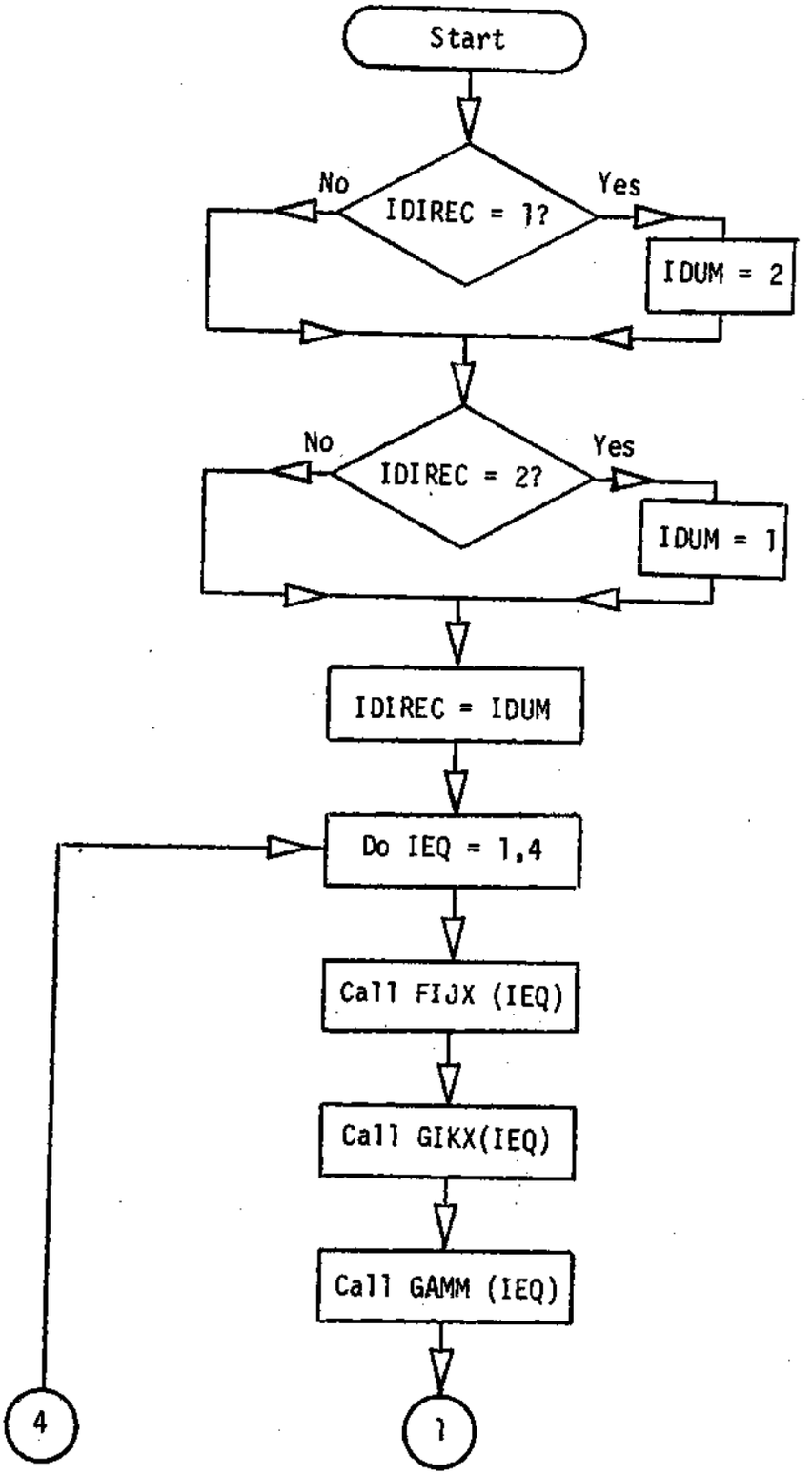

Figure 39. Flow Chart of the Subroutine LW1

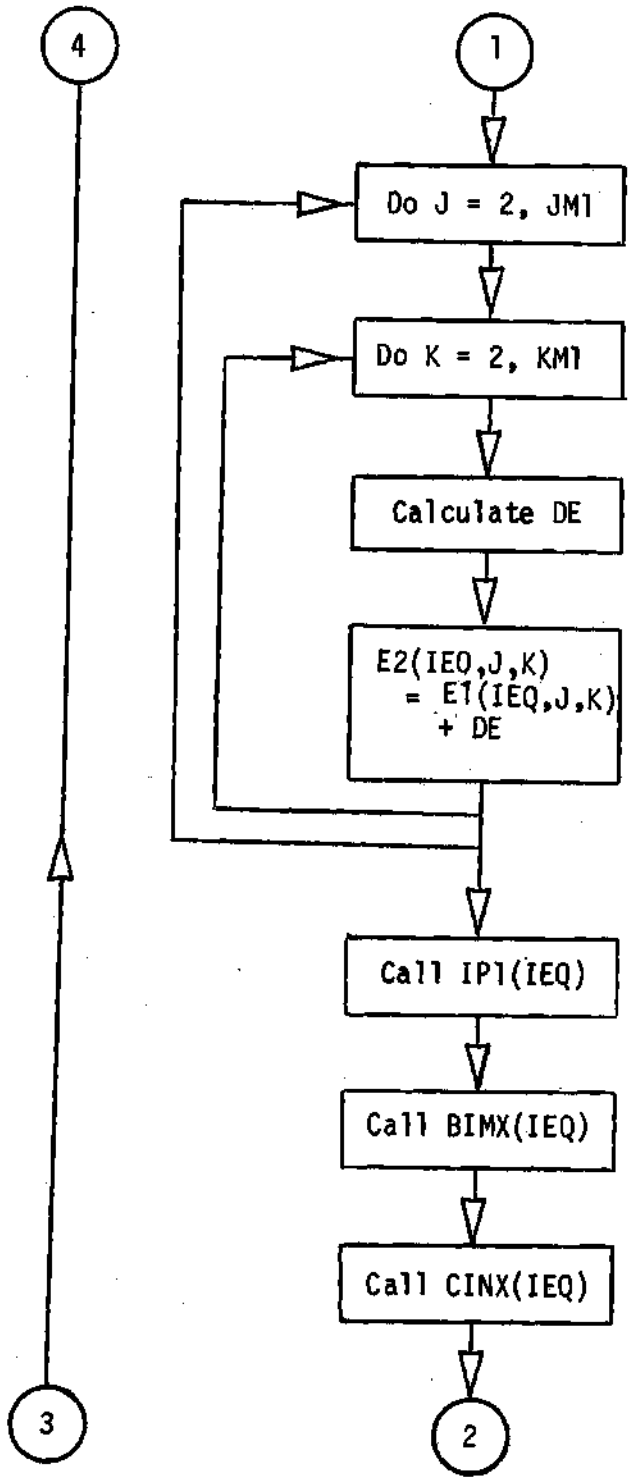

Figure 39. Flow Chart of the Subroutine LW1 (Continued)

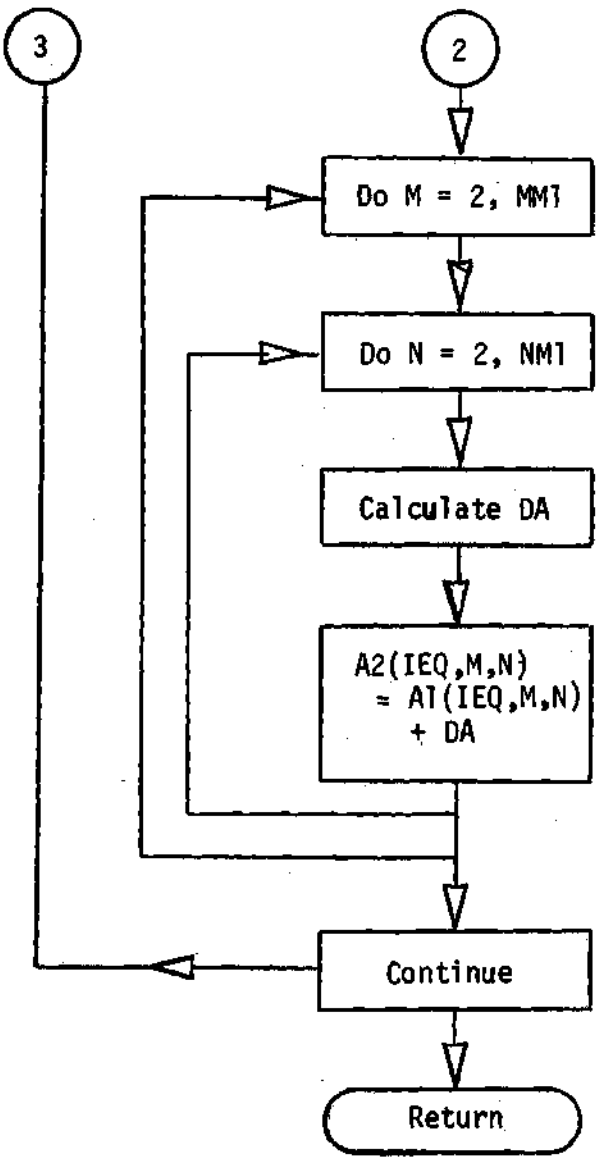

Figure 39. Flow Chart of the Subroutine LW1 (Continued)

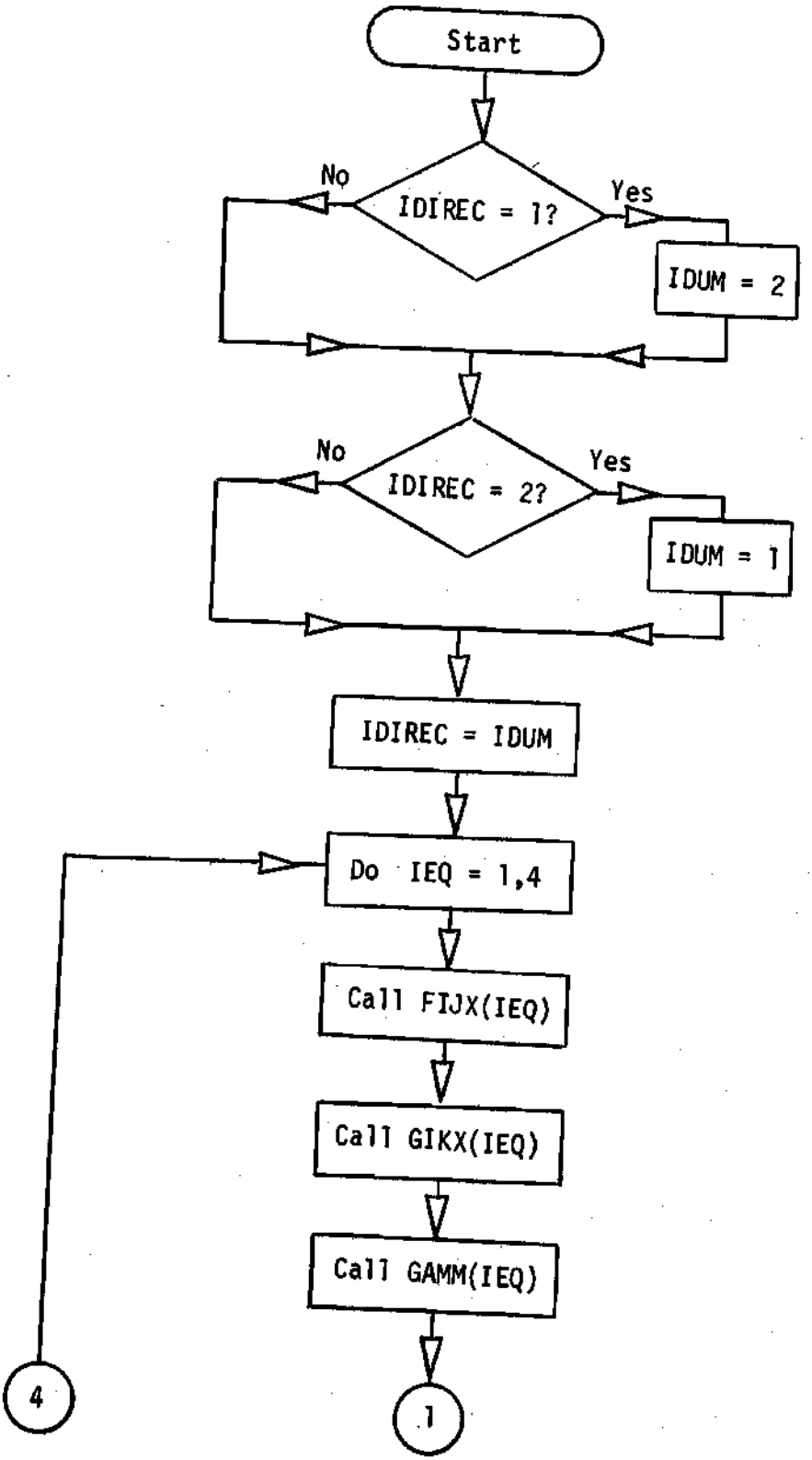

Figure 40. Flow Chart of the Subroutine LW2

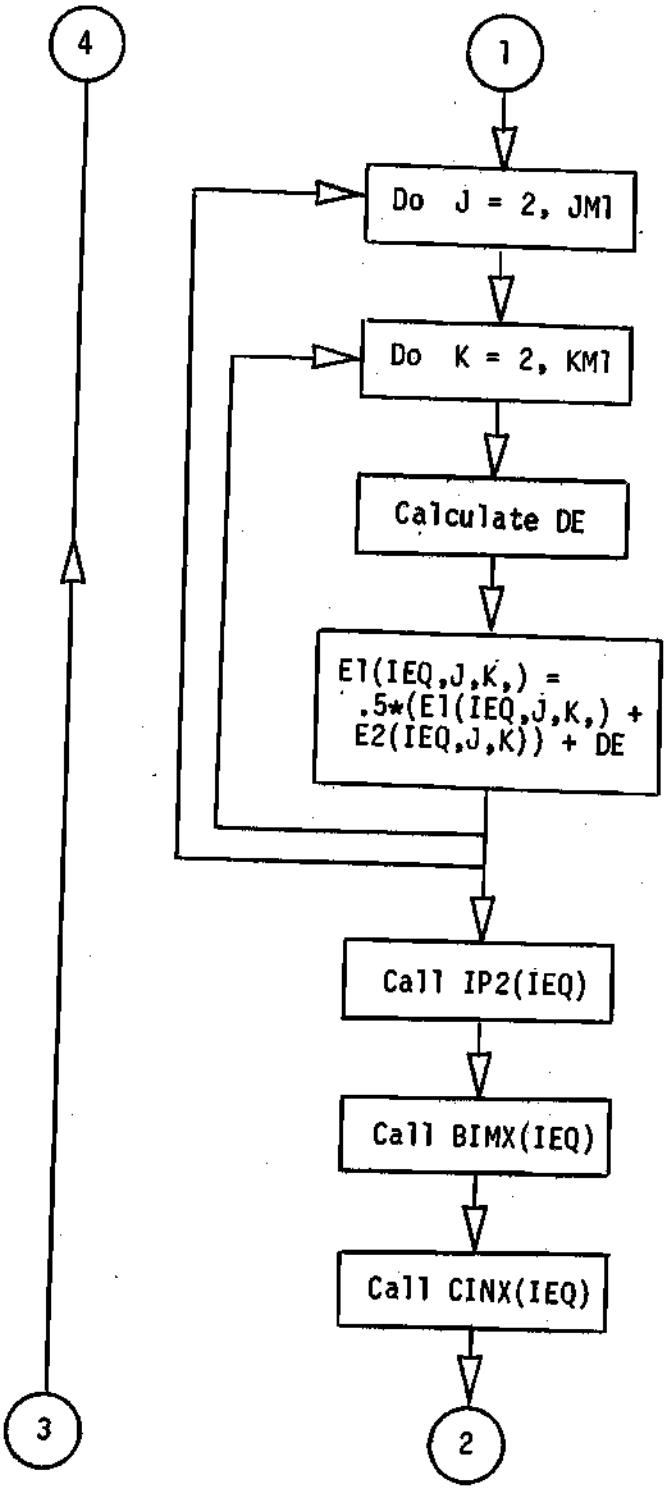

Figure 40. Flow Chart of the Subroutine LW2 (Continued)

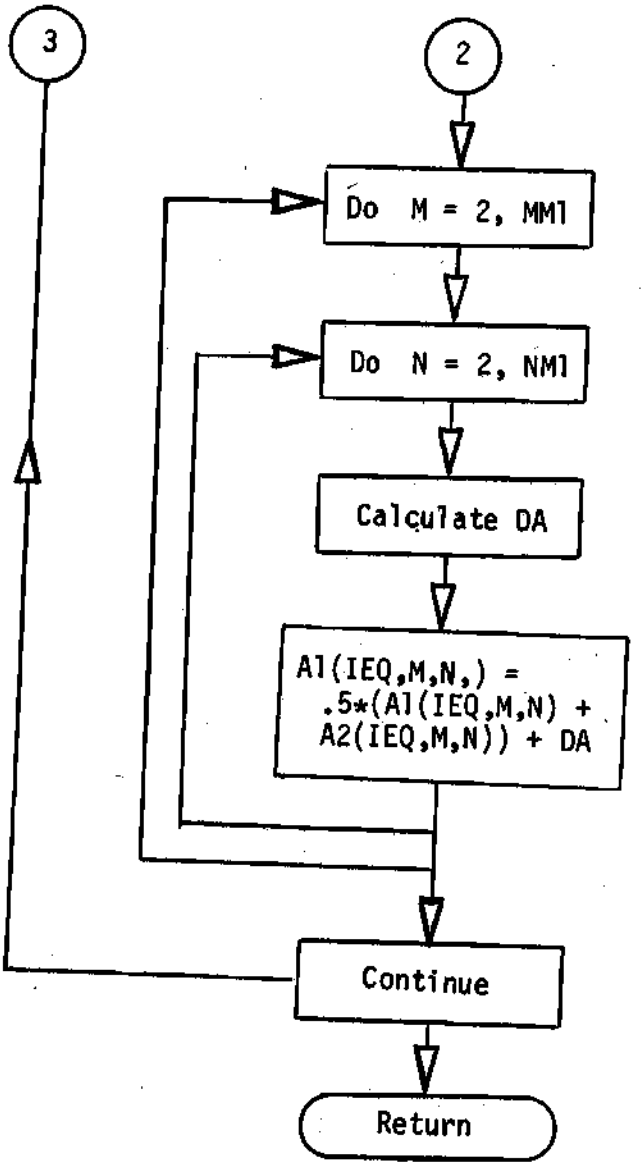

Figure 40. Flow Chart of the Subroutine LW2 (Continued)

APPENDIX I

SIMPLIFIED ANALYSIS OF TRAVERSE OF THE JET BY THE FREE STREAM

The concept of the jet being traversed by streamlines, originating in the free stream, is contrary to some extent to intuition. A simplified analysis combined with experimental observation is useful in providing an explanation for such penetration.

As shown in Figure 41, the streamline originating at the trailing edge of the slot is designated ψ_{tes} while the streamline originating at the leading edge of the slot is ψ_{les}. Based on conservation of mass and the definition of stream functions

$$\psi_{les} - \psi_{tes} \approx \rho_{je} w_{je} b_w \tag{I-1}$$

Downstream of the point of reattachment of the jet the y-coordinate of ψ_{tes} can be seen to be

$$y(\psi_{tes}) = 0 \quad (x \geq x_{rp}) \tag{I-2}$$

Furthermore it is assumed that at some distance downstream of the point of reattachment the jet velocity, temperature and pressure approach the free stream values as the jet disappears.* In such a region the

*This assumption is crucial to the entire analysis but its validity is not entirely clear.

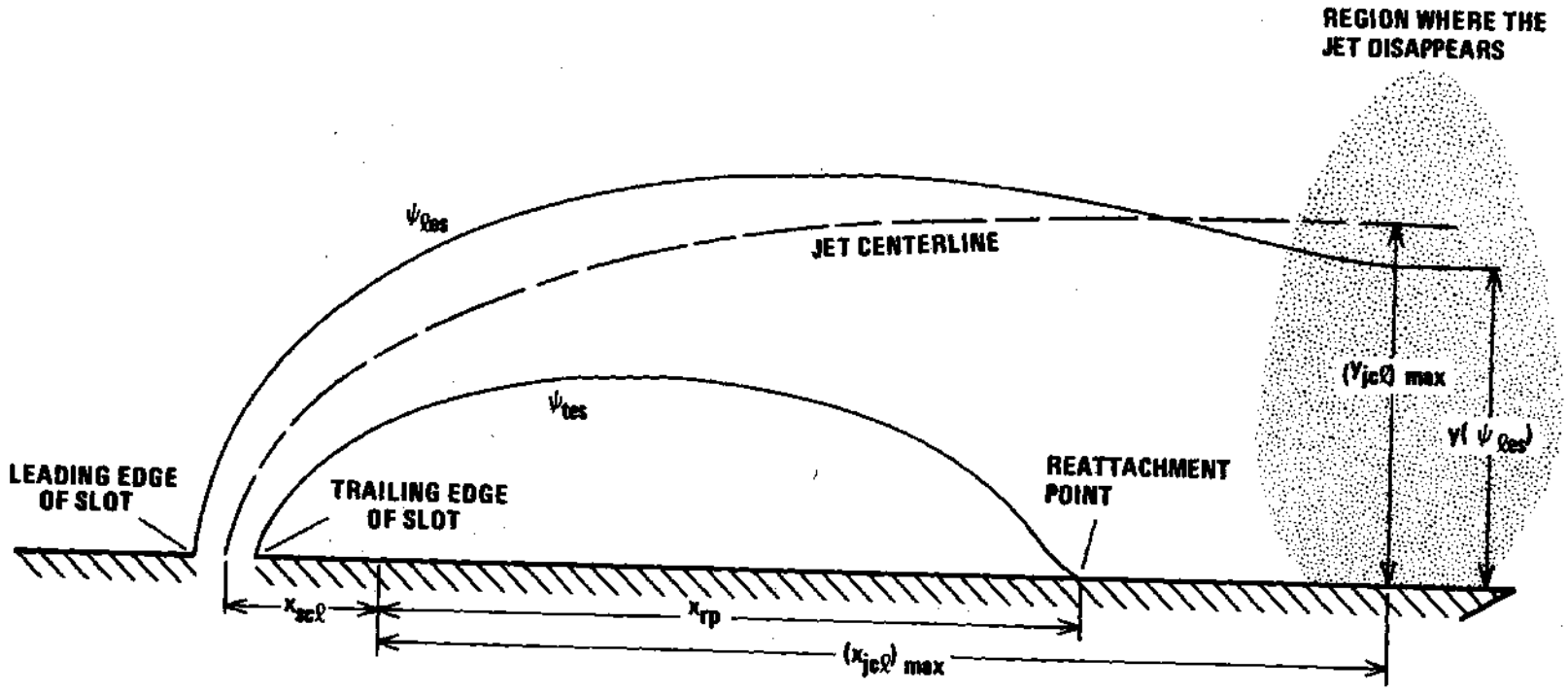

Figure 41. Relative Position of Streamlines $\psi_{\ell es}$ and ψ_{tes} with Respect to Jet Centerline

y-coordinate of $\psi_{\ell es}$ can be expressed as

$$y(\psi_{\ell es}) \approx b_w \rho_{je} w_{je} / (\rho_\infty w_\infty) + \delta^*_{b\ell} \quad (x \geq x_{rp}) \tag{I-3}$$

If penetration of the jet by the free stream does not occur, the y-coordinate of the jet centerline clearly should be less than $y(\psi_{\ell es})$ in the region where the jet disappears. Based on Equation (III-18) for the jet centerline,

$$y_{jc\ell} = b_w \left[\frac{\rho_{je} w_{je}^2}{1.25 \rho_\infty w_\infty^2} \frac{(x_{jc\ell} - x_{sc\ell})}{b_w} \right]^{1/2} \tag{I-4}$$

According to the data of Ivanov [8] for Test Case No. 1 the jet persisted downstream for a distance of

$$(x_{jc\ell})_{max} - x_{sc\ell} \approx 41.8 b_w \tag{I-5}$$

For Test Case No. 1, as noted in Chapter V,

$$\bar{\rho}_{je} \approx \bar{\rho}_\infty \tag{I-6}$$

and

$$\bar{w}_{je} \approx 5 \bar{w}_\infty \tag{I-7}$$

Based on a combination of Equations (I-3), (I-6) and (I-7),

$$y(\psi_{\ell es}) \simeq 5b_w + \delta^*_{b\ell}(x \geq x_{rp}) \tag{I-8}$$

In the current simplified analysis *precise* evaluation of $\delta^*_{b\ell}$ is not appropriate or practical. Based on the assumption that this thickness would be of the same order of magnitude as that occurring in the same region in the absence of the jet† the resulting thickness is

$$\delta^*_{b\ell} \simeq 0.4b_w \quad (x \simeq x_{rp}) \tag{I-9}$$

A combination of Equations (I-8) and (I-9) produces

$$y(\psi_{\ell es}) \simeq 5.4b_w \quad (x \geq x_{rp}) \tag{I-10}$$

while a combination of Equations (I-4) and (I-5) yields

$$(y_{jc\ell})_{max} \simeq 33b_w \quad [x \simeq (x_{jc\ell})_{max}] \tag{I-11}$$

An inspection of Equations (I-10) and (I-11) reveals that based on this simplified analysis, compared with the location of the streamline $\psi_{\ell es}$, the jet centerline is approximately six times as far from the plate. This result would support the concept of the streamline penetrating the jet.

---

†This assumption is consistent with the earlier assumption regarding the nature of the flow in the region where the jet disappears. If the latter is not valid then the former is not justified.

It is important to note that the jet centerline equation as originally developed by Vizel and Mostinskii [16] was based primarily on conservation of momentum. Equation (I-3), describing the location of the streamline $\psi_{\ell es}$ is based simply on conservation of mass. The fact that the two paths, which were generated by the two separate approaches, intersect in the manner described, appears consistent with the idea that, in the deflected jet, momentum in the y-direction is transported deeper into the free stream than is the actual fluid mass of the jet.

BIBLIOGRAPHY

1. E. F. Coxe, "Interaction of a Two-Dimensional Jet with a Deflecting Stream," Ph.D. Dissertation, University of South Carolina, Columbia, South Carolina, 1967.

2. D. J. Spring, T. A. Street, and J. L. Amick, "Transverse Jet Experiments and Theories--A Survey of the Literature," U. S. Army Missile Command, RD-TR-67-4, Redstone Arsenal, Alabama, 30 June, 1967.

3. R. F. Davis, "The Mechanics of Flame and Air Jets," *Institution of Mechanical Engineers Proceedings*, Vol. 137, 1937, pp. 11-72.

4. E. W. Robey and W. F. Harlow, "Heat Liberation and Transmission in Large Steam-Generating Plant," *Institution of Mechanical Engineers Proceedings*, Vol. 125, 1933, p. 201.

5. Yu. V. Ivanov, "Plane Jet in an External Cross Stream of Air," *Izvestia Akademii Nauk Estonskoi SSR*, Vol. 2, No. 2, 1953, pp. 216-234.

6. J. G. Lowry and T. R. Turner, "Low-Speed Wind Tunnel Investigation of Jet Control on a 35° Swept Wing," National Advisory Committee for Aeronautics, RM L53I09a, October, 1953.

7. G. I. Taylor, "The Use of a Vertical Air Jet as a Windscreen," *Jubile' Scientifique de M. Dimitri P. Reabouchinsky*, 1954, pp. 313-317.

8. Yu. V. Ivanov, *Effective Combustion of Overfire Fuel Gases in Furnaces*, Estrosizdat, Tallin, 1959.

9. J. Williams, S. F. J. Butler, and M. N. Wood," The Aerodynamics of Jet Flaps," Aeronautical Research Council, R&M 3304, January, 1961.

10. J. Williams and A. J. Alexander, "Wind-Tunnel Experiments on a Rectangular Wing Jet-Flap Model of Aspect-Ratio 6," Aeronautical Research Council, R&M 3329, June, 1961.

11. M. N. Wood, "Further Wind-Tunnel Experiments on a Rectangular Wing Jet-Flap Model of Aspect-Ratio 6," Ministry of Aviation, unpublished report.

12. S. F. J. Butler, M. B. Guyett, and B. A. Moy, "Six-Component Low-Speed Tunnel Test of Jet-Flap Complete Models with Variation of Aspect-Ratio, Dihedral, and Sweepback," Ministry of Aviation, unpublished report.

13. A. Heyser and F. Maurer, "Experimental Investigations of Solid Spoilers and Jet Spoilers at Mach Numbers of 0.6 to 2.8," *Zeitshrift für Flugwissenschaften,* Vol. 10, No. 45, 1962; issued by Jet Propulsion Laboratory as Astronautics Information Translation No. 32, February 21, 1964.

14. G. N. Abramovich, *The Theory of Turbulent Jets,* The M.I.T. Press, Cambridge, Massachusetts, 1963.

15. L. Ting, P. A. Libby, and C. Ruger, "The Potential Flow Due to a Jet and a Stream with Different Total Pressures," Polytechnic Institute of Brooklyn, PIBAL Report No. 855, 1964.

16. Ya. M. Vizel and I. L. Mostinskii, "Deflection of a Jet Injected into a Stream," *Inzhenerno-Fizicheskii Zhurnal,* Vol. 8, No. 2, 1965, pp. 238-242.

17. R. C. Ackerberg and A. Pal, "On the Interaction of a Two-Dimensional Jet with a Parallel Flow," Polytechnic Institute of Brooklyn, PIBAL Report No. 889, September, 1965.

18. T. A. Girshovich, "The Turbulent Jet in a Crossflow," *Mekhanika Zhidkosti i Gaza,* Vol. 1, No. 1, 1966, pp. 151-153.

19. T. A. Girshovich, "Theoretical and Experimental Study of a Plane Turbulent Jet in a Crossflow," *Mekhanika Zhidkosti i Gaza,* Vol. 1, No. 5, 1966, pp. 121-126.

20. H. Endo, "Effects of Curvature on the Similarity Structure and Turbulent Mixing of Two-Dimensional Curved Jet," National Aerospace Laboratory, TR 1560, Tokyo, 1968; issued by the National Aeronautics and Space Administration as TT F-12, 274, June, 1969.

21. L. J. S. Bradbury, "The Structure of a Self-Preserving Turbulent Plane Jet," *Journal of Fluid Mechanics,* Vol. 23, Part 1, 1965, pp. 31-64.

22. J. O. Hinze, *Turbulence,* McGraw-Hill Book Co., Inc., New York, 1959.

23. T. V. Boussinesq, "Theorie de l'Ecoulement Tourbillant," *Mémoires presentés par divers savants à l'Academie des sciences de l'Institut de France et imprimés par son ordre,* Vol. 23, Paris, 1877.

24. L. Prandtl, "Ueber die ausgebildete Turbulenz," *Zeitschrift für Angewandte Mathematik und Mechanik*, Vol. 5, 1925, p. 136.

25. G. I. Taylor, "The Transport of Vorticity and Heat through Fluids in Turbulent Motion," *Proceedings of the Royal Society*, Vol. A135, 1932, p. 685.

26. Th. von Karman, "Mechanische Aehnlichkeit und Turbulenz," *Nachrichten von der Gesselschaft der Wissenschaften zu Goettingen, Mathematisch-Physikalische Klasse*, Vol. 5, 1930, pp. 58-76.

27. H. Reichardt, "Laws of Free Turbulence," *Verein Deutscher Ingenieure Forschungsheft 414*, 1951.

28. M. L. Albertson, Y. B. Dai, R. A. Jensen, and H. Rouse, "Diffusion of Submerged Jets," *American Society of Civil Engineers Papers*, December, 1948, pp. 1571-1596.

29. H. Schlichting, *Boundary Layer Theory*, McGraw-Hill Book Co., Inc., New York, 4th Edition, 1960.

30. H. Goertler, "Berechnung von Aufgaben der frien Turbulenz auf Grund eines neuen Näherungsansatzes," *Zeitschrift für Angewandte Mathematik und Mechanik*, Vol. 22, 1942, pp. 244-254.

31. V. Zakkay and E. Krause, "The Radial Variation of the Eddy Viscosity in Compressible Turbulent Jet Flows," Wright-Patterson Air Force Base, ARL 65-89, May, 1965.

32. H. H. Korst and W. L. Chow, "Non-isonenergetic Turbulent (Pr_t=1) Jet Mixing Between Two Compressible Streams at Constant Pressure," National Aeronautics and Space Administration, CR-419, 1966.

33. L. J. S. Bradbury and J. Riley, "The Spread of a Turbulent Plane Jet Issuing into a Parallel Moving Airstream," *Journal of Fluid Mechanics*, Vol. 27, part 2, 1967, pp. 381-394.

34. J. F. Tomich and E. Weger, "Some New Results on Momentum and Heat Transfer in Compressible Turbulent Free Jets," *American Institute of Chemical Engineering Journal*, Vol. 13, No. 5, September, 1967, pp. 948-954.

35. P. T. Bauer, "An Eulerian Numerical Method for Multispecie, Turbulent Supersonic Jet Mixing," Ph.D. Dissertation, Oklahoma State University, Stillwater, Oklahoma, July, 1968.

36. S. Pai, *Viscous Flow Theory II--Turbulent Flow*, D. Van Nostrand Co., Inc., Princeton, New Jersey, 1957.

37. E. R. Van Driest, "Turbulent Boundary Layer in Compressible Fluids," *Journal of the Aeronautical Sciences*, Vol. 18, No. 3, March, 1951, pp. 145-160.

38. G. Kleinstein, "Generalized Law of the Wall and Eddy-Viscosity Model for Wall Boundary Layers," *American Institute of Aeronautics and Astronautics Journal*, Vol. 5, No. 8, August, 1967, pp. 1402-1407.

39. G. Maise and H. McDonald, "Mixing Length and Kinematic Eddy Viscosity in a Compressible Boundary Layer," *American Institute of Aeronautics and Astronautics Journal*, Vol. 6, No. 1, January, 1968, pp. 73-80.

40. P. Bradshaw, "Turbulent Boundary Layers," *The Aeronautical Journal of the Royal Aeronautical Society*, Vol. 72, May, 1968, pp. 451-459.

41. T. Cebeci, A. M. O. Smith, and L. C. Wang, "A Finite-Difference Method for Calculating Compressible Laminar and Turbulent Boundary Layers," McDonnell Douglas, Report No. DAC-67131, March, 1969.

42. J. G. Knudsen and D. L. Katz, *Fluid Dynamics and Heat Transfer*, McGraw-Hill Book Co., Inc., New York, 1958.

43. J. Nikuradse, "Gesetzmäbigkeit der turbulenten Strömung in glatten Rohren," *Verein Deutscher Ingenieure Forschungsheft 356*, 1932.

44. J. Laufer, "The Structure of Turbulence in Fully Developed Pipe Flow," National Advisory Committee for Aeronautics, TR 1174, 1954.

45. F. Page, Jr., W. G. Schlinger, D. K. Breux, and B. H. Sage, "Point Values of Eddy Conductivity and Viscosity in Uniform Flow between Parallel Plates," *Industrial and Engineering Chemistry*, Vol. 44, February, 1952, pp. 424-430.

46. J. Laufer, "Investigation of Turbulent Flow in a Two-Dimensional Channel," National Advisory Committee for Aeronautics, TR 1053, 1951.

47. S. I. Pai, "On Turbulent Flow Between Parallel Plates," *Journal of Applied Mechanics*, Vol. 20, March, 1953, p. 109.

48. T. B. Drew, E. C. Koo, and W. H. McAdams, "The Friction Factor for Clean Round Pipes," *Transactions of the American Institute of Chemical Engineers*, Vol. 28, 1932, pp. 56-72.

49. S. Eskinazi and H. Yeh, "An Investigation on Fully Developed Turbulent Flows in a Curved Channel," *Journal of the Aerospace Sciences*, Vol. 28, 1956, pp. 23-24 & 75.

50. J. W. S. Rayleigh, "On the Dynamics of Revolving Fluid," *Proceedings of the Royal Society*, Vol. A93, 1916, pp. 148-154.

51. P. Bradshaw and M. T. Gee, "Turbulent Wall Jets with and without an External Stream," Aeronautical Research Council, R&M 3252, June, 1960.

52. R. A. Sawyer, "Two-Dimensional Reattaching Jet Flows Including the Effects of Curvature on Entrainment," *Journal of Fluid Mechanics*, Vol. 17, 1963, pp. 481-498.

53. R. A. Sawyer, "The Flow Due to a Two-Dimensional Jet Issuing Parallel to a Flat Plate," *Journal of Fluid Mechanics*, Vol. 9, 1960, p. 543.

54. D. P. Margolis and J. L. Lumley, "Curved Turbulent Mixing Layer," *The Physics of Fluids*, Vol. 8, No. 10, October, 1965, pp. 1775-1784.

55. D. E. Guitton, "A Corrigendum and Addendum to MERL Report 64-7 Entitled 'Two-Dimensional Turbulent Wall Jets Over Curved Surfaces'," McGill University, Technical Note 67-1, February, 1967.

56. J. C. Wyngaard, H. Tennekes, J. L. Lumley, and D. P. Margolis, "Structure of Turbulence in a Curved Mixing Layer," *The Physics of Fluids*, Vol. 11, No. 6, June, 1968, pp. 1251-1253.

57. C. K. Chu (editor), *Computational Fluid Dynamics*, American Institute of Aeronautics and Astronautics, Selected Reprint Series, Vol. IV, February, 1969.

58. S. M. Scala, Private Communication, General Electric Company, Valley Forge Space Center, August 12, 1969.

59. A. V. Bitsadze, *Equations of the Mixed Type*, Macmillan Company, New York, 1964.

60. J. Von Neumann and R. D. Richtmyer, "A Method for the Numerical Calculation of Hydrodynamic Shocks," *Journal of Applied Physics*, Vol. 21, March, 1950, pp. 232-237.

61. R. Courant, E. Isaacson, and M. Rees, "On the Solution of Nonlinear Hyperbolic Differential Equations by Finite Differences," *Communications on Pure and Applied Mathematics*, Vol. V, 1952, pp. 243-255.

62. P. D. Lax and B. Wendroff, "Systems of Conservation Laws," *Communications on Pure and Applied Mathematics*, Vol. 13, No. 2, May, 1960, pp. 217-237.

63. V. V. Rusanov, "The Calculation of the Interaction of Non-Stationary Shock Waves and Obstacles," *Zhurnal Vychislitel'noi Matematiki i Matematicheskoi Fiziki*, Vol. 1, No. 2, pp. 267-279, 1961; issued by National Research Council of Canada as Translation No. 1027, 1962.

64. R. D. Richtmyer, "A Survey of Difference Methods for Non-Steady Fluid Dynamics," National Center for Atmospheric Research, Technical Note 63-2, 1963.

65. H. U. Thommen, "A Method for the Numerical Solution of the Complete Navier-Stokes Equations for Steady Flows," General Dynamics/Convair, GDC-ERR-AN733, April, 1965.

66. L. Crocco, "A Suggestion for the Numerical Solution of the Steady Navier-Stokes Equations," *American Institute of Aeronautics and Astronautics Journal*, Vol. 3, No. 10, October, 1965, pp. 1824-1832.

67. H. U. Thommen, "Numerical Integration of the Navier-Stokes Equations," *Zeitschrift für Angewandte Mathematik und Physik*, Vol. 17, 1966, pp. 369-384.

68. S. Z. Burstein, "Finite Difference Calculations for Hydrodynamic Flows Containing Discontinuities," Courant Institute of Mathematical Sciences, New York University, Report NYO-33, 1965.

69. G. Morretti and M. Abbett, "A Fast, Direct, and Accurate Technique for the Blunt Body Problem," General Applied Science Laboratories, Report No. TR-583, January, 1966.

70. J. G. Trulio, W. E. Carr, W. J. Niles, and R. L. Rentfrow, "Calculation of Two-Dimensional Turbulent Flow Fields," National Aeronautics and Space Administration, CR-430, May, 1966.

71. R. D. Richtmyer and K. W. Morton, *Difference Methods for Initial-Value Problems*, 2nd Edition, Interscience Publishers, John Wiley & Sons, Inc., New York, 1967.

72. A. Lapidus, "Detached Shock Calculation by Second-Order Finite Differences," Courant Institute of Mathematical Sciences, New York University, Report NYO-1480-69, February, 1967.

73. S. M. Scala and P. Gordon, "Solution of the Time-Dependent Navier-Stokes Equations for the Flow of Dissociating Gas Over a Circular Cylinder," General Electric Company, R67SD56, May 10, 1967.

74. S. M. Scala and P. Gordon, "Solution of the Time-Dependent Navier-Stokes Equations for the Flow around a Circular Cylinder," *American Institute of Aeronautics and Astronautics Journal*, Vol. 6, No. 5, May, 1968, pp. 815-822.

75. S. M. Scala and P. Gordon, "Reflection of a Shock Wave at a Surface," *The Physics of Fluids*, Vol. 9, No. 6, June, 1966, pp. 1158-1166.

76. P. Gordon, "Nonsymmetric Difference Equations," *Journal of Society for Industrial and Applied Mathematics*, Vol. 13, No. 3, September, 1965, pp. 667-673.

77. A. M. O. Smith and T. Cebeci, "Numerical Solution of the Turbulent Boundary-Layer Equations," McDonnell Douglas, Report No. DAC 33735, May 29, 1967.

78. R. F. Probstein and D. Elliot, "The Transverse Curvature Effect in Compressible Axially Symmetric Laminar-Boundary-Layer Flow," *Journal of the Aeronautical Sciences*, Vol. 23, No. 3, March, 1956, pp. 208-224 & 236.

79. W. D. Hayes and R. F. Probstein, *Hypersonic Flow Theory*, Academic Press, New York and London, 1959.

80. A. J. Chorin, "A Numerical Method for Incompressible Viscous Flow Problems," *Journal of Computational Physics*, Vol. 2, No. 1, August, 1967, pp. 12-26.

81. E. C. DuFort and S. P. Frankel, "Stability Conditions in the Numerical Treatment of Parabolic Differential Equations," *Mathematical Tables and other Aids to Computation*, Vol. 7, 1953, p. 135.

82. V. J. Skoglund, J. K. Cole, and E. F. Staiano, "Development and Verification of Two-Dimensional Numerical Techniques for Viscous Compressible Flow with Shock Waves," New Mexico University, Albuquerque, New Mexico, Report No. SC-CR-67-2679, August, 1967.

83. B. Z. Jenkins, "A Survey and Introduction to the Use of Finite Difference Methods in Fluid Dynamical Problems," U. S. Army Missile Command, RD-TR-68-1, Redstone Arsenal, Alabama, 21 March, 1968.

84. G. Moretti, "The Importance of Boundary Conditions in the Numerical Treatment of Hyperbolic Equations," Polytechnic Institute of Brooklyn, PIBAL Report No. 68-34, November, 1968.

85. R. W. MacCormack, "The Effect of Viscosity in Hypervelocity Impact Cratering," *American Institute of Aeronautics and Astronautics*, Preprint 69-354, June, 1969.

86. H. Lomax, "An Analysis of Finite-Difference Techniques Applied to Equations Governing Convective Transfer," *Analytic Methods in Aircraft Aerodynamics*, National Aeronautics and Space Administration, SP-228, 1970, pp. 245-264.

87. M. R. Spiegel, *Vector Analysis and an Introduction to Tensor Analysis*, Schaum Publishing Company, New York, 1959.

88. W. F. Hughes and E. W. Gaylord, *Basic Equations of Engineering Science*, Schaum Publishing Company, New York, 1964.

89. R. B. Bird, W. E. Stewart, and E. N. Lightfoot, *Transport Phenomena*, John Wiley & Sons, Inc., New York, 1960.

90. R. W. Truitt, *Fundamentals of Aerodynamic Heating*, Roland Press Company, New York, 1960.

91. O. Reynolds, "On the Dynamical Theory of Incompressible Viscous Fluids and the Determination of the Criterion," *Philosophical Transactions of the Royal Society*, Vol. 186A, 1895, pp. 123-164.

92. A. H. Shapiro, *The Dynamics and Thermodynamics of Compressible Fluid Flow*, Vols. I and II, Ronald Press Company, New York, 1953.

93. C. Truesdell, "Mechanical Basis of Diffusion," *Journal of Chemical Physics*, Vol. 37, No. 10, November, 1962, p. 2336.

94. P. S. Klebanoff, "Characteristics of Turbulence in a Boundary Layer with Zero Pressure Gradient," National Advisory Committee for Aeronautics, TN 3178, 1954.

95. M. J. Lighthill, "Viscosity Effects in Sound Waves of Finite Amplitude," *Surveys in Mechanics*, Cambridge, 1956, p. 261.

96. W. G. Vincenti and C. H. Kruger, *Introduction to Physical Gas Dynamics*, John Wiley & Sons, Inc., New York, 1965.

97. S. H. Crandall, *Engineering Analysis*, McGraw-Hill Book Company, Inc., New York, 1956.

98. A. J. Chorin, Private communication, Courant Institute of Mathematical Sciences, New York University, New York, August 17, 1969.

99. R. D. Richtmyer, Private communication, University of Colorado, Boulder, Colorado, September 16, 1969.

100. A. S. Householder, *Principles of Numerical Analysis*, McGraw-Hill Book Company, Inc., New York, 1953.

101. W. F. Walker, G. W. Zumwalt, and L. J. Fila, "A Numerical Solution for the Interaction of a Moving Shock Waves with a Turbulent Mixing Region," *Journal of Applied Mechanics*, Vol. 35, June, 1968, pp. 220-228.

102. W. G. Strang, "Accurate Partial Difference Methods II: Non-Linear Problems," *Numerical Mathematics*, Vol. 6, 1964, p. 37.

103. J. W. Daily and D. R. F. Harleman, *Fluid Dynamics*, Addison-Wesley Publishing Company, Inc., Reading, Massachusetts, 1966.

104. F. Maurer, Private communication, Institute of Applied Gas Dynamics, German Research Center for Aeronautics and Space Flight, Linderhöhe, West Germany, January 21, 1970.

105. F. Maurer, Private communication, Institute of Applied Gas Dynamics, German Research Center for Aeronautics and Space Flight, Linderhöhe, West Germany, May 21, 1970.

106. H. Endo, Private communication, National Aerospace Laboratory, Tokyo, Japan, December 18, 1969.

107. H. Endo, Private communication, National Aerospace Laboratory, Tokyo, Japan, July 1, 1970.

VITA

Frank Buck Tatom was born in Montgomery, Alabama, on November 27, 1934, the younger son of Elizabeth Buck Tatom and the late Thomas Athor Tatom. He was educated in the public schools of Montgomery and graduated from Sidney Lanier High School in May, 1952. In June of that year he entered the United States Naval Academy, and in June of 1956 he graduated from that institution with a Bachelor of Science degree and a commission as Ensign in the United States Navy.

As a commissioned officer he initially served for two years aboard the aircraft carrier, USS FRANKLIN D. ROOSEVELT (CVA-42), with duties in fire control and gunnery. Subsequent to this, he spent six months as an officer-student at the U. S. Naval Combat Information Center School, Glynco, Georgia. Upon completion of this training he reported to the destroyer, USS ZELLARS (DD-777), aboard which he served for 18 months in communications and operations. In August of 1960 Mr. Tatom left active duty and entered the Naval Reserve. He has remained active in the latter organization and currently holds the rank of Commander, U. S. Naval Reserve.

For one year, commencing in August, 1960, Mr. Tatom served as a process engineer with E. I. du Pont de Nemours and Co. in Camden, South Carolina. In the fall of 1961 he enrolled in the graduate program of Auburn University and in December, 1962, he graduated with a Master of Science in Mechanical Engineering. After serving for nine months as

Assistant Professor in the Mechanical Engineering Department of Auburn University, he accepted a position with Northrop Corporation in Huntsville, Alabama. For five years Mr. Tatom was responsible for the Aero/Thermodynamics Branch of Northrop-Huntsville while on a part-time basis continuing his graduate studies at the University of Alabama at Huntsville. In September, 1968, he was enrolled in the graduate program of Georgia Institute of Technology.

Mr. Tatom was married in September, 1959, to the former Roberta Claire Wood, and they have three children, Frank Thomas, John Wood, and Briana Claire.